STUDIES ON CHEMICALLY MODIFIED AND UNMODIFIED ACRYLONITRILE BUTADIENE RUBBER, ETHYLENE PROPYLENE DIENE MONOMER RUBBER AND THEIR NANOCOMPOSITES

Thesis submitted to the
University of Calicut
in partial fulfillment of the requirements
for the award of the degree of

DOCTOR OF PHILOSOPHY IN CHEMISTRY

by

NIHMATH A.

DEPARTMENT OF CHEMISTRY
UNIVERSITY OF CALICUT
KERALA

OCTOBER 2019

DEPARTMENT OF CHEMISTRY
UNIVERSITY OF CALICUT
THENJIPALAM, MALAPPURAM
KERALA-673 635

Dr. M.T Ramesan
Assoc. Professor

Tel: +91-9447837455
E-mail: mtramesan@uoc.ac.in

Date: …….

Certificate

Certified that the research work embodied in the thesis entitled "*STUDIES ON CHEMICALLY MODIFIED AND UNMODIFIED ACRYLONITRILE BUTADIENE RUBBER,ETHYLENE PROPYLENE DIENE MONOMER RUBBER AND THEIR NANOCOMPOSITES*" has been carried out by **Nihmath.A** under my supervision at the Department of Chemistry, University of Calicut, Kerala and further, the results embodied in this thesis, in full or in part have not been submitted previously elsewhere for the award of any other degree or diploma.

Calicut University **Dr. M.T Ramesan**

Declaration

I hereby declare that the research work embodied in the thesis entitled "*STUDIES ON CHEMICALLY MODIFIED AND UNMODIFIED ACRYLONITRILE BUTADIENE RUBBER, ETHYLENE PROPYLENE DIENE MONOMER RUBBER AND THEIR NANOCOMPOSITES*", is based on the original research work carried out by me under the guidance of Dr. M.T Ramesan, Associate Professor, Department of Chemistry, University of Calicut, Kerala and the same has not been submitted elsewhere previously for the award of any other degree or diploma.

Calicut University **Nihmath A**

……

Acknowledgement

"In the name of God, the infinitely compassionate and merciful"

All praises and thanks be to Him for giving me the blessings, strength, opportunity to carry out this research study and to persevere and complete it satisfactorily.

I am deeply grateful to many people who were always there when I needed them the most, during this journey of research and thesis preparation. It is a great pleasure to acknowledge all of those who have provided me all kind of help, inspiration and encouragement that make this Ph.D. thesis a possibility.

At the very outset, I record my sincere gratitude and indebtedness to Dr. M.T.Ramesan, my esteemed supervisor for his aspiring guidance, untiring and ardent interest, critical evaluation and above all the boundless patience. I feel privileged to be associated with a person like Ramesan sir and I shall eternally be grateful to him.

I owe deep sense of gratitude to Dr. A.I.Yahia, Head of the Department for providing necessary facilities for the completion of this research work. I am extremely happy to submit my thesis during his period because he is one of my most beloved and revered chemistry teachers of all time. I extend my sincere thanks to our former HODs, Dr. P.Raveendran, Dr. K.Muraleedharan and Dr. V.M.Abdul Mujeeb. I am delighted to convey my gratitude to Dr. N.K.Renuka, Dr.P.Pradeepan and Dr. Abraham Joseph. I am grateful to all the non teching staff of our department for their whole hearted cooperation and affirmative responses.

With immense love and respect, I remember all my teachers who have enriched me at various learning stages since childhood. It is their blessings and support which enabled me to reach where I am now.

I am indebted to my colleagues in the organic research lab for providing a stimulating and fun environment to learn and grow. They were

with me in all the "off" and "on" conditions I was told I had. One of them is my bestie ; Dr.Jasna. I would never be able to pay back the unwavering and unselfish love and affection given to me at all times. She helped me in collation of data for my work to a great extent. I cannot forget my favorite friends Jayakrishnan, Aparna K Balan, Shaniba teacher, Sreejithettan, Subair sir and Jinitha; the personal and technical help that they had extended to me through out. I am sincerely grateful to them for sharing their truthful and illuminating views on a number of issues related to the work. I am extremely thankful to my juniors Suhailath, Parvathi and Sankar for the stimulating discussions, wholehearted cooperation and selfless help rendered. I thank all the former and present M.Phil scholars of our group for their help and support. A special word of gratefulness to Anilkumar sir for his invaluable assistance in making samples for the study.

My heartfelt thanks to my fellow labmates Soumya, Thasneem, Rajeenatha, Shamsi, Jithin, shyam, Jency and Dipin for all the fun we have had and making this venture a memorable experience.

I acknowledge the University Grants Commission (UGC), Government of India for providing me with the necessary funding and fellowship to pursue research.

I gratefully acknowledge the analytical support offered by CFSE, Manjeri,STIC-CUSAT and NIT,Calicut. I owe my sincere gratitude to Dr.P.P.Pradyumnan,Department of Physics, University of Calicut for facilitating XRD and conductivity studies. I am extremely thankful to Dr.Rosamma Alex, former Joint Director and Dr. Madhusudanan K.M., Scientist RRI, Kottayam for providing me an opportunity to study the cure and mechanical properties of rubber samples.

I would like to make special thanks to Rajeshettan and co-workers, Bina Photostat for the assistance in the beautiful compilation of the thesis.

Deep appreciation and sincere gratitude is expressed to the Principal, Staff and dear students of GHSS, Othukkungal for their unparalleled support which inspired me a lot.

Just like everyone else, the biggest source of my strength is the love and backing provided by my family. Words are inadequate to express my heartful thanks to my parents whose inspiration and faith in me resulted in this achievement. My father, the one who can never ever be thanked enough, for the overwhelming love and care he bestow upon me. I deeply regret the negligence on my part of not completing the work during his lifetime. Whatever I am today is because of my mother's loving, nurturing, unflinching insistence and support. My biggest consolation in these times was that, like under Hen's wing, my little one was in her safety. My acknowledgement would be incomplete without thanking my beloved sisters and brother for goading me in difficult moments where I felt stumped by providing unflinching encouragement and support in various ways. The blessings of my grandmother have made a tremendous contribution in helping me to reach this stage in my life. I will be failing in my duty if I do not mention my sincere thanks to my parents in laws for their love, care, selfless support, encouragement and patience.

My special, profound and affectionate thanks to my better half Dr. Sajid who helped me at every step and stand as backbone. The unabated support both acadamically and emotionally rendered by him made the riding through the rough roads of research a little bit easier. I dedicated all this effort to my Cutie Anjoom whose naughtiness always made me feel refreshed. I also thank Rishukka, Ajukka Azmitha, Amrin, Azeem and Sinu for making her days colourful.

Finally, I am obliged to all my relatives, friends and well-wishers who have loved and encouraged me in the completion of this work.

Nihmath A

To

My beloved Parents

Lil girl and better half

Contents

Preface

The scope of application of both natural and synthetic rubbers has been widened from erasers to flexible conductors. The development of new rubber compound is an interesting area in advanced research. However, the synthesis of new polymers is not always necessary for applications requiring specific properties. One major effort, in the area of polymer technology, is the transformation of existing rubbers to well-defined macromolecules with precisely controlled architecture via chemical functionalization of rubber backbone or by blending of suitable polymers. Various types of particles are also used to fill rubber and to make nanocomposites (depending on the nature of filler) often displaying combinations of synergistic property.

There are opportunities for new chemistries and exploitation which are to be addressed, long-term durability and cost-effectiveness along with unique technological properties so that ready-to-use products with market acceptance could be designed. Further, an attempt to address the health and environmental safety issues to be taken in to consideration. That is the new material should have to satisfy the end properties (service requirements), better processing requirements and maintain a balance between the properties and price.

The main aim of the present work is the chlorination of two commercially exploited synthetic rubbers – NBR and EPDM. The blending of these two modified rubbers was also carried out and the effects of impregnation of bioceramic hydroxyapatite nanoparticles on the cure characteristics, mechanical properties, thermal and electrical properties were investigated in addition to sorption properties. The thesis entitled "**Studies on chemically modified and unmodified**

acrylonitrile butadiene rubber, ethylene propylene diene monomer rubber and their nanocomposites" is divided in to nine chapters.

Chapter 1 gives a brief introduction to rubbers, various chemical modification reactions, an over view of composites and an outline of polymer blends. This chapter also underlines the scope and objectives of the present work. **Chapter 2** deals with the different materials and experimental methods used in this study. **Chapter 3** contains preparation, characterization and studies on electrical properties such as AC conductivity, dielectric constant and dielectric loss tangent of NBR and EPDM rubber based hydroxyapatite (HA) nanocomposites. The chemical functionalization of NBR with dichlorocarbene and its effectiveness on thermal properties, cure behaviors and mechanical properties, flame, oil and solvent resistance with respect to different level of chlorine content have been described in **Chapter 4**. **Chapter 5** deals with the fabrication and characterizations of Cl-NBR /HA nanocomposites by a simple, inexpensive two-roll mill mixing technique. The electrical properties such as AC conductivity, dielectric constant and dielectric loss tangent were also evaluated with respect to the different loading of the nanoparticles. Moreover, this chapter gives the effect of nano hydroxyapatite on mechanical, oil resistance and solvent diffusion properties of chloro functionalized NBR. The preparation, structural characterization, morphology and thermal and electrical properties of chlorinated EPDM and fabrication of its nanocomposite with HA nanofiller have been presented in **Chapter 6.** The effect of nano ceramic HA on mechanical, electrical and oil resistance of chloro functionalized EPDM are also furnished in this chapter. The preparation and characterizations of Cl-NBR and Cl-EPDM elastomer blends with different blend ratio has been given in **Chapter 7**. Besides physical, mechanical and electrical properties, the studies based on the

sorption and transport properties of ASTM oils, petroleum fuels and aromatic solvents are also presented in this chapter. **Chapter 8** discusses on the preparation of Cl-NBR/ Cl-EPDM (50/50) blend nanocomposites with different loading of HA nanoparticles. The compatibility of blend composites have been examined with special reference to the effect of the amount of nanoparticles in terms of their cure and mechanical characteristics, electrical conductivity studies, oil, fuel and solvent resistance. The important conclusions and future outlook of the investigation are presented in **Chapter 9**.

Chapter 1
Introduction

1.1 Rubbers
1.2 Chemical modification of rubber
1.3 Composites
1.4 Polymer Blends
1.5.1 Biodegradability
1.5.2 Flexible electronics
1.5.3 Flammability
1.5.4 Oil and Solvent barrier properties
Scope and objectives

The field of polymer science has been looked at extensively because it touches many scientific disciplines such as Chemistry, Physics, Material Science and Electrical Engineering due to diversity in application and performance characteristics.

A polymer-big chain of specified repeating unit- is an embodiment of monomers or mixtures of monomers of different sizes, shapes, molecular weight and molecular complexity achieving strength and balance through unification. The structural variations ranging from linearity and branching to crosslinking or networking, the natural and synthetic polymer materials offer different range of properties out of the sheer necessity of growing needs and demands in respect of mechanical strength, thermal resistance, toughness and flexibility, rheology and morphology, chemical and solvent resistance etc [1]. The excellent processability, lower cost and low specific gravity, high strength to weight ratio extend the applications of these macromolecules that far exceeds that of any other class of material available to man to adhesives, coatings, foams, and packaging materials to textile and industrial fibers, biomedical and electrochromic devices, antistatic application, polymeric fuel cells, sensors, rechargeable batteries and precursors for many newly developed high-tech ceramics [2-6]. Thus the sustained, imaginative and creative efforts of scientists, engineers and technologists in the polymer field have been made

possible the present level growth, sophistication and advancements of our expanding society in a large measure [7-9].

Elastomers characterized by a unique combination of useful properties such as elasticity, flexibility, toughness and impermeability form a special class of polymeric materials and the modern era of polymers started from the realization of its utility in both industrial and technological settings.

1.1 Rubbers

The rubber technology starts in on with the natural product known as natural rubber (NR) which is a polymer of isoprene. All the materials attract interest on the basis of their property-processing – cost – performance relations. In the last century, the rubber or elastomer materials replaced ceramics and metals in several applications and became interconnected and inseparable with industry due to its inimitable structural characteristics. The freely rotating bonds with 3D zig zag structure allow the rubber chains to change their length by coiling or uncoiling. Unlike most solids which expands in volume upon the application of thermal energy, the stretching and un-stretching of the rubber allows without any change in the internal energy [10]. The major reasons for the use of rubbers in engineering fields are elasticity and durability, applicability in the variety of environments, possibility of convenient equipment designs and corrosion resistance against chemicals, acids and alkalies and can convert to functional products

readily and rapidly at a relatively lower cost. Rubber can act as good construction materials in shock and vibration isolators and/or as dampers due to elasticity and viscosity. It gives excellent performance as protection material against fire, heat and wearing so that finds wide applications in automotive, aerospace, defense and biomedical fields [11-13].

NR, a homopolymers of 2- methyl – 1, 3- butadiene having a cis 1, 4-configuration, is the most widely used naturally occurring elastomer. It is well known for the high tensile strength over a wide hardness range due to its "strain induced crystallization" and the greater resilience is responsible for its very low heat buildup. Also, NR shows very low compression set and stress relaxation, good resistance to abrasion, tear and fatigue and good electrical insulation properties. However, being an unsaturated elastomer NR vulcanizates are susceptible to attack by atmospheric oxygen, ozone and not resistant to petroleum-based oils and fuels, as it contains no polar groups [14].

Eventhough, natural rubber is somewhat an all purpose rubber, its short comings and the advent of the rubber industry prompted the need of synthesizing rubber alternatives which became stronger during the Second World War. Synthetic elastomers, mainly derived from petroleum, initially were based on dienes. That is similar to those present in the repeating unit of NR, most of the polymers that have been derived have unsaturated structural unit in their molecules. The low cost, easy vulcanization

and enhanced performance like gas impermeability triggered the massive production of synthetic elastomers. Currently synthetic rubber materials are used in a variety of industrial applications requiring gum tensile strength, good resilience, oil resistance and low water swell. Neoprene was the first successful rubber reported which is renowned for its resistance to ageing and weathering, ozone attack and flame retardancy [15, 16].

Depending on the chemical saturation of the molecular chain, oil resistance, flame resistance and service performance the elastomers are classified into many groups. Generally, elastomers are classified as commodity or general purpose elastomers such as NR, styrene butadiene rubber (SBR), isoprene rubber (IR) etc. and specialty synthetic elastomers like ethylene propylene diene monomer rubber (EPDM), chloroprene rubber (CR), acrylonitrile butadiene rubber (NBR) etc.

1.1.1 An overview of some special purpose rubbers

Elastomers that are synthesized to full fill some specific functions which cannot be matched by the general purpose rubbers and in many cases of great importance for manufacturing industrial and automotive rubber products.

i. Polychloroprene rubber (CR)

It is the world's first commercial synthetic rubber made available in the market which is known in the trade by the generic

term neoprene. Chloroprene is polymerized by emulsion polymerization using potassium persulphate as free radical initiator. The main component of the polymer usually is trans-1, 4-units. In the vulcanizing of CR, zinc oxide and magnesium oxide blend is usually used. The major applications and uses include heat resistant and flame resistant belting, industrial hoses, wires and cables, rubber rollers gaskets and O rings etc [17].

ii. Ethylene- Propylene-Diene Terpolymer (EPDM)

Ethylene-propylene rubbers are produced mostly by solution polymerization with Ziegler-Natta type catalyst. The random copolymer of ethylene and propylene (EPM) is a soft, easily flowing, amorphous polymer with interesting elastic properties. The letters (E) and (P) stand for ethylene and propylene respectively, while (M) indicates the class of elastomers with fully saturated main chain, as defined in ISO 1629. The lack of chemical functionalities and inadequate compatibility with other polymers limits their applications. To allow for sulfur-curing, ethylene-propylene-terpolymers are developed which is formed by copolymerization of a non conjugated diene as a third monomer in small proportions. Many dienes have been tested as third monomer, and 5-ethylidene-2-norbornene (ENB) is currently the most commonly used· Other commercial dienes are dicyclopentadiene (DCPD) and vinyl-norbornene (VNB). Out of the two double bonds of these dienes, one in the strained ring is most reactive and thus consumed during polymerization, while the second double bond

allows for sulfur vulcanization. The lower reactivity of the second double bond towards polymerization is to minimize branching reactions. It is due to branching that the amount of diene which can be incorporated into the polymer is significantly limited. EPDM has outstanding storage stability, moderate tear strength and good heat stability. Resistance to oxygen or ozone attack is good. It is mainly used in roofing, products of automotive industry such as seals and hoses, isolators, gaskets and hosepipes, liners in building industry, manufacture of wire and cable [18-20].

iii. Poly acrylic rubber or Acrylate rubber (ACM)

ACM is a copolymer of ethyl acrylate (95%) and 2-chloroethyl acrylate or 2- chloroethyl vinyl ether as a cure site monomer. The cured rubber is better than nitrile rubber in oil and heat resistance. Since it doesn't contain unsaturation, resistance to ozone, sunlight and weathering are good. It is commonly used in automotive transmissions and hoses. It is also used in shaft seals, adhesives, beltings, gaskets and O-rings. It is used in vibration damping mounts due to the damping properties.

iv. Fluoro carbon rubber (FKM)

Flouro carbon rubbers are copolymers of vinylidene fluoride and chlorotrifluoro ethylene. They are inert, more expensive than neoprene or nitrile rubber elastomers. FKM exhibit excellent resistance to oils and provide additional heat and chemical resistance, made them superior to almost all other

commercial rubbers. They are flame resistant and exhibit outstanding oxygen and ozone resistance. The applications include fire resistant and protective clothing, wire and cable insulation etc.

v. Acrylonitrile Butadiene Rubber (NBR)

Poly-acrylonitrile-butadiene rubber commonly called nitrile rubber is a random copolymer of butadiene and acrylonitrile in which the acrylonitrile content varies between 18-50%. NBR is produced exclusively by emulsion polymerization. The composition can be varied by changing feeding ratio of monomers, amount of emulsifiers and modifiers of polymerization or temperature. It is particularly used because of its good oil, fuel and fat resistance since it is polar. Increasing the acrylonitrile content improves oil resistance, hardness, abrasion resistance and heat resistance, but raises the glass transition temperature. Nitrile rubbers are used in applications which demand good mechanical properties and oil and fuel resistance. NBR is extensively used in making gasoline hoses, lining for fuel storage tanks, in sheaths for use in oil fields and oil installations etc. PVC/NBR blends produced in a wide range of bright permanent colors are used in materials with good weathering resistance and in footwear soling [21-24].

1.1.1.1 Modified nitrile rubbers

(i) Carboxylated nitrile rubbers (XNBR)

The XNBR rubbers contain randomly placed carboxyl groups that are derived from metacrylate acid or acrylate acid. The XNBR has better abrasion resistance, hardness and tensile strength. It also has better low temperature brittleness and better retention of physical properties after hot-oil and air ageing compared to NBR [25].

(ii) Hydrogenated nitrile-butadiene rubber (HNBR)

The nitrile rubber can also be improved by (partially) saturating the double bonds in main chain butadiene by catalytic hydrogenation. This kind of NBR, HNBR, has been developed to resist better aging in oil and hot air. It shows better high tensile strength, weather resistant than NBR. HNBR is mainly used in vehicle tubing, seals, cables and profiles [26].

The most important invention that regulated the development of rubber technology during industrial revolution is made by Goodyear in 1840. The rubber materials may not have any technical utility if its molecules are not crosslinked. The process of vulcanization gave structural integrity by converting the plastic properties of raw rubber into elastic properties. Vulcanization imparts dimensional stability, strength, and resilience due to the formation of chemical bonds between adjacent elastomer chains.

However, none of the commercially available elastomers even in vulcanized state do exhibit satisfactory strength and performance for the divergent requirements of various products. For the last few decades, it is realized that synthesis of new elastomers are not always necessary for application requiring specific properties but can be bring about by the

i) Chemical modification of existing polymers

ii) Impregnations of fillers

iii) Blending of suitable elastomers.

1.2 Chemical modification of rubber

The prime objective of chemical modification is, altering of the structure and optimizing the physical and chemical properties of macromolecules which depend on the nature of parent rubber and its intended application. Chemical reactions on unsaturated polymers are of particular interest because the olefinic group not only react directly with a multitude of other functional groups but also can activate alternate sites of reaction. For convenience, the modification reactions can be divided in to three categories viz (i) structural modification of polymer chains (ii) bond rearrangement without introduction of new chemical group like isomerised rubber (iii) chemical combination with different polymers resulting in the graft copolymer or block copolymer [27, 28].

1.2.1 Structural modification or attachment of pendant group

The introduction of specific functional groups to rubber surfaces usually involves ionic or polar organic chemical reactions. For that the surface of rubber must contain sites that are vulnerable to electrophilic or nucleophilic attack such as double bonds, halogens, hydroxyl groups etc. Some important chemical functionalization reactions are

1.2.1. a Hydrogenation

Hydrogenation is one of the most familiar modifications that have been continuously studied because of the stability of hydrogenated products than their unsaturated precursors. The reaction can be employed by both catalytic (homogeneous and heterogeneous) and non catalytic methods depending on selectivity, yield, catalytic poison etc [29-31]. In homogeneous catalysis generally Ziegler type (a combination of organo transition metal like Co or Ni, a reducing agent (R_3Al or n- BuLi) and an activator like cyclohexene) catalysts were used while recently rhodium catalysts such as $(PPh_3)RhCl$ and $(PPh)_3$ RhHCO have been used. It was reported that high yields of saturated product have been obtained by homogeneous catalysis. In the non catalytic methods diimide reduction [32] or boranes [33] are used in which former one is more convenient for laboratory scale work. Hydrogenated rubber is a colourless, transparent, elastic waxy solid which on stretching form threads as reported by Singha *et al*. [34]. A tough

rubbery polymer similar to ethylene propylene rubber is obtained by the hydrogenation NR with triisobutyl borane. Depolymerisation and cyclisation occurred when NR hydrogenated with diimide. Due to its insulation properties hydrogenated rubbers are widely used in cable industry. A ‘‘green’’ strategy that is direct hydrogenation of NBR in its aqueous form (i.e. NBR latex) was introduced by Liu *et al.* using two water-soluble rhodium based catalysts, $RhCl(TPPMS)_3$ (TPPMS = monosulfonated triphenylphosphane) and $RhCl(TPPTS)_3$ (TPPTS = trisulfonated triphenylphosphane) [35, 36].

1.2.1.b Halogenation

The extensive research on halogenations of unsaturated rubber is performed due to the considerable interest in terms of chemistry and applications. The chemistry of halogenation is complex which involves addition, substitution, cyclisation, crosslinking and degradation. Chlorination can be done by passing chlorine in to rubber dissolved in a chlorinated solvent or by direct chlorination of rubber latex or solvent-swollen rubber film or by halogen carrying reagents. It has been reported that the dicyclopentadiene termonomer containing EPDM on chlorination form reactive allylic chloride which improve the addition and cure characteristic of the rubber. Though limited works have been reported, it is found that bromination leads to desirable properties than those of the chlorinated counter parts. The acquisition of polar side groups endows the material with increased compatibility with

the adhesion to hydrophilic substrates such as paper and natural fiber. Chlorinated NR has been used in the preparation of heat and chemical resistant paints and is applied to protect wood steel, walls etc and in the paints of road traffic signals [37, 38].

1.2.1. c Hydrohalogenation

The formation of respective rubber hydrochloride, hydrobromide, hydroiodide or hydrofluoride of unsaturated rubbers on reaction with HCl, HBr, HI or HF according to Markovnikov's rule with a small amount of concomitant cyclisation. Bunn and Garner established the structure of rubber hydrochloride. The reaction can also be done by passing HCl through NR dissolved in chloroform, reported by Weber [39]. Harris and Hinrichsen *et al*. [40, 41] studied the HBr addition while HF addition was reported by Tom [42]. The most feasible and cheap reaction is with HCl while rubber bromides formed are unstable. Hydro fluorination reaction is accompanied with cyclisation which can be avoided by selecting appropriate temperature and suitable solvent. Since hydrohalogenation occurs at double bond, the reactivity of rubber become reduced which in-turn increase the oxygen and ozone resistance. The hydro chlorinated 1, 4-polyisoprene give a tough flexible film useful in packaging.

1.2.1. d Epoxidation

Epoxidation is one of the typical modification reactions which results in significant changes in the physical and mechanical

properties. The reaction was first reported by Pummerer and Burkard [43] and later developed by Rouse *et al*. [44]. It involves the transformation of double bond to structures containing oxirane rings under the effect of peroxides and peracids. The inductive effect of newly formed epoxy group decreases the rate of reaction with conversion. Epoxidised NR vulcanizates have improved abrasion resistance, resistance to hydrocarbon solvents, wet traction and high damping performance [45, 46]. The heat stability, solvent resistance and adhesive strength of poly butadiene rubber were greatly improved by epoxidation. Epoxidised EPDM has been used as a viscosity index improver in motor oils. [47].

1.2.1.e Carbene addition

The dihalocarbenes addition to polydienes greatly affects its properties such as viscosity, flow activation energy, refractive index and glass transition temperature which increase with increase in chlorine content. The use of phase transfer catalyst like quaternary ammonium salts facilitate the reaction by enhancing the contact between aqueous reagents with the organic phase containing the polymer. When the NR in dilute aromatic solvent is reacted with dichlorocarbene prepared in-situ from ethyltrichloro acetate with sodium methylate, the double bonds are converted into gem dichloro cyclopropane ring and give a white powder. Similar reactions are also observed with dibromocarbene. It is reported that the dichloro carbene modification of SBR markedly improved its

flame, oil and solvent resistance along with mechanical properties [48].

1.2.1.f Hydrosilylation

The silyl groups can be incorporated in to the unsaturated elastomer by either hydrosilylation or by addition of vinyl silanes. Hydrosilylated rubber shows better heat resistance, improved adhesion to metals, silicates, glass fibers etc. These groups are of great interest as reactive substrates for grafting. Vinylic polymeric structures are more susceptible to silylation reaction and can give 100% yield.

1.2.1.g ENPCAF modification

Ethyl-N-phenylcarbamoylazofonnate (ENPCAF) modification can be carried out in an intermix or mixing mill on dry rubber at 110^0C. Using deammoniated latex, the reaction can also be carried out at 30°C. The ENPCAF modification results in the formation of hydroester pendant groups which increase the glass transition and damping properties of rubber. The modification shows how the physical properties are influenced by polar pendant groups. ENPCAF modified rubber also have the improved gas permeability and solvent resistance.

1.2.1. h Maleic derivatives

Maleic anhydride modification of NR accelerated by benzoyl peroxide was first reported by Bacon and Farmer [49]. The

modification not only provides polarity for non polar rubber but the succinic anhydride group provided can act as site for subsequent functionalization. The technique leads to attachment of single maleic anhydride (MAH) unit at relatively low temperature. The radical nature of reaction makes significant side reactions such as crosslinking and gel formation. Diels-Alder reaction of butyl rubber with maleic anhydride has also been described, which results in addition of 1-2 mol% succinic anhydride units. The Infrared studies of maleic anhydride modification of poly isoprene indicate that there is neither loss of any unsaturation nor any change in the cis-trans ratio.

1.2.2 Bond rearrangement reactions

It includes isomerisation and cyclisation reactions.

Isomerisation of unsaturated macromolecule was first reported by Goulb by converting cis-1, 4-polybutadiene to trans-l,4-polybutadiene with a consequent increase in crystallinity [50]. It can be done by thermal, catalytic, photolytic and irradiative methods. Selenium, NO_2, SO_2 and butadiene sulphone are effective isomerisation agents. NR in thin films, sheets or crumbs undergo isomerisation on heating with SO_2 above 100°C. In all reaction we get 45% cis content.

The oldest known cyclisation modification of NR was reported by Bedford and Wilkinson [51]. The cyclisation reaction of various isoprene butadiene polymers were reported which yield

hard resinous products of commercial importance. This modification can be achieved by thermal, chemical radiation or photochemical activation. Cyclised rubbers have been used as a stiffening agent because it provides stiffness to diene rubber vulcanizates. The cyclised rubber finds application in paints, shoe soles, industrial rollers etc.

1.2.3 Chemical combination with different polymers

Chemical combination of polymers involves the covalent attachment of polymer chains to a polymer substrate. It can be achieved either through graft polymerization or polymer grafting. Graft polymerization is the synthesis of polymer chains from monomer by initiating chain growth directly from reactive sites in the substrate surface. In polymer grafting, the previously synthesized polymer chains are attached to the surface of substrate polymer. Generally, it is based on free radical reaction of vinyl or acrylic monomers. The commonly used monomers for grafting on to NR are methylmethacrylate (MMA), styrene and acrylonitrile [52, 53]. The unpaired electrons can be generated on the substrate surface either by initiators such as UV-photoinitiators, thermoinitiators, such as organic peroxides such as benzophenone and other phenones by bombarding it with high-energy radiation, such as γ-irradiation [54]. The graft polymerization takes place when the vinyl or acrylic monomers, present in the vapor phase or in solution. Methyl methacrylate graft natural rubber, commercially known under trade name Hevaplus MG, is used as a stiffening

agent. In automobile industry it is used in light shield, soft fronts, rear ends, rubbing strips and bumpers. The impact resistant thermo plastic graft polymers in methyl methacrylate of the type acrylonitrile butadiene styrene copolymer (ABS) are used in applications requiring transparent, tough and thermally foamable materials. Recently, Subramaniam *et al*. reported NR latex/ vinyl neodeaconates graft polymer with the formation of a relatively homogeneous semi interpenetrating network or graft mic:rophase [55]. It was reported that non polar EPDM can be blended with polar rubbers by using a graft copolymer as compatibilizer. NBR/EPDM and chloroprene/EPDM blends were compatibilised in presence of EPDM grafted with poly(acrylo-nitrile) and or poly (acrylic acid) [56]. EPDM grafted with maleic anhydride (MAH-g-EPDM) act as good compatibilizer for NR/EPDM blend while Poly (acrylonitrile-co-methyl methacrylate-costyrene) was successfully used as a compatibilizer for NBR/EPDM blend and for chloroprene rubber (CR)/EPDM rubber blends [57]. Botros and Tawfic was studied bromobutyl rubber (BIIR) to improve the compatibility of the EPDM/NBR blends [58]. Block polymers are considered to be simple type of graft copolymer in which the graft chain is attached to the end backbone unit.

1.3 Composites

Recently, the word “composites” is used in various scientific fields, mainly in materials science and engineering. In general, it is the deliberate combination of two or more materials in

a predetermined geometry and scale which complement each other to have new functions or multifunction that the original materials did not possess [59]. Basically composites consist of two distinct constituents or phases in which one is continuous called matrix and the other one is discontinuous reinforcement or filler. Matrix gives the composites their structural integrity and it transmits externally applied loads to the reinforcement via shear stresses at the interface while the reinforcement offers stiffness and strength for the material. Since the end of the last century, the novel design developments have led to the growing popularity of hybrid materials where there is merging of the physical and/or chemical characteristics of individual materials to allow the superposition of their properties.

From the time this concept was first introduced, the development of polymer composites is rapidly emerging as a multidisciplinary research activity whose results could broaden the ever expanding applications of it to the great benefit of many different industries. The fiber reinforced plastic (FRP) developed in the 1940's was the first polymer composite, used for military applications. The widespread acceptance of polymer matrix composite over ceramic and metallic composites is easy processability, lower service temperature and their worth as weight-saving materials characteristics. In polymer systems, the composites can be described either as; (i) homopolymer composite; components in which the filler is embedded in a single matrix or

(ii) Blend composite; the fillers mixed in a combination of different matrices. Fillers added to the vulcanizates are usually cheaper than the polymers in which they are used and can modify the processing performance of gum matrix. However, the enhancement in the properties are achieved at the expense of optical clarity and often increased component weight, due to the higher loading (> 10% by weight) of the filler. The particle size, surface area, shape, and surface activity of the filler directly influence the properties of composite. According to the nature of the product, the fillers are classified in to different groups and the filler classification is summarized in the following scheme

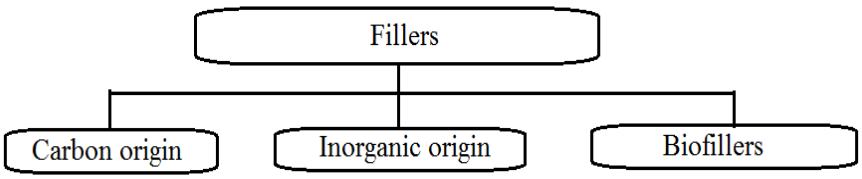

1.3.1 Nanocomposites

Recently, a new class of material has found application as filler in polymer composites namely nanofiller which have at least one dimension in the nano range i.e., 10^{-9} m. Among various fillers available, nanomaterials promote an intimate contact with the matrix phase due to high aspect ratio; extraordinary high surface area provide more contact areas for the filler with the matrix. Thus the class of the composite with one of the phase in nanometer range is considered to be an exciting route for creating innovative

materials with low cost and better physico-mechanical properties [60, 61]. Based on the matrix used nanocomposites are grouped in to ceramic matrix composites, metal matrix composites and polymer matrix composites out of which polymer matrix composites got ample attention over the other two.

1.3.1.1 Polymer matrix nanocomposites

The potential applications of the nanomaterials have been fully exploited by using conventional polymers as one of the component of the nanocomposite to endow them with good processability. In 1990, Toyota used nylon – nanoclay composites in their automobile by in-situ polymerization method which was the earliest application of nanofiller in polymeric material [62]. Compared to the pristine polymers or traditionally micro filled composites, there is remarkable improvements in characteristic properties of nanocomposites which include higher modulus, increased strength and heat resistance and decreased gas permeability and flammability due to the efficient reinforcement without loss of ductility. It is reported that the fine size alone cannot guarantee good reinforcement as fine particles tend to form agglomerates. The properties, synergistically derived from both polymer and the filler are really depending on the degree of dispersion and distribution of nanofillers without affecting the particle size so that the number of possible interaction between the components will increase which in-turn determine the final properties of the materials. These made polymer- nanocomposites

as ideal candidates for a broad range of applications ranging from strong, heat resistant automotive components to high-barrier packaging materials, optical, medical, aerospace and electronic devices. Early research, the property modification of polymer nanocomposites was mainly focused on development of nanoclay filled thermoplastic systems. Subsequently, research diversified into other polymer systems like thermosets and elastomers and many kinds of fillers like nano silica particles, carbon black, carbon nanotube and graphitic particles are incorporated for their effective reinforcement **[**63-70**]**.

1.3.1.2 Rubber based nanocomposites

Elastomers are very promising polymeric matrices for the preparation of nanocomposites because it retain large strain resilient behavior and large strain-to break. Nano-filler reinforcement provides fabrication of stronger, lighter weight due to low filler loading and less expensive due to fewer amounts of filler composites having better processability with increased toughness and fracture resistance. In nanocomposites, a stronger filler/matrix interaction at the interface exists which leads to a more immobilized rubber shell compared with filler particles of micro dimensions. The properties and performance of the elastomeric nanocomposites depend on the structure of the rubber matrix, nature of nanofillers, the degree of filler dispersion in the rubber matrix, the cross linking chemistry of rubber, the physical and chemical interaction of the fillers with the rubber matrix, and the

methods by which they are prepared [71]. There are several methods for the fabrication of elastomer based nanocomposites such as intercalation method, in situ polymerization, sol gel method and direct mixing of rubber and nanofiller. Each method has its own advantage and limitation. Generally, solution mixing technique is used for latex blending, where a polymer is dissolved in a suitable solvent along with nanofiller followed by evaporation of solvent to obtain the nanocomposite. However, for bulk production dissolution of elastomer in the solvent and subsequent removal of it pose environmental problems and engineering difficulties. In the case of rubbers that are available in latex form nanocomposites are prepared by mixing of latex and nanofiller followed by coagulation and drying. Hermann *et al*. described a two step mixing in an internal mixer followed by addition of curative on a two roll mill for preparation of elastomer – layered silicate nanocomposites [72].

The chemical compatibility between the elastomer and the filler greatly depend on the type of nanofiller used and the interaction of active sites on the filler surface with the polymer matrix. The presence of carboxyl and other functional groups in its particles, carbon black promotes an intimate contact with elastomers while less affinity and surface activity of non black fillers can be compensated to an extent by using certain surface treatments. The popularly studied nano fillers include clay

nanoparticles, carbon nanotubes, carbon black, and carbon nanofibers, etc.

1.3.1.2.a. Carbon black and nanotube reinforced rubber nanocomposites

Carbon black (CB) is the oldest most extensively used reinforcing filler which can improve mechanical strength abrasion, and wear characteristics. The carbon black filled NBR composites prepared by Lee *et al*. showed the close relation between the microstructure of elastomer and the curing characteristics and mechanical properties of the composite [73]. Sumio Iijima first discovered multiwalled carbon nanotubes (MWNTs) in 1991 by the arc-discharge method. A few years later, he observed single wall carbon nanotubes (SWNTs), which were long, slender fullerenes with hexagonal carbon (graphite structure) tube walls that were often capped at either end [74, 75]. Carbon nanotubes (CNTs) are excellent candidate as reinforcement for polymer matrix composites due to high aspect ratio in combination with exceptionally high strength low density and stiffness. Yue *et al*. [76] studied the effect of CNT on HNBR and silicone rubber and found that mechanical properties of composites increased with increasing of the content of CNTs in HNBR rubber. The effect of CNT in NR rubber composites was investigated by Manchado *et al*. [77]. They found that both carbon black and SWNT increases the modulus of the NR nanocomposite due to the hydrodynamic reinforcement upon introducing the filler. The fracture toughness of

epoxy resins had significantly improved on mixing it with double-wall carbon nanotubes and carbon black; reported by Gojny *et al*. [78]. The effect of addition of nano graphite fillers in NBR using liquid NBR as dispersion media was investigated by Rajkumar *et al*. [79]. Improved mechanical and functional properties of elastomer/graphite nanocomposites prepared by NBR latex compounding were reported by Yang *et al.* [80]. Yaragalla *et al*. studied the effect of interaction between epoxidised natural rubber and thermally reduced grapheme oxide on the barrier and dielectric properties [81]. Graphene filled natural rubber prepared by Zhan *et al.* achieved consistent improvement in the electrical and mechanical properties [82].

1.3.1.2.b. Nanoclays reinforced rubber nanocomposites

The low cost inorganic material; clays are commonly used in various industrial, engineering and scientific fields as catalysts, discolorations agents and adsorbents. Polymer clay nanocomposites have acclaimed wide appreciation because of their high surface to volume ratio, good reinforcing property, wide availability and non-toxic nature. The most widely used clays for designing high-performance polymer nanocomposites include natural and synthetic montmorillonite, hectorite, kaolinite, saponite, laponite, sepiolite, layered double hydroxide, halloysite nanotube etc. Among them montmorillonite clay is the most widely studied due to high aspect ratio and large surface area which impart good polymer filler interactions, leading to the improvements in physical properties,

such as tensile strength and modulus, gas permeability, lower coefficient of thermal expansion without changing the optical homogeneity of the material**.** In the open literatures, polymer clay nanocomposites are of three types, namely intercalated, flocculated and exfoliated. Among them, the greatest reinforcement is showed by the completely exfoliated nanocomposites. Clay particles in their pristine form are hydrophilic in nature so that surface treatment and modification of are compulsory to improve the compatibility between them and the hydrophobic polymer matrix. The most common way to overcome the immiscibility of clay with the matrix is by treating clays with surfactants; quarternized ammonium or phosphonium cations. The rubber clay nanocomposite can be prepared by in-situ polymerization, intercalation of rubber via solution blending, direct melt intercalation method and or intercalation of rubber via latex compounding. Natural rubber reinforced with organic-modified layered silicate reinforcement with a fully exfoliated structure was reported by many authors. Many authors investigated NBR/organoclay nanocomposites. It was reported that NBR containing 10 phr organoclay exhibit reduction in the relative vapor permeability for water and methanol up to 85% and 42%, respectively, compared to the neat matrix. Toyota group synthesized intercalated NBR-clay nanocomposites (4% clay by volume) which had hydrogen and water vapor permeability 30% lower than pure rubber [83]. Silica reinforced EPDM find versatile applications for case-bonded solid rocket motors inclusive as a

thermal insulator [84]. The dispersion of impermeable O-MMT with a planar orientation in EPDM/O-MMT nanocomposites prepared by melt compounding with EPDM-g- MAH, leads to improved solvent and thermal resistance and gas barrier properties [85]. The partially intercalated and exfoliated 10 phr OMMTs in low temperature grade HNBR prepared by thermal mixing has significant improvement in properties to satisfy engineering applications [86]. Sadhu and Bhowmick studied a series of nanocomposites acrylonitrile–butadiene rubber, SBR, and BR with Na-montmorillonite and stearyl amine modified montmorillonite and showed improved mechanical properties which depend on the nature of the base rubber and its polarity [87].

1.3.1.2.c. Inorganic nanoparticles reinforced rubber nanocomposites

Rubber matrices reinforced with modified inorganic nanoparticles combine the the unique features of the inorganic nanoparticles after appropriate treatments with the low weight and easy formability of rubber can lead to improvements in several areas such as optical, mechanical, electrical, magnetic, rheological, and fire retardancy properties. Selection of the correct nanoparticle including metals (e.g., Al, Fe, Au, and Ag), metal oxides (e.g., ZnO, $CaCO_3$, and TiO_2), non-metal oxides (e.g., SiO_2) and others (e.g., SiC) depends on the desired thermal, mechanical, and electrical properties of the resulting nanocomposites. Also, calcium carbonate ($CaCO_3$) particles polymer composites are selected

because of their low cost, magnesium hydroxide, is known as an efficient flame retardant, Fe_2O_3 nanoparticles can be used for their high magnetic properties [88]**.** Nanometal oxides reinforced rubbers become popular every day for their better chemical, electrical, and optical properties due to the improved mechanical strength as well as flexibility in design [89]. Sahoo *et al*. [90] prepared natural rubber composite with nano ZnO and evaluated dispersion degree of it in comparison with that containing the conventional rubber grade ZnO. Nano ZnO presents a more uniform dispersion. The better nanoparticle dispersion is achieved by introducing specific organic groups at the inorganic particles, which are able to interact with the organic polymeric matrix. Kalaee *et al*. compared the morphology thermal degradation and dynamic mechanical properties of EPDM with nano ZnO and ordinary ZnO and found that the nano filler considerably increased the final performance [91]. Kofod *et al*. [92] have developed hydrogenated styrene-b-butadiene block copolymer / TiO_2 nanocomposite for dielectric actuators. Lin *et al*. [93] blended two kinds of TiO_2 nanoparticles in NR or NBR using two roll milling and concluded that all nanocomposites have good antimicrobial ability. Ong *et al*. [94] produced NBR latex composite with a mixture of Fe_3O_4 magnetite and γ-Fe_2O_3 magnetite; the film with improved thermal stability and good magnetic properties was formed. Jasna *et al.* synthesized nanocomposites of chlorinated SBR and manganous tengstate with enhanced processability, mechanical, electrical and barrier properties [95]. Ramesan *et al.*

studied the reinforcement of NBR with nano ZnS and reported that mechanical properties such as tensile and tear strength increases with increase in concentration of ZnS up to 7 phr of loading [96].

1.3.1.2.d. Ceramic reinforced Rubber Nanocomposites

Development of the composite materials for high frequency applications such as mobile electronic devices, stationary power systems, hybrid electric vehicles etc requires the unique combination of dielectric and mechanical properties. Organic based elastomer materials are easy to process into mechanically strong components due to higher breakdown strengths but generally suffer from a low dielectric constant while typical high dielectric materials like ceramics are brittle and have poor mechanical strength because they require high sintering temperature. The ideal solution would be a high dielectric material is combined with polymer materials that are mechanically robust and processable at ambient temperatures which may combine desired properties of the components. [97, 98]. The ferroelectric ceramic particles are more important due to functional or self tunable properties which can be disclosed to the composite structure. Ferrites like strontium ferrite ($SrFe_{12}O_{19}$) and barium ferrite ($BaFe_{12}O_{19}$) are best magnetic materials because they are inexpensive, stable and have a wide range of technological applications [99-101]. The magnetic and dynamic mechanical properties of barium ferrite-natural rubber composites were studied by Makled *et al* and reported that the properties are highly influenced by size, shape and volume fraction of ferrite particles [102]. Recently, the use of Al_2O_3 nanoparticles

has been used in rubber formulation to impart the desired reinforcement, electric breakdown resistance thermal conductivity and to improve electrical and dielectric properties [103]. A 'Switch' type polarization response was found to be offered by the epoxy resin- ceramic $BaTiO_3$ composites with low or moderate filler content [104].

Hydroxyapatite ($Ca_{10}(PO_4)_6(OH)_2$, HA), a natural composite of calcium phosphate crystals in a collagenous matrix, is the emerging and most promising bioceramic material for biomedical applications in orthopedics and dentistry. HA has been extensively used in medicine for implant fabrication due to the good bone binding ability and bone regeneration which is attributed to its structural similarity to the mineral component found in hard tissue [105]. Additionally, the porous nature promotes much faster tissue growth. However, due to low mechanical reliability it cannot be used for heavy load-bearing applications specifically in aqueous environments [106,107]. Thus, generally HA act as biocompatible phase reinforcement in composites, coatings on metal implants and granular fill for direct incorporation into human tissues and coatings on metal implants. Many efforts have been made to prepare HA nanocomposites based on polymers such as polylactic acid [108, 109], collagen [110], chitosan [111], polyethylene [112,113] etc. HA filled PLLA (HAP/PLLA) composites are proposed to be suitable for bone tissue engineering applications because the scaffold is comparable with cancellous bone in terms of microstructure and mechanical strength. Multi-walled carbon nanotubes (CNTs)/ HA composite have potential applications in the

field of coating materials for metal implants under high load-bearing conditions. The thermal degradation and flame retardancy studies on polycarbonate/ hydroxyapatite (PC/HAP) composite with different HA content concluded significant improvement even with a low content of HA in PC matrix. In addition to excellent affinity to biomaterials, the surface-OH groups adsorb CO_2, NO_x, H_2O etc. Under UV (254 nm) irradiation, the oxidative decomposition of odor compounds such as methyl mercaptane (MM) and dimethyl sulfide (DMS) occurred effectively on HA [114]. The systematic study on CO_2 gas sensing of HA thick film revealed that it can act as an excellent sensor at relatively lower operating temperature (165^0C) as compared to CO2 gas sensors available in the market today [115]. The nanocrystals of titanium-substituted hydroxyapatite (CTHAp) shows good photo catalytic activity, examined by using decomposition of methylene blue (MB) under visible light and UV irradiation [116].

1.4 Polymer Blends

None of the commercially available elastomers satisfy the divergent requirements in terms of processing characteristics, durability and cost for the growing needs of polymer industry. Therefore, in order to attain desirable technical compromise it is to pre design material systems leading to unique combinations of properties in an economic way which can be done by blending between two or more rubbers. The blends for precise application depend on both the chemical composition and configuration of each component [117].

The basic classification of polymer blends is illustrated as

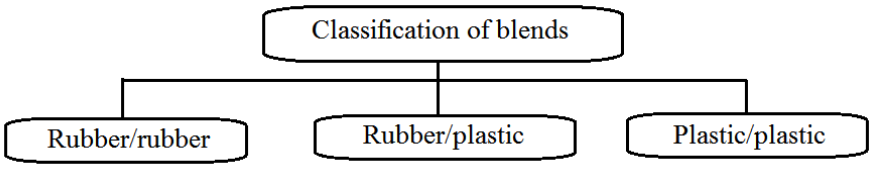

Figure 1.1 Classification of blends

The major factors that affect the properties of elastomer based blend include interfacial adhesion/crosslinking, morphology, compatibility or miscibility between constituents and the blend ratio. The level of homogeneity obtained depends on the nature of the components and the blending technique employed. The major blending techniques include

1.4.1. a Mechanical Blending

Mechanical blending can be done by melt blending of constituent rubbers using an open two-roll mixing mill, kneader or Banbury mixer. In the open mill blending process mixing is carried out between two contrary rotors. The pressure due to variation in tangential speed and nip constriction increases the displacement energy to break the bonding between rubber molecules. The high heat input, necessary to maintain a low melt viscosity and the high shearing rates needed for thorough blending may leads to the formation of block and graft copolymer structures due to some degree of chain branching or chain extension. However, the effectiveness of mixing in these techniques depends on the

protection against dust, the operator's skill as well as the quality of components.

Kneader is an internal mixing mill where the rolls are enclosed in a chamber provided with consecutive projections over the surface to generate a cutting effect which is heated to a high temperature (around 100^{o}C) to facilitate uniform mixing.

Banbury internal mixing mill is sophisticated processing equipment capable of mixing thick, viscous and tough materials in a very short span of time (5-6 minutes). The enclosed mixing chamber contain opposing spiral-shaped rotors operate a hopper to receive the feed, and a hydraulically operated discharge door. Mixing in a Banbury mixer is impressively rapid and efficient. However, it is critical to have exactly the right volume of the melt.

1.4.1. b. Chemical and Mechano-Chemical Blending

In this technique long monomeric sequences of one kind are chemically linked to similar long monomeric sequences of a different kind in either the axial direction or in the cross direction giving block copolymer or graft copolymer structures respectively. The mutual grafting, or intercross linking due to the selective or random crosslinking of mechanical blends generate mechano-chemical blends.

1.4.1.c Solution Blending

This is a very useful technique for preparing extremely viscous blends in which selected diluents are used to dissolve the

component polymers. The morphology of the resultant polymer blend strongly depends on the reaction temperature, nature of solvent and concentration. The main limitation of this technique is the availability of a suitable common solvent for all the components to be blended.

1.4.1. d. Latex Blending

Latex blending is a promising technique for emulsion polymerization of rubber toughened plastic blends in which the components are present as suspended, stabilized microspheres of a specific size distribution. The stabilizers present in the medium prevent the interactions between the neighboring particles. The excellent distribution of different phases due to the absence of water contents and processing of micro-sized constituents is the advantage of this technique.

The additivity of properties is the most important concept in the preparation polymer blends. That means when an elastomer is mixed with another one, the resulting blend has a property which is the weighted average of the properties of the individual components. However, the additivity relationship of the blends will be sensitive to its morphology. The blend properties with composition can be described by the following equation:

$$P=P_1C_1+P_2C_2+IP_1P_2$$

where P_1 and P_2 are the properties of the individual components, C_l and C_2 are their respective concentrations and I is the interaction parameter which can be positive, zero or negative;

positive value indicate the property is synergistic, zero indicate the property is additive and when I is negative the property is nonsynergistic [118] .

A lot of reports by various researchers are present in literature for different types of possible blends particularly used in automobile and household appliances and their optimum properties. Xu *et al*. [119] have prepared highly toughened poly-(vinylidene fluoride)/nitrile butadiene rubber (PVDF/NBR) blends with Izod-impact strength of 6-7 times higher than pure PVDF via peroxide-induced dynamic vulcanization. Manshaie *et al*. **[**120**]** reported NR/SBR blend, prepared via two roll mills and cured through irradiation, with increased tensile strength, hardness, thermal stability, and abrasion resistance. Maity and Xavier studied the rheological properties of Ethylene-propylene block copolymer/ EPDM rubber prepared via melt mixing [121]. The molecular transport of aromatic solvents in isotactic polypropylene/acrylonitrile-co-butadiene rubber blends was analyzed by George *et al***. [**122**].**

The goal of blending is to achieve a combination of the favorable properties from each component which will be governed by the intermolecular bonding force between the molecules of the homopolymers. When blending of suitably selected rubbers with either plastics or even another type of rubber with desirable properties are taken into consideration, the question of whether they are compatible is of particular importance as far as their various properties are considered. Some of these commercially

important elastomers are immiscible; the blending of these will leads to inferior mechanical properties due to weak interfacial adhesion. In such blend system there requires only the breaking of van der Waals bonds during fractures due to poor interface which will limit the stress-transfer across the phase boundaries.

The following figure shows idealized property combinations by the blending of two polymers, A and B.

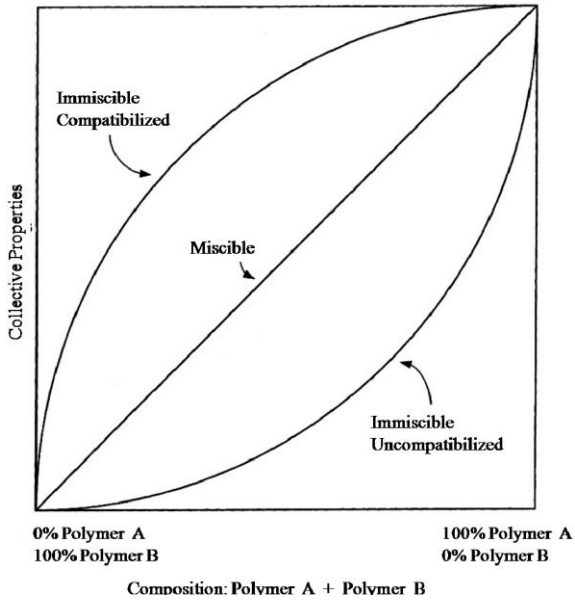

Therefore successful blending of incompatible elastomer systems that can be carried out to suit the requirement of both the producer and the user got ample research interest both in the academic and industrial fields.

1.4.2 Reinforcement of immiscible polymer blends

1.4.2. a Compatibilization

There are many reports on different strategies employed to increase the interfacial adhesion and to minimize the phase separation that includes the addition of physical or chemical compatibilizers. A compatibilizer is an additive intentionally added to immiscible blend system which resists gross phase segregation, provide stability of morphology and reduce the macroscopic inhomogeneities through interfacial tension between the components. Good interfacial adhesion enables efficient stress transfer from one phase to the other and prevents crack initiation for catastrophic failure. Generally, functionalized polymers and block or graft polymers can act as compatibilizers which has to penetrate deeply enough to be entangled with the constitutive chains and thus enhance interfacial adhesion in addition to reduction in the average size of the dispersed phase. For a polymer or copolymer to act as compatibilizer, that must have segments identical to component polymers and should have specific interaction with them.

The different techniques used for compatibilization include

i) Physical compatibilization

In physical or non-reactive compatibilization, pre-synthesized copolymers are added such a way that they could be

able to locate at the interface between the components so as to promote the adhesion between the phases. Lee and Chen prepared immiscible blends of poly vinyl chloride (PVC)/ EPDM with chlorinated poly ethylene (CPE) as a compatibilizer [123]. Schulze *et al*. reported the preparation of polypropylene (PP)/ polystyrene (PS) blends with highly efficient PP-g-PS as compatibilizer and found that the efficiency of the copolymer increases with short PS side than that with long PS side chains at comparable compositions [124]. Ramesan and Alex [125] examined dichlorocarbene modified SBR (DCSBR) as a compatibilizer in SBR/NBR blends and showed that the compatibilization effect was prominent for a system with higher proportions of NBR.

ii) Reactive compatibilization

In reactive compatibilization, a graft or a block copolymer is generated via in-situ chemical reaction during the development of immiscible blends. Reactive compatibilization is more efficient than physical compatibilization because the compatibilizer is formed directly at the interface. The functionalization can be done in a compounding extruder which can bring about reactions such as halogenations; sulphonation, hydro peroxide formation and in-situ formation of block and graft polymers. Ide and Hasegawa reported the formation of maleic anhydride grafted polypropylene (PP) in PP/PA-6 blend [126]. Soares *et al*. performed the reactive compatibilization of EVA/NBR blends have been performed using

partially hydrolyzed EVA in combination with oxazoline functionalized NBR [127].

Nowadays, a number of blends whose importance arises from the new desirable properties have been commercially exploited. Zhu and Chan studied morphology of PVC (50 wt %) / SBR (40 wt %) blend with 10 wt% of NBR as the compatibilizer with respect to the change in sulphur concentration and acrylonitrile content of NBR [128]. Intrinsic viscosity measurements and scanning electron microscopy revealed that EPDM/NBR blends compatibilised with maleated ethylene propylene diene monomer rubber (MAH-g-EPDM) showed improved morphology and compatibility [129]. Ismail *et al*. reported higher stabilization torque, mechanical energy, stress at peak and stress at 100% elongation but lower elongation at break and swelling index for maleic anhydride (MAH) compatibilised NBR/waste poly (vinylchloride) (PVCw) [130]. Setua and Gupta blended NBR with phenolic resin modified high-density polyethylene (HDPE) and studied on its thermal properties [131]. Microfibrillar blends were prepared from polypropylene and poly (ethylene terephthalate) and their thermal decomposition studies revealed that microfibrillar blends delay the degradation better than the microfibrillar composites; reported by Jayanarayanan *et al.* [132]. Botros and Abdel-Nour prepared blends of butyl rubber (IIR) with nitrile rubber (NBR) on a laboratory open mill with satisfactory thermal and oil resistance properties [133]. Khalaf *et*

al. fabricated high performance oil resistant rubber products based on NBR, PVC and CR blends to be utilized in automobiles industry [134]. The blend vulcanizates shows improved rheological, physical and mechanical characteristics.

1.4.2. b Role of nanoparticles in compatibility and miscibility of blends

The addition of certain nanoparticles has been noticed to be a new approach to modify interfacial properties of immiscible blends and therefore these are also termed as compatibilizers [135, 136]. The kinetic and thermodynamic effects, localization and transfer of particles are the major factors which are responsible for influencing the compatibilising mechanism in the filler reinforced elastomeric blends. The viscosity of matrix increases and reduces interfacial tension through compatibilization, structuration, and selective localization of nanofillers that offers the desired mechanical, thermal, and rheological properties. Blending components having a high filler wetting speed give a good localization of filler and its interaction with the corresponding blending components via relocalization of fillers within the blend. NR and its blends with polyurethane reinforced with layered silicates assists for significant reduction in permeant diffusion and therefore enhance the barrier properties of blended composites due to dispersion via exfoliation of fillers [137-139]. Chow *et al*. [140] blended PA6 having good mechanical strength with PP which has high moisture resistance and supports easy processability,

reinforced with 4 phr organoclay (organophilic modified montmorillonite) in presence of maleic anhydride grafted ethylene-propylene rubber (EPR-g-MA) as a compatibilizer. The blend showed decrease in melt flow index improvement in rheological properties and increase in strength and ductility. Magda [141] investigated the high abrasion furnace (HAF) carbon black filled NBR/EPDM (50/50) rubber blends with enhanced mechanical properties, swelling behaviour in oils, electrical properties and thermal behaviour. The effect of organoclay as an emulsifier in a polystyrene/poly(ethyl methacrylate) (PS/PEMA) blend was analyzed by Voulgaris and petridis [142]. Gelfer *et al*. [143] reported a huge reduction in domain size of PS/PMMA blends reinforced with organoclay as an emulsifier. Frounchi *et al*. were the first to investigate the improved gas barrier properties against oxygen and carbon dioxideof nanoclay reinforced PP/EPDM blends (50:50) via the solvent blending method [144]. Mottaghi *et al*. [145] studied the efficiency of nano-ZnO in increasing the cross-linking density of NR/BR and NR/SBR blends by using the swelling behavior technique. Mahmood *et al*. [146] showed the significant improvement in tensile modulus as well as tensile strength for multiwalled carbon nanotubes (MWCNTs) reinforced thermoplastic polyurethane-urea (TPUU)/carboxylated acrylonitrile butadiene rubber (XNBR) blend nanocomposites. It has been reported that the nano reinforcement can considerably reduce the percolation threshold in blend nanocomposites. Nair *et al*. [147] observed varying percolation mechanisms in each blend

composition PP and NR reinforced with CNTs. Stephen *et al*. [148] studied solvent resistant properties of layered silicates (sodium bentonite and sodium fluoro hectorite) filled NR/XSBR (carboxylated styrene butadiene rubber) blends through the equilibrium swelling method using benzene, toluene, and p-xylene as solvents. TiO_2 nanoparticles have been also used as a reinforcing agent for NR/EPDM blends in which nanoparticles are preferentially located inside the NR phase [149]. EPDM/NBR blend compatibilised with 10 phr PVC and loaded with different contents of silica (30–90 phr) was used for the production of automotive brake hoses, automotive radiator hoses, motor mounts, conveyor belts etc [150].

All materials attract interest on the basis of their property—processing-cost—performance relationships**.** To date, the recent attempts to incorporate rubber materials to industry-relevant polymer materials include the enhancement of biodegradability, flame retardancy, electrical and barrier properties in addition to good processability and mechanical properties of existing rubber materials.

1.5.1 Biodegradability

Recently, there has been an increase in the use of biopolymer-blended materials in composites because of the concerns about environmental waste problems and petroleum resource limitations. Thus new environmental regulations and

growing global environmental concerns have led to increased interest in developing polymers from renewable resources. The fully biodegradable polymers with hydrolysable backbones such as poly(caprolactone), poly(lactic acid) (PLA), poly(ethylene glycol), poly(hydroxyalkanoates) etc. are expensive and their abilities to be blown seem limited. The bio-based polymers which are directly extracted from biomass include NR, starch, chitosan etc.

Nanoclay such as montmorillonite (MMT) incorporated into an inert polymer as a potential ingredient play a vital role in the degradation of polymers since they are environmentally friendly, toxin-free and could be used for food packaging. The addition of nanoclay as filler into the polymer matrix also offers a reduction in raw material use, elimination of secondary processes, less complex structures and a reduction in machine cycle time. The positive environmental impact with respect to ultimate disposability forced researchers to enhance utilization of the polymeric materials in several applications via incorporation and blending of bio-based polymers. Mengjiao *et al*. reported that acrylonitrile butadiene rubber / MMT nanocomposite show excellent mechanical properties due to the interaction of MMT and polymer segments [151].

Composites reinforced with biofiber are finding tremendous applications in various fields for the production of biosustainable materials ranging from the construction industry to automotive industry**.** Abraham *et al.* [152] developed nanocomposite materials

based on NR latex and aqueous suspension of cellulose nanofibrils obtained from banana fiber. The permeability and diffusion coefficients of sorption processes of carbon dioxide, oxygen, methane, ethylene and propylene in films of vulcanized NR pure gum and with 15 phr and 30 phr of regenerated cellulose is found to be decrease with increasing pressure [153]. A nanocomposite of 75/25 NR / EPDM blend having ethylene content of 64.6 mol % (EP1) and 74.2 mol% (EP2) was mixed with 15 phr of nano cellulose, is also reported [154]. Transport studies of NR-thermoplastic polyurethane in aromatic solvents were studied by Minnath *et al*. [155].

1.5.2 Flexible electronics

In the last couple of decades electronic systems that can cover large areas on flexible substrates have received increasing attention because they enable classes of applications from space exploration to water purification, and from displays to conformally integrated automotive batteries. An emerging direction in research is to develop flexible electronics lie on a host of advantages such as low weight, mechanical flexibility and durability, low-cost, large area compatibility, and high scalability in addition to seamless heterogeneous integration.

Since the discovery of intrinsically conducting polymers, researchers have explored varying applications in thin film transistors, sensors, super capacitors, organic light emitting diodes,

electrochromic displays and organic solar cells due to their unusual electronic properties. The metallic properties of conducting polymers were first reported with the discovery of polyacetylene in 1977. The conjugated π-electron backbone is responsible for the conductivity which allows efficient transfer of electrons or positive charges along the backbone. It was reported that the conductivity arises only when the polymer is in oxidized state or from the delocalization of radical cation or polaron charge carriers formed by the loss of an electron, which are capable of both inter and intra chain transfer. Conducting polymers may be intrinsically conducting in which polymeric material itself conduct or extrinsically conducting in which a conductive material is embedded in a non conducting polymer. The most important challenge in application of this class of polymers include tailoring of properties such as appropriate processability, mechanical properties, electrical conductivity as well as acceptable biocompatibility. Some of these limitations had been overcome by the development of composites of conducting polymers with conducting nanoparticles along with non-conducting polymers. The polypyrrole (PPy) based nanocomposites with ZrO_2 and Fe_2O_3 showed increased dc conductivity to a large extent in addition to thermal and environmental stability [156,157]. The attractive magnetic behaviour of polyaniline (PAn) and PPy has been got a great deal of attention over the past few years. It has recently been reported by Tang et al that a super paramagnetic nanocomposite film based on PAn incorporated with ultrafine γ-Fe_2O_3

nanoparticles with appreciable electrical conductivity [158]. Cho *et al*. reported the fabrication of a dry type conducting polymer actuator using nitrile rubber (NBR) as the base material on which poly(3,4-ethylenedioxythiophene) (PEDOT), was synthesized by using a chemical oxidation polymerization technique, and room temperature ionic liquids (RTIL) were absorbed into the composite film [159].

Rubber/carbon black conductive composite materials are widely used for rubber contact switches, floor heating, electromagnetic interference shielding and various other electronic and electrical applications characterized by high flexibility, low density and in particular, specific structures that enable the formation of conductive network inside the polymer matrix at relatively low filler concentration, low cost, good physical and mechanical properties [160-162]. The effect of high abrasion furnace black (HAF), graphite and acetylenic carbon black on the electrical and mechanical properties of NBR composites were studied in which the conductivity of acetylenic carbon black is found to be 7 orders of magnitude higher than that of the filler-free NBR whereas NBR/HAF composites have the highest tensile strength [163]. The addition of carbon black in to EPDM/NR (75: 25) blend increased its dielectric permittivity ***E'*** and dielectric loss ***E"*** drastically in addition to the mechanical properties; reported by Ghoneim and Ismail [164]. Shin *et al*. identified several mobility-reducing factors such as polar functional groups, rough topography

and interface charges as a result of O_2 plasma treatment and aging of PMMA/Al_2O_3 gate dielectrics on the characteristics of field-effect transistors (FETs) [165]. In literature, it was compared the conductivity of styrene-butadiene rubber (SBR) nanocomposites containing graphene nanoparticles, thermally expanded graphene (TEG) and MWCNTs and found that SBR/MWCNTs nanocomposite had the lowest percolation threshold and highest conductivity [166]. Polyaniline coated cellulose nanofibrils incorporated natural rubber (NR) could meet the demands for antistatic applications. Polypyrrole, polyaniline, polythiophene and its derivatives such as poly(3,4-ethylenedioxythiophene) are considered as "smart" biomaterials and find applications in biosensors; coatings on conventional electrodes used in neural sensing and stimulation; electrically induced drug release and delivery systems; modulators of activities of nerve, cardiac, skeletal muscle, and bone cells; and in emerging technologies such as tissue engineering [167].

Praveen *et al*. also explained nano-unit'like microstructure formation in case of a clay loading of 10 phr along with 20 phr of CB in SBR nano-composite, resulting in dramatic improvement of technical properties [168]. Etika *et al*. put forward a theory based on haloing effect that involve stabilization of the nano clay platelets by surrounding CB particles [169]. This unique microstructures development ultimately influences the electrical and mechanical

properties of rubber nanocomposites having both carbon black and nano-clay as a filler system.

1.5.3 Flammability

The high flammability and insufficient thermal stability under specified exploitation conditions are the two major undesirable features of polymeric materials which depend on the chemical structure of polymer macromolecules, method of polymer cross-linking and composition of polymeric composites. From the point of view of flame retardancy, natural and synthetic organic polymers are combustible in a fire compared with ceramics or metals which is an important issue for producers and consumers. To enhance the intumescent flame retardancy of polymers, many attempts were done by the scientific community. In 1976, Unitika Ltd., Japan, first presented the potential flame retardant properties of PA6 /layered silicate nanocomposites. The barrier formation during combustion and increase of the melt viscosity are the two general mechanisms that can be found in all of the polymer nanocomposites with a significant impact of fire characteristics. Compared with NR, the fabricated NR/O-MMT (3 wt %) nanocomposite showed a delay in the ignition time with about 150%. The Limitting Oxygen Index (LOI) measurement proved both O-MMT and halloysite nanotubes (HNTs) decrease flammability of vulcanized SBR. The LOI value keeps increasing with the amount of aluminum hypophosphade (AlHPi), a class of phosphorous containing flame retardants, when added to EPDM/

nano silica composite. In a review, Feldman reported that the LOI value of pristine thermoplastic polyurethane (TPU)/NBR was significantly improved from 19.6% compared to the nanocomposites containing 1,3,5 and 8 wt% dodecyl sulfate intercalated Mg-Al based layer double hydroxide (DSLDH) nanofillers which had LOI values 20.7, 21.3, 22.1, and 23.9% respectively [170].

1.5.4 Oil and Solvent barrier properties

Some vibration isolators and dampers, particularly those used in automotive products, have contact with oils or solvents. The effect of a liquid on a particular rubber depends on the solubility parameters of the two materials. Elastomer nanocomposites with gas and liquid barrier properties have important applications in many traditional areas and new fields. The influence of polymer structure and its interactions with the penetrant molecules are the main features to be considered in the area of polymeric barrier materials. The well-established and most accepted mass transport model for the membrane separation processes is the solution-diffusion model. In this, a concentration gradient is established across some arbitrary reference section and the concentration difference or the chemical potential of the penetrant in the phases separated by the membrane is slowly tries to equalize by the transport process. Generally, the transport mechanism within the rubber matrix follows Fick's law and it mainly depend on the nature of matrix, nature of penetrants,

distribution of crosslinks, temperature, presence of fillers and plasticizers. As far as the rubber matrix is concerned the free volume, segmental mobility of the chains and the glass transition temperature has significant influence on its transport properties. Moreover, the transport properties of elastomer nanocomposites mainly depend on the filler dispersion and morphology, elastomer–filler interactions, geometry and intrinsic physical/chemical properties of the filler. There are three types of diffusion (i) Fickian diffusion, in which the rate of diffusion is much less than that of sorption and the sorption equilibrium is rapidly established. (ii) Non-Fickian diffusion process, in which the diffusion rate is very rapid compared with the sorption rate, therefore, sorption is the key step for the transfer process. (iii) Anomalous diffusion, which occurs when the diffusion rate and the sorption rate are comparable.

The transport behaviour of liquids through conventionally vulcanized natural rubber filled with high-abrasion furnace black and silica at the same loading was investigated by Unnikrishnan *et al*. [171]. It was found that the black-filled samples sorb a lesser amount of solvents under study than the silica loaded NR due to higher rubber filler interactions which can be explained in terms of the high bound rubber content and cross link density. The swelling and stress-strain data of SBR/NBR blends compatibilised with dichlorocarbene modified SBR (DCSBR) showed enhanced thermal and oil aging resistance; reported by Ramesan and

Rosamma Alex [125]. Mathai *et al.* [172] studied the effects of blend ratio, penetrant size and temperature on the transport properties of aromatic solvents through NBR/ENR blend membranes. Magda reported NBR/EPDM (50/50) rubber blends loaded with high abrasion furnace (HAF) carbon black which were subjected to gamma radiation doses up to 250 kGy to induce radiation vulcanization have attained considerable improvement in mechanical properties, swelling behaviour in oils, electrical properties and thermal behaviour compared to the unloaded sample [141].

Scope and objectives

Efforts are currently being carried out to develop innovative elastomeric materials from existing ones to achieve commercially viable products that range from common household goods to gate dielectrics in transistors, high-voltage insulation and capacitors in power electronics etc. Among the synthetic elastomers NBR and EPDM are two extensively studied rubbers having potential commercial applications.

As it is known NBR is a synthetic oil resistant rubber that has been the logical elastomer of choice for service in the oil seals and gas industry. However, its mechanical properties such as tensile and tear strength are poor and subject to degradation at high temperature, that limits their applications. Since the production temperatures logically increased when oil wells became deeper,

occasional field failures would surface due to excessive elastomer hardening which will lead to leaks and inoperative controls. It is highly susceptible to attack by atmospheric ozone, oxygen and heat like all unsaturated elastomers.

Many studies were conducted to improve the physical properties and especially the ageing resistance of NBR because in extractive media the high temperature ageing resistance is important for these rubbers where there often leaches out the antioxidants in the vulcanizates. The inclusion of various types of nanofillers in NBR has attracted ample attention due to large improvement in mechanical, thermal, and barrier properties. It is also reported that the more practically useful approach to improve the ageing resistance of NBR is by blending it with saturated rubbers like butyl rubber, EPDM etc without sacrificing nitrile rubber's oil resistance.

EPDM is familiar for its outdoor applications due to good physical properties such as high heat resistance, ozone resistance and cold and moisture resistance. The flexibility and outstanding weathering ability due to saturated polymer back bone make it suitable for automobile weather protection and water channeling application. The presences of double bonds which form crosslinks between two ethylene propylene chains are responsible for elasticity even at low temperature. However, EPDM has relatively poor surface chemical properties and hydrophobicity due to low

reactivity and inadequate compatibility with other polymers. Also, the EPDM vulcanizates are extremely swell in petroleum fuels.

The blending of NBR and EPDM rubber was performed to achieve the best properties from each component. This blend will expected to have excellent oil and fuel resistance, ozone resistance, heat resistance with desirable mechanical properties. The major problem with NBR/EPDM blend system is its inherent immiscibility due to the difference in chemical nature and viscosity. Many research groups have extensively investigated the effect of compatibilizers and fillers on the miscibility of these elastomers [173-175].

In general, the olefinic elastomers are very useful to scientist and engineers for applications requiring a combination of properties because they may be used as a base for a variety of chemical modification. In our group, there has been done a systematic study on dichlorocarbene modified SBR and its nanocomposites which showed excellent improvement in the ageing, fuel, oil and fire resistance while maintaining its comparatively good mechanical properties. The improvement in properties can be attributed to reduction in double bond and increase in the polarity in the molecule as a whole [176-179].

No systematic study has yet been carried out on the chemical modification of NBR and EPDM highlighting the structure-property relationships. Also, the nanocomposites based on

these elastomers with bioceramic materials making use of flexibility of elastomer and high dielectric constant of ceramics hardly been studied. Well aware of the situation, the present work focused on the development of chemically modified NBR and EPDM their nanocomposites, their blends & blend nanocomposites with hydroxyapatite nanoparticles. Also the characterization and vulcanization are carried out with special reference to mechanical, electrical and sorption studies.

The major objectives include

- Preparation and characterization of hydroxyapatite (HA) nanoparticles
- Development and characterization of NBR/HA and EPDM /HA rubber nanocomposites
- To study the thermal and electrical properties of rubber nanocomposites
- Preparation of chlorinated NBR and EPDM.
- Characterization of chlorinated elastomers by different techniques like ^{1}HNMR, FTIR and UV-visible spectroscopy, XRD, SEM,TGA and DSC
- To study the effect of chlorine content on vulcanization behaviour, oil and flame resistance, mechanical and electrical properties of chemically modified rubber.

- ❖ Development and characterization of chlorinated NBR/HA and chlorinated EPDM /HA rubber nanocomposites.
- ❖ To study the thermal, mechanical, electrical and oil diffusion properties of fabricated nanocomposites.
- ❖ To determine the transport properties of the nanocomposites by using aromatic and industrial solvents.
- ❖ Preparation, characterization and studies on mechanical, electrical and transport properties of the Cl-EPDM/Cl-NBR blend.
- ❖ Preparation, characterization and studies on mechanical, electrical and transport properties of the Cl-EPDM/Cl-NBR/HA blend composites.

2.1 Materials

2.1.1 Acrylonitrile butadiene rubber or Nitrile rubber (NBR)

Nitrile rubber is a copolymer of acrylonitrile and butadiene. The excellent resistance to a wide variety of non-polar oils, fats and solvents of NBR depend upon its acrylonitrile content. In the present study NBR having a molecular weight of $\overline{MW}=275000$ (acrylonitrile content of 18%) was procured from Synthetics and Chemicals Ltd, UP, India. The structure of NBR is as shown in **Scheme 2.1**

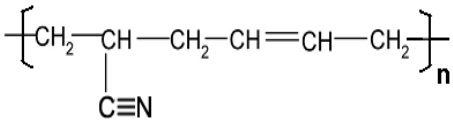

Scheme 2.1 Structure of NBR

2.1.2 Ethylene-propylene diene monomer rubber (EPDM)

EPDM is a nonpolar rubber which exhibits good heat stability, aging resistance and elasticity. It is a copolymer of ethylene, propylene and 3 to 9 percent of non-conjugated diene monomers (usually dicyclopentadiene, ethylidene nobornene, or 1, 4 hexadiene). The (EPDM)-502 with molecular weight of $\overline{MW}=296000$ was used for the present investigation was supplied by Herdillia Unimers Ltd., Bombay. Its structure is given in **Scheme 2.2**

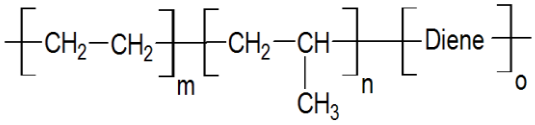

Scheme 2.2 Structure of EPDM

2.1.3 Chemicals and Solvents

The commercial grade dicumyl peroxide (DCP; 40 % active) is the vulcanizing agent used for crosslinking the matrix, purchased from local chemical suppliers. The other chemicals such as potassium permanganate ($KMnO_4$), concentrated hydrochloric acid (HCl), calcium chloride ($CaCl_2$), ammonium hydrogen phosphate ($(NH_4)_2HPO_4$), ammonium hydroxide (NH_4OH), chloroform ($CHCl_3$), sodium hydroxide (NaOH), ammonium thiocyanate (NH_4SCN), silver nitrate ($AgNO_3$) and isopropyl alcohol were of analytical grade obtained from Merck India, were used as received. The capping agent, cetyl trimethyl ammonium bromide (CTAB) was purchased from Himedia chemicals. Tetra butyl ammonium bromide (TBAB), used as the phase transfer catalyst, was also procured from Merck India. The petroleum fuels petrol, diesel and kerosene were obtained from Indian oil Corporation. **Table 2.1** sum up the physical properties of all the solvents used in the diffusion studies.

Table 2.1 Characteristic properties of solvents used

Solvents used	Characteristic properties	
Benzene	Molecular weight ($gmol^{-1}$)	78.11
	Density (gcm^{-3})	0.874
	Boiling point (°C)	80
	Solubility parameter $(cal\ cm^{-3})^{1/2}$	9.2
	Molar volume	89.17
Toluene	Molecular weight ($gmol^{-1}$)	92.14
	Density (gcm^{-3})	0.867
	Boiling point (°C)	109
	Solubility parameter $(cal\ cm^{-3})^{1/2}$	8.9
	Molar volume	105.90
Xylene	Molecular weight ($gmol^{-1}$)	106.17
	Density (gcm^{-3})	0.860
	Boiling point (°C)	138
	Solubility parameter $(cal\ cm^{-3})^{1/2}$	8.8
	Molar volume	123.45
Petrol	Molecular weight ($gmol^{-1}$)	80-100
	Density (gcm^{-3})	0.710-0.737
	Boiling point (°C)	70-150
Kerosene	Molecular weight ($gmol^{-1}$)	150-170
	Density (gcm^{-3})	0.810-1.817
	Boiling point (°C)	140-230
Diesel	Molecular weight ($gmol^{-1}$)	170-330
	Density (gcm^{-3})	0.82-0.95
	Boiling point (°C)	240-350

The ASTM reference oils, ASTM #1, 2 and 3 (IRM 901, IRM 902 and IRM 903), purchased from Calumet Lubricants

Company, were of commercial grade and used as received. The characteristic properties of oils used are given in **table 2.2**.

Table 2.2 Characteristics of oils

Property	ASTM 1	ASTM 2	ASTM 3	ASTM methods
Aniline point (°C)	124±1	93±3	70±1	D 611
Viscosity – gravity constant	0.790-0.805	0.860-0.870	0.875-0.885	D 2140
Refractive index	1.4848	1.5105	1.5026	D 1747
Aromatics (C_A %)	3	12	14	D 2140

2.2 Methodology

2.2.1 Synthesis of hydroxyapatite (HA) nanoparticles

Hydroxyapatite ($Ca_{10}(PO_4)_6(OH)_2$) nanoparticles were prepared by a simple co-precipitation technique. Equimolar concentrations of $CaCl_2$ and $(NH_4)_2HPO_4$ were prepared in an aqueous solution and these solutions were preheated, mixed under vigorous stirring. NH_4OH was added to the reaction mixture immediately after mixing until the pH reached to 10. After stirring for 24h, the precipitate was filtered, washed with distilled water and dried. Finally the HA powder was sintered at 600^0C for 6h [180].

2.2.2 Preparation of (NBR/HA) nanocomposites

The NBR/HA nanocomposites were prepared by direct solution casting method. NBR, 100 phr (parts per hundred rubbers) was added to toluene with stirring the solution at room temperature to complete the dissolution. Various amount of HA nanoparticles (3, 5, 7, 10, 15 and 20 phr) were mixed with CTAB in toluene solution and ultrasonicated for 15 min. The NBR homogenous solution was then mixed with various content of HA nanoparticles (3, 5, 7, 10, 15 and 20 phr filler particles in toluene with CTAB) and ultrasonicated again for 20 min and allowed to stir it for 2h. For comparison, a blank compound was also prepared by mixing NBR with toluene. These solutions were then coagulated with ethanol and dried in oven to get a constant weight.

2.2.3 Preparation of EPDM/HA nanocomposite:

EPDM/HA nanocomposites were prepared by adding various amount of hydroxyapatite nanoparticles in an open two roll mill mixing technique. Rubber (100phr) was mixed with curing agent DCP (6phr) and HA nanoparticles (5, 10, 15 and 20 phr). The samples were vulcanized to their respective cure time in hydraulic press at 160^0C. For comparison a blank compound was also prepared by mixing EPDM and DCP.

2.2.4 Synthesis of chlorinated NBR (Cl-NBR)

The introduction of chlorine groups on NBR was done by the alkaline hydrolysis of chloroform ($CHCl_3$) using a phase

transfer agent, TBAB [181, 182]. Acrylonitrile butadiene copolymer (10 g) was dissolved in toluene in a round - bottomed flask. Approximately 0.002 mol of TBAB was added to this solution and stirred well. $CHCl_3$ (30 mL) and 60% NaOH (40 mL) solution were added to the above mixture and stirred continuously for various time of reaction (4, 8, 12, and 24 h). Chlorinated NBR was removed from aqueous solution at different time intervals and washed several times with hot and cold water. The product was then coagulated with isopropyl alcohol and dried in a vacuum temperature at 70°C.

2.2.5 Chlorine content of chemically modified NBR (Cl-NBR)

The chlorine content of the chemically modified NBR was determined by Volhard method [3]. In brief, Cl-NBR (0.5 g) was mixed with Na_2CO_3 (0.002 mol) and K_2CO_3 (0.002 mol) and fused at 750°C for 1 hour. The residual ash was extracted with deionized water, and the sludge was filtered and washed with deionized water several times to obtain the chlorine solution. To this, a known volume (excess) of 0.1 M $AgNO_3$ solution was added to precipitate the chlorine as AgCl. The residual AgNO3 in the supernatant was filtered with 0.1 M NH_4SCN solution by using ferric alum as an indicator. The chlorine content was estimated from **equation 2.1**.

$$Amount\ of\ chlorine\ (\%) = \frac{[(B-V)\times N\times 35.5]/1000}{W} \times 100 \qquad \textbf{(Eq : 2.1)}$$

where B and V (mL) are the volume of NH_4SCN required for titration of the blank and sample solutions, N is the normality of NH_4SCN, and W (g) is the weight of Cl-NBR.

2.2.6 Preparation of NBR and Cl-NBR rubber vulcanizates

Nitrile rubber (100phr) and Cl - NBR (100phr) compounds were prepared as per the ASTM D - 15 - 627 method by mixing the rubber with 6 phr of dicumyl peroxide in a two roll mill (1.5 m× 0.3 m) with a nip gap of 1.3 mm and a friction ratio of 1:1.4 at room temperature. The mill speed ratio, nip gap and time of mixing of the rolls were kept the same for all mixes. The compounds were then vulcanized at 160°C in a compression molding machine [183].

2.2. 7 Preparation of Cl-NBR/HA nanocomposites

The Cl-NBR/HA nanocomposites were prepared by mill mixing technique. Cl-NBR was first masticated for 3 min, followed by addition of different weight percentage nano HA (0, 3, 5,7,10 and 15phr). The crosslinking agent DCP (6 phr) was incorporated in accordance with ASTM D-15-627 method with special attention paid to maintain the uniform mixing.

2.2.8 Preparation of chlorinated EPDM (Cl-EPDM)

Chlorination of EPDM was done by passing chlorine gas, produced by the simple and inexpensive chemical reaction between concentrated HCl and $KMnO_4$. The EPDM was dissolved in toluene in an RB flask and stirred the solution continuously on a magnetic stirrer. To this solution different amount of chlorine was directly passed and the various amount of reagents used for the

chlorination studies are given in **table 2.3**. The product was coagulated with isopropyl alcohol and dried at 80^0C for 6hrs.

Table 2.3: Amount of reagents for production of chlorine

Sample code	KMnO4 (g)	HCl(mL)	% of Chlorine
S1	2	15	0.79
S2	2.5	20	1.32
S3	3	30	1.80
S4	3.5	40	2.64
S5	1.5	10	0.53
S6	4	40	3.32
S7	6	60	3.80
S8	8.5	80	3.71

2.2.9 Preparation of Cl-EPDM/HA nanocomposites

The nanocomposites were prepared in an open two-roll mill mixing technique. Chlorinated EPDM rubber (100 phr) was mixed with different content of HA nanoparticles (5, 10, 15, and 20 phr) and DCP (6 phr). For comparison, a blank compound was also prepared by mixing Cl-EPDM and DCP. The samples were vulcanized to their respective cure time in hydraulic press at 160^0C.

2.2.10 Preparation of Cl-NBR/ Cl-EPDM blends and its nanocomposites

As per ASTM D-15-627 (1994), blends of Cl-NBR and Cl-EPDM were prepared in a two-roll mixing mill. Initially, Cl-NBR was masticated for four minutes and then blended with Cl-EPDM for an additional 3 min. The formulations of the mixes viz. Cl-NBR/ Cl-EPDM and Cl-NBR/ Cl-EPDM /HA nanocomposite are given in **table 2.4**.

Table 2.4: formulation details of Cl-NBR/ Cl-EPDM blends and its nanocomposite with HA

Cl-NBR/ Cl-EPDM	DCP (phr)	HA (phr)
70/30	6	0
30/70	6	0
50/50	6	0
50/50	6	3
50/50	6	5
50/50	6	7
50/50	6	10
50/50	6	15

2.3 Characterization techniques

2.3.1 ^{1}H - NMR spectroscopy

The ^{1}H - NMR spectra of elastomer samples were recorded with a 90 MHz JEOL EX90 FT NMR spectrometer in $CDCl_3$ (10% w/v solution) with tetramethylsilane as the internal reference.

2.3.2 FT-IR spectroscopy

The IR spectra of the samples were recorded with a JASCO model 4100 Spectrophotometer in the region 500 to 4000 cm^{-1}. Absorption bands in the spectrum results from energy change arising as a consequence of molecular vibrations of the bond stretching and bending type. The samples were dissolved in chloroform and the solution is put on the surface of KBr pellet and dried. This pellet was subjected to FTIR.

2.3.3 UV-Visible spectroscopy

The UV-Vis absorption spectra of samples were carried out by a Hitachi U-300 spectrophotometer. The light source produces a beam of UV radiation, which is divided into two parallel beam of equal intensity radiation. The sample is in the path of one beam and the other may use as a reference beam when the solution is to be analyzed. A slowly rating refraction grating or prism varies the wavelength of the radiation reaching the sample and then the detector. The detector records the difference in wavelength between the two beams on a recorded sharp as absorbance. The samples were dissolved in chloroform and the solution was used for the analysis. The diffuse reflectance UV (UV-DRS) of some solid samples were also taken.

2.3.4 X-ray diffractometry (XRD)

X-ray diffraction pattern of the sample was recorded on Rigaku miniflex 600 X-ray diffractometer using CuKα radiation (λ

= 1.5406 Å) with an accelerating voltage of 30 KV. The diffractogram was recorded in terms of 2θ in the range 10–80^0 at a speed rate of 2 ^{0}/min. XRD is a rapid analytical technique used for phase identification of a crystalline material and can provide information on unit cell dimension. The interaction of the incident rays with the sample produces constructive interference and a diffracted ray when conditions satisfy Bragg's Law. These diffracted X-rays are then detected, processed and counted. The Bragg's diffraction angle (**2θ**), along with interplanar spacing (**d**), and the relative intensity of the peaks were calculated using Bragg's equation,

$$n\lambda = 2d \sin\theta \qquad \textbf{(Eq :2.2)}$$

where, `**θ**' is one half of the angle read from diffractogram.

Scherrer's equation was used to estimate the particle size & the equation is, [4]

$$D = \frac{K\lambda}{\beta \cos\theta} \qquad \textbf{(Eq : 2.3)}$$

where K is the particle shape factor generally taken as 0.89, λ is the wavelength of CuKα radiation λ = 1.54 Å, θ is the diffraction angle of the intense peak, and β is the half height of diffraction angles in radians.

2.3.5 Morphology Studies

2.3.5.1 Scanning Electron Microscopy (SEM)

The surface morphology of the rubber was investigated by using Field Emission Scanning Electron Microscopy - Hitachi, SU 6600 (FESEM) [184]. For SEM analysis, the rubber compounds were immersed in liquid nitrogen for 5 minutes and then fractured. These samples were mounted on the stubs, and the rubber surface was sputtered at 0^0 tilt angle with platinum - palladium to resist the charging on the surface before examining under SEM. Area ranging from approximately 1cm to 5 microns in width was imaged in a scanning mode using SEM technique.

2.3.5.2 Optical microscopy

The optical images of the composites were carried out by trinocular microscope Model Axio Lab.A1attached AxioCam ERc5s Carl Zeiss Microimaging GmbH analyzer.

2.3.6 Thermal analysis:-

2.3.6.1 Differential Scanning Calorimetry (DSC)

Differential scanning calorimetry (DSC) was carried out by Mettler Toledo DSC 22e. The samples were heated at a rate of 5^0C/min (atmosphere N2; flow 40 ml/min) from -80^0C to room temperature. The glass transition temperature (*Tg*) of each sample was observed as the transition from the DSC traces**.**

2.3.6.2 Thermogravimetric Analysis (TGA)

Thermal decomposition behavior of the nanocomposites was investigated by a Perkin Elmer thermogravimetric analyzer in a dry nitrogen atmosphere. The samples were scanned from 30 to 800^0C at a heating rate of 10^0C min^{-1}. From the TG curves, the thermal degradation characteristics and temperatures at different weight losses were recorded.

2.3.7 Cure characteristics and vulcanization

The cure characteristics of the rubber mixes were carried out by a Monsanto Rheometer R - 100 at a rotational frequency of 100 cycles min^{-1} as per ASTM standard D - 5289 (2001) at 150^0C. The molding of samples was done in a hydraulic press at 40 - MPa pressure as per the corresponding optimum cure time obtained from Rheometer.

2.3.8 Mechanical properties

The tensile strength and tear resistance of the dumb-bell shaped samples were tested in a Zwick Universal Testing Machine (UTM) with a load cell of 10 kN capacity at 28^0C and at a crosshead speed of 500mm/min according to ASTM D 412 (2016) and ASTM D 624-00 (2012) respectively. Average of at least of five sample measurements represents each data point. The hardness of rubber and chemically modified rubber and their composites were measured at room temperature by using a Shore - A hardness

tester (Durometer - Mitutoyo Shore - A meter) as per ASTM D - 2240 (2004). The durometer reading was taken at room temperature on each rubber specimen at different locations, and the average of all readings was reported as hardness values.

2.3.9 Flame retardancy

The flame retardancy of the samples was carried out by a Stanton Red croft FTA flammability tester, under mixed nitrogen–oxygen atmosphere. The minimum concentration of the oxygen in the oxygen–nitrogen gas mixture environment just sufficient to sustain the flame for 30s was taken as the limiting oxygen index (LOI). LOI is determined by the equation

$$LOI = \left[\frac{Volume\ of\ oxygen}{Volume\ of\ oxygen + Volume\ of\ nitrogen}\right] \times 100 \qquad \textbf{(Eq : 2.4)}$$

2.3.10 Electrical properties

AC-conductivity and dielectric properties

The dielectric constant of the elastomeric materials were analyzed by automatic Hewlett Packered LCR meter (HP: 4284A) in the frequency range 10^2 to 10^6 Hz. Disc shaped samples were used to find out the dielectric constant. The capacitance 'C', loss tangent 'tan δ' and resistance 'R' were obtained. Dielectric constant or relative permittivity were calculated using the formula,

$$\varepsilon_r = C.d/\varepsilon_0.A \qquad \textbf{(Eq : 2.5)}$$

where d be the thickness of the sample, C the capacitance, A the area of cross section of the sample and ε_0 be the permittivity of free space. The relative permittivity of the material (ε_r), is a dimensionless quantity.

AC conductivity can be calculated using the formula,

$$\sigma_{AC} = \omega . tan\delta . \varepsilon_0 . \varepsilon_r \text{ (S cm}^{-1}\text{)} \qquad \textbf{(Eq : 2.6)}$$

where; 'ω' is the angular frequency.

2.3.11 Oil resistance

According to ASTM D 471, the oil resistances of samples were carried out by immersing ASTM oils # 1, 2 and 3 (IRM 901, IRM 902 and IRM 903) at different temperatures. After 72 h immersion in oil, the samples were taken out, dipped in acetone and wiped off with filter paper to remove excess oil from the surface. From the relative weight difference of samples, oil resistance of was assessed.

2.3.12 Examination of sorption characteristics

The diffusion and transport mechanism of samples were carried out by circular samples punched out from the vulcanized sheets using sharp edged steel die. Initially, the original weight of the samples was measured and their thickness was also determined using a screw gauge. Thus, the pre weighed samples were immersed in different penetrants taken in the specially made

diffusion bottles kept at constant temperature. The samples were then weighed using an electronic balance (Shimadzu, Libror AEU-210 Japan) in preset time intervals and again immersed in the respective solvents, taking maximum care to avoid error due to solvent evaporation. This solvent immersion and the weighing process were continued until the equilibrium weight was obtained [185-189].

The sorption results were expressed as mol percentage uptake of solvents by 100 grams of sample (Q_t mol%)

$$Q_t(mol\%) = \frac{mass\ of\ solvent\ sorbed/molecular\ weight\ of\ penetrant}{initial\ weight\ of\ polymer\ sample} \times 100$$

(Eq: 2.7)

The solvent uptake experiments were repeated at different temperatures. The penetrants used include petroleum fuels (petrol, diesel and kerosene) and aromatic solvents (benzene, toluene and xylene). The kinetic and thermodynamic parameters, mode of transport and activation energy was also determined.

3.1 Introduction

The diversity and novelty in performance characteristics of rubber based composite materials have extensively attracted by researchers because of their wide applications in electromechanical systems [190,191]. Many scientists have investigated the synthesis and applications of polymer–metal composites and the overall response of the composite depends on the interfacial behaviour and phase morphology of the components [192,193]. Recently, the polymer nanocomposites have been the subject of extensive studies over conventional microcomposites due to exceptionally large interfacial area per unit volume of dispersed phase. This high aspect ratio helps to increase the interaction with the matrix phase which enhances the mechanical, electrical, thermal and optical properties of nanocomposites [194,195].

NBR and EPDM are two commercially exploited rubbers having versatile utilization in material industry ranging from automotive to household application. NBR is well known for its excellent oil and heat resistance. The moderate cost, processability, better resistance to acids; aliphatic hydrocarbons etc. made it an ideal material for industrial applications. It is commonly used in petroleum and auto-mobile industry to make fuel hoses, gaskets, rollers etc. It is used as sealant in rubber industry especially for lip seal of ball-bearings [196]. However, NBR has poor green strength, flexibility, flame retardancy and electrical conductivity properties. Recently, many researchers are focused on the fabrication of NBR based nanocomposites not only to enhance the mechanical

properties of NBR but also for making use of its oil and solvent resistance. Thomas et al. studied the impact of filler geometry and surface chemistry on the degree of reinforcement and thermal stability of nitrile rubber nanocomposites and their studies revealed that the NBR nanosilicate composites showed great impact on the mechanical and thermal properties of the NBR as compared to titanium dioxide and calcium phosphate fillers [197]. Self-extinguishing elastomeric nanomaterials can be prepared by the incorporation of hallosite nanotube and a halogen free flame retardant compound into the NBR matrix was reported by Rybinski and Janowska [198]. EPDM has unique characteristics such as outstanding ozone and heat resistance, weathering ability, aging properties etc due to stable saturated hydrocarbon chains with low percentage of olefinic side chains. But the thermodynamic immiscibility results high interfacial tension due to the lack of polarity, limits its application in engineering fields. To overcome this difficulty, recently many research works were carried out on EPDM by making use of its ability to respond high filler loading due to the presence of high ethylene content [199, 200].

The nanocomposites of polymer with ceramic material as filler have the merits of both polymer and ceramic. Literature reports point out the use of polymeric ceramic nanocomposites as energy storage materials because of the low temperature processability of polymer and high dielectric constant of ceramics. These nanocomposites have enormous applications in electrical and electronic devices such as integrated decoupling capacitors, angular

acceleration accelerometers, acoustic emission sensors, electronic packaging etc.

The nano sized hydroxyapatite (Ca_{10} $(PO_4)_6(OH)_2$; HA) is one of the most studied bio ceramic materials which have excellent biodegradability, biocompatibility and osteoconductive properties [201]. It is the major component of natural bone. It has versatile and diverse biomedical applications in tissue engineering, regenerative medicine, gene therapy, controlled drug delivery system etc. [202]. However HA is brittle, can be crushed easily, high temperature processability and is unfit for direct implant applications [203]. Therefore applications of a number of natural and synthetic polymers have been reported as a scaffold for HA in biomedical applications. Polyamide/hydroxyapatite nanocomposite with greater biocompatibility and mechanical strength was prepared by Li et al [204]. Though polypropylene is a bioinert polymer, its nanocomposite with HA shows bioactive characteristics, dimensional stability and high mechanical strength [205]. However, rubber based HA nanocomposites have hardly been studied yet. Thus in this chapter particular attention has been focused on the preparation, characterization and studies on NBR and EPDM rubber based HA nanocomposites.

The interaction between the functional group of polymer and hydroxyl groups of HA nanoparticles were studied by FTIR and UV spectroscopy. The structural and morphological studies of the composites were examined by XRD and optical microscopy and SEM. The effect of concentration of nanoparticles on the

thermal stability and the glass transition temperature of the polymer matrix was evaluated by thermogravimetry and differential scanning calorimetry analysis. Additionally, the electrical properties such as AC conductivity, dielectric constant and dielectric loss tangent of the composites were studied by an impedance analyzer at different frequencies.

3.2 Result and Discussions

Hydroxyapatite nanoparticles (HA) was synthesized by the chemical precipitation between $CaCl_2$ and $(NH4)_2HPO_4$ in aqueous solution. NBR nanocomposite with different concentration of hydroxyapatite nanoparticles were prepared by solution casting technique. EPDM/HA nanocomposite was prepared by simple two roll mill mixing method in presence of dicumyl peroxide as crosslinking agent.

3.2.1 FTIR Analysis

The FTIR spectra of HA, NBR, NBR/HA, EPDM/HA nanocomposites embedded with different concentrations of HA nanoparticles are shown in **Figure 3.1, 3.2** and **3.3**.

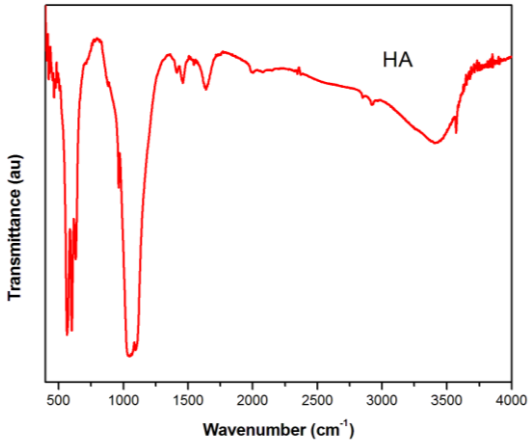

Figure 3.1 FTIR spectrum of hydroxyapatite nanoparticles

The characteristic absorption peak of HA nanoparticle (**Figure 3.1)** observed at 3573 cm^{-1} is assigned to stretching vibration of OH ions and peak at 633 cm^{-1} indicates the O–H deformation mode. The peaks at 470, 569, 604, 964 and 1045 cm^{-1} are the characteristic of PO_4^{3-} entity. The distinguishable peak at 964 cm^{-1} is attributed to P–O stretching vibration of PO_4^{3-} and the sharp peak at 633, 602 and 568 cm^{-1} are corresponding to bending vibration of PO_4^{3-} unit of HA [206].

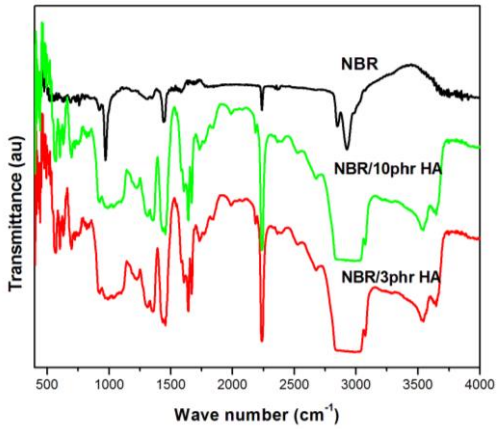

Figure 3.2 FTIR spectra of NBR and NBR/ HA nanocomposites

The **Figure 3.2** NBR shows the characteristic absorption peak at 2239 cm^{-1} which is characteristic of CN stretching vibration. The peaks at 975 and 695 cm^{-1} are assigned to CH wagging of *trans* and *cis* –CH=CH unit of butadiene segment respectively. The peaks at 1444 and 1301 cm^{-1} represent the absorptions of δ(C–H) of $–CH_2$ and for γ (CH_2) of $–CH_2$ respectively. However, in FTIR spectrum of NBR/HA nanocomposites, the stretching and deformation peak of hydroxyl group of nanoparticle is appeared at 3636 and 695 cm^{-1}. In addition, the characteristic absorption peaks of phosphate group (1045, 964 cm^{-1}) in the nanocomposites slightly shifted to a lower wavenumber at 985 and 918 cm^{-1}. It is also clear from the figure that the absorption frequencies of composites below 1000 cm^{-1} are strongly influenced by the presence of nanoparticles. The shift in absorption frequencies and appearance of new peaks in the

composites (the presence of HA particles at 567 and 601 cm^{-1} for 3 phr composite while 561 and 613 cm^{-1} for 10 phr composite) indicates the inter-molecular interaction between the polar groups of NBR with the polar group of HA nanoparticles.

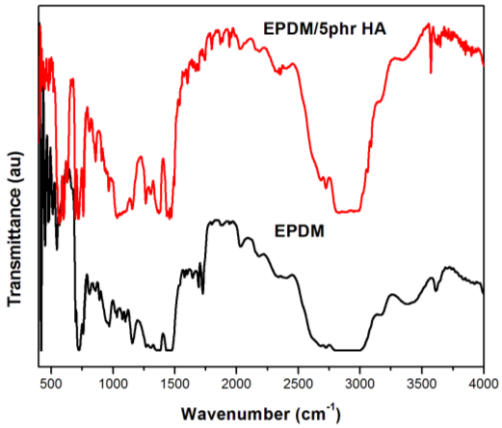

Figure 3.3 FTIR spectra of EPDM and EPDM/5 phr HA nanocomposite

The pristine EPDM shows absorption peaks at 1157 cm^{-1}, 1457 cm^{-1} and 2904 cm^{-1} corresponding to C-H stretching vibration of polypropylene segment and the peak at 721 cm^{-1} is attributed to side ethyl groups of crystalline ethylene blocks [207]. The EPDM/HA nanocomposite contains most of the absorption bands present in the EPDM and HA along with a slight shift in absorption frequency. The OH stretching is shifted from 3573 cm^{-1} to 3568 cm^{-1} and bending vibration is changed from 633 cm^{-1} to 638 cm^{-1}. Furthermore, an absorption band is present in nanocomposite

(at 1022-1164 cm^{-1}), may be due to the combination of C-H stretching vibration of polypropylene in EPDM (1157 cm^{-1}) and PO_4^{3-} entity (1045 cm^{-1}) of HA. These results assure the incorporation of nano HA in EPDM rubber.

3.2.2 UV–VIS Spectroscopy

The UV–Vis spectra of NBR and NBR/ HA nanocomposite is shown in **Figure 3.4**. NBR shows a sharp low intense absorption peak at 285 nm corresponds to n-π^* transition of –CN group in the rubber. In the case of nanocomposite the characteristic peak assigned to n-π^* transition is shifted to a higher wavelength region with an intense broad band at 302 nm. The increase in intensity and broadness of UV absorption peak in the nanocomposite compared to the UV absorption in neat NBR confirms the increase in crystalline phase of the rubber. The orientation of nanoparticles in the polymer is mainly due to the intermolecular interaction between the polar group of rubber and hydroxyapatite nanoparticles.

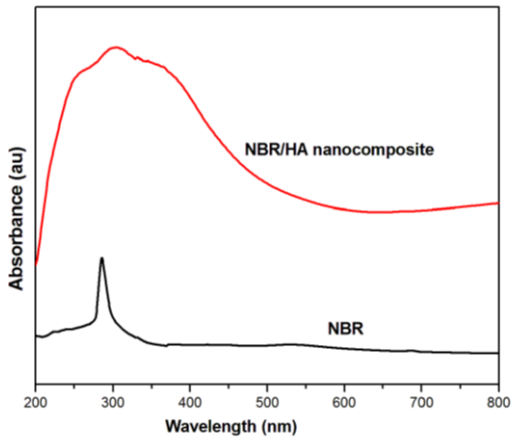

Figure 3.4 UV spectra of NBR and NBR/ HA nanocomposite

The diffuse reflectance UV-Vis spectra scanned at 200-800 nm of HA, EPDM and EPDM/HA nanocomposite is given in **Figure 3.5** and **3.6**.

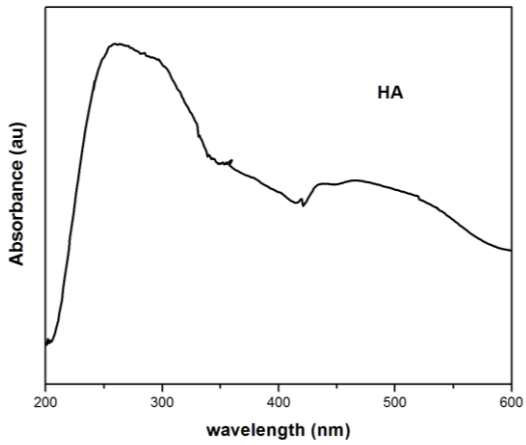

Figure 3.5 UV spectrum of HA

Hydroxyapatite nanoparticle shows an absorption maximum at 263 nm and a dip at 421 nm. EPDM shows a broad absorption band with absorption maxima at 347nm. The chromophore responsible for initial UV light absorption is the carbon-carbon double bond present in EPDM. It is very clear from the figure that the nanocomposites also show a maximum absorption of UV light below 300 nm and an absorption dip in 300-400 nm range which reflects the successful introduction of nanoapatite particles in to the matrix. Moreover, the absorption maximum in the nanocomposite shows a shift to higher energy region than that of EPDM. This hypochromic shift may be due to the interfacial interaction of HA and the chains of EPDM.

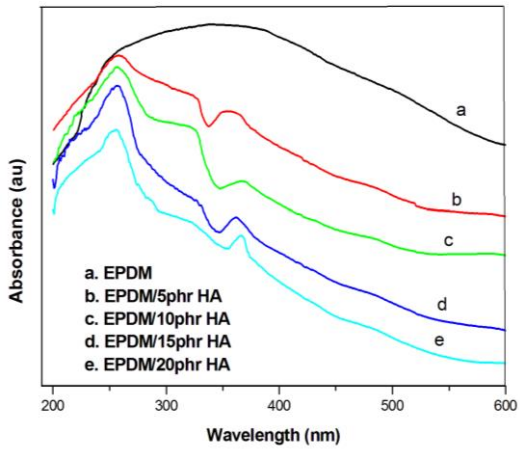

Figure 3.6 UV spectra of EPDM and EPDM/HA nanocomposites

3.2.3 X-ray Diffraction Analysis (XRD)

Figure 3.7 shows the X-ray diffraction pattern of synthesized HA nanoparticles. The XRD pattern has been matched with the JCPDS data (9-432) of HA. The various diffraction peaks observed are at $2\theta = 25.7^0$, 31.6^0, 32.7^0, 34.1^0, 39.7^0, 46.6^0, 49.5^0, 53.09^0, corresponding to the diffraction of 002, 211, 300, 202, 310, 222, 213, 321, 004 crystal planes respectively [208,209]

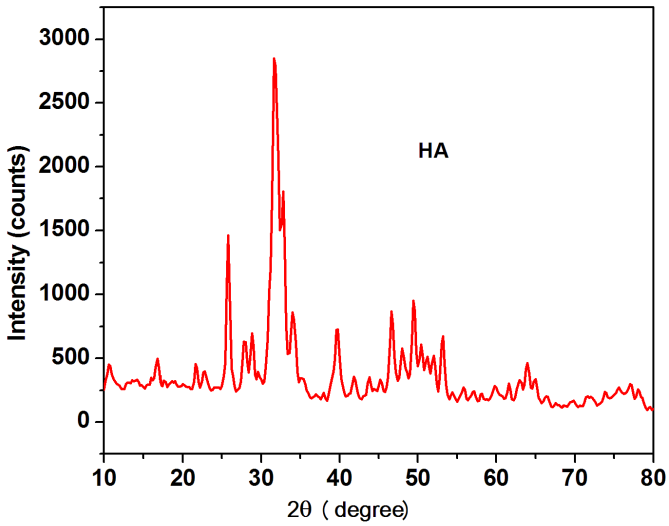

Figure 3.7 XRD pattern of HA

The particle size of HA nanoparticle has determined by using Scherrer' s formula (**Eq : 2.3**). When the reflecting peaks at $2\theta = 31.46^0$, is chosen to calculate the average diameter the particle size of HA is found to be 9.5 nm.

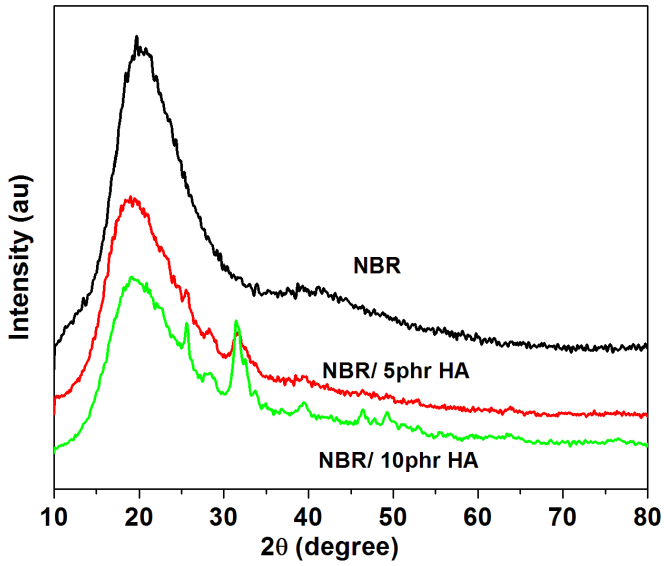

Figure 3.8 XRD pattern of NBR and NBR/HA nanocomposites

The XRD pattern of NBR (**Figure 3.8**) showed a broad diffraction peak at $2\theta = 19.72^0$ correspond to the amorphous nature of the polymer. The XRD pattern of nanocomposite shows some characteristic diffraction peaks of HA nanoparticles with the broad amorphous diffraction of NBR. Moreover, the characteristic amorphous diffraction peak of NBR in the composite is found to be shifted to a lower 2θ value (i.e. from 19.72^0 to 18.94^0) with a decrease in broadness of the amorphous peak. The strong intermolecular interaction between the rubber and HA nanoparticles imparts a regular arrangement of filler particles within the polymer, leading to some extent of crystallinity in the rubber matrix.

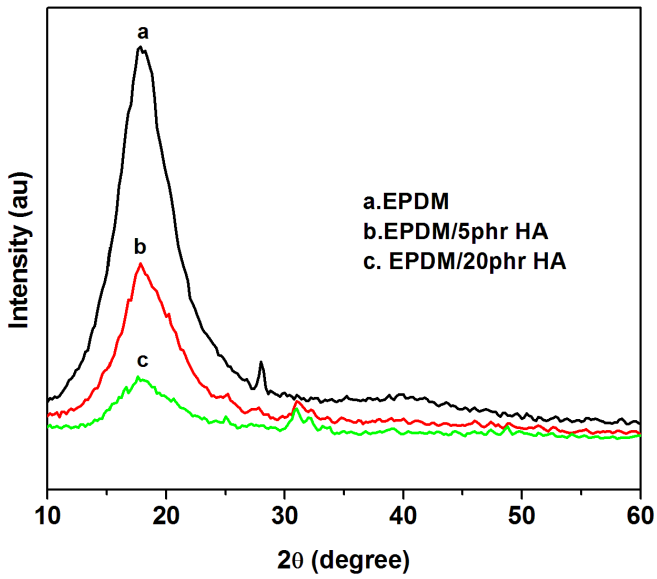

Figure 3.9 XRD pattern of EPDM and EPDM/ HA nanocomposites

EPDM shows (**Figure 3.9**) an intense broad diffraction peak at $2\theta = 17.8^0$ indicating its amorphous nature and a small peak at $2\theta = 28^0$. This small sharp crystalline peak may be due to the presence of side ethylene of polyethylene block. From the plots it is very clear that nanocomposite exhibit very few crystalline peaks of HA with decrease in intensity. The crystalline peak corresponding to polyethylene segment of EPDM is absent in nanocomposite and also a new diffraction peak appeared at $2\theta = 31^0$. It is interesting to see that the amorphous region of the composite is shifted to a lower 2θ region with 20 phr HA nanoparticles. In addition to this the intensity of amorphous and crystalline peaks decreases with increase in the dosage of nanoparticles. This proves that the efficient interfacial interaction

between the elastomer and the ceramic occurs at lower loading of nanoparticles. At higher loading of HA, the variation in amorphous and crystalline region of nanocomposite is attributed to the agglomeration of nanoparticles which is in good agreement with the optical micrographs.

3.2.4 Morphology Studies

3.2.4.1 Optical Microscopy

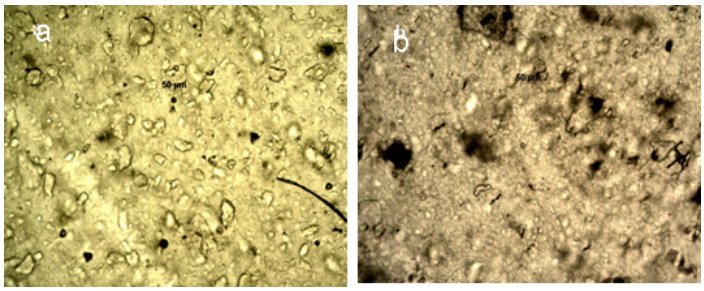

Figure 3.10 Optical micrographs of **a)** NBR/7phr HA and **b)** NBR/15phr HA

The dispersion of nanoparticles into rubber matrices has been characterized by optical microscopy. **Figure 3.10** shows the optical images of different contents of HA nanoparticles with NBR. The optical micrographs of EPDM and its nanocomposites with HA are demonstrated in **Figure 3.11.** It is clear from the micrographs that lower concentration of nanoparticle shows almost uniform morphology with good uniformity of nanoparticles pointing out the good adhesion between nano filler and the polymer matrix. However, when the concentration of nanoparticles

increased to 15 phr, uniformity changes to an irregular nature which may be due to the agglomeration of nanoparticles inside the macromolecular chain of elastomers.

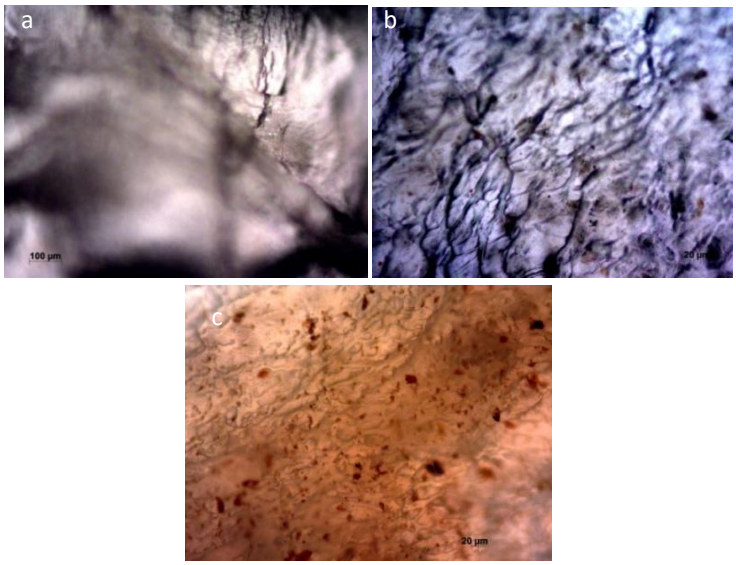

Figure 3.11 Optical micrographs of a) EPDM b) EPDM/5phr HA c) EPDM/15phr HA

3.2.4. b Scanning Electron Microscopy (SEM)

It is already reported that the morphology of polymer nanocomposite depends on compatibility of the polymer and filler particles and also the size of nanoparticles [210].

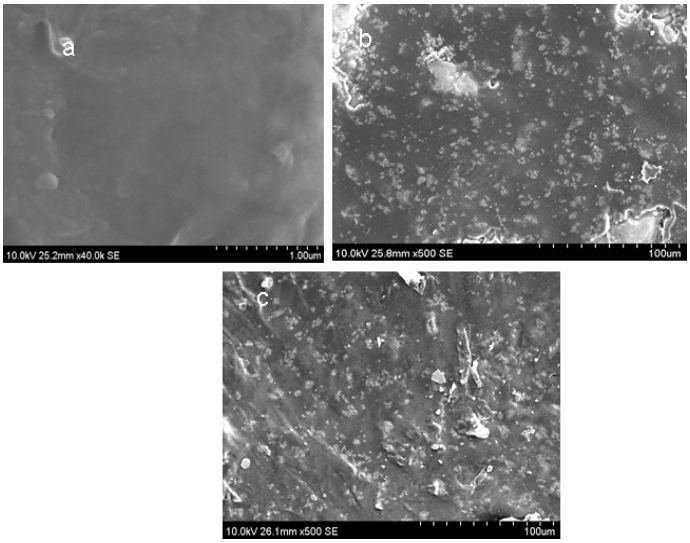

Figure 3.12 SEM images of **a)** NBR, **b)** NBR with 7phr and **c)** NBR with 15phr HA

Figure 3.12 shows the SEM images of NBR with 7 and 15phr of HA nanoparticles. The SEM micrograph of NBR exhibits a smooth surface. The morphology of the composite with 7 phr of HA nanoparticles shows a uniform dispersion of particles in NBR matrix. Since the nanoparticles possess large surface area so that they have high affinity to polar macromolecule leading to a uniform orientation of nanoparticles within the NBR chain. As the loading of filler becomes 15 phr, the composite shows an irregular structure with heterogeneous dispersion of nanoparticles. At higher loadings of fillers, greater stress is developed due to the high external force in the rubber which results in the agglomeration of hydroxyapatite nanoparticles.

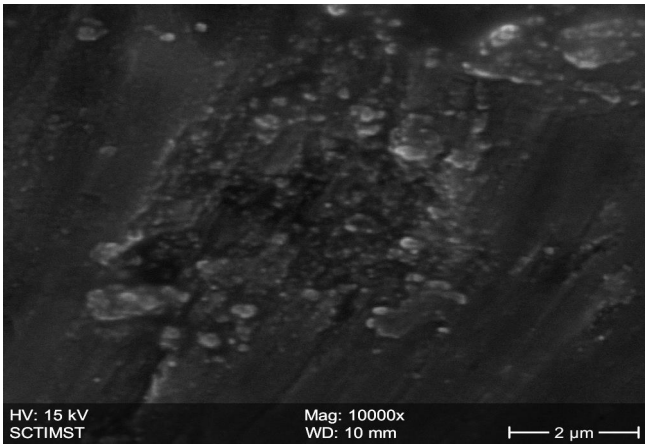

Figure 3.13 SEM images of EPDM/10phr HA

The SEM image of EPDM with 10 phr HA nanoparticle is presented in **Figure 3.13**. It depicts the spherically shaped clusters of nano HA in the host rubber. The dispersed particles are agglomerated due to the self aggregation through strong polar attraction between OH groups within nonpolar macromolecular system.

3.2.5 Thermal Behavior

3.2.5. a. Differential Scanning Calorimetry (DSC)

The glass transition temperature and the thermodynamic properties of fabricated nanocomposites were studied by differential scanning calorimetry (DSC).

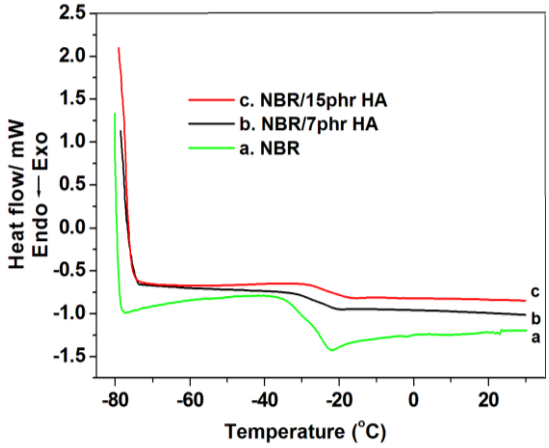

Figure 3.14 DSC thermograms of NBR and NBR/HA nanocomposites

The DSC curve of pure NBR and the composite filled with 7 and 15 phr of HA nanoparticles are presented in **Figure 3.14**. The glass transition temperature (T_g) of pure NBR is occurred at -35.6^0C. The T_g of all composite filled with nano sized HA particles increases significantly as the volume fraction of filler raises. The T_g values obtained for 7 and 15 phr of nano-particles are at -32.5^0C and -30.4^0C respectively. Generally, the glass transition temperature of rubber composite depends mainly on the polarity and crystallinity of polymer and the filler particles. The increment in T_g with respect to filler loading is assigned to the polar–polar interaction between the hydroxyl group of apatite nanoparticles and the nitrile group of NBR creates structural regularity in the rubber and thereby retards the mobility of the rubber chain. It has also been reported that the elastomeric material posses high T_g have higher crystallinity and the knowledge of T_g is much important in the manufacturing process of rubber products. Further, the glass

transition of amorphous rubber may be due to the change in heat capacity of sample undergoing calorimetric measurement. The heat of fusion (ΔH) and corresponding entropy change (ΔS) at glass phase transition was measured from the DSC curve. NBR shows the ΔH value of 227.58 KJ mol^{-1} and ΔS around 14.29 JK^{-1} mol^{-1}. However, the ΔH value of nanocomposite with 7 and 15 phr of nanoparticle exhibits respectively at 83.58 and 72.17 KJ mol^{-1}. Similarly the ΔS value obtained for 7 and 15 phr of nanocomposite is 5.41 and 4.73 JK^{-1} mol^{-1} respectively. From these values it can be inferred that as compared to amorphous NBR, the nano-composite shows lower enthalpy and entropy of transition. Also, the ΔH and ΔS value decreases with increasing the loading of nanoparticles in the macromolecular chain of NBR. Thus the lower of heat of fusion and disorderness of composite with increased glass transition temperature again confirms the interaction of polymer chain with the nanoparticles [211, 212].

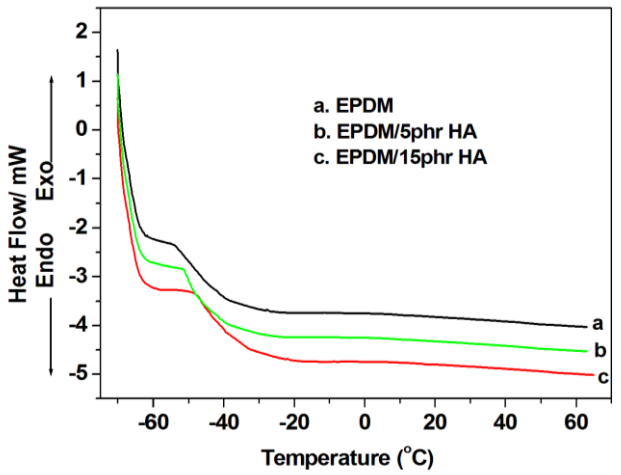

Figure 3.15 DSC thermograms of EPDM and EPDM/HA nanocomposites

The *Tg* obtained as base line shift in thermograms are shown in **Figure 3.15** for EPDM and its nanocomposites with HA. The EPDM shows *Tg* at -53^0C, the nanocomposite with 5 and 15 weight % HA are present at -51^0C and -48^0C respectively. The raise in *Tg* of newly prepared EPDM/HA nanocomposites is attributed to the intermolecular interaction through the enhanced interface of nanocomposite which restricts the rotational motion within the chains. Also, the incorporation of HA increases the compactness of the system as evident from the XRD resulting in the reduction of free volume inside the composite which in turn suppresses the motion of polymer chains [213].

3.2.5. b. Thermogravimetric Analysis (TGA)

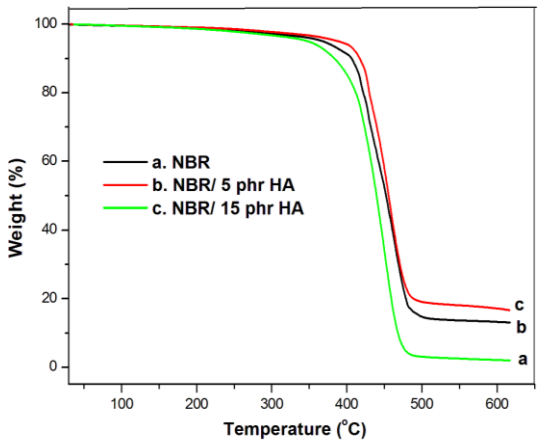

Figure 3.16 TGA curves of NBR and NBR with 5 and 15phr HA

The thermal decomposition behaviour of NBR and NBR with different concentration of HA nanoparticles is given in **Figure 3.16**. It can be observed from the figure that the NBR shows single stage decomposition temperature at 405^0C whereas the NBR nanocomposites with 5 and 15 phr of HA nanoparticles show the thermal degradation at 415 and 413^0C respectively. The degradation temperature of nanocomposite is greater than that of NBR which reveals that the nanocomposites exhibit higher thermal stability than that of raw rubber. This is because of the reduced air permeability in to the macromolecular chain and also due to increased crystallinity as a result of the systematic arrangement of macromolecular chain due to the intermolecular interaction between the nanoparticle and the rubber chain. It can be seen from the figure that the char residue obtained at 600^0C for NBR and nanocomposites with 5 and 15 phr HA are 2.4, 13.3 and 17.1% respectively. This indicates that the nanocomposite shows higher percentage of final char residue than pure NBR. The increased char residue of nanocomposites suggests the better flame retardancy of the prepared nanocomposite.

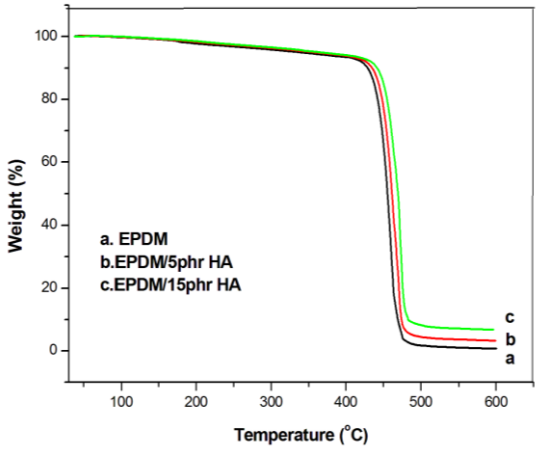

Figure 3.17 TGA curves of EPDM and EPDM/HA nanocomposites

Thermogravimetric analysis of newly prepared EPDM/HA nanocomposites presented in **Figure 3.17** shows single stage decomposition. The degradation temperature of EPDM chain is at 434^0C whereas the decomposition temperature increases as the concentration of nanoparticle increases. That is EPDM with 5 phr HA shows decomposition at 438^0C while EPDM/ 15 phr HA degrades at 445^0C. The elevation in decomposition temperature clearly indicates the improved thermal stability of nanocomposite which is due to the nanoparticle penetrated in to the EPDM reduces the diffusion of oxygen in to the long chain of elastomer. Besides, the char residue obtained at 600^0C for EPDM is 1.2% whereas the nanocomposites with 5 and 15 phr HA are about 4.7% and 9.3 % respectively. The increase in percentages of final char residue with the increase in filler loading indicates that the

nanoparticles act as heat barrier to EPDM and thus enhances the flame retardancy of rubber.

3.2.6 Conductivity Studies

3.2.6.1. AC Conductivity

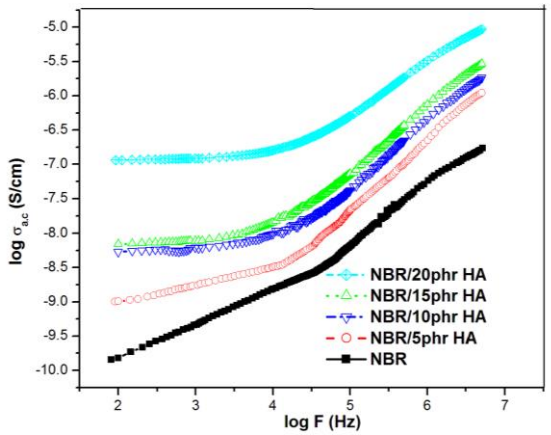

Figure 3.18 AC conductivity of NBR and NBR/HA nanocomposites

Figure 3.18 shows the variation in AC conductivity with various frequencies of pristine NBR and nanocomposite containing different loadings of HA as double logarithmic plots of σ_{AC} *vs.* frequency. The conductivity improved with the increase in frequency indicates the electronic conduction in the composite materials is of hopping type. Thus the transportation of charge carriers which are decoupled from the elastomer segmental motion occurs through hopping process. It is well clear from the figure that the conductivity of nanocomposites are much higher than the pure NBR which is due to the uniform dispersion of nanoparticles and thereby the regular arrangement of nanoparticles in the polymer

matrix. Moreover, the extensive interfacial zone, the orientation of dipoles associated with the nitrile group of NBR and the hydroxyl group of hydroxyapatite nanoparticle is responsible for the higher conductivity in the nanocomposite. Also, the conductivity is related to the polarity of the composite material, crystallinity of the sample and the orientation of dipoles in the macromolecular chain of NBR. It is evident from the XRD studies that the crystallinity of the nanocomposite increases with the loadings of nanoparticles. The same results are also found in the literatures [214,215]. The conductivity of nanocomposites is found to be improved with the concentration of nanoparticles. The compactness of composite materials is increased by the addition of apatite nanoparticles, which improves the links between the grains and therefore coupling through grain boundaries became stronger, that leads to a higher conductivity values.

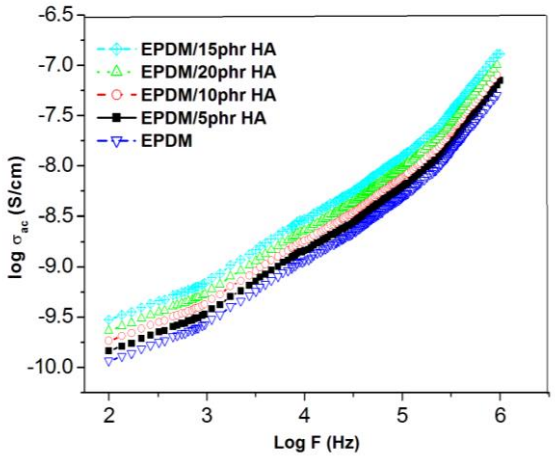

Figure 3.19 AC conductivity of EPDM and EPDM/HA nanocomposites

The AC electrical conductivity as a function of frequency of EPDM and EPDM with different contents of HA nanoparticles are depicted in **Figure 3.19**. The conductivity goes on increasing with frequency which is due to the hopping of charge carriers through the conducting networks formed as a result of polarity induced by the hydroxyl group of hydroxyapatite to the EPDM chains. Further, the electrical conductivity of nanocomposite is better than neat EPDM and the conductivity increases proportionately with increase in concentration of HA. It can be explained on the microscopic conductivity arising from the matrix-filler interaction, polarity and chain entanglements in the host matrix. As it is revealed from XRD studies the crystallinity of EPDM increases with the incorporation of nano HA resulting in the improvement of orderness through the interconnection of dispersed filler and the rubber matrix. It can also be seen from the graph that the conductivity of nanocomposite with 20phr HA is less than that of nanocomposite with 15phr HA due to aggregation of nanoparticles at higher loading.

3.2.6.2. Dielectric Constant

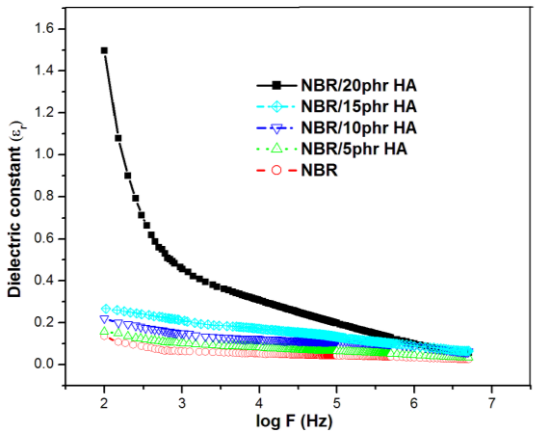

Figure 3.20 Dielectric constant of NBR and NBR/ HA nanocomposites

The dielectric properties are measured to understand the polarization mechanism arising from the alignment of charge carriers under applied electric field. **Figure 3.20** depicts the variation of dielectric constant with frequency for NBR and NBR containing different concentration of HA nanoparticles. It is clear from the figure that the dielectric constant continuously decreases with increase in frequency and attains a constant value at higher frequencies. The increase in dielectric constant may be due to interfacial polarization which arises from the polar interaction of functional groups present in the surface of polymer and hydroxyl group of nanoparticles [163]. The high dielectric value at lower frequency is due to the dipoles get enough time to align before it changes its direction while as the applied frequency increases there will be insufficient time for dipoles to align before the reversal of

field. The dielectric constant continuously increases with increasing the loadings of nanoparticles and an abrupt increase in dielectric constant of composite is noticed when the volume fraction of filler particles reached to 20 phr. This sharp increase is a direct consequence of enhanced interfacial polarization effect between the nanoparticles and rubber [216]. The higher dielectric constant indicates higher capacitance density of the nanocomposites which is proportional to the quantity of charge stored on the surface of composite materials under an applied electric field. In the present study, the quantity of the accumulated charge is high due to the polarization of NBR with the HA nanoparticles at the interface. From this point of view, it can be inferred that the dielectric constant of nanoparticles are much higher than pure NBR and the dielectric constant depends on the loadings of nanoparticle in the rubber matrix [217].

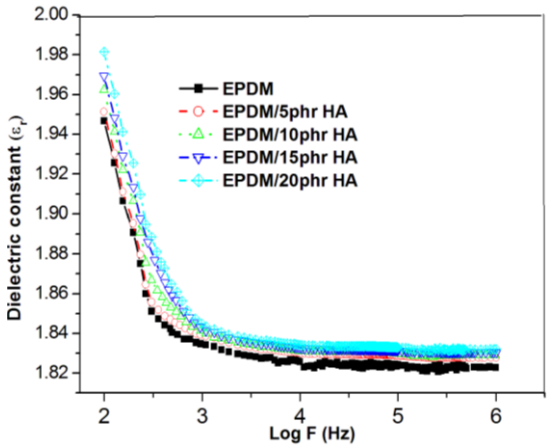

Figure 3.21 Dielectric constant of EPDM and EPDM/HA nanocomposites

The dielectric constants of the EPDM composites are portrayed in **Figure 3.21**. It can be observed that dielectric constant shows frequency independent behaviour at high frequency and strong distortion of permittivity at lower frequency region and also the dielectric constant increases with the concentration of nano HA. At lower frequencies the interfacial polarization raised by the introduction of polar filler into the rubber matrix is the reason for high dielectric constant while at higher frequencies the orientation polarization plays important role [218]. That is up to about 10^4Hz the AC current is in phase with the applied potential whereas above 10^4Hz the filler aggregates do not get enough time for hoping before the reversal of the field. As the filler concentration increases the electrical polarization of the elastomer matrix increases due to the presence of more number of polar groups.

3.2.6.3. Dielectric Loss

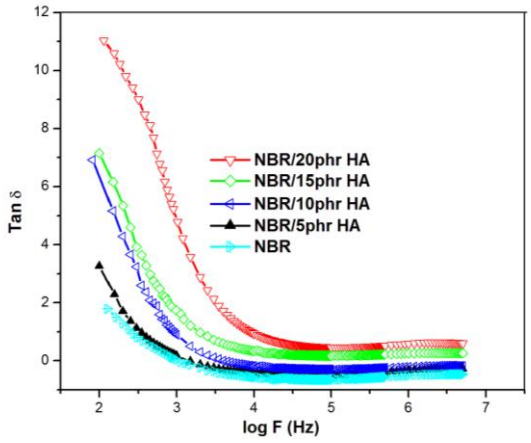

Figure 3.22 Dielectric loss tangent of NBR and NBR/HA nanocomposites

The variation of the dielectric loss tangent (tan δ) of NBR/ HA nanocomposites as a function of frequency at room temperature is reproduced in **Figure 3.22**. The relaxation processes arising from the structural reorganization of the material is responsible for the dielectric loss factor. The dielectric loss tangent decreases steeply at lower frequencies and reaches a constant value at higher frequencies (10^4 Hz). This is mainly due to the induced charges gradually loses to follow the reversing field, which leads to a reduction in the electronic oscillation as the frequency is increased [219]. The tan δ values of the composites are significantly higher than pure NBR and the dielectric loss tangent improved with the volume fraction of nanoparticles. The maximum dielectric loss tangent is noted for 20 phr of composite and this is because of the strong intermolecular interaction between the filler surface and the NBR chain which leads to higher crystallinity. Thus the influence of HA on dielectric loss of composite can be ascribed to the increased regularity of polymer chain which is in good agreement with XRD studies.

3.3 Conclusions

The effect of hydroxyapatite nanoparticles on two industrially important rubbers – NBR and EPDM - was studied and characterized by FTIR, UV, XRD, TGA, DSC and electrical conductivity measurements. FT-IR spectra indicated the incorporation of hydroxyapatite with the elastomer chain. UV-Visible spectroscopy confirms the enhanced interfacial

interaction of nanoparticles and the elastomeric chain. XRD analysis showed that the HA nanoparticles were inserted in to the elastomer segments and the intensity of the XRD peaks increased with the loadings of nanoparticles. The intercalation and flocculation of inorganic nanoparticles in organic matrix can be revealed from optical micrographs and also from SEM images. The thermal behaviour of newly prepared nanocomposites increased with increase in concentration of nanoparticles. DSC analysis showed glass transition temperature of nanocomposites was higher than neat matrix and the Tg increases with increase in content of nanoparticles in the polymer, indicating the interfacial interaction between matrix and the nanoparticles. The nanocomposites with higher weight percentage of HA nanoparticle shows higher AC conductivity than pristine rubber due to the improved interconnection between nanoparticles and the polymer. Dielectric constant and loss factor of nanocomposites exhibit similar behaviour to the applied frequency and was significantly increased with increase in concentration of HA nanoparticles. The enhanced dielectric and electrical conductivity of composites are also due to the increased interaction between nanoparticles and the polymer that result in an ordered arrangement of filler inside the macromolecular chain.

4.1 Introduction

In recent years, polymers became demanding stuff in both technical and commercial areas due to the widely varying static and dynamic properties that are drastically different from other engineering materials. Thus, the designing of new polymeric materials and modification of existing polymers for superior properties got great research emphasis [220-223]. The polydiene elastomers are particularly good candidates for various chemical reactions due to the olefinic group present on the backbone of polymer chain [224-226] and nowadays it drawn exciting research interest as conducting or dielectric elastomers [227].

The modification of spatial network structure of macromolecules by the introduction of polar groups got ample attention due to the increase in the mutual interaction of elastomer chains [228]. The presence of polar groups in rubber also improves the flame retardant behavior, optoelectronic properties, and oil and solvent resistance of the material. Chlorination is one of the extensively used functionalization reactions for unsaturated elastomers because chlorinated derivatives show low vapor permeability, good chemical resistance and flame retardant properties which give an insight into the service behavior of materials [229, 230]. It also reduces the tackiness and frictional resistance found especially in surgical household natural rubber gloves. The different methods of chlorination on various commercial diene polymers are done by many researchers. Among

a number of methods, the most adapted one is the steriospecific cyclo-addition of carbene which is an important synthetic intermediate. The most convenient and efficient method reported for the generation of dihalocarbene is the hydrolysis of chloroform with aqueous alkali metal hydroxide in presence of a phase transfer agent [231]. It was reported that the dichlorocarbene modified SBR shows better flame retardancy and excellent oil resistance compared to other chlorine containing rubbers. The oil and solvent diffusion process depends on free volume within the elastomer matrix, polarity of polymer, crosslink density, temperature and the size of the penetrant molecules [232].

In automotive vehicles, nitrile rubber is utilized as a fundamental material in the fuel handling system which must have superior heat and gasoline permeation resistance while retaining the flexibility and bendability. However, the automotive applications of NBR are limited due to the thermal oxidative aging associated with the butadiene part of the polymer. Moreover, nitrile rubbers used to seal oil well tubing undergo degradation due to hydrolysis as a result of its contact with fluids like $ZnBr_2$ brine. Literature reports show that the reductions of unsaturation present on the backbone of NBR by hydrogenation and fluorination give materials with enhanced oil and chemical resistance in addition to excellent aging resistance [181]. The hydrogenated NBR (HNBR) has excellent oil and fuel resistance at high temperatures coupled with good mechanical properties has found important applications in

automobile and petroleum industries. Studies of Mandal on carboxylated nitrile rubber (XNBR) neutralized by metal oxide showed the profound change in physical properties due to the presence of physical cross links produced by ionic clusters [233].

There is an increased demand for flexible conductive elastomer which can offer many useful technological applications such as microwave absorbers, sensors, automobile, petroleum and in chemical industries. The introduction of polar groups in rubber enhances the dielectric properties along with tensile properties, resistance to oil, ozone, flame, and solvents. In this chapter, we describe the chemical functionalization of NBR and its effectiveness on thermal properties, flame, oil and solvent resistance, cure behaviors, and mechanical properties with respect to the different level of chlorine content. The dichlorocarbene addition on NBR was analyzed through ^{1}H-NMR, UV, Fourier transform infrared (FTIR), X-ray diffraction analysis (XRD), and scanning electron microscopy (SEM).

4.2 Results and Discussion

Chlorinated acrylonitrile butadiene rubber (Cl-NBR) was prepared from NBR by the alkaline hydrolysis of chloroform using phase-transfer catalysis.

4.2.1 Estimation of degree of chlorination

The percentage of chlorine present in the macromolecular chain of chemically modified NBR was monitored by chemical titration method (Volhard method). The reaction of dichlorocarbene with NBR conducted at various time intervals (4, 8, 12, and 24 h) shows 15, 18, 22, and 24% of chlorine content respectively. This means that the percentage of chlorine attached to the rubber molecule increases with the time of reaction.

4.2.2 ^{1}H-NMR characterization

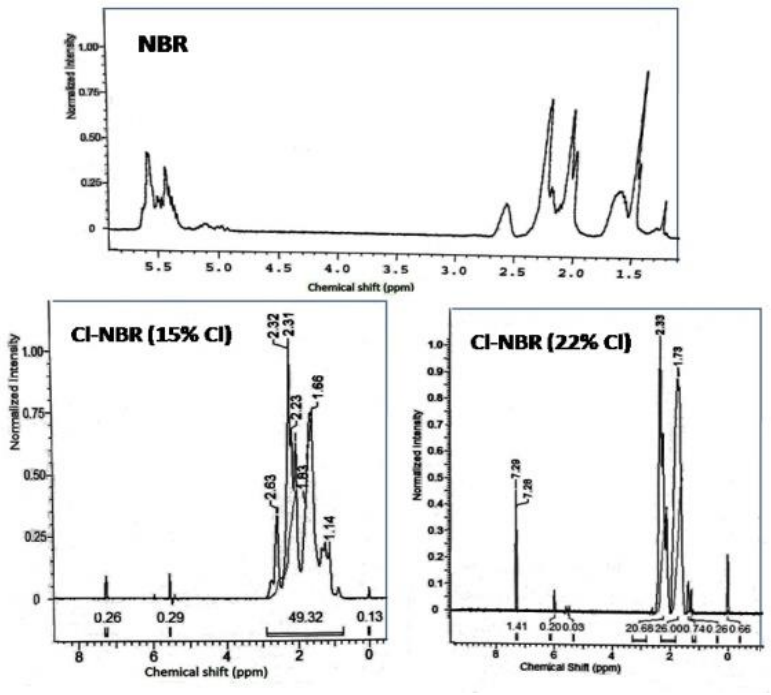

Figure 4.1 ^{1}H - NMR spectra of NBR and Cl - NBR with different chlorine contents

Figure 4.1 shows the ^{1}H-NMR spectra of NBR and Cl-NBR with 15 and 22 percentage of chlorine content. The major signals obtained in the range of 5 to 6 ppm are assigned to the protons on the unsaturated carbon atom and of those obtained at 1.5 to 2.5 ppm is attributed to the aliphatic protons (–CH_3, –CH_2, and –CH) of NBR. The peaks at 5.1 and 5.7 ppm in NBR represent the hydrogen atoms of vinyl pendant group, and the peaks at 5.3 to 5.6 ppm are from the protons of 1, 4-polybutadiene units of rubber [36]. From the figure, it is clear that due to chlorination, the relative intensity of signals of aliphatic protons increased, while that of olefinic protons reduced. In addition to that, new signals appeared from 1.1 to 1.3 ppm due to methylene hydrogen next to cyclopropyl ring produced during carbenization. The most noticeable result obtained is the generation of a signal below 0.8 ppm in Cl-NBR, which is assigned to one of the protons present on the cyclopropyl ring, and the spectrum clearly depicts that the height of this peak increases as the chlorination time increases. This confirms that the extent of modification is increased with time of chlorination.

4.2.3 FTIR analysis

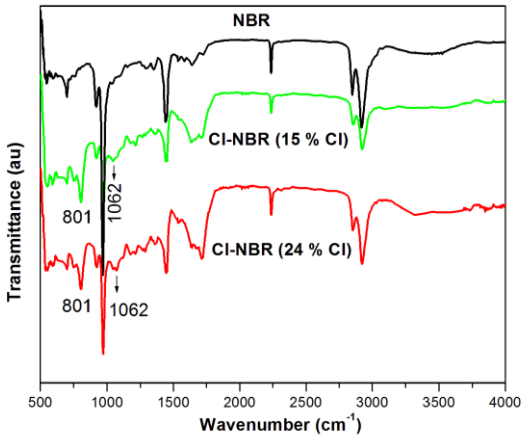

Figure 4.2 FTIR spectra of NBR and Cl - NBR with different percentage of chlorine

The IR spectra of NBR and Cl-NBR are given in **Figure 4.2**. The spectrum of NBR shows a significant absorption at 2239 cm^{-1} which is characteristic of –CN stretching vibration. The absorption peaks that appeared at 972, 920, and 692 cm^{-1} are attributed to CH wagging of 1,4 trans, CH_2 wagging for pendent CH_2═CH– (vinyl) unit, and CH wagging of 1,4 cis –CH═CH unit of butadiene segment, respectively. The IR absorption found at 1444 and 1310 cm^{-1} corresponds to the δ(C–H) of –CH_2 and for γ(CH_2) of –CH_2, respectively. Also, the peaks at 2920 and 2840 cm^{-1} are due to –CH– stretching vibrations of –CH_3 and CH_2– of NBR [234]. It can be seen from the figure that the Cl-NBR shows two additional peaks, one at 801 cm^{-1} (characteristic C–Cl stretching), and another at 1062 cm^{-1} is the absorption of

cyclo-propyl ring. In the Cl-NBR, the position of the peak at 2239 cm^{-1} in NBR remains intact and supports that the chlorination reaction is more favored at the butadiene part of NBR unit. From these results, it can be inferred that the dichlorocarbene formed due to alkaline hydrolysis of chloroform which successfully added on the double bond of butadiene unit of NBR. The reaction mechanism of carbenization of NBR is displayed in **Scheme 4.1**.

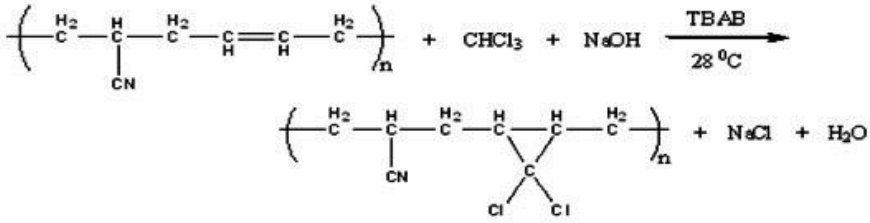

Scheme 4.1 Schematic representation of the chemical modification of acrylonitrile butadiene copolymer

4.2.4 UV-Vis spectra

Figure 4.3 displays the UV-Vis absorption spectra of pristine NBR and Cl-NBR with different chlorine content. The absorption maxima of NBR at 285 nm is attributed to the π to π* transition of the polymer. It can be seen from the figure that the π to π* transition of all the chlorinated samples shifted to a higher wavelength region with an increase in broadness of the absorption peak. The increase in broadness with the level of chemical modification indicates the attachment of chlorine on the backbone of the butadiene unit of NBR. Also, the chemical modification introduces more polarity in the NBR, which restricts the

mobilization of macromolecular chain and gives regularity in the arrangement of molecules in the amorphous elastomer. So this observation implies a clear evidence for the addition of dichlorocarbene to the double bonds of the butadiene units of NBR.

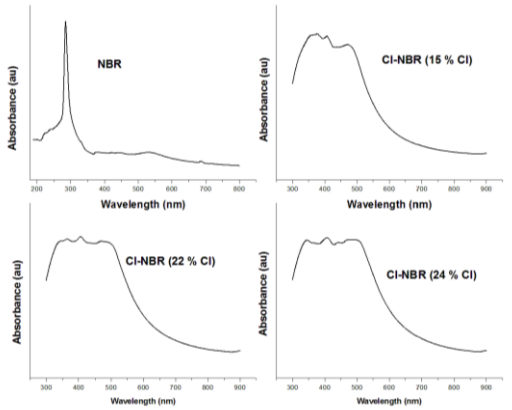

Figure 4. 3 UV - Visible spectra of NBR and chlorinated NBR

4.2.5 X-ray diffraction analysis (XRD)

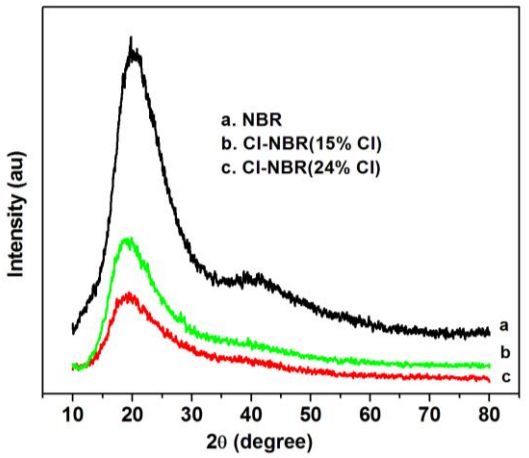

Figure 4.4 XRD patterns of NBR and Cl-NBR with different chlorine content

Figure 4.4 shows the XRD pattern of NBR and NBR with different chlorine content. The broad diffraction peak obtained for NBR is at $2\theta = 19.72^0$ with an interplanar spacing of 4.54. In chlorinated samples, it can be observed that the amorphous peak of NBR is shifted to a lower Bragg's angle with a decrease in intensity and increased interlayer spacing. That is, the Cl- NBR (15% Cl) shows 2θ value at 18.82^0 corresponding to a basal spacing of 4.75 and Cl-NBR (24% Cl) shows diffraction at 19.64^0 corresponding to d spacing of 4.57. Further, the area under the diffraction curve decreases as the level of chlorination increases. This reduction in the broadness of diffraction peak is attributed to the decreased amorphous nature of chlorinated samples compared with bare rubber due to the stereo-regular addition of dichlorocarbene, which decisively increased the degree of orderness inside the elastomer. The expanded interlayer height and the decreased amorphous nature are due to the polar-polar interaction between the chlorinated segments and the nitrile group of NBR. This is another evidence for supporting the formation of chlorinated segments in the backbone of nitrile rubber.

4.2.6 Scanning electron microscopy (SEM)

The surface morphology of modified elastomer for microstructural analysis, studied by SEM, is given in **Figure 4.5**. It is clear from the figure that the chlorinated samples show an inhomogeneous surface and the surface porosity increases as the chlorination level increases. This apparently rough surface may be

due to increase in the chemical interaction of adjacent polymer chains due to the introduction of a polar group in the elastomers. The relative increase in the stiffness of the chlorinated samples with the increase in the amount of chlorine confirms the formation of chlorinated segments in NBR chain.

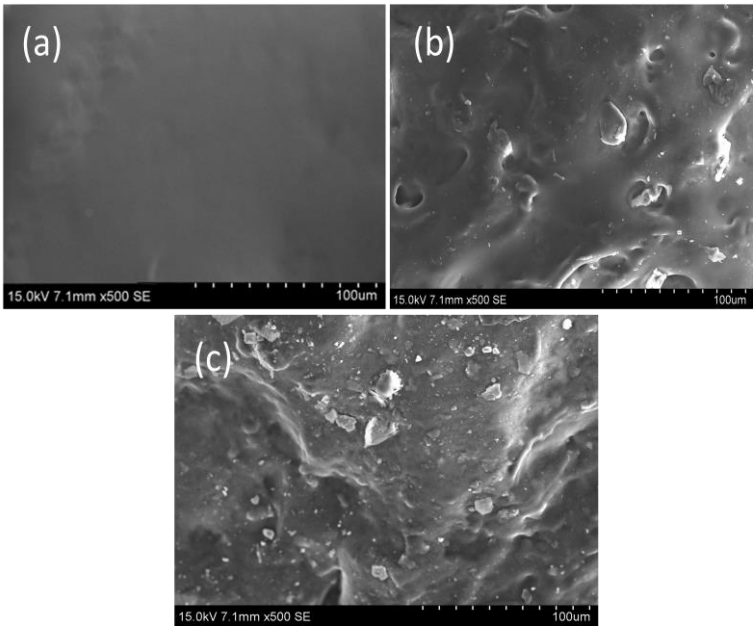

Figure 4.5 SEM images of a) NBR b) Cl-NBR (15% Cl) and c) Cl-NBR (24% Cl)

4.2.7 Thermal Behaviour

4.2.7. a Differential Scanning Calorimetry (DSC)

Differential scanning calorimetry measurement is used to identify and characterize the physical changes in states in terms of heat evolved or absorbed. It helps to identify the extent of

amorphous nature of polymer through the change in the glass transition temperature (*Tg*). The *Tg* mainly depends on the segmental mobility and the free volume between the polymer chains.

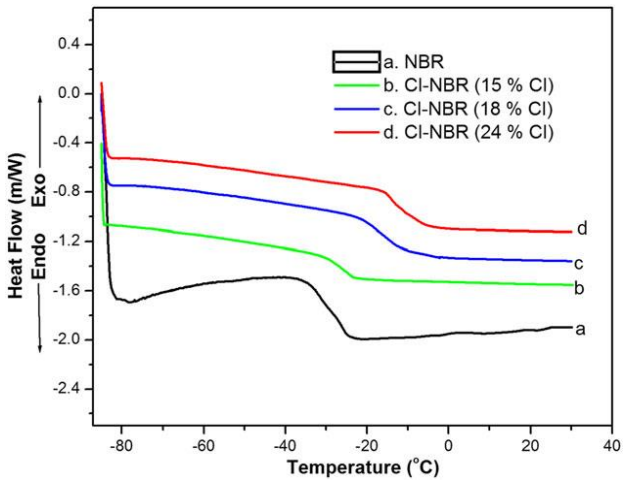

Figure 4.6 DSC thermograms of NBR and chlorinated NBR with different chlorine content

The DSC thermograms of NBR and Cl-NBR having different chlorine content are depicted in **Figure 4.6**. Acrylonitrile butadiene copolymer showed glass transition at −35.6°C. However, the Cl-NBR with 15, 18, and 24% of Cl showed the glass transition temperatures at −30.5°C, −22.4°C and −15°C, respectively. The result demonstrates that the glass transition temperature of NBR increases with the increase in the level of chemical modification. The increased *Tg* of Cl-NBR is ascribed to the confinement of polymer chains and this is because of the increased polar-polar

interaction developed due to the introduction of two Cl molecules through cyclopropyl ring in the polar nitrile rubber. Further, the spatial network structure formed due to the polar attraction decrease the free volume which resists the segmental motion of polymer matrix which increases the stiffness of the samples [235].

4.2.7. b Thermogravimetric analysis (TGA)

Figure 4.7 shows the thermal degradation behavior of NBR and Cl-NBR. The thermal decomposition of NBR occurs at a temperature of initiation of 405°C; however, the chain scission of Cl-NBR occurs in two distinct steps. The first degradation of the chlorinated sample is due to the dehydrohalogenation, and the second weight loss is due to the removal of residual organic components. The Cl-NBR with 18% of chlorine content shows the first degradation at 233°C and the second at 404°C, while chlorinated sample with 24% of chlorine content has the first decomposition at 228°C and second at 402°C. Comparing the decomposition temperature of chlorinated samples, it is found that as the level of chlorination increases, the decomposition temperature decreases.

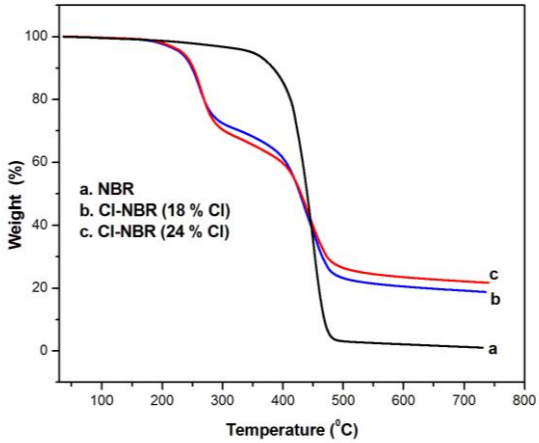

Figure 4.7 TGA curves of NBR and chlorinated NBR with different chlorine content

4.2.8 Flame retardant behavior

Flame retardant elastomeric materials have witnessed great importance due to economic and health concern. Limiting oxygen index (LOI) test gives a numerical measure of polymer flammability that has been used for assessing the achieved flame retardant properties of Cl-NBR containing different weight percentage of chlorine.

The LOI value of NBR is 18.8, while the Cl-NBR with 15, 18, 22, and 24% Cl containing sample shows the LOI value around 22.2, 24.8, 27.6, and 28.8, respectively. The oxygen content in the ambient air is about 21% so material having LOI value <21% is typically classified as flammable, the LOI between 21 and 28% is

classified as slow burning, and any material with a LOI value >28% is classified as self extinguishing. The LOI values are significantly increased by increasing the amount of chlorine content in the elastomer. This improved fire-proofing action of Cl-NBR is due to the presence of chlorine, which acts as an intumescent agent and thereby catalyzes hard char formation on the rubber [236]. This insulating boundary carbon layer formed on the surface of rubber is an obstacle to the flow of mass and energy between sample and fire. As the dosage of chlorine increases, the thickness of protective layer increases, this may delay the fire propagation. Moreover, the flammability and thermal stability are interrelated.

4.2.9 Cure characteristics

The cure properties such as variation in maximum torque (M_H), minimum torque (M_L), scorch time (ts_2), and optimum cure time (t_{90}) of NBR and chemically modified NBR with different chlorine contents are presented in **table 4.1**. It can be seen that the maximum and minimum torque of Cl-NBR is higher than that of NBR. The M_H and M_L values of chlorinated samples are found to be increased with increase in chlorine content up to 22% and after that a slight decrease in torque values is observed. The variation in torque particularly M_H or maximum torque is an indication of relative stiffness and a measure of the extent of crosslinking [237]. The higher *M*H value of chemically modified NBR with 22% chlorine content can be attributed to its high viscosity compared with others. In addition to this, the peroxide vulcanization creates

more rigid C–C linkages in Cl-NBR system, which is responsible for the higher torque values. The scorch and optimum cure time values of Cl-NBR are higher than those of NBR, and the magnitude of these values increases with the increase in the level of chemical modifications. This is due to the reduction in the number of double bonds by the dichlorocarbene attack on NBR. Also, the negative inductive effect of chlorine (-I effect) reduces the active sites of vulcanization.

Table 4.1 Processing characteristics of NBR and chlorinated NBR

Samples	Cure time t_{90} (min)	Scorch time t_2 (min)	Maximum Torque (dNm)	Minimum torque (dNm)
NBR	13	1.95	17	2.2
Cl-NBR (15 % Cl)	14.2	3.75	19	2.5
Cl-NBR (18 % Cl)	15.4	3.52	21	3.7
Cl-NBR (22 % Cl)	16.5	3.26	25	4.5
Cl-NBR (24 % Cl)	18.6	3.04	24	3.9

4.2.10 Mechanical properties

The mechanical properties are the ability to transfer stresses to the system which depends on the nature of material and degree of vulcanization. The mechanical properties of NBR and Cl-NBR

including the ultimate tensile strength, tear strength, hardness, and elongation at break (EB) are displayed in **table 4.2**. The tensile strength and tear resistance of Cl-NBR vulcanizate is greater than the NBR vulcanizates. In the case of Cl-NBR, the tensile and tear strength of vulcanizates increases progressively up to the sample containing 22% chlorine and then decreases. It can be seen from the table that the tensile strength of 22% chlorinated sample is 4 times higher than that of the pure NBR vulcanizate. The higher mechanical strength of Cl-NBR is due to the stereo-specific addition of dichlorocarbene unit to the double bond of the macromolecular chain of NBR which induces strain induced crystallization to Cl-NBR. Moreover, the dipolar interaction induces effective orientation of molecular chains of the elastomeric matrix which result in better stress transfer through the rubber and thus the improved tensile and tear properties [238]. The decrease in mechanical properties of Cl-NBR beyond 22% Cl may be due to the steric hindrance and the loss of strain induced crystallization at a higher level of chlorination. It can be seen from table 4.2 that the Shore A hardness of Cl-NBR increases with increasing chlorine content of chemically modified NBR. The increase in hardness is due to the attachment of rigid dichlorocarbene segments in NBR chain. The elongation at break is the ability to stretch several times its original length. The EB of NBR and Cl-NBR is also displayed in the **table 4.2**. The EB is found to decreases with an increase in chlorine content of NBR. This indicates the lower flexibility of elastomer with an increase in the level of chlorination [239].

Table 4.2 Mechanical properties of NBR and chlorinated NBR

Samples	Tensile strength (MPa)	Elongation at break(%)	Tear strength (kN/m)	Hardness (Shore A)
NBR	2.34	412	14	38
Cl-NBR (15 % Cl)	4.21	302	18.61	41
Cl-NBR (18 % Cl)	5.19	259	21.07	43
Cl-NBR (22 % Cl)	8.95	204	23.48	47
Cl-NBR (24 % Cl)	7.81	174	22.29	50

4.2.11. Electrical properties

4.2.11.1 AC Conductivity Studies

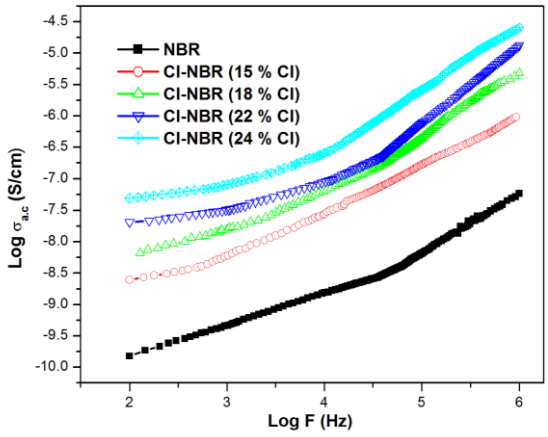

Figure 4.8 AC conductivity plot of NBR and chlorinated NBR with different chlorine content

The variation of conductivity of NBR and chlorinated NBR with different extent of chlorination as a function of applied AC frequency is presented in **Figure 4.8**. It is evident from the figure that all the chlorinated samples have much higher conductivity than parent rubber and the conductivity of the chlorinated samples increases not only with frequency but also with the increase in chlorine content. The increase in AC conductivity with increasing frequency is due to the hopping of charge carriers from one localized site to another site. Again, the higher content of dichlorocarbene functionality in the polar elastomer increases the hopping probability due to the presence of greater number of localized sites. Furthermore, the microscopic conductivity arises from the interaction of polar dichlorocarbene group along with the polar nitrile group generate interfacial polarization which alters the chain mobility due to the formation of cross-links within the system is also responsible for improved conductivity. Thus the AC conductivity of chlorinated NBR increases with the increase in level of chlorination is due to systematic attachment of chlorinated segments to the polymer matrix [240, 241].

4.2.11.2 Dielectric Constant

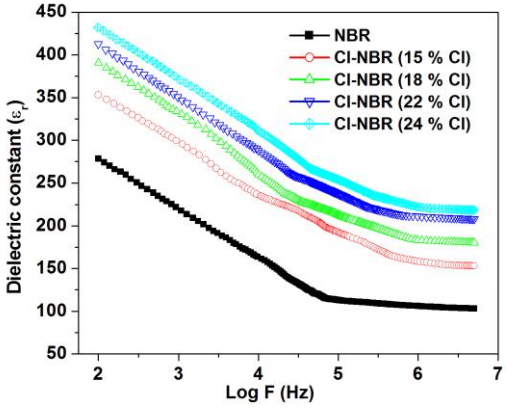

Figure 4.9 Dielectric constant of NBR and chlorinated NBR with different chlorine content

Figure 4.9 shows that variation of dielectric constant (ε_r) with different frequency at room temperature for NBR and modified NBR with different level of chlorination. It can be seen that the dielectric constant continuously decreases with increase in frequency and attains a constant value at higher frequencies. The alignment of dipoles under the applied field is arising from the resultant polar- polar interaction between the adjacent macromolecular chains of NBR which contributes towards the dielectric behaviour of the polymeric samples. The frequency dependence of dielectric behavior is attributed to interfacial polarization induced as a result of alignment of dipoles associated with the polar groups present on the back bone of NBR. Moreover,

NBR shows a linear plot eventhough it is a polar rubber may be due to the absence of electron hopping from one site to the other site. Thus at a given frequency the dielectric behavior gives a picture about the polarization mechanism [242].

4.2.11.3 Dielectric loss (Tan δ)

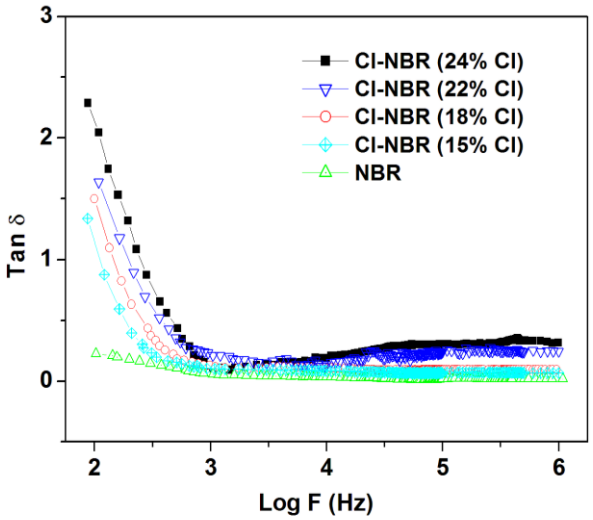

Figure 4.10 Dielectric loss tangent of NBR and chlorinated NBR with different chlorine content

The variation of loss tangent (tan δ) of NBR with different time of chlorination at various frequencies is shown in **Figure 4.10**. Dielectric loss is the function of relaxation process which depends on the change in the viscoelastic nature of the polymer. The molecular interaction is a measure of polymer segmental relaxation process. Tan δ shows similar behavior to the applied frequency as that of dielectric constant and at low frequencies interwell hopping is responsible for dielectric relaxation. The increase in dielectric

loss tangent with the increase in chlorination is attributed to the space charge distribution in the macromolecule due to the ordered arrangement of dipoles [243].

4.2.12 Oil resistance measurements

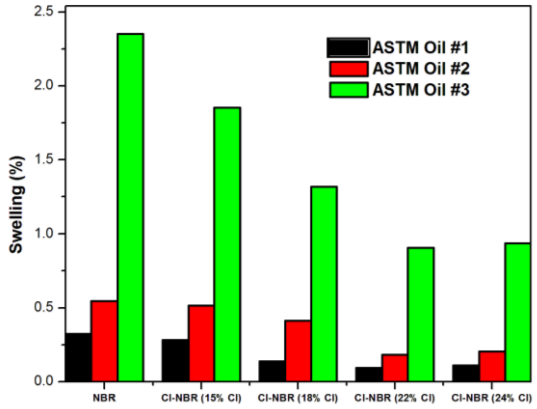

Figure 4.11 (a) ASTM oil resistance of NBR and Cl-NBR at room temperature

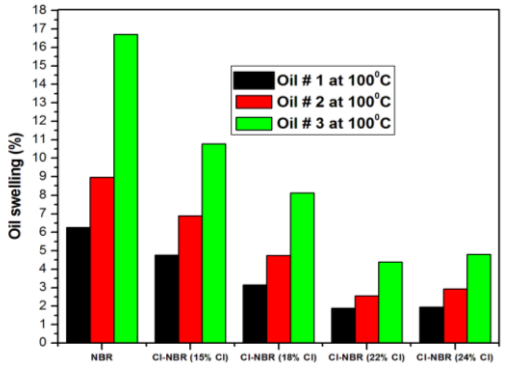

Figure 4.11 (b) ASTM oil resistances of NBR and Cl - NBR at 100^0C

The increased demand for the rubber seal products particularly in the automobile industry has aroused special attention to extend the lifetime of oil resistant elastomers [244]. NBR is used mainly for the manufacture of seals where oil resistance is the basic requirement is more prone to both physical and chemical changes depending on the working medium and temperature. The chemical resistance to hydrocarbon oils can be assessed by determining the degree of swelling of rubber samples in petroleum based industrial reference oils according to ASTM D 471. As the relative weight difference of sample immersed in ASTM oils increases, its oil resistance property decreases. The variation of percentage swelling of NBR and Cl-NBR with different amount of chlorine content at room temperature and 100^0C are presented in **Figure 4.11 (a)** and **(b)** respectively. The oil resistance of Cl-NBR is significantly higher than that of pure NBR. The degree of swelling decreases with the increase in amount of chlorine in the modified rubber. This declination in oil absorption can be explained on the basis of the increased polarity of Cl-NBR which leads to the ordering of macromolecular chains in amorphous structure of NBR which is already confirmed by the XRD. The negative inductive effect of chlorine will generate a slight negative charge on it and a delta positive charge on the nearby carbon. The presence of a high fraction of dichlorocarbene unit induces dipole moment to the elastomer chain, and the chlorine atoms act as crosslinking points through which the chain network is formed. This results in the restricted diffusion of oil molecules into the chlorinated rubber.

Further, the profound enhancement in hot oil resistance of chlorinated samples better than NBR, it can be inferred that due to the post curing effect which result in the increase in mutual interaction of elastomer chains, the chlorinated samples can withstand exposure to oil at 100^0C for reasonable period of time. As far as the oils are concerned, it is reported that the lower the aniline point the swelling action is more severe. Thus having a high aniline point (124 °C), ASTM oil # 1 causes a slight swelling compared to oil # 2 (aniline point of 93 °C) and oil # 3 (aniline point 70 °C). This indicates that IRM 903 oil having more aromatic hydrocarbon content is less compatible with the modified elastomer and the hot oil resistance of chlorinated NBR increases in the order ASTM oil # 1> ASTM oil # 2> ASTM oil # 3 the volume change is more pronounced in ASTM oil # 3 than oil # 1 and oil # 2 [245-247].

4.2.13 Diffusion Studies

4.2.13.1 Mol % uptake of aromatic and petroleum fuels

NBR dominate as barrier material for many commercial applications because it is highly chemically resistant and can retain its dimensional stability and mechanical strength. The permeation of solvents through the elastomer matrix mainly depends on the chemical composition, the way of formation and type of curative, nature and size of penetrants used etc. [248]. In order to understand the effect of modification of vulcanizates on their service

performance while using in contact with different solvents, the equilibrium swelling studies were carried out in terms of mol percentage uptake of solvents by 100g of polymer using the equation

$$Q_t = \frac{(M_t/M_s)}{M_p} \times 100 \qquad \textbf{(Eq: 4.2)}$$

where Mt represent the mass of solvent absorbed at a given time 't', Ms is the molar mass of the solvent and Mp is the mass of elastomer. The diffusion, sorption and permeation were characterized by their swelling behavior in aromatic solvents such as benzene, toluene and xylene and its fuel resistance is checked with industrial solvents such as petrol, kerosene and diesel.

Effect of chlorination on mol % uptake

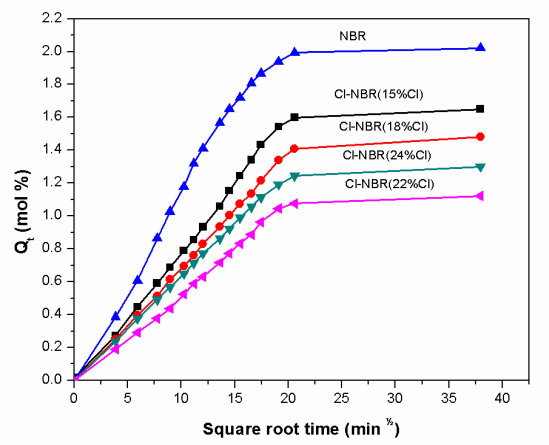

Figure 4.12 Mol % uptake of NBR and Cl-NBR with different percentage of chlorine in benzene

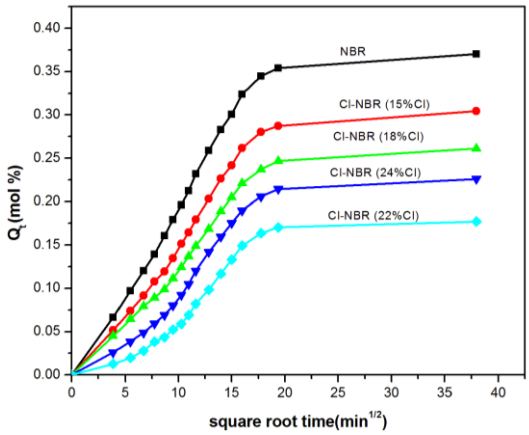

Figure 4.13 Mol % uptake of NBR and Cl-NBR with different percentage of chlorine in petrol

The sorption curve plotted by taking Qt percentage against square root time (√t) of chlorinated NBR in benzene and petrol is given in **Figure 4.12** and **4.13** respectively. The percentage solvent uptake was decreased with increase in the weight percentage of polar chlorine groups up to Cl-NBR containing 22% chlorine content. The diffusion of other aromatic and industrial solvents under study showed similar behavior as that of benzene and petrol. It is needless to mention that as the level of chlorination increases, the rigidity of the samples increases due to the increased crosslinking produced by the dipolar interaction between the chlorine groups of adjacent chains in addition to the attraction between chlorine and nitrile group. Moreover, the rigid C-C bond formed as a result of DCP vulcanization restricts the permeation of solvents in to the intermolecular gaps of the modified nitrile rubber.

As the chlorination level increases above 22% the molar absorption of solvent slightly increased which may be due to the steric hindrance produced by the bulky dichlorocarbene group made the chain packing inefficient.

Effect of penetrant size

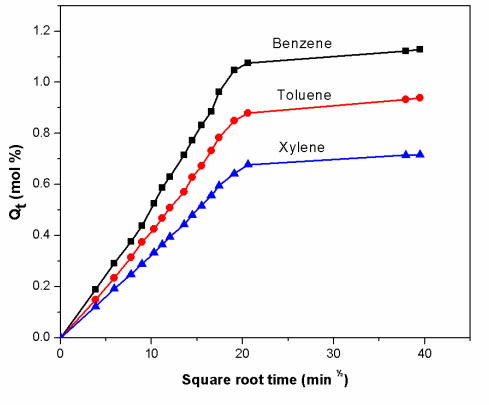

Figure 4.14 Solvent uptakes of Cl-NBR containing 22% chlorine content in different aromatic solvents

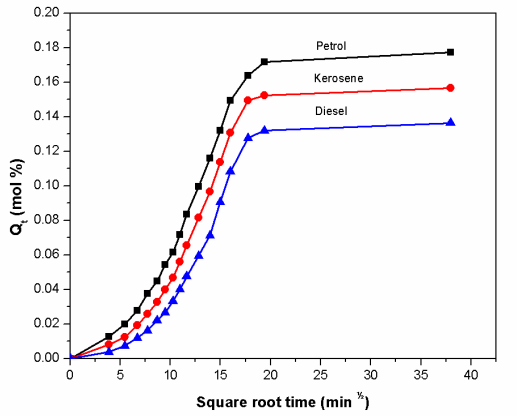

Figure 4.15 Solvent uptakes of Cl-NBR containing 22% chlorine content in different petroleum fuels

The sorption of solvents in a homologous series of aromatic and petroleum fuels by chlorinated NBR was estimated in terms of penetrant size and shown in **Figure 4.14 and 4.15**. The mol % uptake decreases in the order petrol> kerosene>diesel in case of fuels while the aromatic solvents showed the decreasing trend as benzene>toluene>xylene. Higher the molecular weight and molecular volume of the penetrant molecule, lower will be its rate of diffusion into the macromolecular chains. This is because transport of penetrants through the elastomer matrix depends on the segmental mobility and free volume theory [249]. That is on increasing the molecular size; the solvent molecules cannot easily exchange the position of polymer chains according to free volume theory and thus decreases the diffusivity.

Effect of Temperature

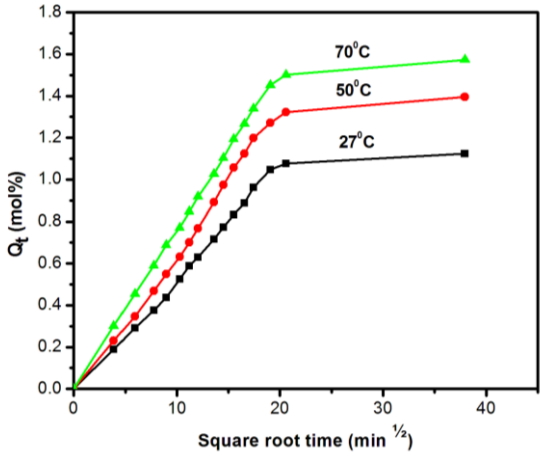

Figure 4.16 Solvent uptakes of Cl-NBR (22% Cl) in benzene at different temperature

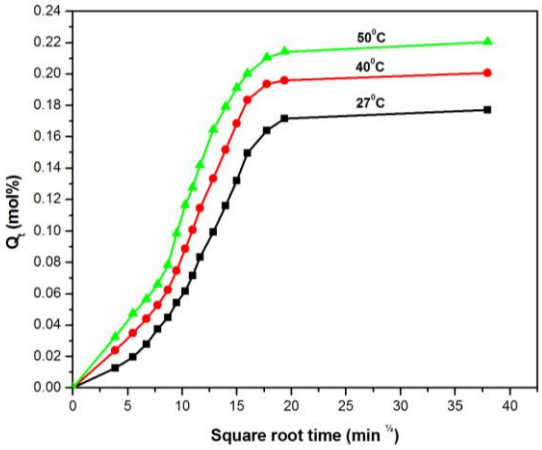

Figure 4.17 Solvent uptakes of Cl-NBR (22% Cl) in petrol at different temperature

To analyze the effect of temperature on fuel and solvent resistance, the transport properties of functionalized NBR has been studied at different temperature. The variation of rate of diffusion of petroleum fuels for Cl-NBR containing 22% chlorine content at 27, 40 and 50^{0}C were studied while that of aromatic solvents were estimated at 27, 50 and 70^{0}C. The change in penetration of petrol and benzene through the samples is displayed in **Figure 4.16** and **4.17** respectively. The rate of sorption and accordingly the equilibrium solvent uptake increases significantly with raise in temperature. All the samples exhibit similar trend in other solvents also. The increase in temperature will increase the kinetic energy of the system due to intermolecular collision of solvent molecule which may escort these molecules to very circuitous path through

the chlorinated NBR. Moreover, the raise in temperature may forcefully increase the segmental motion of the macromolecular chain, providing the activation energy needed.

4.2.13.2 Kinetic parameters

The rate of transport of different solvents through the chlorinated derivative of NBR is explained in terms of diffusion (D) sorption (S) and permeation (P) coefficient and their values obtained is presented in **table 4.3** and **4.4**. The diffusion coefficient depends on segmental motion of macromolecular chains while sorption and permeation depend on extent of unsaturation, nature of substituent and the degree of crystallinity.

Diffusion Coefficient (D)

Diffusion coefficient can be found out using the equation

$$D = \pi \left(\frac{h\theta}{4Q_{\infty}} \right)^2 \qquad \textbf{(Eq: 4.3)}$$

where h is the initial sample thickness, θ is the slope of the linear portion of the sorption curve of the plot of % Qt versus √t, and Q∞ is the equilibrium absorption.

Table 4.3. Diffusion, Sorption and Permeation of NBR and Cl-NBR in aromatic solvents.

Samples	Diffusion Coefficient D × 10^5 (cm^2/s)			Sorption Coefficient S			Permeation Coefficient P × 10^5 (cm^2/s)		
	Benzene	Toluene	Xylene	Benzene	Toluene	Xylene	Benzene	Toluene	Xylene
NBR	4.19	4.12	4.01	1.91	1.66	1.52	8.003	6.839	6.095
Cl-NBR (15% Cl)	4.11	4.02	3.93	1.82	1.50	1.43	7.480	6.03	5.619
Cl-NBR (18% Cl)	4.02	3.88	3.81	1.73	1.38	1.24	6.955	5.354	4.724
Cl-NBR (22% Cl)	3.71	3.63	3.52	1.66	1.44	1.18	6.159	5.227	4.154
Cl-NBR (24% Cl)	3.89	3.76	3.67	1.72	1.49	1.23	6.691	5.602	4.514

Table 4.4 Diffusion, Sorption and Permeation of NBR and Cl-NBR in petroleum fuels

Samples	Diffusion Coefficient $D \times 10^5$ (cm^2/s)			Sorption Coefficient S			Permeation Coefficient $P \times 10^5$ (cm^2/s)		
	Petrol	Kerosene	Diesel	Petrol	Kerosene	Diesel	Petrol	Kerosene	Diesel
NBR	3.98	3.88	3.64	1.86	1.59	1.29	7.403	6.169	4.696
Cl-NBR (15% Cl)	3.74	3.69	3.49	1.79	1.54	1.22	6.695	5.683	4.258
Cl-NBR (18% Cl)	3.42	3.38	3.28	1.75	1.49	1.16	5.985	5.036	3.805
Cl-NBR (22% Cl)	3.12	3.09	3.06	1.61	1.38	1.04	5.023	4.264	3.182
Cl-NBR (24% Cl)	3.29	3.17	3.16	1.69	1.42	1.11	5.560	4.501	3.508

The numerical value of diffusion coefficient varies with the free volume inside the elastomer and the size of diffusing molecule. **Table 4.3** and **4.4** demonstrate that, for all the solvents under study, chlorinated NBR shows a low diffusion coefficient compared to NBR and its value decreases with increase in the amount of chlorine on rubber. As the time of chlorination increases, higher percentage of dichlorocarbene group is added to the olefinic group which induces more polarity to the polar NBR chain. The polar - polar attraction of elastomeric chain through both the chlorine and nitrile group result in the chain entanglements. The decrease in diffusion coefficient can be attributed to the formation of more uniform network of NBR which act as obstacle for the flow of solvent molecules. That is the crosslinking reduces the segmental mobility which force the penetrant molecule to diffuse along longer path lengths. Further, the rate of movement of solvent molecules decreases with increase in the molar volume of penetrants; petrol showed highest uptake and diesel exhibit the lowest and the decreasing order is petrol>kerosene>diesel. Diesel molecules, being large cannot easily exchange the position of elastomer chains. For the same reason the solvent diffusion values of aromatic solvents are higher than that of petroleum fuels.

Sorption Coefficient (S)

Just like diffusion coefficient, the sorption coefficient (S) decreases with increase of chlorination. It can be determined as

$$S = \frac{W_\infty}{W_p} \qquad \textbf{(Eq: 4.4)}$$

where W_∞ is the mass of the solvent at equilibrium swelling and W_p is the mass of the polymer sample.

The equilibrium sorption values presented on **table 4.3** and **4.4** is greater for NBR compared to the chlorinated derivatives and S value decreases with increase in the dosage of polar groups in the polymer. This may be due to regularity in the orientation of amorphous elastomer chain imparted by the stereo specific addition of dichlorocarbene reduces the area for solvent transport.

Permeation Coefficient (P)

The permeation rate of both aromatic and industrial solvents through uniform area of samples per second was also determined in terms of permeation coefficient (P), calculated by using the equation

$$P = D \times S \qquad \textbf{(Eq: 4.5)}$$

Since P depend upon D and S, it also decreases with increase in the weight % of chlorine which is very clear from the **table 4.3** and **4.4** respectively. It indicate the reduction of mobility of penetrant molecule through chlorinated derivative than neat NBR. In NBR the chains are more flexible so that the solvent ingression takes place more easily compared to modified rubber where there is extended chain network is present [250].

Arrhenius parameters

From these kinetic parameters the activation energy for diffusion and permeation were calculated using Arrhenius equation

$$X = X_0 e^{-(E_X/RT)} \qquad \textbf{(Eq: 4.6)}$$

where *X* can be D or P and X_0 is D_0 or P_0 which is a constant.

From **table 4.5** (aromatic solvents) and **4.6** (petroleum fuels) it is clear that E_D and E_P values are higher for chlorinated derivative than NBR and increases with increase in chlorination time. The diffusion process involves the jumping of solvent molecules through the chains and cavities of elastomer which will disrupt the rubber-rubber and rubber-solvent interactions. Since in chlorinated NBR the macroscopic network is formed due to statistically distributed branching unit, the permeation of solvent molecules are very difficult and needs more energy. Further, the C-C linkage formed as a result of vulcanization increase the cohesive energy density while solvent penetrating power remains constant; also contribute to the increased activation energy.

Table 4.5 E_P (KJ/mol) and E_D (KJ/mol) values of NBR and Cl-NBR in aromatic solvents.

Samples	Benzene		Toluene		Xylene	
	E_P	E_D	E_P	E_D	E_P	E_D
NBR	4.68	3.48	4.83	3.54	5.06	3.69
Cl-NBR (15% Cl)	4.84	3.59	5.02	3.68	5.18	3.76
Cl-NBR (18% Cl)	4.92	3.63	5.18	3.79	5.39	3.91
Cl-NBR (22% Cl)	5.11	3.74	5.39	3.94	5.69	4.13
Cl-NBR (24% Cl)	4.98	3.67	5.26	3.86	5.6	4.09

Table 4.6 E_P (KJ/mol) and E_D (KJ/mol) values of NBR and Cl-NBR in petroleum fuels.

Samples	Petrol		Kerosene		Diesel	
	E_P	E_D	E_P	E_D	E_P	E_D
NBR	4.79	3.67	4.94	3.71	5.21	3.86
Cl-NBR (15% Cl)	4.92	3.74	5.08	3.81	5.3	3.92
Cl-NBR (18% Cl)	5.03	3.82	5.23	3.93	5.37	3.97
Cl-NBR (22% Cl)	5.18	3.92	5.57	4.21	5.72	4.26
Cl-NBR (24% Cl)	5.09	3.85	5.39	4.07	5.6	4.18

4.2.13.3 Thermodynamics parameters

From the equilibrium absorption constant (Ks) of the solvents, as determined by **equation 4.7**, thermodynamic parameters such as ΔH_S and ΔS were calculated using Van't Hoff's equation given as **equation 4.8** .

$$Ks = \left(\frac{\text{Number of moles of the solvent absorbed at equilibrium}}{\text{Mass of the vulcanizates}}\right) \qquad \textbf{(Eq: 4.7)}$$

$$Log\ K_s = \left(\frac{\Delta S}{2.303R}\right) - \left(\frac{\Delta H_s}{2.303RT}\right) \qquad \textbf{(Eq: 4.8)}$$

The values of ΔH_S, ΔS and ΔG_S obtained for NBR and chlorinated NBR with different chlorine content in aromatic and industrial solvents are given in **table 4.7** and **4.8** respectively. The heat of sorption increased with increase in penetrant size which indicates Henry's mode of absorption is taking place in the modified rubber which is associated with the flexibility of linkages present in it [251]. The rigid C-C covalent bonds formed as a result of vulcanization hinder the flow of penetrant molecules and require more energy to generate sites to occupy for the molecules of solvent. Again, the ΔS values for all the solvents were positive. ΔS values are found to be decreasing with increase in the % of chlorine due to decrease in solvent diffusion.

The Gibbs free energy for sorption of petroleum fuels are calculated by the expression,

$$\Delta G_s = \Delta H_s - T\Delta S \qquad \textbf{(Eq :4.9)}$$

The negative value of Gibbs free energy indicates the sorption process is spontaneous. ΔG_s values are found to be increasing with increasing polarity of the rubber. That might be due to decrease in the spontaneity of the diffusion process through the matrix.

Table 4.7 ΔH, ΔS and ΔG values of NBR and Cl-NBR in aromatic solvents.

Samples	ΔH (KJ/mol)			ΔS(J/mol)			-ΔG(KJ/mol)		
	Benzene	Toluene	Xylene	Benzene	Toluene	Xylene	Benzene	Toluene	Xylene
NBR	1.20	1.29	1.37	37.32	35.8 2	33.97	9.996	9.456	8.821
Cl-NBR (15% Cl)	1.25	1.34	1.42	34.25	33.79	32.86	9.025	8.797	8.438
Cl-NBR (18% Cl)	1.29	1.39	1.48	33.18	32.93	31.17	8.664	8.489	7.871
Cl-NBR (22% Cl)	1.37	1.45	1.56	29.9	27.95	24.80	7.6	6.935	5.88
Cl-NBR (24% Cl)	1.31	1.40	1.51	31.26	31.98	29.82	8.068	8.194	7.436

Table 4.8 ΔH, ΔS and ΔG values of NBR and Cl-NBR in petroleum fuels

Samples	ΔH (KJ/mol)			ΔS(J/mol)			-ΔG(KJ/mol)		
	Petrol	Kerosene	Diesel	Petrol	Kerosene	Diesel	Petrol	Kerosene	Diesel
NBR	1.12	1.22	1.34	34.37	33.28	32.97	9.191	8.764	8.551
Cl-NBR (15% Cl)	1.19	1.26	1.36	33.55	32.04	31.86	8.875	8.352	8.198
Cl-NBR (18% Cl)	1.23	1.30	1.41	32.89	31.63	30.17	8.637	8.189	7.641
Cl-NBR (22% Cl)	1.28	1.38	1.46	28.74	26.45	23.08	7.342	6.555	5.464
Cl-NBR (24% Cl)	1.25	1.33	1.43	30.26	29.98	27.82	7.828	7.664	6.916

4.2.13.4 Transport mechanism

In rubbery polymers, the free volume, chain flexibility and unsaturation are important properties. The transport phenomenon is governed by Fick's diffusion laws. In order to find the transport mechanism, the results obtained from sorption experiment were fitted to the following equation

$$\mathrm{Log}\left(\frac{Q_t}{Q_\infty}\right) = \log k + n \log t \qquad \textbf{(Eq :4.10)}$$

Where *Qt is the* the mol% uptake of solvent at time *t* and Q_∞ is the mol% increase in sorption at equilibrium, *k* is a constant which depends on the structural characteristics of the polymer and its interaction with the solvent molecule.

The value of *n* denotes the mode of transport mechanism. The n can have values in between 0.5 and 1. For n=1, the mechanism of diffusion is said to be non Fickian and then the rate of relaxation of polymer chain is slower than diffusion of solvent molecules. For the Fickian mode the value of n is 0.5 and this indicates a rapid chain relaxation process occur in the elastomer as compared to rate of diffusion of permeant molecule into it. If the value of n lies in between 0.5 and 1, then the rate of relaxation of elastomer chain and rate of diffusion of solvent molecules are similar and mechanism of transport is said to be anomalous. **Table 4.9** and **4.10** shows the values of n and k for the bare NBR and modified NBR with different extent of chlorination obtained by

regression analysis of log (Qt/Q∞) against log t. The n value of NBR is closer to Fickian behaviour while that of chlorinated samples shows the mechanism of diffusion is deviating from Fickian. That is the values of n increase with increase in the percentage of chlorine content and lies in between 0.5 and 1 which indicate that the transport mechanism is changed from Fickian to anomalous mode. Thus as a result of chlorination, diffusion and the sorption rate of solvents through the NBR matrix become comparable. Further the decrease in k value with increase in chlorination suggests the reduced interaction of elastomer chains with the solvent molecules.

Table 4.9 n and k values of NBR and Cl-NBR in aromatic solvents at room temperature

Samples	Benzene		Toluene		Xylene	
	n	k (min^{-1})	n	k (min^{-1})	n	k(min^{-1})
NBR	0.51	0.29	0.52	0.26	0.55	0.24
Cl-NBR (15% Cl)	0.57	0.23	0.61	0.21	0.64	0.19
Cl-NBR (18% Cl)	0.62	0.18	0.69	0.18	0.71	0.16
Cl-NBR (22% Cl)	0.77	0.12	0.80	0.10	0.82	0.08
Cl-NBR (24% Cl)	0.69	0.14	0.74	0.12	0.78	0.10

Table 4.10 n and k values of NBR and Cl-NBR in petroleum fuels at room temperature

Samples	Petrol		Kerosene		Diesel	
	n	k (min^{-1})	n	k (min^{-1})	n	k (min^{-1})
NBR	0.39	0.28	0.47	0.26	0.52	0.22
Cl-NBR (15% Cl)	0.44	0.24	0.56	0.24	0.66	0.21
Cl-NBR (18% Cl)	0.62	0.24	0.61	0.19	0.68	0.17
Cl-NBR (22% Cl)	0.74	0.17	0.79	0.13	0.78	0.13
Cl-NBR (24% Cl)	0.69	0.15	0.66	0.15	0.72	0.11

4.2.14 Crosslink Density Measurements

Most of the properties of rubber depend on the degree of crosslinking present in it. Since modified rubber is characterized with both covalent and non-covalent bonding, the observed solvent uptake behaviour might be related with the crosslink distribution in the matrix. Therefore, the network density is determined in terms of the average molar mass between rubber segments situated between two cross-links (Mc) using Flory-Rehner equation given as

$$Mc = -\left(\frac{\rho_p V_s (V_r)^{1/3}}{\ln(1 - Vr) + V_r + \chi (Vr)^2} \right) \qquad \textbf{(Eq: 4.11)}$$

Where ρ_p is the density of the elastomer, Vs is the molar volume of the solvent and Vr is the volume fraction of vulcanizates in the fully swollen state. Vr gives the degree of tortuosity of solvent molecule which is actually depending on the orientation of rubber chains. It can be calculated by the formula

$$Vr = \frac{(d - fw)(\rho_r)^{-1}}{(d - fw)(\rho_r)^{-1} + A_0(\rho_s)^{-1}} \qquad \textbf{(Eq: 4.12)}$$

χ is the polymer-solvent interaction parameter computed as

$$\chi = \beta + \frac{V_s}{RT}(\delta_s - \delta_p)^2 \qquad \textbf{(Eq: 4.13)}$$

Where β is the lattice constant (0.34), Vs is the molar volume of the solvent, R is the universal gas constant, T is the absolute temperature (300 K), δs is the solubility parsssameter of the solvent and δp is the solubility parameter of polymer

From these the degree of crosslinking (υ) can be directly evaluated by the Equation

$$\upsilon = \frac{1}{2Mc} \qquad \textbf{(Eq : 4.14)}$$

Table 4.11 gives the values of Mc and crosslink density of NBR and its chlorinated derivatives with different level of chlorination using petrol as solvent. It can be seen from the table that the Mc values noticeably decreases with increase in the extent of chlorination up to the sample having 22% chlorine content. This decrease in Mc value suggests that the number of crosslinks per unit volume is highest for Cl-NBR (22% Cl) and hence has highest crosslink density value. Thus the better distribution of crosslinks supports the least capability of Cl-NBR (22% Cl) to accommodate the solvent molecules in it. This can be explained in terms of the

increased strength of dipolar interaction due to the presence of chlorine content between adjacent chains. This will decrease the segmental mobility and free volume inside the elastomer so that they may admit considerably less amount of solvent molecule to penetrate through it [178, 252, 253].

Table 4.11 Mc and υ values of NBR and Cl-NBR with different content of chlorine in petrol.

Samples	Mc (g/mol)	υ(g-1mol)
NBR	460.05	10.87×10^{-4}
Cl-NBR (15% Cl)	435.51	11.48×10^{-4}
Cl-NBR (18% Cl)	416.00	12.02×10^{-4}
Cl-NBR (22% Cl)	373.03	13.40×10^{-4}
Cl-NBR (24% Cl)	408.02	12.25×10^{-4}

4.3. Conclusions

Highly polar elastomer was successively prepared from NBR by the alkaline hydrolysis of chloroform using phase transfer catalyst. The amount of chlorine content attached to the macromolecular chain was quantitatively estimated. The ^{1}HNMR spectrum gives additional signals for methylene hydrogen due to the addition of dichlorocarbene in NBR. The FTIR spectrum of chemically modified NBR showed the characteristic absorption peak of C–Cl and cyclopropyl ring. The attachment of chlorine in the backbone of NBR was confirmed from UV-Vis spectroscopic

studies through the shift and broadness of the absorption peak as compared with pure NBR. The decrease in amorphous nature and the changes in morphology of Cl-NBR were confirmed from XRD and SEM analysis. The results from DSC showed the higher *Tg* of Cl-NBR than NBR, and the *Tg* value increased with the increase in level of chemical modification. The thermal stability of NBR decreases with increase in chlorine content while the flame resistance of Cl-NBR increased with the level of chemical modifications. Chemically modified NBR showed an enhancement in rheometric torque and optimum cure time. Mechanical properties such as tensile strength, tear resistance, and hardness were increased by the attachment of chlorinated segment in NBR. The chemical functionalization improved the AC conductivity of the unmodified NBR and the conductivity increased with increase in chlorine content over the whole frequency range due to combined effect of increased hopping probability and crosslink density in the elastomer. The dielectric constant and loss tangent shows similar behavior and the increase of dielectric properties with the increase in chlorination is attributed to interfacial polarization and space charge distribution in the macromolecule. The noticeable result obtained from the study is that chlorination significantly enhanced the oil resistance property of virgin NBR, especially hot oil resistance. The interaction of petroleum fuels and aromatic solvents with the modified samples was investigated. The solvent uptake tendency decreases up to sample containing 22% chlorine content and then increased. The change in transport properties such as

diffusion, sorption and permeation coefficients of these solvents also showed the same trend which can be correlated with the crosslink density calculated using Flory-Rehner theory. Thus, it can be concluded that the chemically modified NBR showed excellent tensile strength and oil and flame resistance than NBR, and hence, it can be used as a substitute in NBR in various applications such as pump diaphragms, oil seals, aircraft hoses, oil-lined tubing, and gasket materials.

5.1 Introduction

Over the last two decades nanocomposites open a new perspective in the field of science to upgrade the structural and functional properties of existing polymers. The inherent high surface area of nanomaterials increases their dispersion capability in the matrix which offers ample scope for the improvement in properties as compared to conventional micro and macro composites. There have been many investigations dedicated to processing of thermoplastic elastomer based composites with enhanced performance without recourse to expensive synthesis procedures. Also, earlier studies on this topic have indicated that the physical and chemical interaction of the fillers with the rubber matrix, the crosslinking chemistry of rubber, nature of nanofillers are the key factors which affect the processability and performance of the elastomeric nanocomposites. It is a great task to configure appropriate density of crosslinking networks in a material because it determines the elasticity, mechanical reinforcements and solvent resistance of rubbers. It was reported that noncovalent chemical bond and supramolecular interactions such as metal ion crosslinking, electrostatic attractions etc seem to improve the properties of elastomer based composite [60,254-256].

A number of papers have been published on NBR based composites using various kinds of nanofillers such as nanoclay, nanosilica, nanocalcium carbonate, carbon nanotube etc. Composite of NBR with waste dispersion phases from the

extraction metallurgy like electrostatic precipitator powder from a sinter plant can be used for production of protective materials against influence of electromagnetic waves, reported by Grigorova et al [257]. In majority of these works the effective reinforcement is achieved by the surface modification of fillers with organo modifiers through ion exchange reactions since the strong interparticle interaction in nanomaterials due to high surface energy and the hydrophobicity of rubber is not favorable for blending of these two phases [258]. Reported studies on matrix modified elastomer composites are scarce. Previous studies revealed that the polarity and hydrophilicity of elastomer surface can be considerably improved by a simple and inexpensive chlorination and result in a product with enhanced chemical and mechanical properties. The chloro group will increase the compatibility of filler with the matrix [178].

Higher demand of environmental protection along with new technology and business opportunities leads a continuous increase of research on bioresorbable polymer nanocomposite [259]. There are a lot of reports based on polymer/HA composite materials [260]. Dong et al investigated the thermal properties and flame retardancy behaviour of polycarbonate/ hydroxyapatite nanocomposite [261]. Bhomik et al studied the load carrying behaviour of polymer and response of interfaces when load is applied in ex-situ HA composites using MD and SMD simulations [262]. Scratching test results indicated that the as-alloyed HA

composite coatings exhibit improved wear resistance and lower friction coefficient with increasing the amount of CNTs in the precursor material powders, reported by Chen et al [263].

This chapter focuses the fabrication of novel Cl-NBR (22%Cl)/HA nanocomposites by a simple, inexpensive two-roll mixing technique. The formation, structural characterization, morphology, and thermal behavior of new Cl-NBR/HA nanocomposites were done by Fourier transform infrared spectroscopy (FTIR) and UV–VIS spectroscopic techniques, X-ray diffraction (XRD), scanning electron microscopy (SEM), thermogravimetric analysis (TGA), and differential scanning calorimetry (DSC). The electrical properties such as AC conductivity, dielectric constant, and dielectric loss tangent were also evaluated with respect to the different loading of the nanoparticles. Moreover, this work demonstrates the effect of nano hydroxyapatite on mechanical, oil resistance and solvent diffusion properties of chloro functionalized NBR.

5.2 Results and Discussion

5.2.1 FTIR Spectroscopy

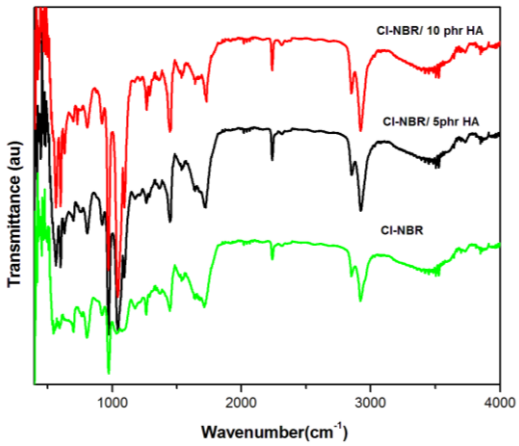

Figure 5.1 FTIR spectra of Cl-NBR and Cl-NBR/HA nanocomposites

The chemical structure characteristics of Cl-NBR/HA nanocomposites with different concentrations of HA nanoparticles were identified by Fourier Transform Infrared (FTIR) Spectroscopic measurement and given in **Figure 5.1**. The IR spectrum of Cl-NBR shows characteristic bands corresponding to the nitrile group, butadiene segment and dichlorocarbene groups. That is chlorinated NBR shows absorption peaks at 801cm^{-1}(assigned to C–Cl stretching vibration), 1062 cm^{-1} (corresponding to cyclopropyl ring) along with significant absorption at 2239 cm^{-1} characteristic of –CN stretching vibration and at 972 cm^{-1} and 692 cm^{-1} corresponding to –CH stretching vibration of cis and trans counterparts of butadiene segment respectively [180]. As it is

given in the previous chapter, the -OH stretching and bending vibrations of hydroxyapatite nanoparticles are present at 3,376 cm^{-1} and 633 cm^{-1} due to OH stretching and OH bending vibrations respectively. The υ1, υ2, υ3, and υ4 vibration modes of phosphate group present in HA are obtained at 964, 470, 1045, 569, and 604 cm^{-1} respectively [206]. The FTIR peaks of the Cl-NBR/ HA nanocomposites are manifested by most of the peaks present in both Cl-NBR and HA nanoparticles with slight shift in IR bands. In the case of nanocomposites, it is to be noticed that there is a decrease in intensity of the OH stretching peak at 3,376 cm^{-1} and also a partial shift in the bending vibration from 633 to 625 cm^{-1}. It signifies the formation of better dipolar interaction between the OH of nano HA with the polar groups present on chlorinated rubber surface which decreases the strength of IR absorption. These observations would shed light on the incorporation of hydroxyapatite nanoparticles on the surface of chlorinated NBR chains and its schematic representation is given in **Scheme 5.1**.

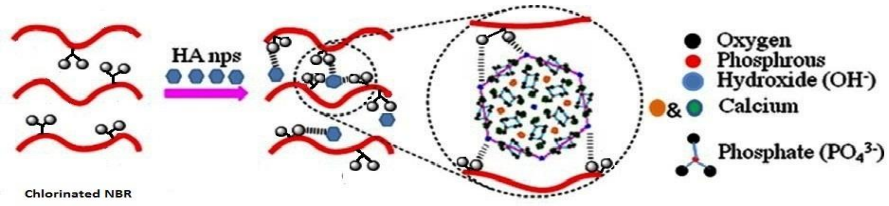

Scheme 5.1 Schematic representation of the interaction of Cl-NBR with hydroxyapatite nanoparticles.

5.2.2 X-ray diffraction Analysis (XRD)

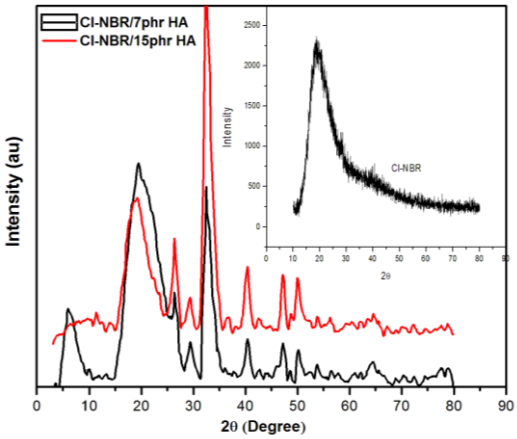

Figure 5.2 XRD patterns of Cl-NBR and Cl-NBR/HA nanocomposites

X-ray diffraction patterns indicate the state of dispersion of nano HA in the chlorinated rubber matrix. **Figure 5.2** represent the XRD pattern of Cl-NBR nanocomposites with different loading of HA nanoparticles. The main peaks of synthesized HA appeared at $2\theta = 25.7^0$, 31.6^0, 32.7^0, 34.1^0, 39.7^0, 46.6^0, 49.5^0 and 53.09^0 corresponding to the crystal planes 002, 211, 300, 202, 310, 222, 213, 321, 004 respectively. Also chlorinated NBR shows a broad diffraction peak at 19.85^0. From the plots, it can also be observed that the nanocomposite contain broad diffraction peak of Cl-NBR along with the peak corresponding to (002), (300), (310), (222) and (213) crystal planes of HA with a slight deflection to 26.4^0, 32.4^0, 40.3^0, 47.3^0, 49.8^0. From the result it is to be highlighted that both HA and nanocomposites exhibit a high intense peak but that peak in HA at $2\theta = 31.6^0$ (assigned to 211 plane) is shifted to 32.4^0 (assigned to (300) plane of HA) in the nanocomposite which is a

clear evidence for the intercalation of HA nano particles in to the macromolecular chain of Cl-NBR due to the dipolar interaction between the chlorinated butadiene segments of NBR and –OH group of nano filler. As far as the broad peak is concerned, the angle of diffraction is present at $2\theta = 19.47^{o}$ corresponding to an interlayer spacing of 4.55 A^{o} and $2\theta = 19.2^{\circ}$ corresponding to a gallery gap of 4.61 A^{0} for Cl-NBR with 7 and 15 phr HA respectively. Further, the peak width at half of the maximum is considerably reduced with increase in the phr of HA which confirm the narrow size distribution of the nanoparticles in the elastomer matrix. These results suggest that the nanoparticles act as a nucleating agent for the improved crystallinity of chlorinated NBR matrix.

5.2.3 Scanning Electron Microscopy (SEM)

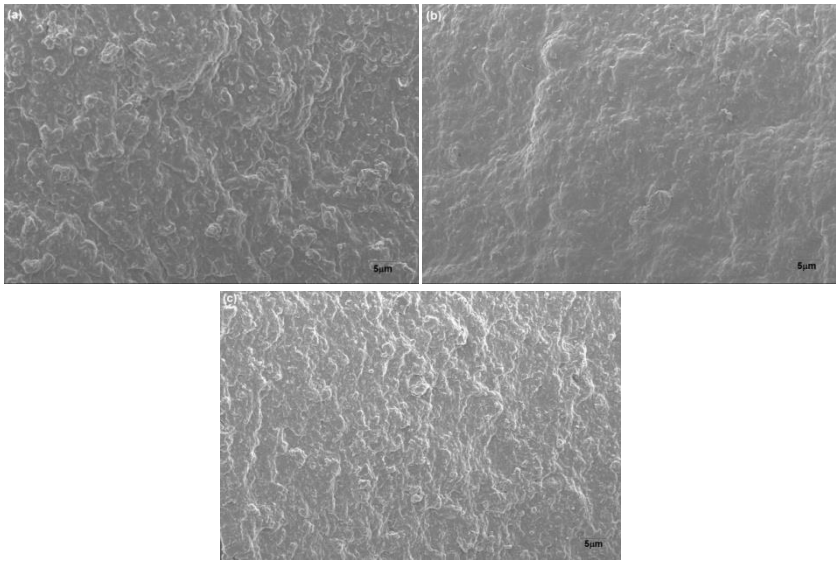

Figure 5.3 SEM images of a) Cl-NBR/ 5phr HA b) Cl-NBR/ 7phr HA c) Cl-NBR/ 15phr HA

The morphology of the fabricated composite materials was evaluated by using scanning electron microscopy. In **Figure 5.3**, the SEM micrographs of Cl- NBR and representative images of the Cl-NBR nanocomposite with 5, 7 and 15 phr of HA are displayed. It is reported that chlorination of the matrix induces surface roughening which is paralleled by reduction in surface friction. From the micrograph, it can be visible that at lower loading of the filler the nanoparticles are more dispersed in the jaggy matrix with relatively lesser stacks of HA while the surface uniformity is somewhat changed as the concentration of filler increased . In addition to the polar interaction between the chlorine attached to the rubber matrix and –OH of the filler, the rough surface of Cl-NBR with increased surface area also can provide more sites for interlocking of the HA particles. This will enhance the homogenous distribution of nanoparticles on the polar rubber. However, as the loading of nanoparticles increases, more and more stress is developed in the composite material with an initiation of flocculation tendency for the nanoparticles as seen in the SEM image of Cl-NBR/ 15phr HA. This is due to the strong interparticle interaction through hydroxylated edge which will extend the interface and the increased domain size will decrease the interfacial interaction between matrix and filler. These agglomerated HA heaps gave rise to the greater number of peaks as observed in the XRD pattern of Cl-NBR/ 15phr HA.

5.2.4 Thermal Behaviour

5.2.4. a Differential Scanning Calorimetry (DSC)

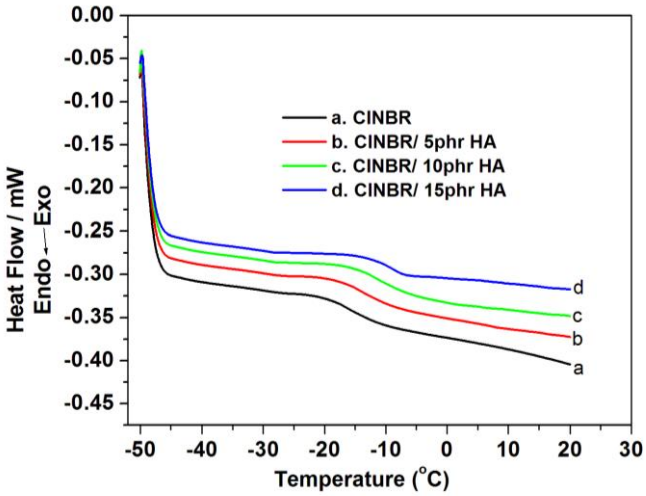

Figure 5.4 DSC thermograms of Cl-NBR/ HA nanocomposites

The segmental motion of elastomer chain can be characterized by evaluating its glass transition temperature (*Tg*) which is strongly depend on the strength and nature of interfacial interaction present in the composite. The *Tg* values are determined from DSC measurement for Cl-NBR and Cl-NBR/HA nanocomposites with different content of HA presented in **Figure 5.4**. It can be seen that the glass transition temperature value move to higher temperatures with an increase in filler concentration in the polymer. That is, *Tg* of Cl-NBR is -18.7^{0}C while Cl-NBR containing 5, 10 and 15 phr HA nanoparticles shows *Tg* at − 15.4, − 13.6 and − 11.25^{0}C respectively. The large increase in *Tg* indicate a substantial confinement effect of nano HA particles on the

segmental motion of Cl-NBR chains. This may be due to the increased chain packing density which in turn decreases the free volume inside the matrix due to strong adhesion through polar attraction at the interface [264].

5.2.4. b Thermogravimetric Analysis (TGA)

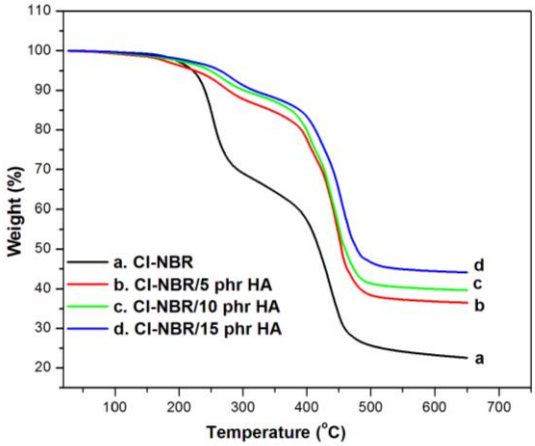

Figure 5.5TGA thermograms of Cl-NBR and Cl-NBR/HA nanocomposites.

In TGA, the loss in weight after decomposition due to the formation of volatile product is monitored as a function of temperature. The TGA curves of Cl-NBR and Cl-NBR/HA nanocomposites with different contents of HA are given in **Figure 5.5**. The non oxidative degradation trend of nanocomposites is similar to that of neat Cl-NBR. That is all the samples show two-step decomposition process whereas the Cl-NBR/HA nanocomposite samples start to degrade at a higher temperature than that of pure rubber matrix with the increase of heating as seen

in thermograms. This is due to the homogeneously incorporated hydroxyapatite nanoparticles having high aspect ratio may hinder the thermal degradation of rubber in the earlier stages of decomposition by acting as a superior insulator. The significant weight loss delay can also be attributed to intimate contact between rubbers and HA through polar attraction which may slow down the volatilization as well as assist the formation of char after decomposition. The volatile products generated retard the diffusion of oxygen into the polymer matrix and shift the decomposition to higher temperature at the early stages of decomposition and thus increases the thermal stability of the nanocomposites [265].

5.2.5 Cure characteristics

Table 5.1 summarize the cure parameters derived from the rubber process analyzer such as maximum torque (M_H), minimum torque (M_L), scorch time (ts_2), and optimum cure time (t_{90}) with respect to the amount of filler for the fabricated composites. The maximum torque (M_H) value gives a clue about the network density and thus the nature of reinforcement of filler in the polymer matrix. A dramatic increase in M_H value is observed for the nanocomposites with increase in HA content as compared to pristine Cl-NBR. This increase in rheometric torque directs to the increase in the shear modulus of the composites due to the interaction of nanoparticles which in turn increases the rigidity of the vulcanizates. As far as the nanocomposite is concerned, the

magnitude of M_H increases up to the sample containing 7phr HA and thereafter a slight decrease is observed. That is Cl-NBR/ 7phr HA, which contributes higher reinforcing efficiency in the elastomer matrix.

Table 5.1 Processing characteristics of Cl-NBR and Cl-NBR/HA nanocomposites

Samples	Cure time t_{90} (min)	Scorch time t_2 (min)	Maximum Torque (dNm)	Minimum torque (dNm)
Cl-NBR	16.5	3.26	25	4.5
Cl-NBR/ 3 phr HA	15.4	3.15	28	5.2
Cl-NBR/ 5 phr HA	14.6	2.91	31	6.4
Cl-NBR/ 7 phr HA	13.5	2.65	35	8.5
Cl-NBR/ 10 phr HA	12.3	2.44	34	8.3
Cl-NBR/ 15 phr HA	11.6	2.18	32.9	7.8

Upon further increase in HA loading, forms aggregation of nanofillers at few spots at the interface of the two phases. Since M_L value is related to the viscosity, it can be deduced that the nano HA particles certainly increases the viscosity of nanocomposites. This is due to the dispersed filler decreases the mobility of macromolecular chains of the matrix. The scorch time and optimum cure time shows a decreasing trend with increase in

concentration of filler in Cl-NBR. That is on addition of hydroxyapatite the system gets more heated due to the friction created by the generation of higher degree of cross linking. The good number of polar chlorine and hydroxyl groups may promote the adsorption of curatives which also leads to decrease in both t_{90} and t_2 [135].

5.2.6 Mechanical Properties

Cl-NBR/ nano HA matrices under different ratios of filler content was subjected to mechanical testing and the variation is studied with respect to pristine Cl-NBR. As it is known, the tensile strength is the micro voids initiated catastrophic tearing of cracks at the surface of the samples.

Table 5.2 Mechanical properties of of Cl-NBR and Cl-NBR/HA nanocomposites

Samples	Tensile strength (MPa)	Elongation at break (%)	Tear strength (kN/m)	Hardness (Shore A)
Cl-NBR	8.95	204	23.48	47
Cl-NBR/ 3 phr HA	12.31	194	27.81	48
Cl-NBR/ 5 phr HA	16.12	188	29.69	49
Cl-NBR/ 7 phr HA	20.98	179	33.11	50
Cl-NBR/ 10 phr HA	19.19	164	31.55	52
Cl-NBR/ 15 phr HA	17.67	151	29.12	54

From the table (**table 5.2**) it can be observed that there is a momentous increase in tensile strength for the nanocomposites compared to bare rubber, as expected. Since the mechanical strength of elastomers is a function of the polarity of the rubber, the nature of the filler and their mutual interaction, the nano hybrid shows higher strength due to higher glass - transition temperature and increased compatibility between Cl-NBR chains and the nano-fillers via dipolar interaction between chloro and hydroxyl groups. In the case of nanocomposites, the incorporation of filler gradually increases the tensile properties up to the sample containing 7phr of nano HA and then decreases. This may be due to the effective reinforcement of filler-elastomer interaction occurs up to Cl-NBR/ 7phr HA so that the input energy is dissipated through the elastomeric network and less elastic energy will be available to break the adhered Cl-NBR/HA network. Above 7phr loading the interparticle interaction predominates over rubber–filler interactions consequently, uniform distribution of stress throughout the matrix is disrupted. Tear strength (given in **table 5.2**) also shows a similar trend as that of the tensile strength. That is the inclusion of structured HA increases stiffness and resistance to fracture because they interact more intensely with the elastomer by making use of the higher surface area. This will result in the effective orientation of polar Cl-NBR chains in the direction of strain upon loading. **Table 5.2** also displays the percentage

elongation at break and hardness of filled and unfilled Cl-NBR matrix. In view of the fact that the insertion of nano filler resists the deformations of the macromolecular chains due to better interfacial adhesion between filler and matrix to a greater extent, the elongation at break continuously decreased with the incorporation of nanoparticles up to 7phr loading. The hardness of nanocomposites and gum vulcanizates show a consistent increase with filler loading due to the increased physical and chemical interlocking between filler and matrix which can give raise to a three dimensional net work structure [79, 266].

5.2.7 Electrical Properties

5.2.7.1 AC Electrical Conductivity

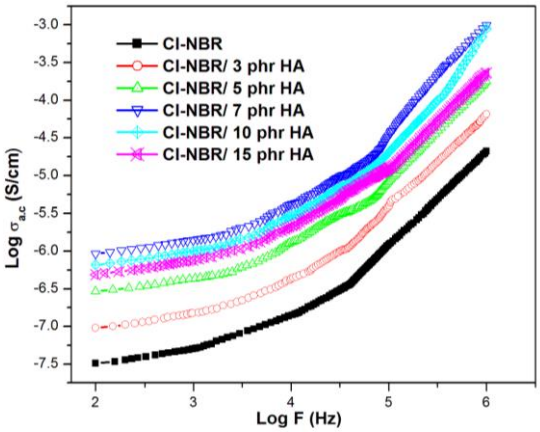

Figure 5.6 AC conductivity of Cl-NBR and Cl-NBR /HA nanocomposites

The variation of σ_{ac} of Cl-NBR and Cl-NBR/HA nanocomposites with frequency of applied electric field is shown in **Figure 5.6**. The conductivity patterns show a dispersion behaviour as the frequency applied in the experiment increases and also there is a tremendous increase in the ac electrical conductivity with increase of filler loading. It has been explained previously that the major factor responsible for the conductivity of composite is electron tunneling mechanism which in turn directly related to polarity of polymer matrix, the conductivity of filler and the characteristic of conductive network formed. Here, the chloro functionalized NBR contain a number of localized polar dichlorocarbene groups in addition to the nitrile group and the dipoles associated with these groups strongly interact with hydroxyl group of HA nano particles. The effectively confined HA particles within the macromolecular chain will facilitate the formation of three dimensional electro conducting pathways through the interface charge polarization due to dipolar attraction of matrix and filler. Thus the enhanced conductivity at higher frequencies can be attributed to the increased probability for the correlated forward–backward hopping of charge carriers through the dense network of macromolecular hybrid. Also, there will be some intrinsic electric polarizations due to the individual dipoles connected to the polar segments of both matrix and filler. Furthermore, polarized system formed will hamper the filler aggregation and favor its better dispersion in the rubber matrix up to 7phr. Further increase in concentration of HA will disturb better

ordering of the macromolecular chain due to agglomeration of the nanoparticles. So the interfacial and intrinsic polarization, both enhances the AC electrical conductivity of nanocomposites [267, 268].

5.2.7.2 Dielectric Constant

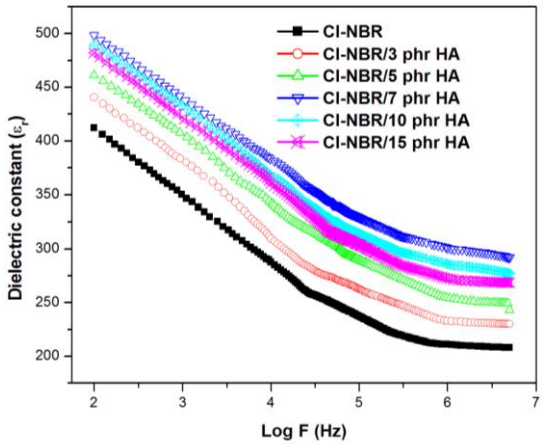

Figure 5.7 Dielectric constant of Cl-NBR and Cl-NBR /HA nanocomposites

Dielectric measurement detects the fluctuation of dipoles derived from atomic, electronic, interfacial and orientation polarizations. **Figure 5.7** compares the variation of relative dielectric constant ($\in_r$) with frequency for Cl-NBR and Cl-NBR/HA nanocomposites having different loading of HA at room temperature. It is obvious that, at lower frequency region a strong dispersion of permittivity is observed while at higher frequency $\in_r$ become nearly constant. The sharp decrease in dielectric constant with increase in frequency may be attributed to the electrical

relaxation processes which are a result of the lag in the orientation polarization. That is the orientation of dipoles belonging to different polar groups takes more response time to reach the equilibrium static field compared with electronic and atomic polarizations. Certainly, the Cl-NBR/HA nanocomposites show higher dielectric value than the corresponding bare Cl-NBR matrix. This may be due to the presence of large number of permanent dipoles spontaneously following the direction of the polarization which increases with the increase in filler content. The addition of HA enhance the interfacial polarization due to the diverse structure of nanocomposites, also contributed to the increased dielectric constant [269].

5.2.7.3 Dielectric loss (Tanδ)

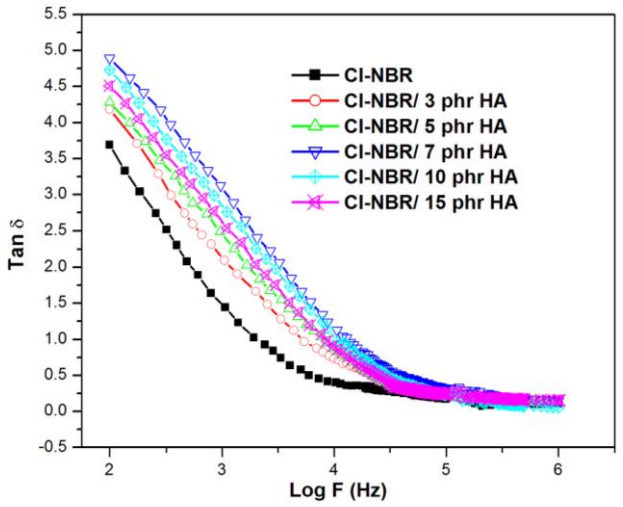

Figure 5.8. Dielectric loss of Cl-NBR / HA nanocomposites

It is generally believed that dielectric data of elastomer nanocomposite provides information on correlated local motion of their backbone. **Figure 5.8** shows the variation of dielectric loss with frequency of Cl-NBR and Cl-NBR/HA nanocomposites having different loading of HA at room temperatures. It is found that the abrupt change in loss tangent is very sharp at lower frequencies similar to the variation of dielectric constant. The higher dispersion of dielectric loss at low frequency is attributed to the easy flow of charge carriers within the materials due to their low inertia and binding forces between the molecules. Beyond a certain critical frequency the exchange energy of dipoles connected with electric charge carriers in the system cannot follow the alternation of applied AC frequency. Specifically, being a function of relaxation process dielectric loss increases with increase in filler loading due to interfacial polarization. The difference in conductivity of Cl-NBR and HA leads to local displacement of electrons in the direction of applied electrical field which induces polarization at the anchoring region of filler and matrix. The conductive network thus formed will allow easy motion of trapped charge carriers through the electrically heterogeneous system so that tan δ shows a slight decrease after sample containing HA above 7phr [210].

5.2.8 Oil resistance measurement

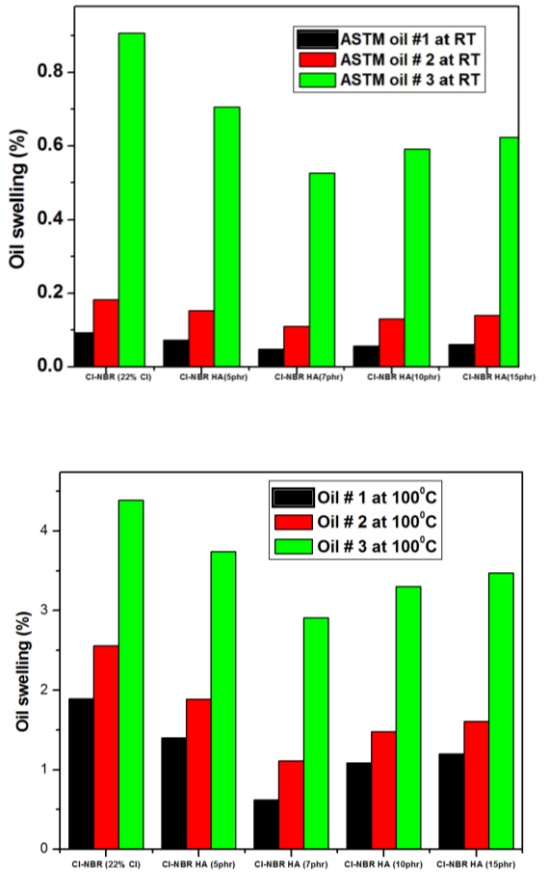

Figure 5.9 ASTM oil resistance of Cl-NBR and Cl-NBR /HA nanocomposites

One of the key characteristics of NBR rubber that made it to be used in seal applications is its oil resistance property which is closely related to its molecular structure. In our previous studies, it was found that the chlorinated NBR shows much better oil resistance than NBR due to increased polarity and cross-linking

density induced by the dichlorocarbene group. **Figure 5.9** compares the ASTM oil swelling percentage of Cl-NBR and its nanocomposites with different contents of HA at room temperature and 100^0C. A sharp decrease in the swell with the addition of HA up to 7phr is observed and the rate of decrease lessens at higher concentrations. This can be explained on the basis of increased number of crosslinks formed through the intermolecular interaction due to the polarity of Cl-NBR, by chlorine and acrylonitrile content and the polarity of HA, by hydroxyl content. As the intermolecular forces increased the energy required to separate all the molecules (Cohesive energy density) in the samples for the diffusion of oil molecules become stronger and thus leading to a reduction in mass swell of the nanocomposites. Resistant to the oil attack decreases due to the softening of polymer matrix at elevated temperature so that the penetrants can easily diffuse in to the thermally relaxed sample matrix. As might be expected, Cl-NBR/ 7phr HA shows the maximum oil resistance at 100^0C also. Besides, it can be seen that the all samples exhibit higher swelling resistance in ASTM oil 1 than in oil 2 and 3. That is the viscosity and aniline point of penetrating oils greatly influence its diffusion through the samples. The volume swelling continued to increase with decrease in viscosity and increase in aromatic content of the oil [229, 247].

5.2.9 Diffusion Studies

5.2.9.1 Mol % uptake of aromatic solvents and petroleum fuels

Nitrile rubber is well known for its use in lip seal application due to the high polarity of elastomer. For more technological applications, it is necessary to improve fuel permeation properties of NBR by introducing additional polar functional group into it. The transport behavior through the elastomer materials depends on the nature of filler, interfacial interaction and morphology of the system, temperature etc. The effect of nano hydroxyapatite in the chloro functionalized NBR nanocomposites on the transport properties were characterized by their swelling behavior in aromatic solvents such as benzene, toluene and xylene and industrial solvents such as petrol, kerosene and diesel. The solvent sorption of Cl-NBR/HA nanocomposites was assessed by calculating their mol percentage uptake (Q_t) using the **equation 4.2**

Effect of filler loading

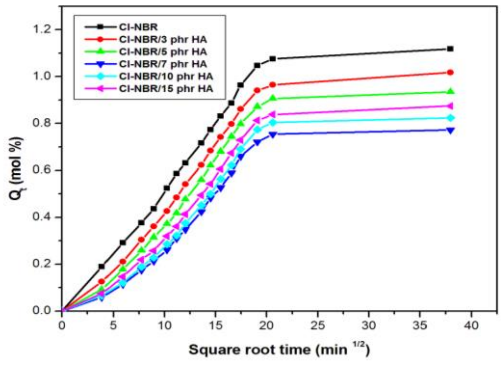

Figure 5.10 (a) Mol % uptake of Cl-NBR and Cl-NBR /HA nanocomposites in benzene

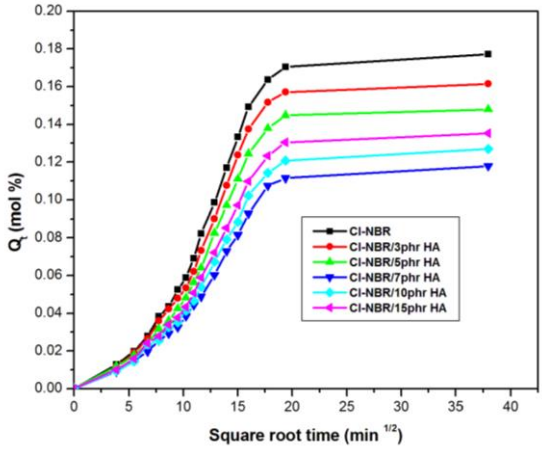

Figure 5.10 (b) Mol % uptake of Cl-NBR and Cl-NBR /HA nanocomposite in petrol

Figure 5.10 (a) and (b) represent the sorption curves (Q_t Vs. $\sqrt{t}$) of petrol and benzene through Cl-NBR/HA nanocomposites for varying nanoapatite content, respectively. It is clearly seen from all the curves that, an initial increase in the solvent uptake due to large concentration gradient of the solvent and the mass of the absorbed solvent levels off near the saturation equilibrium. Also, the percentage weight gain is too reduced with increase in concentration of filler for the nanofilled composites compared to chlorinated rubber. The decreased sorption of the filled composites can be explained in terms of homogenous dispersion of apatite nanoparticles in the rubber matrix. The strong polar interaction at the interface in addition to the C-C covalent bond formed as a result of DCP vulcanization restricts both the local segmental mobility and long range movements of rubber chain which may create tortuous path for the transport of the penetrant molecules.

Further, it is to be noticed that beyond 7 phr loading the solvent uptake increased slightly which indicate the effective reinforcement in the composite occurs up to 7 phr of filler content. This is due to the formation of agglomerates of nano hydroxyapatite which is evident from the SEM micrographs. The trend remains the same for both aromatic and industrial solvents under study [270, 271].

Effect of penetrant size

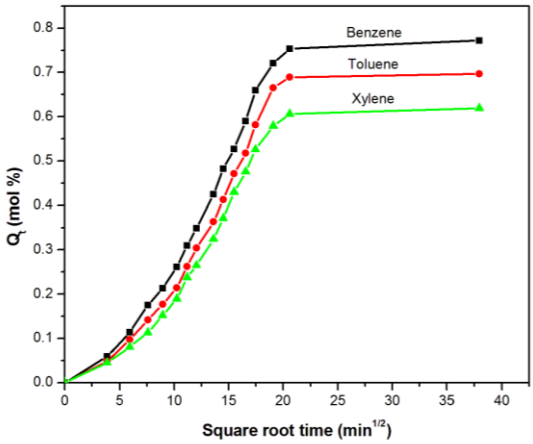

Figure 5.11 (a) Solvent uptakes of Cl-NBR/7 phr HA in different aromatic solvents

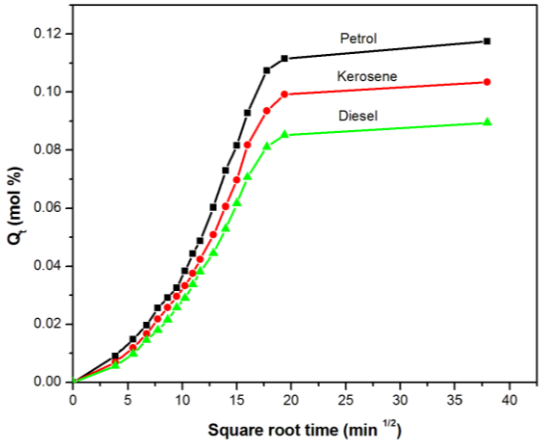

Figure 5.11 (b) Solvent uptakes of Cl-NBR/7 phr HA in different petroleum fuels

Solvent properties such as structure, molecular weight and polarity seem to exert a considerable effect on sorption phenomena. **Figure 5.11 (a)** presents the percentage uptake of petrol, kerosene and diesel by Cl-NBR/7 phr HA. For instance, petrol shows higher sorption than that of kerosene and diesel and the equilibrium sorption trend observed in the order petrol > kerosene > diesel. In the case of aromatic solvents, depicted in **Figure 5.11 (b)**, the sorption trend is in the order benzene > toluene > xylene. This can be explained on the basis of size and molecular weight of probe molecules. The molar volume of petroleum fuels taken follows the order petrol < kerosene < diesel while aromatic solvents follow the order benzene < toluene< xylene. As said by free volume theory, the penetration of molecules primarily depends on the free volume inside the matrix so that the penetrants can easily exchange the position of polymer chain segments. As the penetrant size

increases, the exchange of chain segments become difficult and needs more energy, particularly in the case of filled matrices [272].

Effect of Temperature

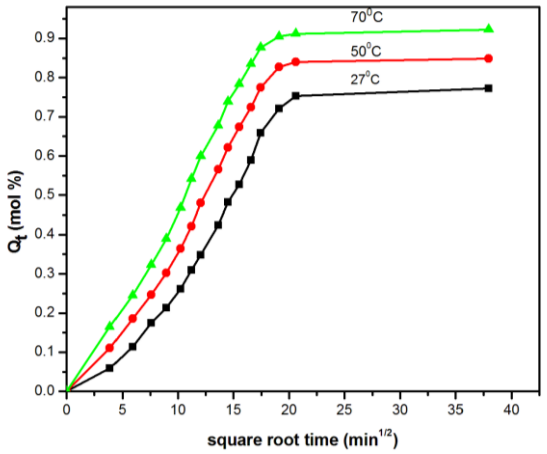

Figure 5.12(a) Solvent uptakes of Cl-NBR/7 phr HA in benzene at different temperature

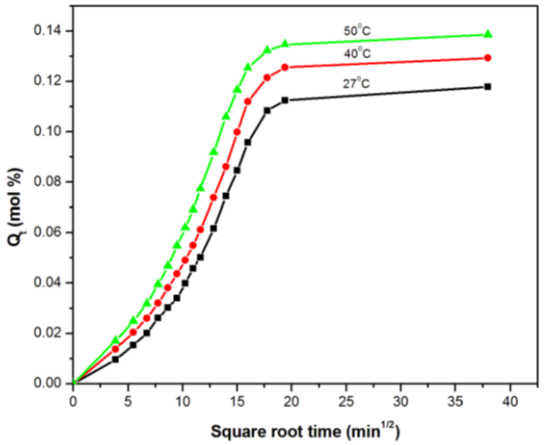

Figure 5.12 (b) Solvent uptakes of Cl-NBR/7 phr HA in petrol at different temperature.

The mol percentage uptake of nanocomposite containing 7phr HA is compared at various temperatures by conducting the experiments at 27, 50 and 70^0C for aromatic solvents and at 27, 40 and 50^0C in petroleum fuels. From the figures (**Figure 5.12 (a) and (b)**), it is obvious that the amount of solvent uptake and thus the diffusion rate increases as the temperature is increased. Similar behaviour is observed with other solvents also. This is due to the combined effect of increased segmental mobility of elastomer chain and kinetic energy of penetrant molecules. This will lead to the weakening of filler matrix adhesion and thus the voids generated will increase the free volume of the system.

5.2.9.2 Kinetic parameters

The transport properties such as diffusion, sorption and permeation coefficients were evaluated for the system under study to characterize the nature of interfacial interaction between Cl-NBR and HA.

Diffusion coefficient (D)

The diffusivity D of the nanocomposites was calculated using **equation 4.3.** The estimated values of D for the nanocomposites are given in **table 5.3** for aromatic solvents and **5.4** for industrial solvents**.** It is obvious from the table that the diffusion coefficient of nanocomposite is greatly reduced as compared to bare Cl-NBR matrix and a systematic decrease is observed up to the nanocomposite with 7 phr HA, after that a slight increase in

sorption is observed. The solvent diffusion through the nanocomposite materials is a kinetic parameter which depends on the concentration, orientation, size distribution and interaction of the filler with the matrix at the interface. The diffusion of probe molecules through a membrane occurs due to random motions of individual molecule**.** As the solvent molecule diffuse into the elastomer matrix the system will expand and weaken the molecular interaction between the chains. However, filler reinforced matrix restrict the chain flexibility. The evenly dispersed nanoparticles orient in a regular manner in the macromolecular chain which decreases the free space inside the system. Also, the high aspect ratio of the nanofiller ensures better interfacial adhesion which further reduces the D values for the nanocomposite. The minimum value of diffusion coefficient for the Cl-NBR/7 phr HA is attributed to its maximum reinforcement effect due to optimum crosslink density. Also, diffusivity decreases when going from petrol to diesel in case of fuels and benzene to xylene in case of aromatic solvents due to the increased molar volume.

Table 5.3 Diffusion, Sorption and Permeation values of Cl-NBR/HA nanocomposites in aromatic solvents.

Samples	Diffusion Coefficient D × 10^5 (cm^2/s)			Sorption Coefficient S			Permeation Coefficient P × 10^5 (cm^2/s)		
	Benzene	Toluene	Xylene	Benzene	Toluene	Xylene	Benzene	Toluene	Xylene
Cl-NBR	3.71	3.63	3.52	1.66	1.44	1.18	6.159	5.227	4.154
Cl-NBR/HA (3 phr)	3.63	3.51	3.44	1.52	1.35	1.07	5.518	4.738	3.681
Cl-NBR/HA (5 phr)	3.52	3.43	3.30	1.41	1.29	1.04	4.963	4.425	3.432
Cl-NBR/HA (7 phr)	3.21	3.14	3.09	1.37	1.19	1.01	4.398	3.737	3.121
Cl-NBR/HA (10 phr)	3.39	3.22	3.16	1.42	1.23	1.05	4.814	3.961	3.318
Cl-NBR/HA (15 phr)	3.42	3.25	3.19	1.45	1.26	1.07	4.959	4.095	3.413

Table 5.4 Diffusion, Sorption and Permeation values of Cl-NBR/HA nanocomposites in petroleum fuels.

Samples	Diffusion Coefficient $D \times 10^5$ (cm^2/s)			Sorption Coefficient S			Permeation Coefficient $P \times 10^5$ (cm^2/s)		
	Petrol	Kerosene	Diesel	Petrol	Kerosene	Diesel	Petrol	Kerosene	Diesel
Cl-NBR	3.12	3.09	3.06	1.61	1.38	1.04	5.023	4.264	3.182
Cl-NBR/HA (3 phr)	3.09	3.04	3.01	1.56	1.32	1.01	4.820	4.013	3.040
Cl-NBR/HA (5 phr)	3.01	2.93	2.89	1.51	1.28	0.99	4.545	3.750	2.861
Cl-NBR/HA (7 phr)	2.87	2.81	2.76	1.32	1.17	0.86	3.788	3.288	2.374
Cl-NBR/HA (10 phr)	2.92	2.89	2.85	1.38	1.23	0.96	4.029	3.555	2.736
Cl-NBR/HA (15 phr)	2.97	2.94	2.91	1.40	1.24	0.98	4.158	3.645	2.852

Sorption Coefficient (S)

The matrix- solvent interaction can also be determined in terms of sorption coefficient (S) which can be calculated using the **equation 4.4**. The S value obtained for equilibrium swelling data is presented in **table 5.3** and **5.4**. From the table, it can be seen that the sorption coefficient decreased with increase in the filler loading and the lowest value has obtained for nanocomposite containing 7phr HA.

Permeation Constant (P)

Since the permeation of the penetrant into an elastomer membrane is a combination of the diffusivity as well as sorptivity, the permeation coefficient (P) has been computed as the product of diffusion and sorption coefficients as

$$P = D \times S \qquad \textbf{(Eq: 5.1)}$$

The values obtained are also given in **table 5.3** and **5.4**. It is followed that P value also show the same trend as that of D and S with respect to filler loading and penetrant size. Sample with filler loading 7phr shows minimum permeability due to increased chain packing densities which decreased free volume available in the matrix to accommodate the penetrant molecules. However, above 7phr there was an increase in permeation due to aggregation of nanofiller which decrease the interfacial adhesion.

Arrhenius Parameters

From the temperature dependence of D, P and S, the activation energy needed for the process of diffusion, E_D or permeation E_P of solvent molecule were computed using Arrhenius **equation 4.6.** The estimated E_D and E_P values obtained from the slope of ln X versus 1/T plot, displayed in the **table 5.5 and 5.6** are found to be increasing with the amount of nanoparticles and also with the molecular weight of the penetrant molecules. Besides the high aspect ratio of nanofillers, the dipolar attraction between chlorine segment of Cl-NBR and –OH group of HA leads to enhanced matrix-filler interaction resulting in enhanced reinforcement. Cl-NBR/ 7phr HA has the highest activation energy which can be explained on the basis of maximum reinforcement and greater crosslink density in this sample. As filler content increases above 7phr, the homogeneity of distribution of filler decreases which creates voids in the interface and lesser energy may be required for the percolation of solvent molecules [273].

Table 5.5 E_P (KJ/mol) and E_D (KJ/mol) values of Cl-NBR/HA nanocomposites in aromatic solvents.

Samples	Benzene		Toluene		Xylene	
	E_P	E_D	E_P	E_D	E_P	E_D
Cl-NBR	5.11	3.74	5.39	3.94	5.69	4.13
Cl-NBR/HA (3 phr)	5.34	3.95	5.54	4.06	5.72	4.11
Cl-NBR/HA (5 phr)	5.45	4.03	5.68	4.15	5.94	4.29
Cl-NBR/HA (7 phr)	5.7	4.14	5.85	4.23	6.03	4.32
Cl-NBR/HA (10 phr)	5.65	4.12	5.79	4.21	5.95	4.27
Cl-NBR/HA (15 phr)	5.6	4.09	5.72	4.18	5.88	4.24

Table 5.6 E_P (KJ/mol) and E_D (KJ/mol) values of Cl-NBR/HA nanocomposites in petroleum fuels.

Samples	Petrol		Kerosene		Diesel	
	E_P	E_D	E_P	E_D	E_P	E_D
Cl-NBR	5.18	3.92	5.57	4.21	5.72	4.26
Cl-NBR/HA (3 phr)	5.36	4.06	5.65	4.26	5.78	4.29
Cl-NBR/HA (5 phr)	5.43	4.09	5.74	4.31	5.87	4.34
Cl-NBR/HA (7 phr)	5.73	4.18	6.05	4.49	6.1	4.5
Cl-NBR/HA (10 phr)	5.66	4.16	5.96	4.44	6.05	4.46
Cl-NBR/HA (15 phr)	5.59	4.15	5.88	4.41	5.96	4.43

5.2.9.3 Thermodynamics parameters

The equilibrium sorption constant Ks have been determined from the amount of liquid sorbed by a given mass of rubber.

Mathematically, it is the ratio of number of moles of solvent sorbed at equilibrium to the mass of the polymer sample.

Using the values of Ks, the enthalpy of sorption ΔH_s and entropy ΔS_s was determined by van Hoff equation

$$Log\ Ks = \left(\frac{\Delta S}{2.303R}\right) - \left(\frac{\Delta Hs}{2.303RT}\right) \qquad \textbf{(Eq: 5.2)}$$

The regression analysis of log Ks against 1/T plot gives the value of ΔH_s and ΔS_s and given in **table 5.7** and **5.8**. The table clearly depicts that all the samples shows positive ΔH value in all the solvents. That is the sorption follows an endothermic reaction path way. The positive ΔS values indicate that the penetrant molecules sorbed are retained as liquid structures within the rubber.

The feasibility of sorption process has been ascertained by calculating the Gibbs free energy of the process by the **equation 4.9**. The values of ΔG of both aromatic and fuel absorption are included in **table 5.7** and **5.8** respectively. The free energy value increases with filler loading and reaches maximum for Cl-NBR/ 7phr HA, indicating a decrease in spontaneity upon filler addition. This may because of the fact that the tortuosity of penetrant molecule increases through the highly packed nanohybrid sample [274].

Table 5.7 ΔH, ΔS and ΔG values of Cl-NBR/HA nanocomposites in aromatic solvents

Samples	ΔH (KJ/mol)			ΔS(J/mol)			-ΔG(KJ/mol)		
	Benzene	Toluene	Xylene	Benzene	Toluene	Xylene	Benzene	Toluene	Xylene
Cl-NBR	1.37	1.45	1.56	29.9	27.95	24.80	7.6	6.935	5.88
Cl-NBR/HA (3 phr)	1.38	1.48	1.61	25.37	24.23	22.58	6.231	5.789	5.164
Cl-NBR/HA (5 phr)	1.42	1.53	1.64	23.09	21.19	20.97	5.507	4.827	4.651
Cl-NBR/HA (7 phr)	1.56	1.62	1.71	20.89	19.88	16.54	4.707	4.344	3.252
Cl-NBR/HA (10 phr)	1.52	1.57	1.66	21.74	20.10	18.47	5.002	4.46	3.881
Cl-NBR/HA (15 phr)	1.52	1.56	1.64	22.25	21.46	20.74	5.155	4.878	4.582

Table 5.8 ΔH, ΔS and ΔG values of of Cl-NBR/HA nanocomposites in petroleum fuels

Samples	ΔH (KJ/mol)			ΔS(J/mol)			-ΔG(KJ/mol)		
	Petrol	Kerosene	Diesel	Petrol	Kerosene	Diesel	Petrol	Kerosene	Diesel
Cl-NBR	1.28	1.38	1.46	28.74	26.45	23.08	7.342	6.555	5.464
Cl-NBR/HA (3 phr)	1.31	1.39	1.49	24.73	23.28	21.97	6.109	5.594	5.101
Cl-NBR/HA (5 phr)	1.34	1.44	1.53	22.99	20.88	20.17	5.557	4.824	4.521
Cl-NBR/HA (7 phr)	1.52	1.56	1.61	19.89	18.31	15.41	4.447	3.933	3.013
Cl-NBR/HA (10 phr)	1.49	1.53	1.58	20.74	19.68	17.74	4.732	4.374	3.742
Cl-NBR/HA (15 phr)	1.44	1.47	1.53	21.25	20.02	19.06	4.935	4.536	4.188

5.2.9.4 Mechanism of sorption

To investigate the sorption mechanism, the solvent uptake results of the nanocomposites were fitted to the equation

$$\mathrm{Log}\left(\frac{Q_t}{Q_\infty}\right) = \log k + n \log t \qquad \textbf{(Eq: 5.3)}$$

Where Q_t and Q_∞ are the respective mass uptake of solvents at time t and equilibrium, k and n are constants. The k values given in **table 5.9 (a)** (for aromatic solvents) and **5.9 (b)** (for petroleum fuels) depend on the structural characteristics of the matrix and measures the extent of interaction between the rubber and solvent. On comparing with the unfilled matrix all the filled samples shows lower k value and in the case of composite, this values decrease with increase in filler up to optimum loading and then a slight increase is obtained, indicating lower rubber- solvent interactions due to the insertion of nano HA. The values of n propose the mechanism of sorption. The value of n is 0.5 for normal Fickian mode of transport where the rate of chain relaxation is greater compared to the diffusion rate of the solvent. When the chain relaxation become slower than the rate of diffusion then n value reaches unity and the transport approaches non-Fickian behaviour. If the value of n is in between 0.5 and 1, the mode of sorption is said to be 0.5 and 1. It is noted that the values of n vary from 0.5 to 1, clearly point out an anomalous mode of transport. It is well established that the macromolecular chain relaxation decreases with the degree of reinforcement and become comparable with the concurrent penetrant diffusion rate [275].

Table5.9 (a) n and k values of of Cl-NBR/HA nanocomposites in aromatic solvents at room temperature

Samples	Benzene		Toluene		Xylene	
	n	k(min^{-1})	n	k(min^{-1})	n	k(min^{-1})
Cl-NBR	0.77	0.12	0.80	0.10	0.82	0.08
Cl-NBR/HA (3 phr)	0.78	0.10	0.81	0.08	0.84	0.06
Cl-NBR/HA (5 phr)	0.79	0.09	0.83	0.07	0.85	0.06
Cl-NBR/HA (7 phr)	0.84	0.07	0.87	0.04	0.89	0.02
Cl-NBR/HA (10 phr)	0.82	0.08	0.84	0.05	0.88	0.03
Cl-NBR/HA (15 phr)	0.81	0.08	0.83	0.06	0.86	0.04

Table 5.9 (b) n and k values of of Cl-NBR/HA nanocomposites in petroleum fuels at room temperature

Samples	Petrol		Kerosene		Diesel	
	n	k (min^{-1})	n	k (min^{-1})	n	k (min^{-1})
Cl-NBR	0.74	0.17	0.79	0.13	0.78	0.13
Cl-NBR/HA (3 phr)	0.78	0.14	0.84	0.11	0.82	0.11
Cl-NBR/HA (5 phr)	0.79	0.14	0.85	0.10	0.84	0.10
Cl-NBR/HA (7 phr)	0.82	0.12	0.89	0.06	0.87	0.05
Cl-NBR/HA (10 phr)	0.8	0.15	0.87	0.07	0.86	0.07
Cl-NBR/HA (15 phr)	0.78	0.16	0.86	0.08	0.85	0.08

5.3 Conclusions

In this study, a series of nanocomposites were prepared from chlorinated NBR filled with different loading of hydroxyapatite nanoparticles by a simple two-roll mill mixing technique. The molecular level interactions generated due to the incorporation of HA nanoparticles in Cl-NBR was evaluated by spectral, morphological and thermal analysis. FTIR and UV-Vis spectral studies proved the presence of hydroxyapatite inserted between the macromolecular chains of Cl-NBR. The nanoparticles markedly changed the angle of diffraction of matrix as evident from XRD pattern and the increased inter gallery spacing considerably reduced the amorphous nature of Cl-NBR. SEM study indicates the better dispersion of nano filler at its lower concentration and tendency to form agglomerates at higher concentrations. Addition of nano HA enhanced the thermal stability of nanocomposites. The DSC scans illustrated a shift in the chlorinated elastomer glass transition temperature to higher value in presence of the nano filler due to the confinement of HA within the rubber chains restricting the segmental mobility of the Cl-NBR chains. The decrese in cure time with the addition of HA particles indicates that HA can act as a co-agent for the reducing the vulcanization time. The mechanical properties of nanocomposites also showed remarkable improvement over pristine Cl-NBR. The formulation of nanocomposite improved the AC conductivity of the unfilled Cl-NBR and the conductivity increased with increase in

filler content. The dielectric constant and loss tangent of the composite increases by the addition of HA is attributed to interfacial polarization and space charge distribution in the macromolecule. The addition of filler conferred tremendous changes in the oil resistance property of virgin Cl-NBR, especially its hot oil absorption. The swelling percentage of samples up on immersion in ASTM oils was considerably decreased as the dosage of HA in Cl-NBR is increased due to the increased mutual interaction of elastomer chains. Also, the interaction of petroleum fuels and aromatic solvents with the modified samples was investigated. The magnitude of the transport properties such as diffusion, sorption and permeation were found to decrease with nanofiller content due to the polarization interaction between the rubber chains and filler. The standard free energy data obtained for equilibrium absorption indicate the sorption process is spontaneous. The mechanism of diffusion for chlorinated NBR/ HA hybrids were found to be anomalous due to the comparable rate of diffusion and sorption of solvents through the modified macromolecular chain. Indeed the magnitude of the increase in the physical, mechanical and diffusion properties reached the optimum level at 7 phr nanoceramic HA loading, above that aggregation of the nanofiller leads to poor dispersion. Thus the newly fabricated Cl-NBR/ HA nano hybrid is very promising from the industrial viewpoint due to simplicity of the preparation technique of both matrix and filler and above all good cost/performance ratio.

6.1 Introduction

Ethylene propylene diene monomer (EPDM) rubber is one of the extensively studied industrially important polymer. EPDM valued for its good physical properties such as high heat resistance, ozone resistance, and cold and moisture resistance. EPDM shows elasticity even at low temperature due to the presence of double bonds, which form crosslinks between two ethylene propylene chains. The saturated polymer backbone of ethylene propylene diene monomer rubber is responsible for high oxidative stability and excellent weather resistance. The added advantage of this rubber is its response to high filler loading and the olefinic group present in the hydrocarbon chain could act as template for chemical reactions [200,276-278]. However, the poor conductivity of EPDM limits its applications to some extent.

Nanofillers with large surface area per unit volume are particularly attractive because the electrical characteristics of the hybrid materials depend on the interpenetration and inter-actions of inorganic and organic phases [279,280]. Studies revealed the electrical properties of EPDM can be improved by the incorporation of conducting filler like carbon black [281-283]. It was also demonstrated that the electrical conductivity of polymers having isolated double bonds can be improved by introducing appropriate substituent [284]. The synthesis and characterization of ion-conducting polymeric system based on EPDM blends was reported by Bashir et al [5]. The advantages of conductive

elastomeric materials over conducting metal polymer composite is that they have low temperature flexibility, good elasticity, light weight and can be easily molded in to different shape by vulcanization technique.

Recently, naturally occurring nanoparticles with hierarchical structures are used instead of the conventional metal powder in extrinsically conducting elastomers due to the oxidative degradation of later composites, which limits its long-term applications. There are many instances for which HA can be used including in biomedical field, catalysis, sensors, photoelectric materials, etc. [285]. Usually hydroxyapatite is used as a reinforcing phase in load bearing applications. Due to the non-compatibility, mixing of EPDM rubber with polar nanofillers often leads to a polymer composite with poor mechanical, thermal, and electrical properties. These problems can be overcome by the introduction of functional groups in EPDM. Therefore, the present chapter describe the preparation of chlorinated EPDM (Cl-EPDM) in a cost effective route and fabrication of nanocomposite of Cl-EPDM having higher chlorine percentage with HA nanofiller by a simple, inexpensive two-roll mixing technique. The formation, structural characterization, morphology, and thermal behavior of new elastomer and its nanocomposites were done by Fourier transform infrared spectroscopy (FTIR) and UV–VIS spectroscopic techniques, X-ray diffraction (XRD), scanning electron microscopy (SEM), thermogravimetric analysis (TGA), and differential

scanning calorimetry (DSC). The electrical properties such as AC conductivity, dielectric constant, and dielectric loss tangent were also evaluated with respect to chlorination time and the loading of the nanoparticles. Further, this work demonstrates the effect of nano ceramic HA on mechanical, oil resistance and solvent diffusion properties of chloro functionalized EPDM.

6.2 Results and Discussion

6.2.1 FTIR Spectroscopy

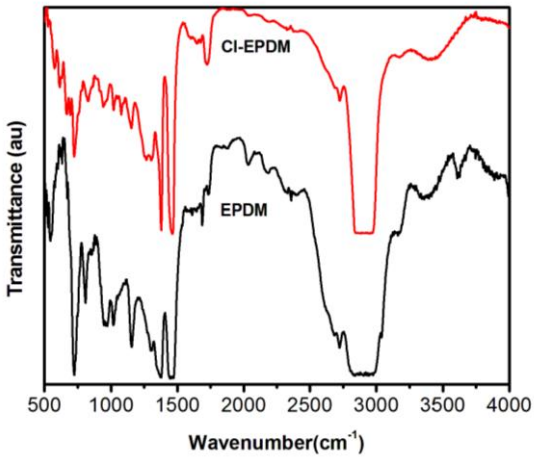

Figure 6.1 FTIR spectra of EPDM and chlorinated EPDM.

Figure 6.1 shows the FT-IR spectra of EPDM and chlorinated EPDM. Cl-EPDM shows characteristic IR absorption from propylene band at 1,157 cm^{-1} while 1,457 cm^{-1} and 2,904 cm^{-1} correspond to –CH stretching vibration and from polyethylene block at 721 cm^{-1} of side ethyl group. A sharp stretching frequency at 808 cm^{-1} due to (–CH=) stretch and the peak at 1686 cm^{-1} is

attributed to bending vibrations of alkenes. However in the case of chlorinated sample, the sharp peak of EPDM at 808 cm^{-1} is shifted to 827 cm^{-1} with a lower intensity. Furthermore, there appears a new absorption peak at 695 cm^{-1}, is due to C-Cl stretching band of chlorinated EPDM [48]. It is also evident from the figure that the characteristic absorption band of –CH = (1686 cm^{-1}) is absent in chlorinated EPDM. These results indicated that the absorption band of polymer is strongly affected by the attachment of chlorine in the main chain of EPDM.

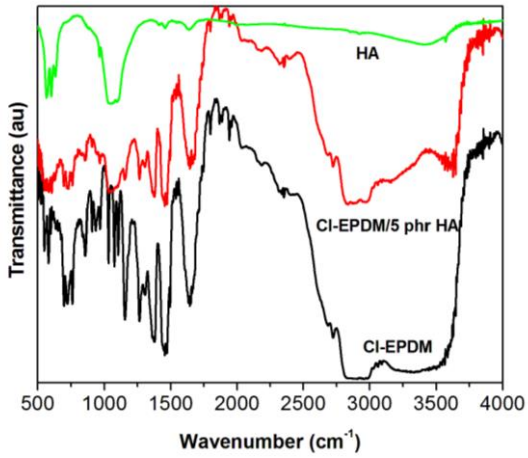

Figure 6.2. FTIR Spectra of HA, Cl-EPDM and Cl-EPDM/HA.

Figure 6.2 demonstrates the FTIR spectrum of HA, Cl-EPDM (3.8 % Cl content) and this chlorinated polymer with 5 phr of HA nanoparticles. The hydroxyapatite nanoparticle gives significant IR peaks at 3,376 cm^{-1} and 633 cm^{-1} due to OH stretching and OH bending vibrations respectively. The peaks

obtained at 964, 470, 1045, 569, and 604 cm^{-1} are the respective υ_1, υ_2, υ_3, and υ_4 vibration modes of phosphate group present in HA [180,286]. In the case of nanocomposite, the absorption frequencies are shifted to higher wavenumber as compared to pure Cl-EPDM vulcanizate. It is interesting to observe from the figure that the –OH stretching frequency of HA nanoparticles in the composite is slightly shifted to higher wavenumber from 3,376 cm^{-1} to 3,589 cm^{-1}, is due to the strong intermolecular interaction between the nanoparticles and polymer chain. Moreover the absorption frequencies of Cl-EPDM around 1,020, 1,073, and 1,107 cm^{-1} are absent in the nanocomposite and these peaks are merged to broad peak at 1,047 cm^{-1}. These observations suggest that the chlorinated EPDM chain is adsorbed on the surface of hydroxyapatite nanoparticles and its schematic representation is given in **scheme 6.1**.

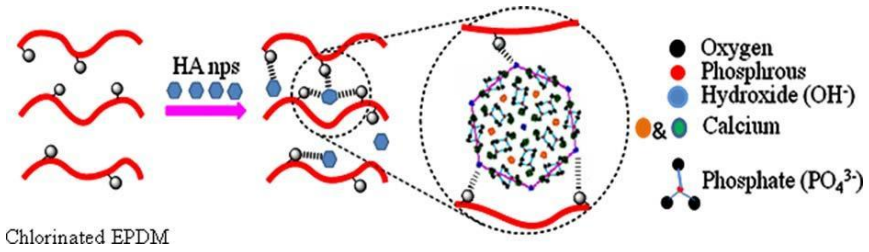

Scheme 6.1. Schematic representation of the interaction of Cl-EPDM with hydroxyapatite nanoparticles

6.2.2 UV–VIS Spectroscopy

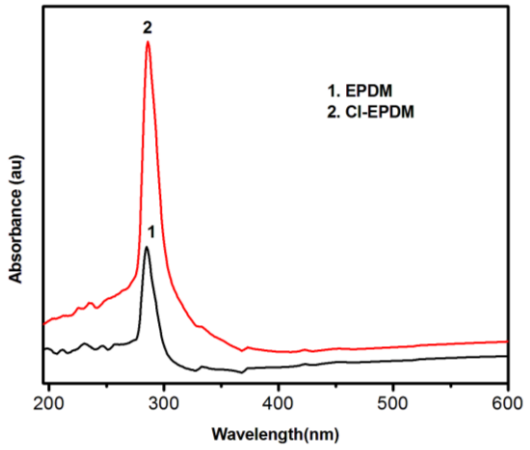

Figure 6.3. UV spectra of EPDM and chlorinated EPDM

UV spectra of EPDM and chlorinated EPDM are shown in **Figure 6.3**. The EPDM shows an absorption peak at 287 nm whereas the absorption peak of chlorinated EPDM slightly shifted to 285 nm. This means that the chlorinated sample shows hypsochromic shift, the shift towards higher energy or shorter wave length region. Hypsochromic shift is due to decrease in the extent of double bond. This result also suggest that the attachment of chlorine to the main chain of EPDM.

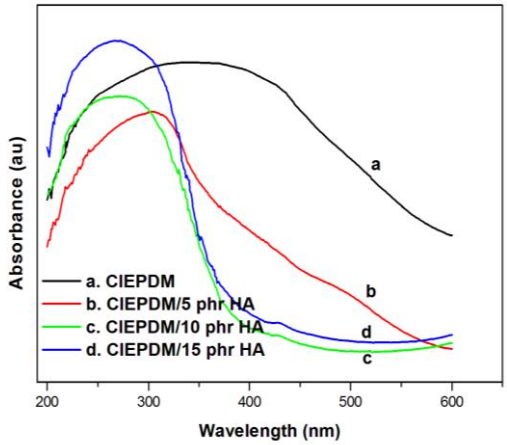

Figure 6.4 UV spectra of Cl-EPDM (3.8% Cl) with different content of HA nanoparticles.

The extent of molecular interaction between Cl-EPDM with the nanoparticle is assessed from UV-DRS spectra presented in **Figure 6.4**. The chlorinated EPDM shows a broad absorption peak at 338 nm is the typical n–π* transition of the EPDM segments. However, the broadness of the UV absorption peak of the nanocomposite is reduced with the increase in concentration of nanoparticle in Cl-EPDM. The decreasing peak width is an evidence for the insertion of nanoparticles within the macromolecular chain of EPDM. The UV absorption maxima of nanocomposite are shifted to a high energy region with the addition of nanoparticles. The polymer composite with 5, 10, and 15 phr of HA nanoparticles shows the absorption maxima at 303, 271, and 265 nm respectively. It is also clear from the figure that the broadness of UV absorption of composite is found to be decreases with the concentration of filler particles up to 10 phr and thereafter

the broadness increases. This clearly indicates that 10 phr of nanocomposite shows strong intermolecular interaction of HA particles with Cl-EPDM segments, which proves better compactness of nanocomposite [216]. Therefore, the decrease in broadness and shift in absorption peaks of nanocomposite confirms the encapsulation of HA nanoparticles by the chlorinated EPDM chain [239].

6.2.3 X-Ray Diffraction Analysis (XRD)

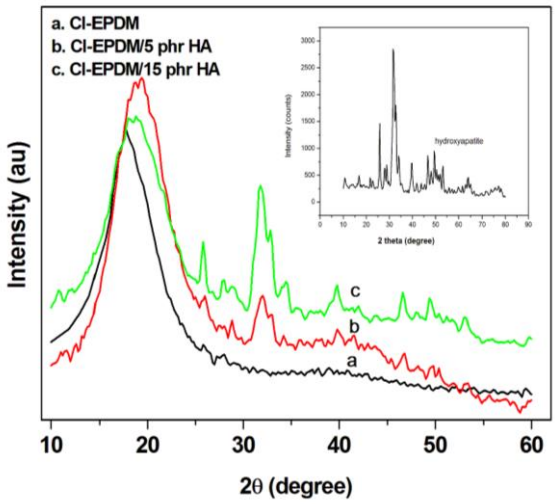

Figure 6.5 XRD patterns of Cl-EPDM (3.8 % Cl), and Cl-EPDM (3.8 % Cl)/HA nanocomposites.

The XRD analysis depicted in **Figure 6.5** clearly shows the structural changes occurred in the functionalized elastomer as a result of introduction of nanofiller. A broad, amorphous peak of Cl-EPDM vulcanizate is appeared at $2\theta = 17.8^0$ with a d spacing of 4.98A^o. It is obvious from the figure that the nanocomposite shows

few characteristic X-ray diffraction peaks of HA with the amorphous peak of Cl-EPDM. In addition, the amorphous peak of chlorinated EPDM in the composite is found to be shifted to higher diffraction angle with a decrease in inter planar spacing. Cl-EPDM with 5 and 15 phr of HA nanocomposite shows 2θ values at 19.4^0 with basal spacing of 4.57Aº and $2\theta=18.8^0$ with basal spacing of 4.71Aº respectively. This confirms that the hydroxyapatite nanoparticles are entrapped in the macromolecular chain of Cl-EPDM. Thus, the polar groups present on the surface of rubber and hydroxyapatite form an effective interaction between polymer and filler at the interfacial zone, which gives a well-ordered microstructure to the nanocomposite.

6.2.4 Scanning Electron Microscopy (SEM)

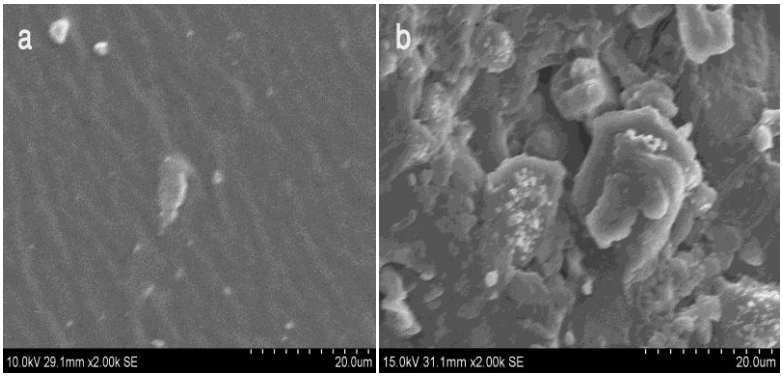

Figure 6.6. SEM images of a) EPDM b) Cl-EPDM with 3.8 % Cl.

The micro-structural analysis of EPDM and chlorinated EPDM has been carried out by using SEM. As in **Figure 6.6**, the micrograph of EPDM exhibits a smooth surface which indicates

that the macromolecular chain of EPDM is uniformly arranged. But in the case of chlorinated sample, the surface became irregularly arranged with a few aggregations. This change in phase morphology is due to the introduction of polarity in the synthesized sample. Hence it can be inferred that the structure of EPDM is influenced by the presence of chlorine in the polymer.

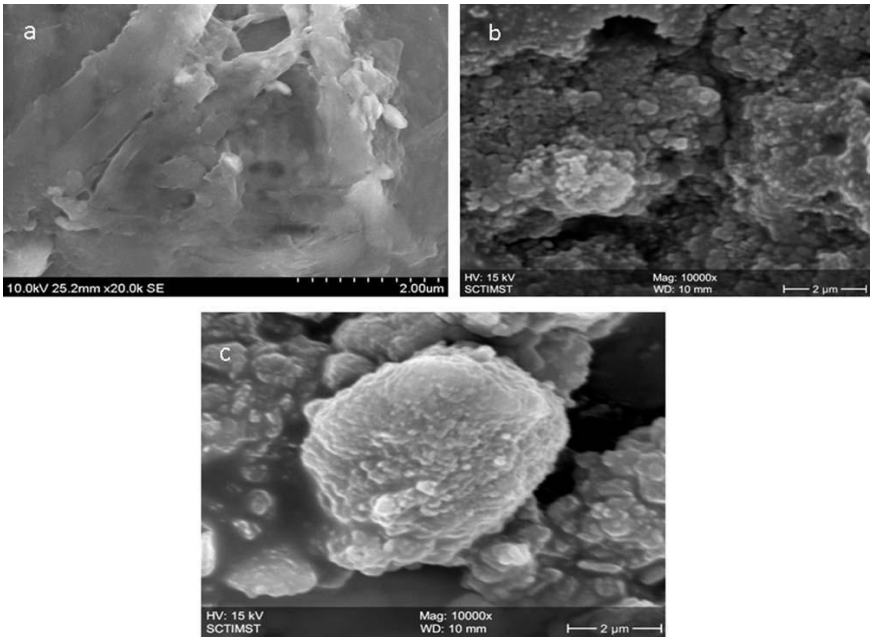

Figure 6.7. SEM images of (a) Cl-EPDM (b) Cl-EPDM/10 phr HA and (c) Cl-EPDM/15 phr HA.

The surface morphology of the synthesized Cl-EPDM and Cl-EPDM/HA nanocomposites with 10 and 15 phr of HA nanoparticles are presented in **Figure 6.7**. The SEM image of Cl-EPDM vulcanizate reveals the presence of a porous structure with an irregularly ordered macromolecular segment in the polymer chain. The sample with 10 phr of composite shows the uniform

dispersion of HA nanoparticles in the polymer with spherically shaped particles. The polar functional group in the inorganic particles having large surface area can effectively interact with the polar segments of modified rubber, which contribute a uniform orientation of nanoparticles within the elastomer matrix and therefore the structure of composite became uniform morphology (confirmed from the increased order-ness of composite from the XRD). As the loading of nanoparticle increased to 15 phr, the surface of the composite became cluster like structure indicating the resistance of composite, which leads to an agglomeration of nanoparticles within the elastomer matrix. In other words, the weak intermolecular interaction between the nano-filler and Cl-EPDM, leads to an increase in free volume in the composites.

6.2.5 Thermal behaviour

6.2.5.1 Differential Scanning Calorimetry (DSC)

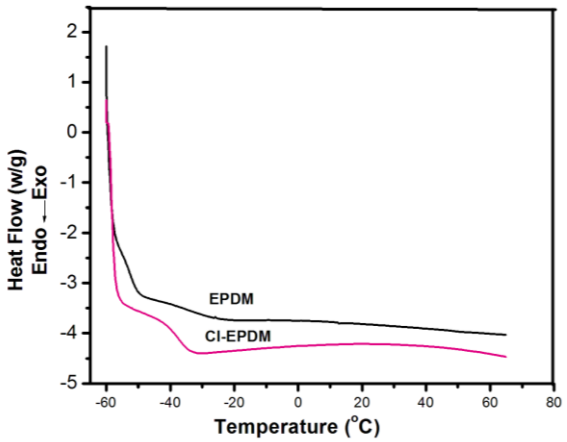

Figure 6.8. DSC thermograms of EPDM and chlorinated EPDM

The physical changes of state in a sample, especially the glass transition temperature (*Tg*) of polymer has been studied from DSC and the curve is given in **Figure 6.8**. EPDM shows the *Tg* at -52.18^0C whereas that of the chlorinated sample is at -40.0^0C. The increase in *Tg* as a result of chlorination is mainly due to the polar nature of the prepared sample and also the change in structural rearrangement of the macromolecular chain present in EPDM. In other words, the chlorine group triggered the ionic interaction between polymer chains which restricts the chain movement by decreasing spacing and thus the free volume in the polymer [287].

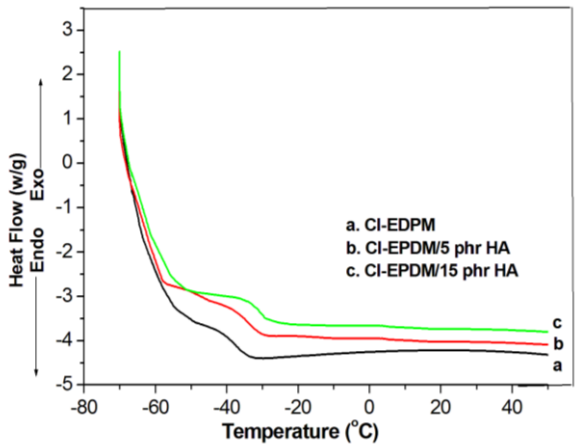

Figure 6.9. DSC thermograms of Cl-EPDM and Cl-EPDM/ HA nanocomposites.

DSC analysis was carried out to determine the glass transition temperature (T_g) of Cl-EPDM vulcanizate and its hybrid with HA and is given in **Figure 6.9**. Cl-EPDM shows the glass

transition temperature at -40^0C, whereas, the composite with 5 and 15 phr of HA nanoparticles are appeared at -36^0C and -34^0C, respectively. It is evident from the figure that the glass transition temperature of the composites is shifted to a higher temperature with an increase in the concentration of nanoparticles. The enhancement in T_g of nanocomposite with respect to that of pure Cl-EPDM is due to the restriction of polymer chain mobility as a result of the strong interfacial interaction between the nanoparticles and the chlorinated EPDM [4].

6.2.5.2 Thermogravimetric Analysis (TGA)

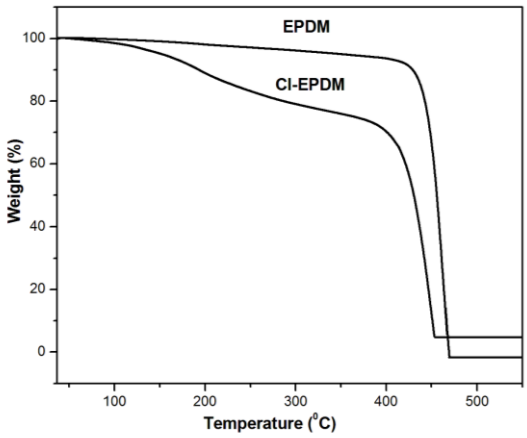

Figure 6.10. TGA curve of EPDM and chlorinated EPDM

The thermal decomposition behaviour of EPDM and chlorinated EPDM are given in **Figure 6.10**. It can be observed from the figure that the EPDM shows single stage decomposition at a temperature of 415 ^{0}C whereas the chlorinated EPDM

decomposes in two steps: the first stage of decomposition begins at 149^0C and the second degradation at 416^0C. The first degradation of polymer is due to the removal of HCl from the main chain of EPDM and the second weight lose is the elimination of residual polymer. Also it is found that the final char residue of chlorinated EPDM is 4.9% whereas EPDM have 1.2% only. The increased char residue for chlorinated EPDM is an indication for the enhanced flame resistance of the chemically modified sample [288].

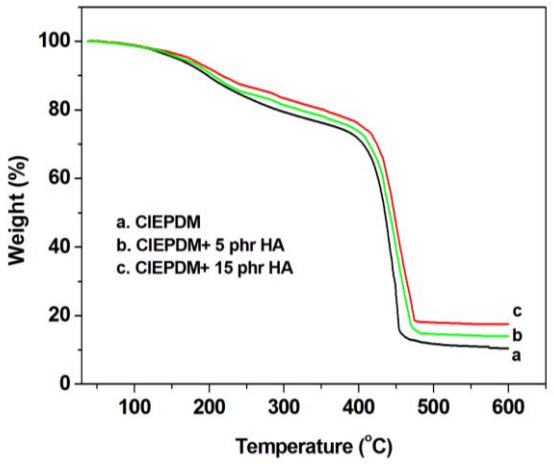

Figure 6.11. TGA thermograms of Cl-EPDM and Cl-EPDM/HA nanocomposites

Thermogravimetric analysis is also performed to study the influence of incorporation of inorganic phase in oxidative degradation of elastomer. TGA of Cl-EPDM and Cl-EPDM with various loading of HA nanoparticle is displayed in **Figure 6.11**. The nanocomposite with 5 and 15 phr of HA shows decomposition initially at 159^0C and 162^0C and the subsequent destruction of

polymeric backbone occurs at 420^0C and 426^0C respectively. As seen from the TGA curves, the thermal stability of chlorinated EPDM/hydroxyapatite nanocomposite significantly improved than that of the pure chlorinated EPDM. The decomposition temperature of the composite material is shifted to a higher temperature with an enhancement of filler content in the nanocomposite. The significant increase in thermal resistance of the composite is mainly attributed to the uniform dispersion of nanoparticles and the strong interaction between the polar segments of the chlorinated EPDM with the hydroxyl group of apatite nanoparticles. Approximately, 12 wt% of char residue remained after 600^0C for chlorinated EPDM, while 20 wt% of char residue is obtained for 15 phr of HA particle in elastomer matrix. This higher weight percentage of char residue for the composite indicates the improved flame resistance. The higher char residue after the decomposition may act as oxygen transport barrier and insulator for the rubber matrix [289].

6.2.6 Cure characteristics

Table 6.1 Processing characteristics of Cl-EPDM and Cl-EPDM/HA nanocomposites

Samples	Cure time t_{90} (min)	Scorch time t_2 (min)	Maximum Torque (dNm)	Minimum torque (dNm)
Cl-EPDM	14.6	4.62	32	7.4
Cl-EPDM/ 3 phr HA	14.2	4.40	35	8.1
Cl-EPDM/ 5 phr HA	13.81	4.18	39	8.5
Cl-EPDM/ 7 phr HA	12.92	3.91	44	8.8
Cl-EPDM/ 10 phr HA	12.53	3.72	47	9.0
Cl-EPDM/ 15 phr HA	12.01	3.56	45	8.8

Table 6.1 represents the cure characteristics such as M_H, M_L, t_{90} and t_2 of Cl-EPDM (3.8% Cl)/HA nanocomposites with respect to filler loading. The maximum and minimum torque (M_H and M_L) values increases significantly with increase in filler loading up to the sample containing 10phr HA and thereafter a slight decrease is observed. Since M_H values signify the reinforcement and cross-link density of the mixes, the increment in M_H with increase in filler loading can be related to greater interaction between filler and rubber matrix. M_L value indicates the extent of filler-filler aggregations. As the filler concentration reached to 10 phr, the crosslink density become optimum and has

maximum reinforcement. The uniformly distributed micro-domains generate large interfacial area and enhance micro-level interactions. The mobility of macromolecular chain thus decreased considerably which result in the rigidity of the vulcanizates. Further addition of the nano HA has been found to reduce the torque; due to interfacial saturation. The decrease in both t_{90} and t_2 with increase in filler loading confirms the heat generation which accelerates the cure reaction [290].

6.2.7 Mechanical Properties

The tensile strength, elongation at break (EB), tear resistance and hardness of Cl-EPDM (3.8% Cl)/ nano HA matrices under different phr of filler content was analyzed with respect to pristine Cl- EPDM. The values obtained are presented in **Table 6.2**.

Table 6.2 Mechanical properties of of Cl-EPDM and Cl-EPDM/HA nanocomposites

Samples	Tensile strength (MPa)	Elongation at break (%)	Tear strength (kN/m)	Hardness (Shore A)
Cl-EPDM	17.5	320	25.38	49
Cl-EPDM/HA (3 phr)	20.4	308	27.69	50
Cl-EPDM/HA (5 phr)	23.2	296	30.12	52
Cl-EPDM/HA (7 phr)	26.9	281	33.44	54
Cl-EPDM/HA (10 phr)	28.8	265	35.89	56
Cl-EPDM/HA (15 phr)	26.4	248	34.11	58

It is seen that tensile strength of polymer composite increases with increase in the filler content up to 10 phr loading. The improvement in tensile strength with filler loading can be attributed to the effective stress transfer between the macromolecular chains. The increased compatibility between rubber chains and the nano-fillers via dipolar interaction between chloro and hydroxyl groups as seen in Cl-NBR/HA nanocomposite (chapter 5) leads to the micro-level interactions and larger interfacial area formed by the uniformly distributed micro domains. Tear strength is an important property which contributes towards resistance to crack growth during production as well as in service. The tear strength also follows the same trend as that of tensile strength. It can be seen from the table that tear strength increases

with the filler loading and the value is maximum for Cl-EPDM/ 10phr HA system. This may be due to the reinforcing nature and the effective distribution of filler particles present at the crack propagation tip will arrest the propagation of cracks. The elongation at break is determined from the force applied to pull the vulcanizates. EB decreased continuously with increase in the filler content indicate higher reinforcement of nanoparticles in the matrix. As expected, the progressive increase in hardness is attributed to the addition of high modulus nano filler to low modulus filler [291, 292].

6.2.8 Electrical properties

6.2.8.1 AC Conductivity

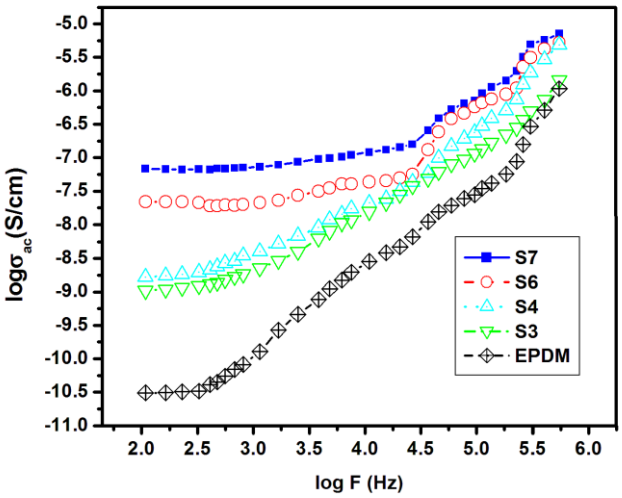

Figure 6.12 Variation of ac conductivity with frequency of Cl-EPDM

The variation of AC conductivity of EPDM and EPDM with different time of chlorination is presented in **Figure 6.12** as double logarithmic plots of σ_{AC} *vs.* frequency. It is clear from the figure that the conductivity of chlorinated samples are considerably higher than that of EPDM and also the conductivity increases with increase in chlorination time. The conductivity of polymeric samples depends on microscopic or macroscopic properties. The microscopic conductivity arises from the interaction of molecules, chain entanglements, polarity whereas macroscopic conductivity depend on the compactness, uniform morphology etc. [293]. In the present study the microscopic conductivity is the major factor responsible for the higher electrical properties of the chlorinated samples. The polar nature of chlorine group present in the modified polymer leads to an ionic interaction which in turn produces many cross -links between the adjacent macromolecular chains [294]. This structural reorganization is already confirmed from SEM and this creates electron carrier paths within the polymer that ultimately result in improved conductivity.

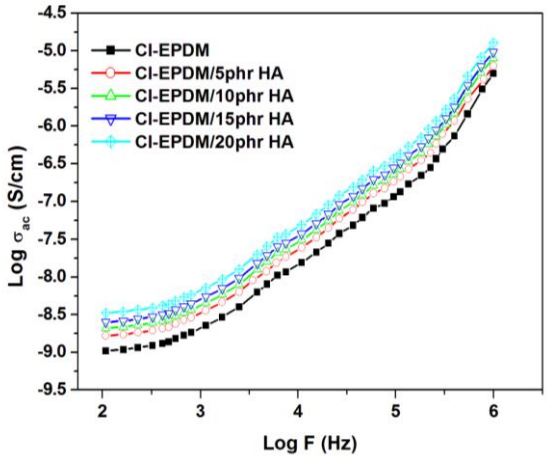

Figure 6.13 AC conductivity of Cl-EPDM and Cl-EPDM / HA nanocomposites

The effect of frequency and the concentration of apatite nanoparticles in the electrical conductivity at room temperature of Cl-EPDM (3.8% Cl)/HA nanocomposites are depicted in **Figure 6.13**. It can be observed that the conductivity of all the samples increases not only with increase in frequency of AC current but also with the concentration of nanofillers. The powerful interconnection formed at the bridging region of the two phases helps the hopping of charge carriers from one site to the other and that is why the conductivity increases with frequency. The increasing trend of AC conductivity of all the samples is high at higher frequencies indicating the formation of charge carriers in the nanocomposite. The conductivity of nanocomposite is higher than pure Cl-EPDM and the conductivity is found to be improved with the addition of nanoparticles. Generally, the conductivity of polymer composite depends on the surface area, polarity of

polymer, and filler particles and the interfacial interaction between them. In the present study, the enhanced conductivity of nanocomposite is attributed to the uniform dispersion and the orderly arranged nanoparticles within the elastomer matrix [295].

6.2.8.2 Dielectric Constant

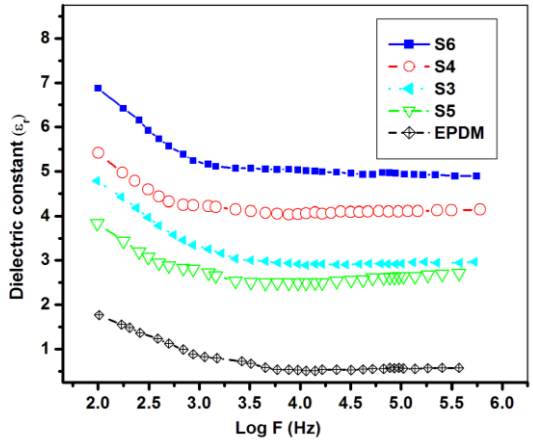

Figure 6.14 Variation of dielectric constant with frequency of Cl-EPDM

Figure 6.14 shows the variation of dielectric constant (ε_r) with frequency at room temperature for EPDM and chlorinated samples at different frequencies.

It can be seen from the figure that the dielectric constant continuously decreases with increase in frequency. In chlorinated samples the high value of dielectric constant is attributed to the interfacial polarization of chlorinated segment with the adjacent macromolecular chain of EPDM. These interfacial polarization

leads to the orientation of macromolecular chain which contributes towards the dielectric behaviour of the polymeric samples. EPDM showed a lower dielectric value which is the characteristics of non-polar matrix. In addition to this, the linearity of the curve obtained for EPDM is the lack of interfacial polarization of the polymeric matrix [296].

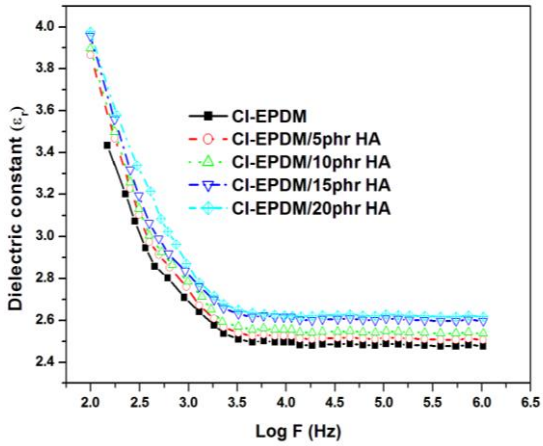

Figure 6.15. Dielectric constant of Cl-EPDM with different content of HA particles.

The dielectric constant has been determined at room temperature in different frequency range for Cl-EPDM (3.8% Cl) with different content of nano-fillers is plotted in **Figure 6.15**. As it is seen from the figure, the permittivity drops steeply up to the frequency reached about 10^3 Hz and after that, it shows a constant plateau at higher frequencies. It is already reported that the dielectric constant depend on the polarizabilities of the system [218]. At lower frequencies, the polarization is induced by the

displacement of charge carriers generated as a result of encapsulation of HA in Cl-EPDM along the direction of applied field is responsible for higher dielectric constant. This interfacial polarization enhances with the concentration of HA due to increased dipole density at the interface. However, as the frequency increases these dipoles cannot reorient with the field reversal. Thus at higher frequencies the orientation polarization decreases because of the increased relaxation time due to the restricted mobility of dipoles. It is obvious from the figure that the unfilled rubber shows the low dielectric constant than nanofiller containing rubber. The high value of dielectric constant is attributed to the increased interaction between the chlorine unit of EPDM and the hydroxyl group of nanoparticles. In addition, the dielectric constant of the composites is improved by the loading of filler particles. The magnitude of increasing trend of dielectric constant with the loading of nanoparticle is marginal when the concentration of nanoparticles increased from 15 to 20 phr. This can be due to the space charge polarization and reversal of the direction of polarization [297, 298]. Hence, the fabricated nanocomposites with improved AC conductivity and dielectric properties may find applications in several electrical and nano-electronic devices.

6.2.8.3 Dielectric Loss Tangent (Tan δ)

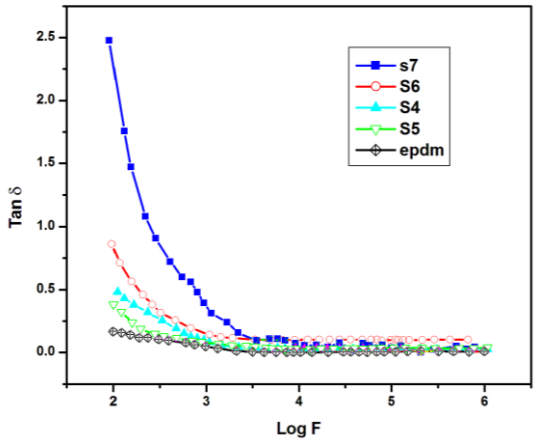

Figure 6.16. Variation of dielectric loss with frequency of Cl-EPDM

Figure 6.16 depicts the variation of loss tangent (tan δ) of EPDM and the samples with different time of chlorination at different frequencies. Dielectric loss is the function of relaxation process which originates from the local motion of polar groups. After the successive addition of chlorine to the double bond of EPDM, the viscoelastic nature of the polymer will change, that may be another reason for the relaxation process. The increase in dielectric properties with the increase in chlorination is due to the development of large number of dipoles, which in turn increases the orientation of polymeric chain that caused the formation of space charges at the interfaces of macromolecules [210].

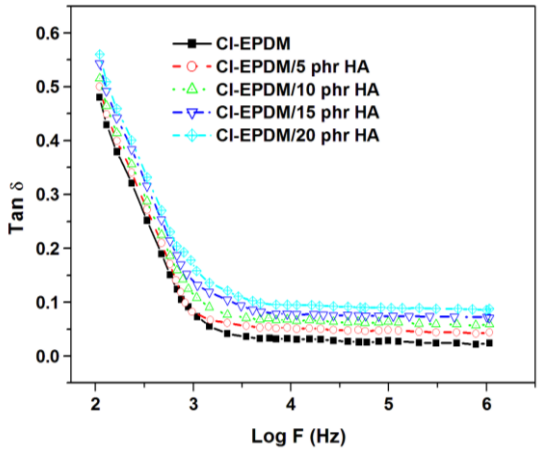

Figure 6.17 Dielectric loss of Cl-EPDM with different content of HA particles

The frequency dependence of dielectric loss tangent (tan δ) at room temperature for Cl-EPDM (3.8 % Cl)/HA nanocomposite is shown in **Figure 6.17**. The dielectric loss tangent of a material depends upon the interfacial or dipolarization ability. The dielectric loss shows similar tendency as that of dielectric constant that is at low frequency region the complex part of permittivity decreases up to 10^3 Hz then it became independent of change in frequency. In addition, the interfacial interaction through the enhanced interface of nanocomposites leads to space charge polarization, which is clearly evident from the UV and FTIR studies. The space charge build up at interface increases as the loading of the nano HA increases and free motion of it through the material is responsible for the high dielectric loss at higher loading [299]. High tan δ values are observed for higher concentration of HA nanoparticles

in the Cl-EPDM composite. Since both the polymer and filler particles have polar nature, more and more polarized interfaces are developed in the polymer matrix which in turn increase the tan δ values.

6.2.9 Oil resistance measurement

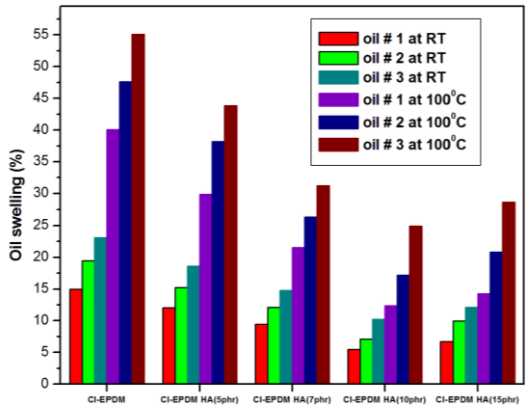

Figure 6.18 ASTM oil resistance of Cl-EPDM (3.8% Cl) with different content of HA nanoparticles

Figure 6.18 represent the percentage of mass swell of HA filled EPDM in petroleum based industrial reference oils IRM 901, IRM 902 and IRM 903 at room temperature and 100^0C. As we know the percentage of oil swelling is influenced by filler loading, temperature, nature of penetrating oil etc. It is evident from the figure that the percentage of oil uptake is higher for the unfilled sample, which has been considerably reduced upon loading with HA fillers and a minimum value is obtained for Cl-EPDM/10phr HA nanocomposite. The movement of the oil molecules

through the rubber matrix is significantly controlled by the presence of fillers. That is the crosslinks formed by the molecular interaction between HA nanoparticles and rubber chains will restrict the extensibility of rubber chains induced by the diffusion of penetrants. The polarity of the system also has a significant effect in preventing the penetration of oils [300, 301]. Further, the percentage of swellings in oils increase with temperature is due to the increase in the segmental mobility, free volume and kinetic energy of the penetrants. Swelling in IRM 903 oil is higher for all samples than IRM 901 and 902 due to lower aniline point.

6.3 Conclusions

The chemical modification of EPDM rubber was done by passing chlorine gas through a simple chemical reaction between concentrated hydrochloric acid and potassium permanganate. The chlorination on EPDM was confirmed by various characterization techniques such as FTIR, UV, SEM, DSC and TGA. FTIR spectrum showed the characteristic absorption peak of C-Cl and UV spectroscopy supports the attachment of chlorine to the double bond of ethylidene group by the change in wave length as compared to that of pure EPDM. The SEM analysis revealed the change in morphology of virgin rubber as a result of the polarity in macromolecular chain. The DSC analysis revealed that the glass transition temperature of the chlorinated sample was much higher than that of EPDM because of the increased orderness via cross linking between polymer chains. TGA studies proved that the

chlorination reaction affected the basic thermal decomposition pattern of EPDM and the final char residue obtained from the analysis indicated the better flame retardancy of chlorinated EPDM. The increase in AC conductivity with frequency was mainly attributed to the polar interaction between polymer chains that triggered by the chlorine group. The dielectric properties increased with increase in chlorination but decreased with frequency.

Chlorinated EPDM nanocomposite with different concentrations of hydroxyapatite nanoparticles were prepared by a simple and inexpensive two-roll mill mixing technique using DCP as vulcanizing agent. FTIR and UVspectra of nanocomposite showed the simultaneous shift of absorption frequencies, indicating the successful insertion of HA nanoparticles in to the chlorinated EPDM rubber segments. The XRD studies established the presence of HA nanoparticles in the polymer composite and the amorphous nature of the elastomer was decreased by the addition of the nanoparticle. SEM images showed the extent of dispersion of nanoparticles in the matrix, which confirms the enhanced adhesion between filler and rubber. DSC analysis indicated that the interaction of HA nanoparticles with polymer improve the glass transition temperature of the composite. The better thermal stability of the newly prepared nanocomposite was revealed from the thermogravimetric analysis. The addition of fillers in the rubber resulted in a significant increase in the interfacial interaction as

evidenced by the values of maximum torque during the rheological studies. The tensile and tear properties of filled rubber increases with increase in concentration of HA, reached the maximum for Cl-EPDM/10phr HA nanocomposite and then decreased. Oil swelling studies revealed that incorporation of HA nanoparticles enhances oil resistance of nanocomposites.

The chlorinated EPDM rubber showed a lower AC conductivity than Cl-EPDM/HA nanocomposites, the conductivity of composite increased with the increase in loading of HA nanoparticles. Dielectric properties such as dielectric constant and dielectric loss tangent were also increased with the increase in the loading of hydroxyapatite nanoparticles. The marked increase in electrical and dielectric properties suggests that the Cl-EPDM/ HA nanocomposite has potential application in the field of nanotechnology where flexibility is important criteria and in various electronic industries.

7.1 Introduction

The blending of elastomers is an effective method which has been found to offer substantial improvement in the performance of materials to fulfill both scientific challenges and industry needs for a specific set of properties. When a polymer is mixed with another polymer, the resulting blend is expected to obey some additivity relationship. That is blending will bring about a series of good properties via the improvement in the inferior properties such as processability, mechanical, thermal, electrical and barrier properties of the original material in addition to cost dilution, which one constituent alone cannot supply. Properties of polymer blends depend mainly on blend ratio, miscibility of the polymers, morphology, component polymer properties, viscosity ratio and type of interaction between the components [302,303]. It is reported that the overall physicomechanical properties of elastomeric blends strongly depend on the proper interfacial tension which leads to macroscopic homogeneity and an interphase adhesion which should be enough to assimilate stresses and strains without disruption of the established morphology. Extensive research works on this topic reveal that, optimum properties are commonly observed for compatible polymer blends and generally the miscibility of dissimilar elastomers can be achieved by the addition of a suitable compatibilizer during the processing stage or by exposing to radiation with suitable power. The compatibilizers used should be either chemically identical with the different phases

of the blend or miscible with or adhered to one of the phase [304-306].

Acrylonitrile butadiene rubber (NBR) is commonly used where a combination of excellent oil resistance and good aging resistance is needed with satisfactory physical and processing properties. Still, the deficiencies such as poor gum strength, ozone and environmental resistance etc in some aspect limit the range of their applications in practical industry. Review on literature accounts that many of these drawbacks can be solved by blending NBR with saturated elastomers. Ethylene-propylene diene monomer (EPDM) rubber is a well studied rubber having excellent resistance to heat, oxidation, ozone and aging properties due to long saturated hydrocarbon backbone with the presence of double bonds in side chains [307, 308]. Many investigators studied on NBR/ EPDM blends to tailor a blend which withstands ozone, heat aging, oil and solvents swelling with desirable mechanical characteristics and reported a number of beneficial combinations of properties of these vulcanizates [309-311]. Oliveira and Soares studied the effect of the efficiency of both maleic anhydride and mercapto-modified ethylene–propylene–diene rubber (EPDMMA) and ethylene–vinyl acetate copolymer (EVAMA) on the mechanical, dynamic mechanical and morphological properties of NBR/EPDM blends [312]. Lohmar et al investigated the mechanical dispersion of the incompatible EPDM and NBR rubbers was favored by transoctylenylene rubber (TOR) [313]. The

non polar EPDM can be compatibilised with polar NBR by grafting of EPDM with different functional monomers based on (meth)acrylates, styrene, or acrylonitrile using an atom transfer radical polymerization (ATRP) process. It was proposed that the formation of interfacial ionic aggregate is responsible for the compatibility of zinc salts of maleic anhydride–grafted EPDM rubber and carboxylated nitrile rubber. That is grafting of EPDM with another polymer having an active functional group can improve its interaction with polar elastomers. Also, earlier reports show that the non polar elastomers can be made polar by chemical modification via halogenations, amination etc [314,315].

This chapter describes the preparation of compatible, technologically feasible blends comprising of chloro functionalized EPDM and dichloro carbene modified NBR without a compatibilizer. The Cl-NBR/ Cl-EPDM blends were characterized by FTIR, UV-VIS spectroscopy, XRD, SEM, TGA and DSC. The compatibility of blends was also be evaluated in terms of their cure and mechanical characteristics, electrical conductivity studies, oil, fuel and solvent resistance.

7.2 Results and Discussion

7.2.1 FTIR Spectroscopy

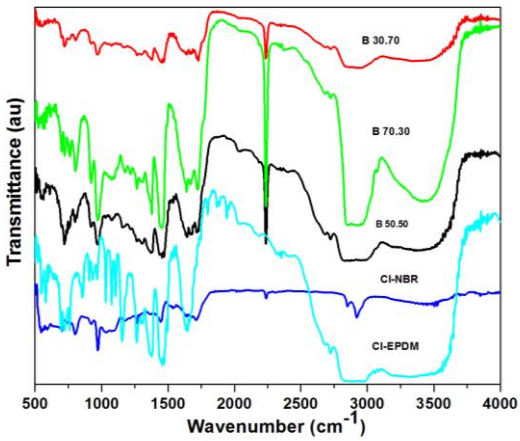

Figure 7.1 FTIR Spectra of Cl- NBR, Cl-EPDM and Cl- NBR/ Cl-EPDM blends

The FTIR spectra of Cl-NBR, Cl-EPDM, and Cl-NBR/Cl-EPDM mixtures with different ratios are shown in **Figure 7.1**. It can be seen from the IR spectrograph and IR absorption data of blends presented (table 7.1), the peaks at 2236 cm^{-1}, 972 cm^{-1}, 801 cm^{-1} and 1062 cm^{-1} identify the Cl-NBR while the peaks at 1448 cm^{-1}, 722 cm^{-1} and 695 cm^{-1} are characteristic for the Cl-EPDM, indicating the dispersion of the two binary phases in the blends. It is known that the compatibility of blend components is achieved by specific interactions that enhance the packing efficiency of the molecules. Since each elastomer under study has polar and nonpolar ends there would be a strong polar- polar interaction between the chlorine groups and also between highly polar nitrile

ends which leads to effective miscibility of these components. So the presence of characteristic IR absorption with a slight shift in frequency in the Cl-NBR/ Cl-EPDM blends with different blend ratios assures that the chlorine groups attached to each elastomer itself act as compatibilising agent [316].

Table 7.1 Assignments of the infrared bands of blends

Materials	Wave number (cm^{-1})	Assignments
Cl-NBR	2236	υ(CN–) stretching vibration
	1062	υ-cyclopropyl ring
	801	υ(C-Cl) stretching vibration
Cl-EPDM	1448	-CH stretching vibration from polyethylene band
	722	stretching vibration side ethyl group
	695	υ(C-Cl) stretching
Cl-NBR/Cl-EPDM (30/70)	965	*Trans* δ (–CH=CH–) wagging motion vibration
	813	υ(C-Cl) stretching vibration
	726	stretching vibration side ethyl group
	1457	-CH stretching vibration from polyethylene band
	2239	υ(CN–) stretching vibration
Cl-NBR/Cl-EPDM (50/50)	1463	-CH stretching vibration from polyethylene band
	969	*Trans* δ (–CH=CH–) wagging motion vibration
	803	υ(C-Cl) stretching vibration
	717	stretching vibration side ethyl group

	609	υ(C-Cl) stretching
	2239	υ(CN–) stretching vibration
Cl-NBR/Cl-EPDM (70/30)	707	stretching vibration side ethyl group
	803	υ(C-Cl) stretching
	1454	-CH stretching vibration from polyethylene band
	959	*Trans* δ (–CH=CH–) wagging motion vibration
	2239	υ(CN–) stretching vibration

7.2.2 X-Ray Diffraction Analysis (XRD)

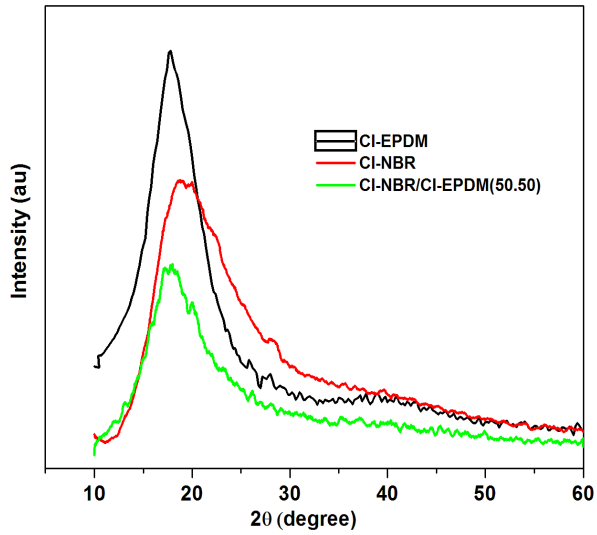

Figure 7.2 XRD patterns of Cl- NBR, Cl-EPDM and Cl- NBR/ Cl-EPDM (50/50) blend

Figure 7.2 displayed the XRD spectra for the pristine Cl-NBR, Cl-EPDM and Cl-NBR/Cl-EPDM blend with 50/50 blend ratio. The pristine showed a broad intense peak at $2\theta = 19.52^0$ corresponding to d spacing of 4.54Aº for Cl-NBR while the amorphous peak of Cl-EPDM appeared at $2\theta = 17.8^0$ with a d spacing of 4.98º. In blend samples, it can be seen that the area under the amorphous peak obtained is shorter to that of Cl-EPDM. The blend with 50/50 ratio shows diffraction at 17.41^0 corresponding to inter gallery spacing of 4.93. The most appealing result is that broadness of diffraction peak is considerably lowered by the blending of Cl-EPDM with Cl-NBR indicating the increased compatibility of blend at 50/50 ratio. In view of the fact that the dipolar interaction between chloro functionalized blend components is preferentially located at the interface the dispersion of both elastomers will become easy and lead to the formation of macroscopically homogeneous blend.

7.2.3 Scanning Electron Microscopy (SEM)

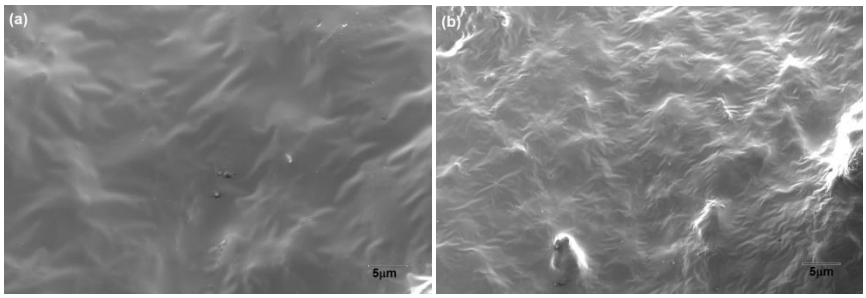

Figure 7.3 SEM images of a) Cl-NBR/Cl-EPDM (50/50) b) Cl-NBR/Cl-EPDM (70/30)

The SEM photograph of Cl-NBR/ Cl-EPDM blends with different blend ratios are presented in **Figure 7.3**. It is well known that the phase structure of the blend is influenced by several factors, including the surface characteristics, blend ratio, viscosity of each component and compounding process [317]. As mentioned earlier the surface morphology of both Cl-NBR and Cl-EPDM are rather bumpy and these structural changes occurred after chlorination provides more sites for interlocking of the two phases. These crosslink points soften the molecular chains of blend compared to Cl-NBR. Thus the increased surface area along with stronger polar interaction increases the interfacial adhesion by decreasing the surface energy which will lead to better dispersion of one phase in another, which is more pronounced when the blend ratio is 50/50.

7.2.4 Thermal behaviour

7.2.4.1 Differential Scanning Calorimetry (DSC)

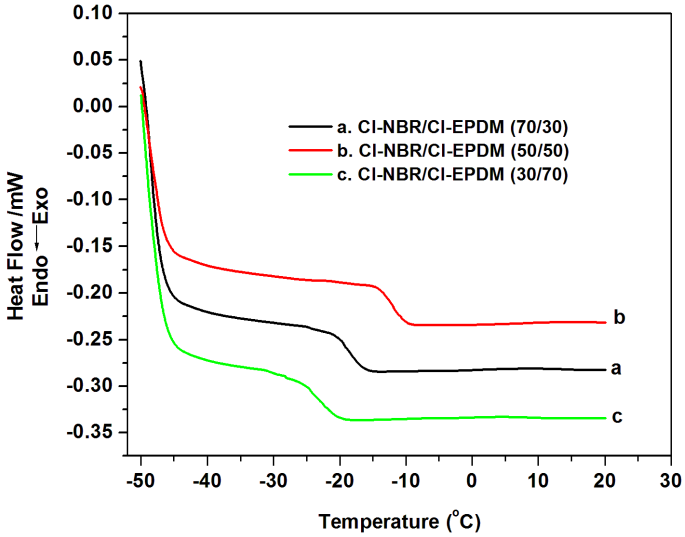

Figure 7.4 DSC thermograms of Cl- NBR/ Cl-EPDM blend samples

DSC analysis is also used to predict the compatibility of polymer blend systems. **Figure 7.4** gives the DSC thermograms of 70/30, 50/50 and 30/70 Cl-NBR/Cl-EPDM blends. The blend samples exhibit a single transition indicative of the occurrence of coupling reaction between the components. – 21.07, – 14.18 and – 25.43^{0}C are the respective *Tg* values of Cl-NBR/Cl-EPDM 70/30, 50/50 and 30/70 blend samples. Therefore, Cl-NBR/ Cl-EPDM interpolymer is formed with effectual miscibility due to the "across-phase" interaction which led to increase in the extent of the coupling reaction between functionalized elastomers [318].

Moreover 50/50 blend may show maximum miscibility which can be deduced from the highest *Tg* value obtained.

7.2.4.2 Thermogravimetric Analysis (TGA)

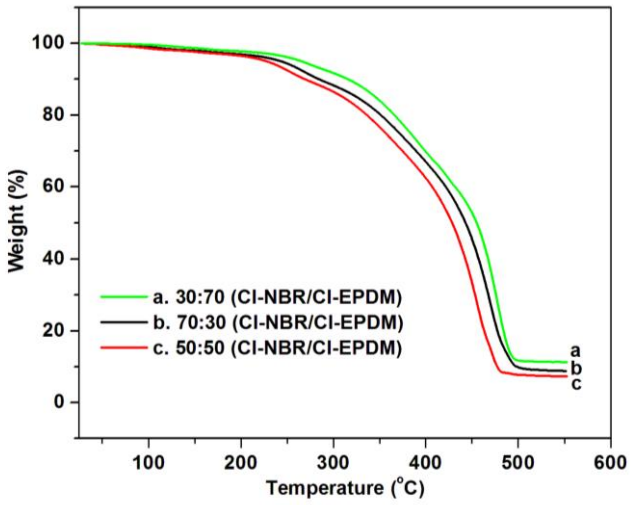

Figure 7.5 TGA thermograms of Cl- NBR/ Cl-EPDM blend samples

A detailed understanding of the thermal degradation behaviour is necessary to understand the material performance to fulfill the demands of contemporary engineering materials. The thermal stability of the prepared samples is analyzed by TGA in order to obtain the variation of the sample mass as a function of temperature. **Figure 7.5** shows typical TG curves for the Cl-NBR/Cl-EPDM blend at a constant heating rate. As in TGA plots, the sample with 30/70 Cl-NBR/Cl-EPDM shows single step degradation while 70/30 and 50/50 Cl-NBR/Cl-EPDM sample show two steps. The initial step corresponds to expulsion of

chlorine as HCl while the second degradation is due to leftover rubber chain. This clearly indicates that the homogeneity of the blends along with better interfacial adhesion via coreaction of functionalities hold back the easy transport of thermal energy which delay the breakdown of rubber molecules [177].

7.2.5 Cure Characteristics

Table 7.2 Processing characteristics of Cl-NBR, Cl-EPDM and Cl-NBR/ Cl-EPDM blends

Samples	Cure time t_{90} (min)	Scorch time t_2 (min)	Maximum Torque (dNm)	Minimum torque (dNm)
Cl-EPDM	14.6	4.62	32	7.4
Cl-NBR/Cl-EPDM (30/70)	15.6	4.36	33.5	7.7
Cl-NBR/Cl-EPDM (50/50)	15.4	3.89	34.5	7.9
Cl-NBR/Cl-EPDM (7 0/30)	15.0	3.56	31	7.2
Cl-NBR	16.5	3.26	25	4.5

The cure characteristics of Cl-NBR/Cl-EPDM rubber blends as a function of different blend ratio are summarized in **table 7.2**. The shorter M_L and higher M_H value of blend samples are indicators for the stronger interactions between gum components. The difference in torque (ΔM) attained increases with concentration of Cl-NBR and then decreases. Thus ΔM obtained is

highest for the 50/50 blend; hence at this blend ratio crosslinking is higher with the formation of interdiffused chains. Thus the presence of entanglements between the components resulted from the reaction between the functional groups can be the reason for increase in modulus. The optimum cure time (t_{90}) and scorch time (ts_2) decreases with increase in the Cl-NBR content. This is due to the fact that the cure process of Cl-NBR rubber is much slower as compared to Cl-EPDM because for the former component higher activation energy is needed to produce proper crosslink points for the curative due to the reduction in the double bonds on backbone [319, 320].

7.2.6 Mechanical properties

The variation of mechanical properties of Cl-NBR/Cl-EPDM blend with different blend ratio including the ultimate tensile strength, tear strength, hardness and elongation at break are displayed in **table 7.3**. The data reveal that the tensile and tear strength improves with increase in concentration of Cl-NBR and maximum at 50/50 ratio of rubber components; with further increase in ratio of Cl-NBR tensile and tear value drops. The increase in tensile strength with increase in Cl-NBR content may be attributed to the expected strain crystallization of Cl-NBR as a result of the stereoregular addition of polar dichlorocarbene unit under the applied stress. However, in 70/30 Cl-NBR/Cl-EPDM blend, the poor adhesion and thermodynamic miscibility owing to the increased self cross linking in Cl-NBR between the polar dichlorocarbene and polar nitrile group than with Cl-EPDM phase,

decreases its mechanical strength. The 50/50 blend shows optimum property because of the even distribution of finer domains which effectively prevent the dissemination of stress. Hardness shows a weighted average of the hardness of the individual elastomers. Also, the penetrating tip of durometer experience more resistance with increasing the content of Cl-NBR. Elongation at break shows a linear decrease for all blend samples. This is attributed to the network which is so dense that there is little energy dissipation in the matrix and the energy supplied is utilized for breaking the bonds. At higher cross link density, the segments of macromolecule become immobile, the system became stiffer and the elasticity decreases [321-323].

Table 7.3 Mechanical properties of Cl-NBR, Cl-EPDM and Cl-NBR/ Cl-EPDM blends

Samples	Tensile strength (MPa)	Elongation at break(%)	Tear strength (kN/m)	Hardness (Shore A)
Cl-EPDM	17.5	320	25.38	49
Cl-NBR/Cl-EPDM (30/70)	18.6	300	26.8	48.5
Cl-NBR/Cl-EPDM (50/50)	19.2	276	28.1	48
Cl-NBR/Cl-EPDM (7 0/30)	14.4	249	27.5	47.4
Cl-NBR	8.95	204	23.48	47

7.2.7 Electrical properties

7.2.7.1 AC Conductivity

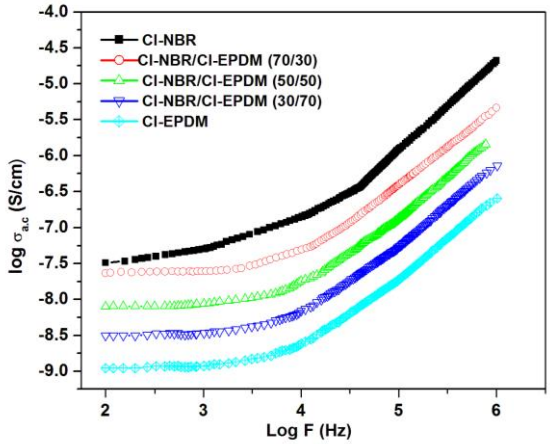

Figure 7.6 AC conductivity of Cl- NBR, Cl-EPDM and Cl- NBR/ Cl-EPDM blend

Figure 7.6 shows the variation of alternating current (AC) conductivity of Cl-NBR, Cl-EPDM and Cl-NBR/ Cl-EPDM blend with different blend ratio at different frequencies. The conductivity of all the samples shows an increasing trend with increase in frequency and also with the concentration of Cl-NBR. On increasing frequency, up to 10^4 Hz there is not much variation in conductivity while marked increase in σac is observed after 10^4 Hz due to the enhancement of hopping frequencies of charge carriers associated with the polar functional groups of each component. Further, the frequency dependence of conductivity can be described in terms of intrinsic electric dipole polarization along with interface charge polarization. The noticeable result obtained is that

conductivity increases with increase in Cl-NBR content due to the presence of dichlorocarbene group in addition to highly polar nitrile group. This will definitely increase microscopic conductivity of the system which arises from the interaction of molecules, chain entanglements and polarity [324, 325].

7.2.7.2 Dielectric constant

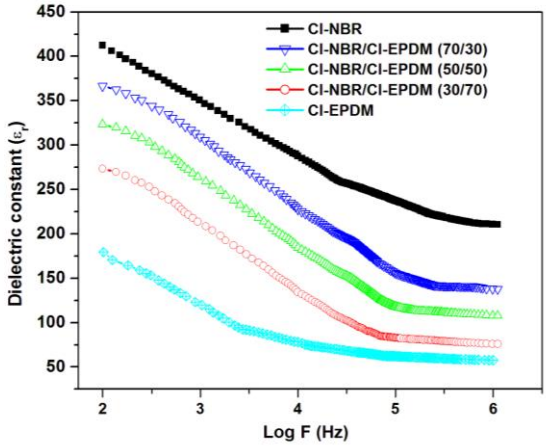

Figure 7.7 Dielectric constant of Cl- NBR, Cl-EPDM and Cl-NBR/ Cl-EPDM blend

Figure 7.7 shows the variation of dielectric constant with frequency for the Cl-NBR, Cl-EPDM and Cl-NBR/ Cl-EPDM blend with different blend ratio at room temperature. It is clear from figure that dielectric constant decreases with increase in frequency and reaches a constant value at higher frequencies. It is well known that owing to mismatch of conductivities an interfacial polarization is most likely to occur in the multi component system

at lower frequencies of dielectric measurement. But, at higher frequencies the probability of these space charges to drift and accumulate at interface usually take large time lags for mobility and do not get enough time for long range hopping before the field reversal. The dielectric permittivity has contribution from orientation, atomic and electronic polarization. The increase in εr with increase in the content of Cl-NBR can be attributed to orientation of dipoles associated with –CN dipoles and that of chlorine [326]

7.2.7.3 Dielectric loss (Tan δ)

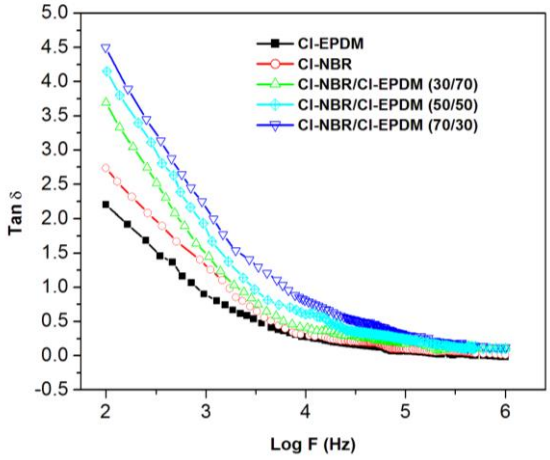

Figure 7.8 Dielectric loss tangent of Cl- NBR, Cl-EPDM and Cl- NBR/ Cl-EPDM blend

The variation of imaginary part of complex permittivity (tan δ) with frequency for the Cl-NBR, Cl-EPDM and Cl-NBR/ Cl-EPDM blend with different blend ratio is given in **Figure 7.8** . It is found that at room temperature, tan δ decreases with increasing

frequency. The higher value of dielectric loss at low frequency is due to the free charge motion within the materials. That is in this heterogeneous system, there will be a number of defects and microporosities which cause a space charge build-up at interfaces which leads to field distortions [269]. The increase in dieelectric loss value with Cl-NBR content can be attributed to the increased polarity will decrease the degrees of freedom so that the respective relaxation time also increases. Thus, it has been proposed as a good damping material.

7.2.8 Oil resistance measurement

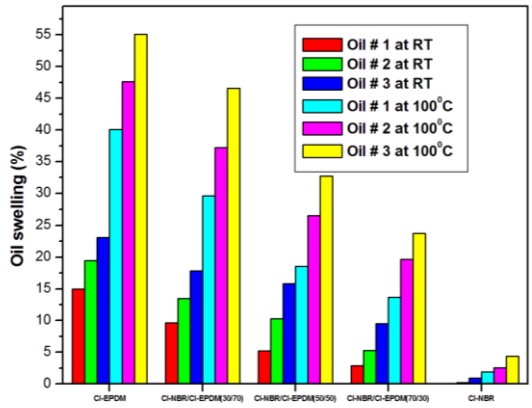

Figure 7.9 ASTM oil resistance of Cl- NBR, Cl-EPDM and Cl-NBR/ Cl-EPDM blend

Swelling studies in ASTM oils were done at 25 and 100^{0}C for the blend systems and presented in **Figure 7.9**. It is obvious from the figure that better oil resistance is obtained for the three blend ratio and the oil resistance increases with increase in concentration of Cl-NBR. As it is reported the oil resistance is

directly related to the polarity of the system, the Cl-NBR unit contains a dichlorocarbene group in addition to highly polar nitrile group. Therefore, when the blends are immersed in oil Cl-EPDM dispersed phase is markedly swollen than Cl-NBR phase [327].

7.2.9 Diffusion Studies

7.2.9.1 Mol % uptake of aromatic solvents and petroleum fuels

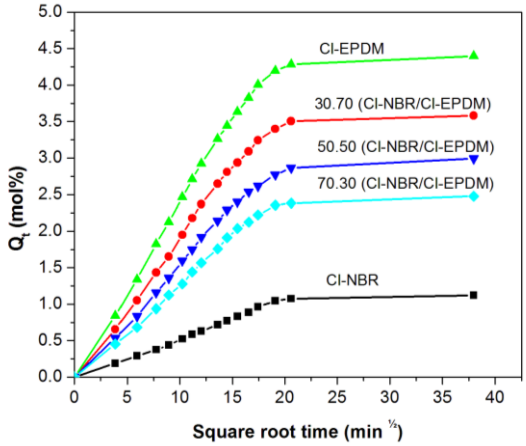

Figure 7.10 (a) Mol % uptake of Cl- NBR, Cl-EPDM and Cl-NBR/ Cl-EPDM blend in benzene

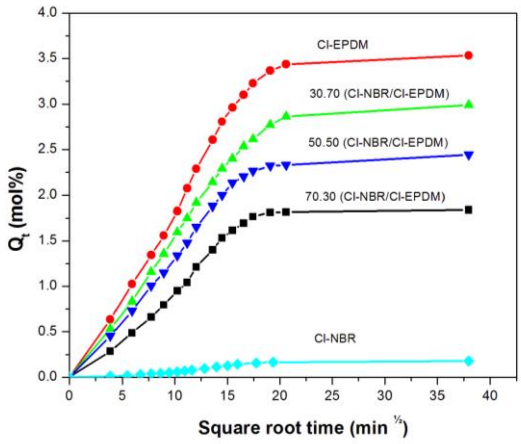

Figure 7.10 (b) Mol % uptake of Cl- NBR, Cl-EPDM and Cl- NBR/ Cl-EPDM blend in petrol

For sorption studies, circular samples, punched out from the vulcanized sheets, of known weight and thickness were immersed in about 15-20ml solvents in closed diffusion bottles, kept at a thermostatically controlled oven. At regular intervals, the samples were taken out, wiped with tissue paper to remove excess solvent and immediately weighed using an electronic balance. The samples were put back in solvents and the process is continued until equilibrium swelling was achieved. The results of the experiment are expressed in terms of mol % uptake of solvent by 0.1 kg of the sample specimen, Q_t (mol %). [328, 329]

Mathematically, Q_t can be determined by **equation 2.7**

The sorption curves are constructed by plotting the obtained Q_t values as a function of square root of time. The solvent uptake

behaviour depends on the microstructure of polymer, nature of permeants and temperature of experiment. **Figure 7.10 (a)** and **(b)** shows the variation of the Q_t (mol %) of Cl-NBR/Cl-EPDM blend with different blend ratio when benzene and petrol as the penetrants at 27^0C. It is found that the blend samples showed a lower solvent uptake tendency with increase in the percentage of Cl-NBR. Upon chlorination, the polarity of polar nitrile rubber and EPDM increases prominently which result in the chain entanglements through dipolar attraction at the interface. Also, the DCP vulcanization produces inflexible C-C covalent bonds between elastomer chains which restrict the swelling of blend in corresponding solvents. Due to these two factors the crosslink density significantly increased in the system. Thus the reduction in solvent uptake can be attributed to the increased degree of crosslinking in the matrix which relatively lower the free volume inside and decreases the rate of movement of polymer chains with solvent molecules. Besides, as the amount of Cl-NBR increases the rubbery nature of blend decreases, confirmed from XRD by the reduction in the area of amorphous peak, also supports the enhanced solvent permeation resistance of vulcanizates. [330].

Effect of nature of solvent molecules

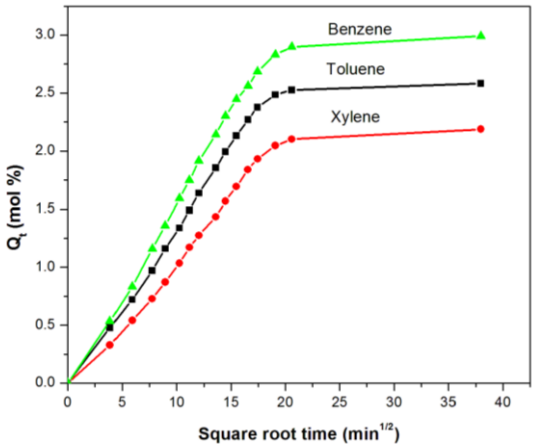

Figure 7.11 (a) Solvent uptakes of Cl- NBR/ Cl-EPDM (50/50) blend in different aromatic solvents

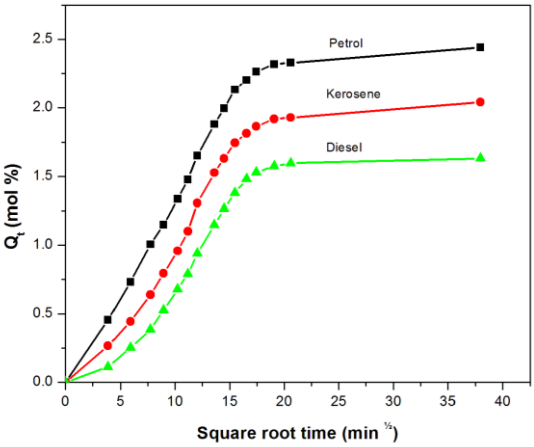

Figure 7.11 (b) Solvent uptakes of Cl- NBR/ Cl-EPDM (50/50) blend in different industrial solvents

The dependence of size of diffusing molecules on Qt values of blend is studied by using three aromatic solvents viz. benzene, toluene and xylene and three industrial solvents viz. petrol, kerosene and diesel; given in **Figure 7.11 (a)** and **(b)**. From the figure it is obvious that the transport performance of aromatic solvents is in the order benzene > toluene > xylene. That is diffusivity of solvent molecules decreases with increase in its molecular volume. Having one and two methyl side chains the toluene and xylene cannot easily diffuse into the available free volume of the modified rubber while benzene being flat can exchange the position of elastomer segments, according to free volume theory. By the same reason petroleum fuels follow the order petrol > kerosene > diesel.

The kinetics of sorption process can be studied in terms of diffusion (D), sorption (S) and permeation (P) coefficients. Table gives the estimated values of D, S, and P of blends with different ratios of Cl-NBR and Cl-EPDM in aromatic and industrial solvents.

Effect of temperature

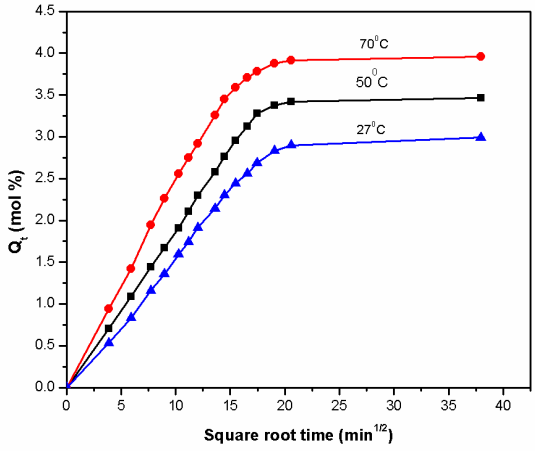

Figure 7.12 (a) Solvent uptakes of Cl- NBR/ Cl-EPDM (50/50) blend in benzene at different temperature

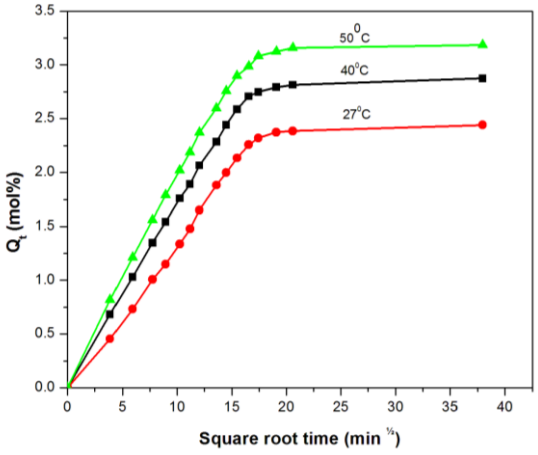

Figure 7.12 (b) Solvent uptakes of Cl- NBR/ Cl-EPDM (50/50) blend in petrol at different temperature

The diffusion studies were also conducted at higher temperature with the above mentioned three aromatic and industrial solvents for Cl-NBR/ Cl-EPDM (50/50) blend, since it shows lower

solvent uptake at room temperature. Figure 7.12(a) represents the mol% uptake of 50/50 blend at 27, 50 and 70^0C with benzene as probe molecule and Figure 7.12(b) represent sorption curve for petrol. As it is evident from the figure the solvent uptake increases with increase in temperature. The increase in sorption with temperature can be explained by the increased kinetic energy of penetrant molecules and enhanced free volume of the system due to increased macromolecular flexibility of the matrix.

7.2.9.2 Kinetic parameters

Diffusion coefficient (D)

The diffusivity of vulcanizates- solvent system can be determined using Fickian law as the ratio of the diffusing substance per unit area of cross section to the space gradient of concentration using the expression

$$D = \pi\left(\frac{h\theta}{4Q_\infty}\right)^2 \qquad \textbf{(Eq: 7.1)}$$

Where θ is the slope of the linear portion of sorption curves before reaching 50% of the Q_∞ and h is the initial thickness of the test specimen. The D values of blend samples are considerably decreased with increasing the ratio of Cl-NBR and the lowest value has been obtained for Cl-NBR/ Cl-EPDM (70/30) vulcanizates. Since chlorination generate more and more crosslinking in addition to the bonds formed as a result of vulcanization, the availability of free space to occupy solvent molecule is getting reduced. Also the high degree of crosslinking create tortuous path for transport of

solvent due to the restriction of the segmental mobility of rubber chains [331].

Sorption Coefficient (S) and Permeation Constant (P)

The sorption coefficient (S) was obtained from the plateau regions of the equilibrium sorption curves and is presented in **table7.4 (a) and (b)** for the vulcanizates in different solvents. From the table it is clear that the sorption coefficient decreases with Cl-NBR content in the rubber vulcanizate for a given solvent.

The difference in the concentration of penetrant molecules between the two sides of the barrier material also influence the rate of diffusion and it can be quantitatively expressed as permeation constant (P). P is given by

$$P = D \times S \qquad \textbf{(Eq: 7.2)}$$

where D is the diffusion constant and S is the sorption coefficient.

Permeation coefficient also decreases with increase in the weight percentage of Cl-NBR due to increase in the chain network. Again it can infer from the table that the liquid sorption and permeation behaviour of the vulcanizates in aromatic solvents is highest in benzene, followed by toluene, and then xylene. Further, industrial solvents show much lower values compared to aromatic solvents and in the case of industrial solvents both the sorption and permeation is in the order petrol > kerosene > diesel due to increase in the size of molecules in the same order [332,333].

Table 7.4 (a) Diffusion, Sorption and Permeation values of Cl-NBR/Cl-EPDM blend in aromatic solvents.

Samples	Diffusion Coefficient $D \times 10^5$ (cm^2/s)			Sorption Coefficient S			Permeation Coefficient $P \times 10^5$ (cm^2/s)		
	Benzene	Toluene	Xylene	Benzene	Toluene	Xylene	Benzene	Toluene	Xylene
Cl-NBR	3.71	3.63	3.52	1.66	1.44	1.18	6.158	5.227	4.154
Cl-NBR/ Cl-EPDM (70/30)	3.92	3.81	3.76	1.72	1.53	1.22	6.742	5.829	4.587
Cl-NBR/ Cl-EPDM (50/50)	4.14	4.11	4.03	1.87	1.69	1.31	7.742	6.946	5.279
Cl-NBR/ Cl-EPDM (30/70)	4.28	4.23	4.17	1.98	1.82	1.49	8.474	7.699	6.213
Cl-EPDM	4.39	4.31	4.26	2.19	2.07	1.78	9.614	8.922	7.583

Table 7.4 (b) Diffusion, Sorption and Permeation values of Cl-NBR/Cl-EPDM blend in petroleum fuels.

Samples	Diffusion Coefficient $D \times 10^5$ (cm^2/s)			Sorption Coefficient S			Permeation Coefficient $P \times 10^5$ (cm^2/s)		
	Petrol	Kerosene	Diesel	Petrol	Kerosene	Diesel	Petrol	Kerosene	Diesel
Cl-NBR	3.12	3.09	3.06	1.61	1.38	1.04	5.023	4.264	3.182
Cl-NBR/ Cl-EPDM (70/30)	3.84	3.78	3.71	1.78	1.54	1.17	6.835	5.821	4.340
Cl-NBR/ Cl-EPDM (50/50)	4.02	3.94	3.87	1.84	1.61	1.29	7.397	6.343	4.992
Cl-NBR/ Cl-EPDM (30/70)	4.15	4.09	4.02	1.93	1.79	1.44	8.009	7.321	5.788
Cl-EPDM	4.28	4.19	4.13	2.04	1.83	1.56	8.731	7.668	6.442

Arrhenius Parameters

The activation energy for diffusion and sorption can be computed by using Arrhenius equation, given as **equation 4.6**. The value of E_P and E_D obtained from the slope of lnX versus 1/T plot is displayed in **table7.5 (a)** (for aromatic solvents) and **in table7.5 (b)** (for petroleum fuels).

The activation energy of diffusion and permeation of solvent progressively increases with increase in the ratio of Cl-NBR and highest Ep and E_D value is found for Cl-NBR/ Cl-EPDM (70/30) blend. From the literature, it is found that the mechanism of diffusion of a penetrant molecule is well explained as a series of jumps through a mass of tangled polymer chains and cavities. The thermal fluctuations are responsible for the constant destruction and reformation of cavities. Each jump requires the disruption of rubber-rubber and rubber to penetrant interactions in order that the surrounding chains can rearrange themselves to allow the passage of the diffusing molecules. Chlorination of bare rubbers increases the rigidity of the vulcanizates due to reduction in unsaturation and on blending there form dense crosslinks at the interface of the two homopolymer chains due to enhanced dipolar attraction. Therefore solvent molecule has to impart high energy to penetrate in to the matrix and thus increases activation energy for sorption process.

Table 7.5 (a) E_P (KJ/mol) and E_D (KJ/mol) values of Cl-NBR/Cl-EPDM blend in aromatic solvents.

Samples	Benzene		Toluene		Xylene	
	E_P	E_D	E_P	E_D	E_P	E_D
Cl-NBR	5.11	3.74	5.39	3.94	5.69	4.13
Cl-NBR/ Cl-EPDM (70/30)	5.07	3.72	5.24	3.88	5.36	3.94
Cl-NBR/ Cl-EPDM (50/50)	4.93	3.69	5.12	3.83	5.28	3.89
Cl-NBR/ Cl-EPDM (30/70)	4.81	3.62	4.91	3.72	5.07	3.83
Cl-EPDM	4.72	3.58	4.81	3.65	4.94	3.76

Table 7.5 (b) E_P (KJ/mol) and E_D (KJ/mol) values of Cl-NBR/Cl-EPDM blend in petroleum fuels.

Samples	Petrol		Kerosene		Diesel	
	E_P	E_D	E_P	E_D	E_P	E_D
Cl-NBR	5.18	3.92	5.57	4.21	5.71	4.26
Cl-NBR/ Cl-EPDM (70/30)	5.02	3.87	5.26	4.01	5.52	4.2
Cl-NBR/ Cl-EPDM (50/50)	4.94	3.86	5.14	3.92	5.24	3.98
Cl-NBR/ Cl-EPDM (30/70)	4.86	3.81	4.99	3.87	5.07	3.93
Cl-EPDM	4.81	3.78	4.89	3.83	4.99	3.89

7.2.9.3 Thermodynamics parameters

By van't Hoff equation (**equation 4.8**), the sorption enthalpy (ΔHs) and entropy (ΔSs) were also calculated. The regression analysis of log Ks vs 1/T plot gives the values ΔHs and

ΔSs and presented in table **7.6 (a)** for aromatic solvents and **7.6 (b)** for petroleum fuels. ΔH_S is a composite parameter involving contributions from Henry's law and Langmuir's (hole-filling) sorption mechanism. Here, the positive ΔH_S values obtained for all solvents suggest that sorption in this study is dominated by Henry's mode with an endothermic contribution. That is the formation of a site and the dissolution of the species into that site occurs in an endothermic path way. The enthalpy values increases with increasing the Cl-NBR content in the blends. The ΔS values of the fabricated blends decrease with increase in nitrile content suggest decreased disorderness of solvent molecules.

The calculated values of ΔG_S in different solvents are shown in **tables 7.6 (a)** and **7.6 (b)**. The values obtained reveals that the spontaneity of solvent diffusion decreases with increase in the weight % of Cl-NBR.

Table 7.6 (a) ΔH, ΔS and ΔG values of Cl-NBR/Cl-EPDM blend in aromatic solvents

Samples	ΔH (KJ/mol)			ΔS(J/mol)			-ΔG(KJ/mol)		
	Benzene	Toluene	Xylene	Benzene	Toluene	Xylene	Benzene	Toluene	Xylene
Cl-NBR	1.37	1.45	1.56	29.90	27.95	24.80	7.6	6.935	5.88
Cl-NBR/ Cl-EPDM (70/30)	1.32	1.37	1.43	25.15	24.34	22.86	6.225	5.932	5.428
Cl-NBR/ Cl-EPDM (50/50)	1.24	1.29	1.37	23.18	21.63	20.07	5.714	5.199	4.651
Cl-NBR/ Cl-EPDM (30/70)	1.16	1.19	1.24	22.74	20.65	18.0	5.662	5.005	4.16
Cl-EPDM	1.13	1.15	1.19	21.64	18.24	16.24	5.362	4.322	3.682

Table 7.6 (b) ΔH, ΔS and ΔG values of Cl-NBR/Cl-EPDM blend in petroleum fuels

Samples	ΔH (KJ/mol)			ΔS(J/mol)			-ΔG(KJ/mol)		
	Petrol	Kerosene	Diesel	Petrol	Kerosene	Diesel	Petrol	Kerosene	Diesel
Cl-NBR	1.28	1.38	1.46	28.74	26.45	23.08	7.342	6.555	5.464
Cl-NBR/ Cl-EPDM (70/30)	1.16	1.27	1.3	23.55	22.04	20.86	5.905	5.342	4.958
Cl-NBR/ Cl-EPDM (50/50)	1.08	1.22	1.27	22.89	20.63	18.17	5.787	4.969	4.181
Cl-NBR/ Cl-EPDM (30/70)	1.06	1.13	1.14	21.74	19.45	16.98	5.462	4.705	3.954
Cl-EPDM	1.03	1.06	1.1	20.26	17.98	14.82	5.048	4.334	3.346

7.2.9.4 Mechanism of sorption

The mechanism of transport of solvent molecule through modified rubber has been found out from the swelling data using the empirical **equation 4.10**. The constants n and k are obtained on the linear regression analysis and the values obtained for aromatic and industrial solvents are given in **table 7.7 (a) and (b)**. The constant k, characteristic of sample under consideration, indicates the interaction between penetrant and polymer. As the percentage of Cl-NBR content increases the value of k decreases indicating less interaction between solvent and the samples. This may due to loss of free volume in the blends due to dense packing. It is the value of n which relates the rate of diffusion of solvent molecule and rate of exchange of polymer chain by the permeants. By Ficks diffusion law there are three mechanisms for sorption of solvents based on n value. For Fickian diffusion, the value of n is equal to 0.5 where concentration gradient is the predominant driving force for transport of molecules. For a non Fickian mode of diffusion, n is unity and then the relaxation rate of polymer chain is much less than rate of diffusion. The diffusion is considered as anomalous when the value of n falls in between 0.5 and 1. Here the value of n obtained is in between 0.5 and 1, indicating an anomalous mode of transport because of the comparable rate of diffusivity and chain relaxation. [334,335].

Table 7.7 (a) n and k values of values of Cl-NBR/Cl-EPDM blend in aromatic solvents at room temperature

Samples	Benzene		Toluene		Xylene	
	n	k (min^{-1})	n	k (min^{-1})	n	k (min^{-1})
Cl-NBR	0.77	0.12	0.8	0.1	0.82	0.08
Cl-NBR/ Cl-EPDM (70/30)	0.74	0.17	0.78	0.14	0.78	0.10
Cl-NBR/ Cl-EPDM (50/50)	0.68	0.19	0.76	0.18	0.76	0.15
Cl-NBR/ Cl-EPDM (30/70)	0.67	0.24	0.72	0.19	0.72	0.17
Cl-EPDM	0.59	0.29	0.69	0.22	0.68	0.20

Table 7.7 (b) n and k values of Cl-NBR/Cl-EPDM blend in petroleum fuels at room temperature

Samples	Petrol		Kerosene		Diesel	
	n	k (min^{-1})	n	k (min^{-1})	n	k (min^{-1})
Cl-NBR	0.39	0.28	0.47	0.26	0.52	0.22
Cl-NBR/ Cl-EPDM (70/30)	0.34	0.33	0.46	0.28	0.46	0.24
Cl-NBR/ Cl-EPDM (50/50)	0.32	0.34	0.41	0.29	0.45	0.27
Cl-NBR/ Cl-EPDM (30/70)	0.29	0.37	0.39	0.31	0.43	0.30
Cl-EPDM	0.26	0.41	0.26	0.35	0.39	0.32

7.3 Conclusions

Cl-NBR and Cl-EPDM elastomer blends with different blend ratio were prepared by two roll mill mixing technique. The formation of blend samples was characterized by FTIR, XRD, SEM, TGA and DSC. FTIR spectrum of blend showed the presence of characteristic IR absorption of both the components with a slight shift in frequency indicating effective miscibility of these blend through the chlorine groups attached to each elastomer which itself act as compatibilising agent. XRD result clearly depicts the structural changes occurred in the fabricated samples as the amorphous peak considerably reduced with an increase in the content of Cl-NBR. SEM images showed the uniform mixing of both Cl-NBR and Cl-EPDM in 50/50 blend ratio due to their surface roughness and polarity. The TGA curves indicated the better thermal stability of polymer blend than the individual polymers due to the effective interaction between blend components. The DSC analysis exhibit a single transition due to the "across-phase" interaction, indicative of the coupling reaction between the functional groups of the components. The AC conductivity and dielectric properties increased with increase in the weight percentage of Cl-NBR due to the intrinsic electric dipole polarization along with interface charge polarization. The cure characteristics, mechanical, electrical, oil and solvent transport properties of the blend vulcanizates were also analyzed with respect to blend ratio. The optimum cure time of the blend

increases with Cl-NBR due to fewer number of double bonds left after chlorination. The sample with 50/50 blend ratio showed better tensile and tear strength due to the effective interfacial interactions between the blend components. The studies based on the sorption and transport properties of ASTM oils, petroleum fuels and aromatic solvents support the superior compatibility of Cl-NBR/Cl-EPDM blend.

8.1 Introduction

The production of polymer blends or alloys through the existing commercial polymers offers opportunities for technological success in the synthesis of new materials with desirable properties more rapidly in a cost effective route [23, 336]. The commercially useful elastomer– elastomer combination usually characterized by a coarse and unstable morphology coupled with poor interfacial adhesion between the phases. The immiscibility of the system owing to differences in chemical structure and viscosities of the individual polymers may result in premature failure upon stress transfer. The present day rubber industries use different types of fillers to meet a given service application or sets of performance parameters and to attain compatibility between the components of a polymer blend with weight reduction and cost effectiveness. Fillers specifically in the nano-range reduce macroscopic inhomogeneities and improve the morphological stability by decreasing the interfacial tension and subsequently reducing the dispersed phase size. Thus the nanocomposites formed have been widely used in many fields, such as automobile and tire industries, construction and foot packaging fields, electrical fields and so on [337-340].

Considerable research works has been done by scientists on elastomer based blends because of its good properties and the best properties from each component can be still improved. The blend prepared by mixing conventional rubbers like NBR and EPDM still

deserve attention via nano filler incorporation, especially because of the excellent oil and fuel resistance of NBR and higher environmental resistance of EPDM [341,342]. Sau et al reported that acetylene black filled EPDM / NBR Blend showed greater conductivity and the conductivity increases with increasing temperature [343]. Subramanian et al analyzed various properties under accelerated air ageing of typical formulations based on EPDM and NBR for rubber seal applications [344]. The studies of Jovanovic´et al on carbon black N330 reinforced NBR/EPDM rubber blend explored the effect of filler on the activation energy of crosslink (Eac) and reversion (Ear) process, morphology and thermal behavior of the blends [175]. Zeid reported the effect of radiation and HAF carbon black loading on NBR/EPDM blend [345]. Tiwari et al investigated the properties of polyacetylene coated silica filled NBR/EPDM [346]. The effect of carbon black fillers viz. semi reinforcing furnace (SRF), high abrasion furnace (HAF) and intermediate super abrasion furnace (ISAF) carbon blacks on the cure, swelling and mechanical properties of 70/30 EPDM/NBR blend have been investigated by Manoj et al [347].

Nowadays, the bio-based fillers aroused a significant amount of interest to produce polymer composites for various applications that satisfies our primary concern about the environment [348]. Hydroxyapatite which belongs to inorganic bioceramic category has been extensively used in medicine for implant fabrication as well as in non-medical applications. HA is very compatible with polar group containing polymers due to its

nano-size and porous nature in addition to the presence of several P-OH groups on the surface.

This chapter discusses on the preparation of Cl-NBR/ Cl-EPDM (50:50) blend nanocomposites with different loading of HA nanoparticles. The blend composites were characterized by FTIR, UV-VIS spectroscopy, XRD, SEM, TGA and DSC. The compatibility of blend composites was also be evaluated in terms of their cure and mechanical characteristics, electrical conductivity studies, oil, fuel and solvent resistance.

8.2 Results and Discussion

8.2.1 FTIR Spectroscopy

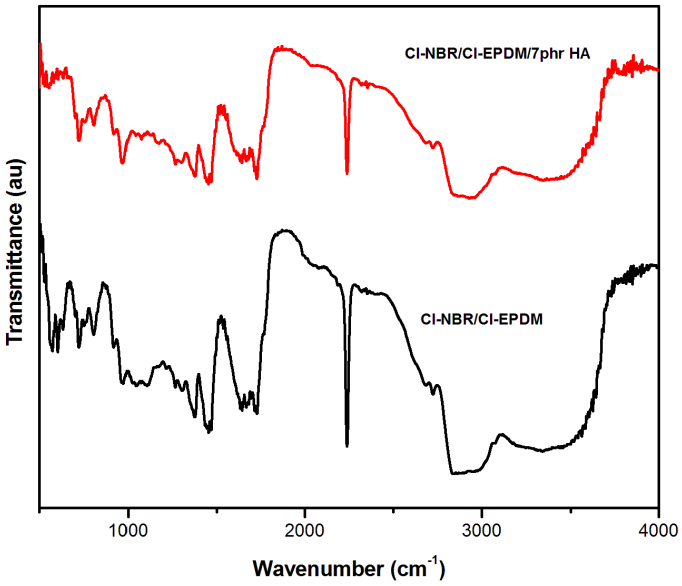

Figure 8.1 FTIR Spectra of Cl- NBR/ Cl-EPDM (50/50) and Cl- NBR/ Cl-EPDM/ 7 phr HA

The FTIR spectrum recorded for the Cl-NBR/Cl-EPDM (50/50) blend with 7 phr of HA particles is shown in **Figure 8.1**. It is worthy to note from the figure that the nanocomposite shows an overlapping IR absorption spectrum with the presence of characteristic peaks corresponding to Cl-NBR, Cl-EPDM and HA nanoparticles with some shifts in wavenumbers. That is the peaks at 969 (*trans* δ (–CH=CH–) wagging motion vibration) 803 (υ(C-Cl) stretching vibration of Cl-NBR), 1463 (-CH stretching vibration from polyethylene band) and 609 cm^{-1} (υ(C-Cl) stretching of Cl-EPDM) are shifted to 974, 807, 1457 and 549 cm^{-1} respectively. The absorption peak at 3392, 606 and 563 cm^{-1} correspond to the typical stretching vibration of at a particle. So the spectrum highlights the presence of polar-polar interaction between the functionalities attached to the surface of matrix and the filler may sensibly affect the IR frequencies of individual components. Similar observations were reported earlier [334]. Or the spectra of nanocomposite unambiguously displays the better dispersion of nanoparticles in the matrix and this suggest that by reducing the interfacial tension the nano HA probably act as compatibilizer between the different phases of the blend matrix. It is expected that the hydroxyl groups on HA are able to interact with the chloro, dichlorocarbene and nitrile groups of base matrix, giving rise to a more homogeneous structure.

8.2.2 X-ray Diffraction analysis (XRD)

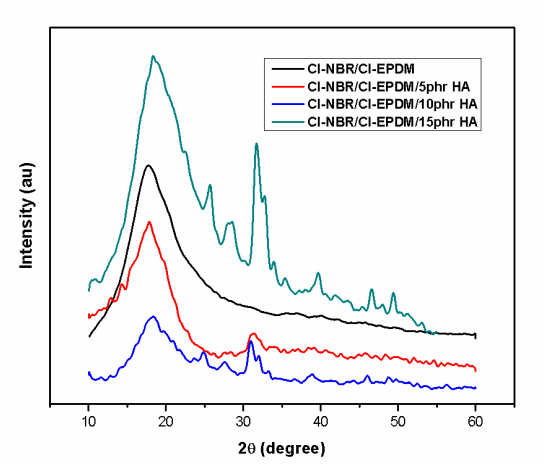

Figure 8.2 XRD pattern of Cl- NBR/ Cl-EPDM/ HA nanocomposites

Figure 8.2 shows the X-ray diffraction profile of HA, Cl-NBR/Cl-EPDM (50/50) blend and its nanocomposites with 5, 10 and 15phr of HA. It is presented in previous chapters; the XRD pattern of pure HA contains many crystalline peaks which have been matched with the JCPDS data (9-432) of HA. As can be seen in the figure, XRD diffractogram of base matrix shows a displacement towards higher angles; from $2\theta = 17.41^0$ to 18.4^0 corresponds to d spacing 4.81 A^o in all the nanocomposite presented along with the crystalline peaks of HA nanofiller. As the concentration of HA increases the number of crystalline peaks also increases. It is important to mention that the intensity of most of the diffraction peaks of HA is found to be increased in both the composite presented; pinpointing to the structural reorganization

occurred in HA particles for the effective insertion in to the macromolecular chains. Also, the polarity of blend matrix favors the uniform dispersion of nano particles [349].

8.2.3 Scanning electron microscopy (SEM)

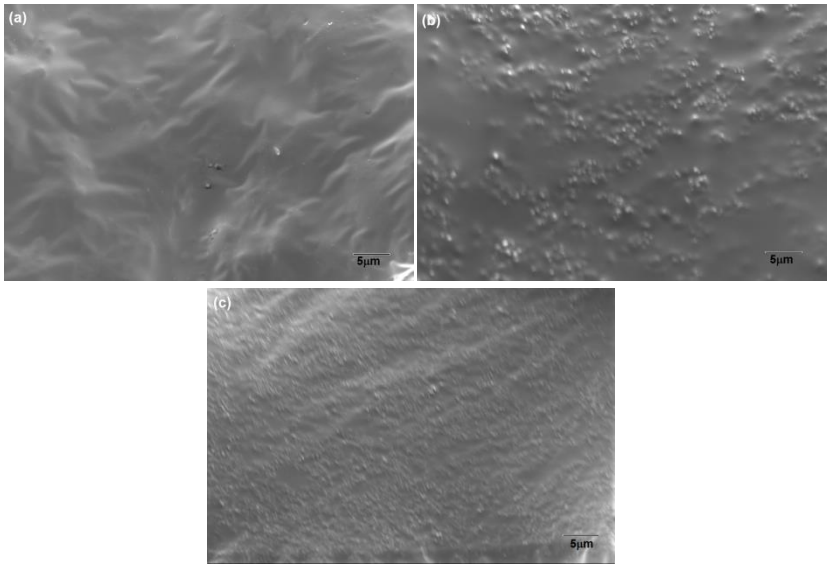

Figure 8.3 SEM images of a) Cl-NBR/Cl-EPDM b) Cl-NBR/Cl-EPDM /5phr HA c) Cl-NBR/Cl-EPDM / 7phr HA

The SEM images of Cl-NBR/Cl-EPDM blend with different contents of HA particles are given in **Figure 8.3.** The texture of bare blend is considerably changing with the addition of HA nanoparticles. Cl-NBR/Cl-EPDM/ 7phr HA shows fairly cleaner surface compared to other samples. That is 7phr HA loading have achieved the maximum dispersion in the matrix with reduced domain size where the intermolecular interaction between filler and matrix chains has also reached the maximum value. At still higher

loading, the filler- filler attraction increases due to close contact between them, than filler- rubber interaction which leads to highly branched and interlinked morphology.

8.2.4 Thermal Behaviour

8.2.4. a Differential Scanning Calorimetry (DSC)

DSC characterizes the interface structure which in turn strongly influences the segmental motion of the rubber chains. That is the nature and strength of interface may change *Tg*.

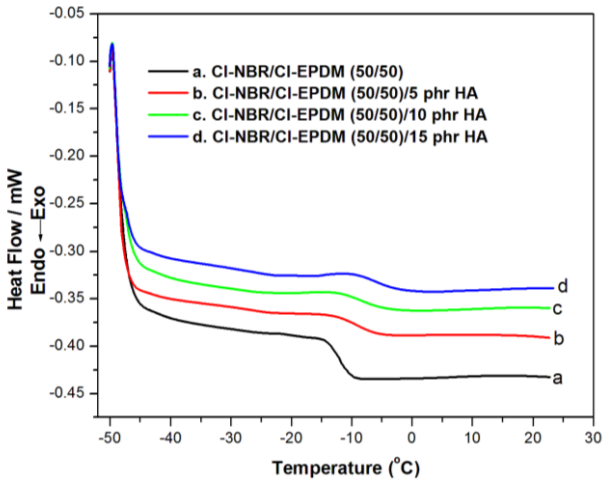

Figure 8.4 DSC thermograms of Cl- NBR/ Cl-EPDM blend with HA nanoparticles

Figure 8.4 shows the DSC thermograms of the Cl-NBR/Cl-EPDM/HA nanocomposites with different content of HA nanoparticles. It can be seen from figure that after the addition of

HA, the glass transition temperature of the composites increases than that of the pure blend matrix. The *Tg*s have been found to be shifted towards a higher temperature region from -14.12^0C (for Cl- NBR/ Cl-EPDM (50:50)) to -9.5^0C (for Cl- NBR/ Cl-EPDM/15phr HA). This observation can be explained by the decrease in the flexibility of the polymer chains in filled cross linked polymeric system. As evident from the previous analysis, the polar network formed between the molecules of the matrix is reinforced by the hydroxyapatite. [125]

8.2.4. b Thermogravimetric analysis (TGA)

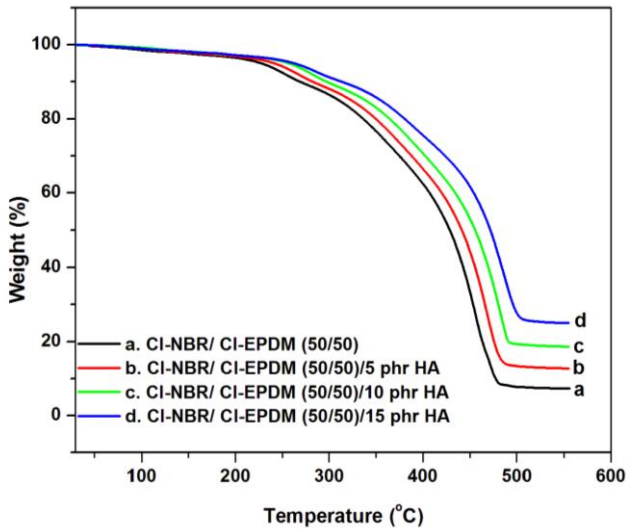

Figure 8.5 TGA thermograms of Cl- NBR/ Cl-EPDM blend with different contents of HA nanoparticles

The thermal stability is among the most important properties of polymers because during processing and/or use they are often exposed to high temperatures. The thermal stability of a material is defined by the specific temperature or temperature–time limit in which the material can be used without excessive mass loss. At a programmed heating rate the temperature beginning of decomposition of the sample determines its stability. The TGA thermograms of 50/50 Cl-NBR/ Cl-EPDM blends along with its HA composite is given in **Figure 8.5**. The value of temperature corresponding to the onset of decomposition for the composites is higher than that of pristine blend. This might be due to the higher interfacial interaction between nanoparticles and polymer chain. It is very clear from the figure that the higher thermal stability and thus the increased char residue obtained for nanocomposites affirmed that rate of weight loss is consistently decreasing with incorporation of nano HA. The effective interaction of the homogeneously dispersed filler particles with the macromolecular chain will restrict the continuous decomposition of the rubber matrix between the nano HA and blend molecules by hindering the evaporation of decomposition products and the access of oxygen. Therefore the addition of HA leads to the increase of the onset and completion of the thermal degradation temperatures in addition to better flame resistance.

8.2.5 Cure characteristics

The typical cure characteristics of Cl-NBR/Cl-EPDM rubber blends as a function of varying concentration of HA nano fillers are summarized in **table 8.1**. As expected, the minimum torque, M_L which is considered as representative of the elastic modulus of uncured blends increase with the loading of nanoparticles. So the M_L value is a sign of filler–filler aggregations. The maximum torque value (M_H) is definitely associated with the effect of physical reinforcement of filler and the network density of the blend vulcanizates. It is clear that the M_H values increase with an increase in the percentage of nano HA reached maximum and then decreased. The 7phr loaded sample shows the highest torque value; revealing the extent of reinforcement is highest in Cl-NBR/Cl-EPDM/ 7phr HA vulcanizates. Thus the strong inter molecular interaction increase the rigidity of the blend system which reduces the mobility of polymer chains in the matrix. However, above 7phr loading, the rheometric torque decreases due to agglomeration and diluent effect resulting in the separation of component phases at the interface. The optimum cure time (t_{90}) and the scorch time decreases regularly with an increase in the percentage of hydroxyapatite in the composites owing to the activation of the blend system for vulcanization by the filler particles. It is assumed that the nanoparticles act as co activators and facilitate the even distribution of curatives due to more homogeneous mixing of blend components [335].

Table 8.1 Processing characteristics of Cl- NBR/ Cl-EPDM (50/50) blend with different loading of HA nanoparticles

Samples	Cure time t_{90} (min)	Scorch time t_2 (min)	Maximum Torque (dNm)	Minimum torque (dNm)
Cl-NBR/Cl-EPDM	15.4	3.89	34.5	7.9
Cl-NBR/Cl-EPDM / 3 phr HA	15.1	3.78	36.1	8.3
Cl-NBR/Cl-EPDM / 5 phr HA	14.8	3.59	37.9	8.6
Cl-NBR/Cl-EPDM / 7 phr HA	14.4	3.41	39.4	9.0
Cl-NBR/Cl-EPDM / 10 phr HA	14.1	3.26	38.6	8.8
Cl-NBR/Cl-EPDM / 15 phr HA	13.9	3.12	38.1	8.7

8.2.6 Mechanical properties

The mechanical properties such as the tensile strength, tear resistance, elongation at break and hardness of Cl-NBR/ Cl-EPDM (50/50) blend and its nanocomposites with different HA content are given in **table 8.2**. It is well known that the effect of reinforcement is directly related to the properties of the interphase; nature of the specific interactions between elastomer and reinforcing fillers, its crystallinity and the optimum reinforcement is achieved when the filler is well dispersed in the rubber matrix. From the table, it can be observed that the tensile strength of the filled systems is higher

compared with the pure blend and with the increase in HA content, the tensile strength increase to its optimal value (7phr loading) and then decreases. In the case of nano HA filled samples, the most strained chains between two filler particles might get a chance of slipping to relieve the tension caused by stretching and this homogenous distribution of stress will improve the strength.

Table 8.2 Mechanical properties of Cl- NBR/ Cl-EPDM (50/50) blend with different loading of HA nanoparticles

Samples	Tensile strength (MPa)	Elongation at break(%)	Tear strength (kN/m)	Hardness (Shore A)
Cl-NBR/Cl-EPDM	19.2	276	28.11	48
Cl-NBR/Cl-EPDM / 3 phr HA	21	268	29.97	49
Cl-NBR/Cl-EPDM / 5 phr HA	23.9	253	31.88	50
Cl-NBR/Cl-EPDM / 7 phr HA	26.7	244	34.22	51
Cl-NBR/Cl-EPDM / 10 phr HA	25.8	230	33.44	53
Cl-NBR/Cl-EPDM / 15 phr HA	24.6	218	32	55

Cl-NBR/Cl-EPDM/ 7phr HA composite has maximum tensile strength values. Since tensile strength is a complex function of crosslink density, it can be deduced that 7 phr HA content form a good anchorage between the phase component of the blends and the interaction between chlorinated segments and the filler excellent compatibility between filler and rubber. Tear resistance show similar behaviour as that of tensile strength which indicates the reinforcement effect of the filler. The maximum tear resistance is also observed for NBR/EPDM/ 7phr HA blend composite which can be explained by favorable interactions at the phase boundaries incorporating the filler, as a result of the homogeneous filler dispersion. On the other hand, further addition of filler led to decrease of these properties most probably due to the aggregation of the filler at higher loading. One can see from the table that that the addition of nano hydroxyapatite increases the hardness of the sample and decreases the % of elongation at break consistently with increase in loading of filler which reflects an improved stiffness for the blend composites due to entanglement of polymer chains. The presence of entanglements between the components is a consequence of both the reaction between the functional groups of homopolymers and the extended interfacial zone due to high aspect ratio of fillers [178,301].

8.2.7. Electrical properties

8.2.7.1 AC Conductivity Studies

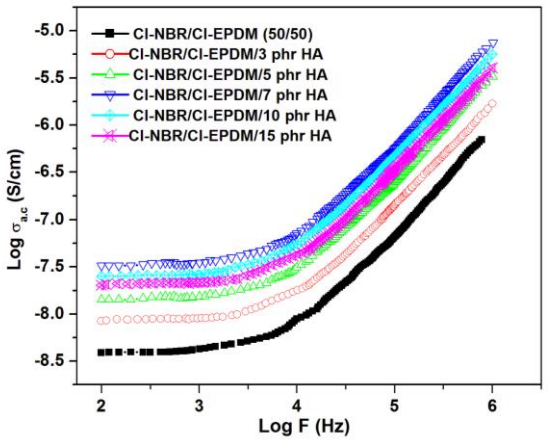

Figure 8.6 AC conductivity of Cl- NBR/ Cl-EPDM (50/50) blend with different loading of HA nanoparticles

Figure 8.6 presents the variation of AC conductivity of Cl-NBR/Cl-EPDM blend with various concentrations of HA particles at room temperature. The AC conductivity of blend and blend composites gradually increases with increase in frequencies and after 10^4 Hz the magnitude of increase become sharper; indicating a hopping type conduction mechanism. That is, on application of electric field the charge carriers associated with the dipoles present in the system will hope from one site into the other. Further, the conductivity of Cl-NBR/Cl-EPDM/HA composites is higher than the unfilled blend and the conductivity increases with the concentration of nano filler particles. In comparison with the bare blend system, the incorporation of crystalline nano HA powder

imparts a well-defined compact structure (as evident from XRD) and more uniform distribution of molecular dipoles in the nanocomposites which significantly improve the linkage through grain boundaries leading to higher conductivity. The composite with 7phr HA powder shows maximum conductivity; further loading of nanoparticles decreases the magnitude of hopping of charge carriers. Therefore tunneling mechanism is more dominant at 7phr loading of HA where optimum interfacial interactions between the nanoparticles and the polar segments of the matrix are achieved. Above optimum concentration of filler, the conductivity decreased due to the high aggregating tendency of nanoparticles leading to poor miscibility at interface [350, 351].

8.2.7.2 Dielectric constant

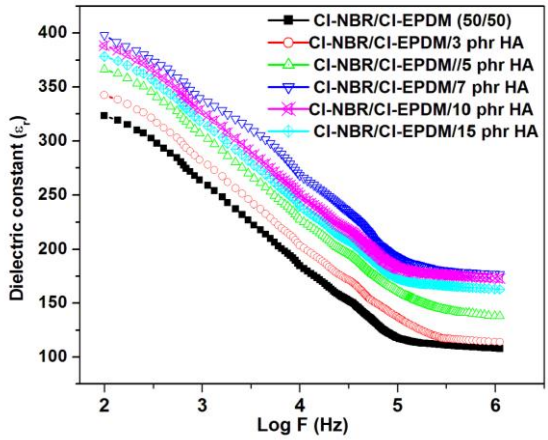

Figure 8.7 Dielectric constant of Cl- NBR/ Cl-EPDM (50/50) blend with different loading of HA nanoparticles

The effect of HA nanoparticles on the dielectric constant of fabricated Cl-NBR/Cl-EPDM with various content of nanoparticle is given in **Figure 8.7**. On increasing the frequency, the dielectric constant of all the samples decreases and the property becomes nearly constant at higher frequencies. At lower frequency the dipoles arrange themselves with the applied field and thus the enhanced relaxation of the dipolar units contribute to the high dielectric value of samples. Also, the dielectric constant of all filled blend sample is much higher than that of pure blend and increases with an increase in the concentration of nano HA particles due to enhancement in conductive interactions. This can be explained by the generation of space charge polarization at the interfaces of the constituents due to the migration of free charge carriers through the composite materials. The Cl-NBR/Cl-EPDM with 7 phr HA shows higher dielectric constant due to high polarization induced as a result of the uniform distribution of nanoparticles and the dense structure of the sample. Beyond 7phr, the dielectric constant decreases with further addition of fillers due to the agglomeration of nanoparticles which restrict segmental motion of the macromolecular chain [240,352].

8.2.7.3 Dielectric loss (Tan δ)

Dielectric loss is a measure of the electrical energy dissipated in an insulating material for the total power applied to the material. **Figure 8.8** shows the variation of tan delta with frequency in the case of Cl-NBR/Cl-EPDM blend and its

nanocomposites containing different filler loadings of HA. It is seen that the tan delta values are found to decrease with an increase in the frequency and increase with increase in the filler loading. The distinct variations in the trends of tan delta (similar to dielectric constant) with respect to frequency are usually associated with the occurrence of additional polarization at the interface. At lower frequency, more energy is required for the polarization of grain boundaries whereas the polarization reduces with increase in frequency. The polar filler present inserted increases the interactions between the polar components of the blend and this leads to the accumulation of space charge, which affects the field distortions and dielectric loss. The maximum dielectric loss is shown for the sample containing 7phr HA, indicates that the nanoparticles concentration at this proportion is optimum. At higher loading space charge accumulation decreases due to agglomeration of filler particles [353, 354].

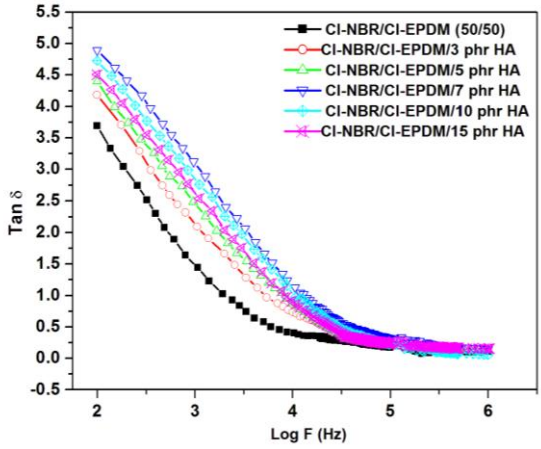

Figure 8.8 Dielectric loss tangent of Cl- NBR/ Cl-EPDM (50/50) blend with different loading of HA nanoparticles

8.2.8 Oil resistance measurement

Figure 8.9 shows the effect of blend ratio on the oil swelling properties of Cl-NBR/Cl-EPDM (50/50) blend and its nanocomposites with different HA Particles. The degree of volume swelling in ASTM oils mainly depends on the polymer- solvent interaction parameter, crosslink density, crystallinity and type of crosslinking. It can found from figure that the extent of swelling decreases with increases in the loading of nanoparticles up to 7phr HA while the filler concentration is at 10phr and above a slight increase is observed. Thus the incorporation of crystalline HA can endow polar network in the material especially at the interface which will hinder the easy diffusion of oil molecules. Further the viscosity of oil molecules plays a vital role in the oil resistance properties of the materials. Oils with reduced viscosity caused greater penetration into the blends. Thus the order of penetration follows the trend IRM 903> IRM 902> IRM 901; the aniline point increases in the same order. However the oil resistance decreases with temperature due to the softening of crosslink points at elevated temperatures [320,355].

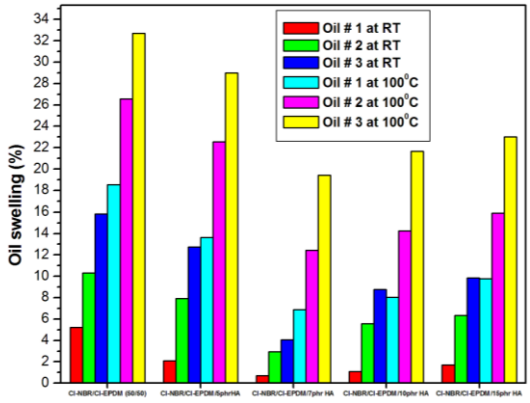

Figure 8.9 ASTM oil resistances of Cl- NBR/ Cl-EPDM (50/50) blend with different loading of HA nanoparticles

8.2.9 Diffusion Studies

8.2.9.1 Mol % uptake of aromatic and petroleum fuels

Effect of HA concentration on mol uptake

The results of sorption of different solvents were expressed in terms of the mole percentage uptake (Q_t) at time‘t’. For comparison, the mole percentage uptake by Cl-NBR/Cl-EPDM/HA blend having varying HA content with benzene and petrol as probe molecules as a function of square root of time were plotted and are represented in figure **8.10 (a)** and **8.10 (b)**.

As it is already said, the solvent uptake behaviour of composite system depends on the filler content, temperature and molecular weight of probe molecules.

It is clear from the sorption curve that all the nanocomposite systems show a reduced solvent uptake tendency compared to the unfilled elastomer blend. This is because of the filler particles modifies the segmental mobility of the rubber matrix and the reinforcement offered by them restricts the long-range movements of the macromolecules. The polarity of both filler and matrix increased the probability of multiple interactions between them which leads to extensive reduction in free volume available for solvent transport. Cl-NBR/ Cl-EPDM/7phr HA nanocomposite imparts the maximum solvent resistance where enhanced surface area of the reinforcing phase leading to the superior homogeneity and interfacial adhesion between filler and matrix with lower free volume compared to other samples [356].

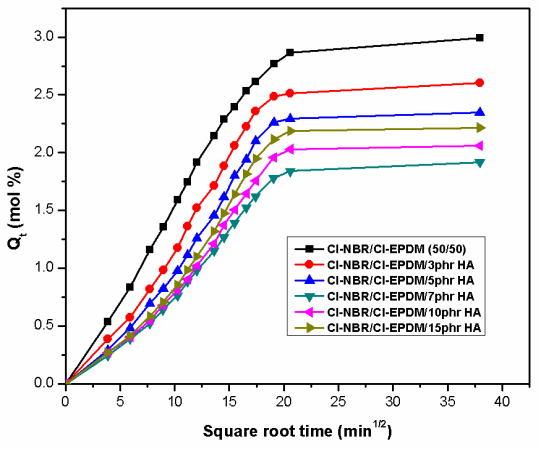

Figure **8.10 (a)** Mol % uptake of Cl- NBR/ Cl-EPDM (50/50) blend with different loading of HA nanoparticles in benzene

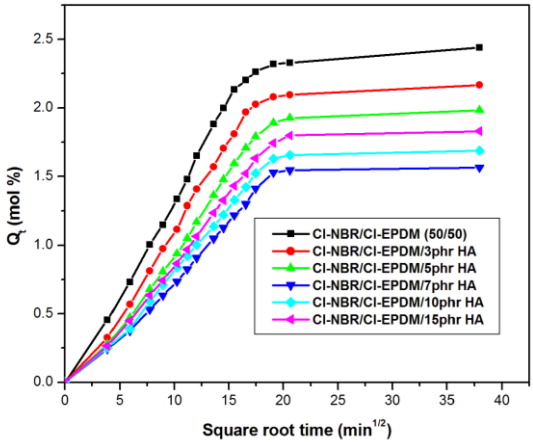

Figure 8.10 (b) Mol % uptake of series of Cl- NBR/ Cl-EPDM/ HA nanocomposites in petrol

Nature of Solvents

The effect of penetrant size on the mol % uptake of the Cl-NBR/ Cl-EPDM/7phr HA by aromatic and industrial solvents is plotted in Figure **8.11 (a)** and **8.11(b)**. Solvents with different molecular size showed a systematic trend in the transport behaviour. In all the systems it can be observed that the value of mole percentage uptake decreases with an increase in molecular size of the solvent molecules. In the case of aromatic solvents, the molecular size increases in the order xylene> toluene > benzene and thus rate of sorption follows the order xylene< toluene< benzene. As far as the petroleum fuels are concerned the maximum sorption is for petrol, kerosene comes at the intermediate and diesel shows minimum equilibrium sorption. This behaviour is in accordance with the free volume theory; primarily the diffusion of

a molecule through a polymer matrix depends on the ease with which polymer chain segments exchange their positions with penetrant molecules according to the availability of free volume in the matrix. The ease of exchange becomes less, particularly in the case of filler reinforced matrices with increase in penetrant size.

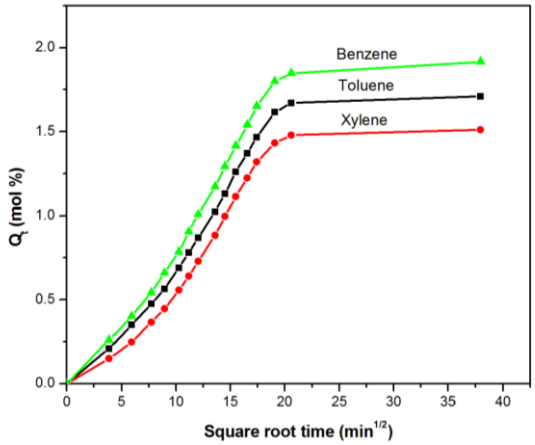

Figure 8.11 (a) Solvent uptakes of Cl-NBR/Cl-EPDM/7 phr HA in different aromatic solvents

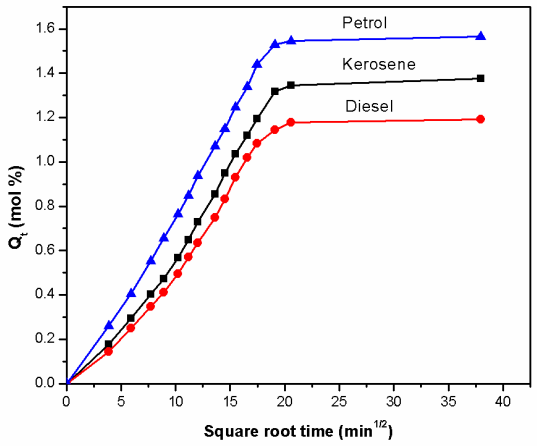

Figure 8.11 (b) Solvent uptakes of Cl-NBR/Cl-EPDM/7 phr HA in different industrial solvents

Effect of Temperature

The dependence of sorption and diffusion behaviour of aromatic solvents through blend composites on temperature was studied by doing the experiments at 27, 50 and 70^0C while that of petroleum fuels were done at 27, 40 and 50^0C. The diffusion curves of Cl-NBR/ Cl-EPDM/7phr HA at different temperatures in benzene and petrol are shown in **Figure 8.12 (a)** and **8.12(b)**. As it is expected, the rate of diffusion and the maximum solvent uptake have been found to increase with temperature.

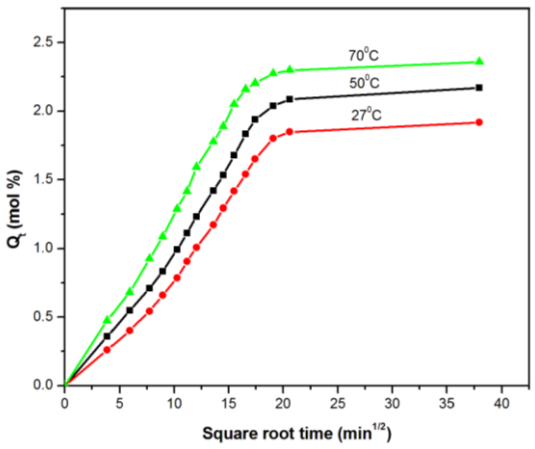

Figure 8.12 (a) Solvent uptakes of Cl-NBR/Cl-EPDM/7 phr HA in benzene at different temperature

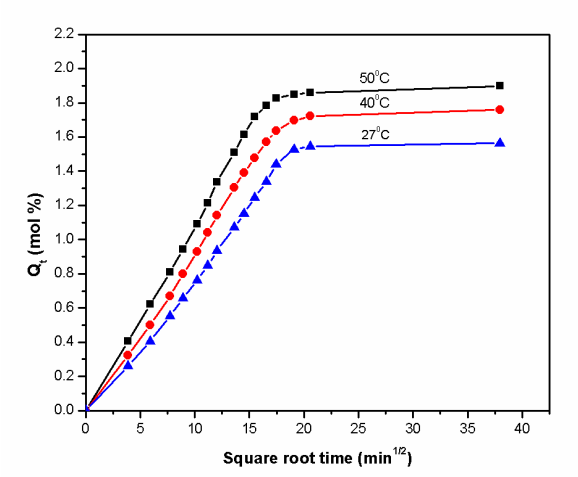

Figure 8.12 (b) Solvent uptakes of Cl-NBR/Cl-EPDM/7 phr HA in petrol at different temperature

8.2.9.2 Kinetic parameters

Diffusion Coefficient (D)

As a result of diffusion of a solvent through the polymer matrix the system will expand and thus the molecular interaction between the neighboring polymer chains weakens. The reinforcing fillers can significantly control the molecular mobility of the network. The overall diffusion coefficient can be calculated using the **equation 4.3**

The estimated values of diffusion coefficient for aromatic solvents and petroleum fuels are given in **table 8.3 (a)** and **table 8.3 (b)**. It can be seen that all the filled systems are showing lower D values compared to bare matrix as seen in many other elastomer based composites. The theoretical explanation given to this

observation is that each filler particle behaves as an obstacle to the diffusing solvent molecule. The increased surface area of reinforcing phase restricts the chain mobility which in turn reduces the free spaces inside for the ingression of solvent molecules. It is also found that the D values are minimum for 7 phr HA filled sample for the given blend ratio. That is 7phr is the optimum loading of nanoparticles which ensures better interfacial adhesion whereas above 7 phr extended filler-filler network is formed in addition to filler–matrix interaction leading to poor interaction. The D value is also influenced by the molar volume of the penetrant molecules so that higher energy is needed for the exchange of positions between molecular chain and penetrant molecules. The low D values obtained for petroleum fuels compared to aromatic solvents summarized in Table is in line with this observation.

Sorption Coefficient (S)

The polymer-solvent interactions can be expressed in terms of the sorption coefficient (S) which is calculated using the **equation 4.4**. Sorption coefficient presented on **table 8.3 (a)** and **table 8.3 (b)** corresponding to aromatic and industrial solvents show similar behaviour as that of diffusion coefficient. That is sorption process is least in 7 phr HA filled blend sample due to the higher interfacial adhesion between the blend components.

Permeation Coefficient (P)

The permeation of a solvent molecule into the rubber matrix depends on the diffusivity as well as on the solubility or sorptivity of the penetrant in the matrix. Hence permeation coefficient (P) has been computed as the product of the diffusion coefficient and sorption coefficient [357]. It is observed that the P values (from **table 8.3 (a)** and **table 8.3 (b))** also follow the same trend as that of D and S, in terms of filler loading as well as penetrant size. In comparison with the unfilled system, the rate of permeation decreases for the filler reinforced system which can be attributed to the better barrier properties imparted by the filler particles in the blend matrix. Cl-NBR/Cl-EPDM/ 7phr HA showed the minimum diffusivity and sorptivity; as a consequence minimum permeability due to more effective interfacial interaction at the interfacial zone of the composite material. That is the rate of polymer chain relaxation of the nanocomposite is higher compared to the diffusion rate of the penetrant.

Table 8.3 (a) Diffusion, Sorption and Permeation values of Cl-NBR/Cl-EPDM/HA blend nanocomposites in aromatic solvents.

Samples	Diffusion Coefficient $D \times 10^5$ (cm^2/s)			Sorption Coefficient S			Permeation Coefficient $P \times 10^5$ (cm^2/s)		
	Benzene	Toluene	Xylene	Benzene	Toluene	Xylene	Benzene	Toluene	Xylene
Cl-NBR/ Cl-EPDM (50/50)	4.14	4.11	4.03	1.87	1.69	1.31	7.742	6.946	5.279
Cl-NBR/ Cl-EPDM/HA (3phr)	4.09	4.03	3.99	1.81	1.57	1.29	7.403	6.327	5.147
Cl-NBR/ Cl-EPDM/HA (5phr)	4.02	3.98	3.92	1.78	1.52	1.22	7.156	6.049	4.782
Cl-NBR/ Cl-EPDM/HA (7phr)	3.71	3.58	3.43	1.71	1.49	1.09	6.344	5.334	3.739
Cl-NBR/ Cl-EPDM/HA (10 phr)	3.89	3.72	3.56	1.75	1.53	1.14	6.807	5.692	4.058
Cl-NBR/ Cl-EPDM/HA (15phr)	3.92	3.75	3.59	1.79	1.56	1.17	7.017	5.85	4.200

Table 8.3 (b) Diffusion, Sorption and Permeation values of Cl-NBR/Cl-EPDM/HA blend nanocomposites in petroleum fuels.

Samples	Diffusion Coefficient $D \times 10^5$ (cm^2/s)			Sorption Coefficient S			Permeation Coefficient $P \times 10^5$ (cm^2/s)		
	Petrol	Kerosene	Diesel	Petrol	Kerosene	Diesel	Petrol	Kerosene	Diesel
Cl-NBR/ Cl-EPDM (50/50)	4.02	3.94	3.87	1.84	1.61	1.29	7.397	6.343	4.992
Cl-NBR/ Cl-EPDM/HA (3phr)	3.78	3.71	3.68	1.77	1.54	1.22	6.690	5.713	4.489
Cl-NBR/ Cl-EPDM/HA (5phr)	3.45	3.37	3.31	1.73	1.49	1.12	5.968	5.021	3.707
Cl-NBR/ Cl-EPDM/HA (7phr)	3.12	3.07	2.99	1.67	1.42	1.04	5.210	4.359	3.109
Cl-NBR/ Cl-EPDM/HA (10 phr)	3.34	3.27	3.21	1.69	1.45	1.07	5.645	4.741	3.435
Cl-NBR/ Cl-EPDM/HA (15phr)	3.38	3.29	3.23	1.71	1.46	1.09	5.779	4.803	3.520

Arrhenius parameters

The activation energy for diffusion and sorption are calculated by using Arrhenius equation**.** Values of E_P and E_D with aromatic solvents and petroleum fuels as the penetrant are presented in **table 8.4 (a)** and **table 8.4 (b)**. It can be observed that as the concentration of HA increases E_P and E_D values increase. The better distribution of nanoparticles induces a higher resistance to solvent permeation and diffusion, as it is explained in the previous chapter. The diffusion of penetrant molecules depend not only on the attraction of rubber and solvent but also on the availability of appropriate molecular size holes in the network which is depend on the chain entanglement densities.

Table 8.4 (a) E_P (KJ/mol) and E_D (KJ/mol) values of Cl-NBR/Cl-EPDM/HA blend nanocomposites in aromatic solvents.

Samples	Benzene		Toluene		Xylene	
	E_P	E_D	E_P	E_D	E_P	E_D
Cl-NBR/ Cl-EPDM (50/50)	4.91	3.69	4.94	3.7	5.07	3.83
Cl-NBR/ Cl-EPDM/HA (3phr)	4.98	3.74	5.15	3.89	5.22	3.95
Cl-NBR/ Cl-EPDM/HA (5phr)	5.06	3.79	5.22	3.93	5.27	3.98
Cl-NBR/ Cl-EPDM/HA (7phr)	5.23	3.91	5.33	3.98	5.4	4.03
Cl-NBR/ Cl-EPDM/HA (10 phr)	5.14	3.88	5.25	3.95	5.35	4.01
Cl-NBR/ Cl-EPDM/HA (15phr)	5.1	3.87	5.21	3.93	5.3	3.98

Table 8. 4 (b) E_P (KJ/mol) and E_D (KJ/mol) values of Cl-NBR/Cl-EPDM/HA blend nanocomposites in petroleum fuels.

Samples	Petrol		Kerosene		Diesel	
	E_P	E_D	E_P	E_D	E_P	E_D
Cl-NBR/ Cl-EPDM (50/50)	4.94	3.86	5.14	3.92	5.24	3.98
Cl-NBR/ Cl-EPDM/HA (3phr)	5	3.89	5.23	3.97	5.32	4.02
Cl-NBR/ Cl-EPDM/HA (5phr)	5.08	3.94	5.31	4.03	5.43	4.09
Cl-NBR/ Cl-EPDM/HA (7phr)	5.24	4.05	5.43	4.09	5.5	4.11
Cl-NBR/ Cl-EPDM/HA (10 phr)	5.19	4.03	5.36	4.06	5.44	4.07
Cl-NBR/ Cl-EPDM/HA (15phr)	5.14	4.01	5.31	4.02	5.41	4.05

8.2.9.3 Thermodynamics parameters

Table 8.5 (a) and **8.5(b)** `represent the respective values of ΔHs, ΔSs and ΔGs of sorption for aromatic solvents and industrial fuels. The positive values of ΔHs indicate that the sorption is endothermic and thus, is dominated by Henry's mode instead of Langmuir type. ΔHs value decreases for the HA filled blends. ΔSs values decreases with HA loading due to increased interfacial interaction between blend matrix and nanoparticles. ΔGs values are increased from unfilled blend to its HA based nanocomposites. Thus, the spontaneity of sorption decreases in nanocomposites with filler loading and a minimum is obtained for blend with 7phr HA where there is better cross link density and optimum reinforcement.

Table 8. 5 (a) ΔH, ΔS and ΔG values of Cl-NBR/Cl-EPDM/HA blend nanocomposites in aromatic solvents.

Samples	ΔH (KJ/mol)			ΔS(J/mol)			-ΔG(KJ/mol)		
	Benzene	Toluene	Xylene	Benzene	Toluene	Xylene	Benzene	Toluene	Xylene
Cl-NBR/ Cl-EPDM (50/50)	1.24	1.26	1.37	23.18	21.63	20.07	5.714	5.229	4.651
Cl-NBR/ Cl-EPDM/HA (3phr)	1.25	1.27	1.39	22.55	19.78	18.86	5.515	4.664	4.268
Cl-NBR/ Cl-EPDM/HA (5phr)	1.27	1.29	1.39	20.96	18.64	17.17	5.018	4.302	3.761
Cl-NBR/ Cl-EPDM/HA (7phr)	1.33	1.35	1.47	15.24	12.37	14.74	3.242	2.361	2.952
Cl-NBR/ Cl-EPDM/HA (10 phr)	1.25	1.31	1.46	16.05	14.55	15.42	3.565	3.055	3.166
Cl-NBR/ Cl-EPDM/HA (15 phr)	1.23	1.29	1.44	17.94	16.02	16.1	4.152	3.516	3.39

Table 8. 5 (b) ΔH, ΔS and ΔG values of Cl-NBR/Cl-EPDM/HA blend nanocomposites in petroleum fuels.

Samples	ΔH (KJ/mol)			ΔS(J/mol)			-ΔG(KJ/mol)		
	Petrol	Kerosene	Diesel	Petrol	Kerosene	Diesel	Petrol	Kerosene	Diesel
Cl-NBR/ Cl-EPDM (50/50)	1.08	1.22	1.27	22.89	20.63	18.17	5.787	4.969	4.181
Cl-NBR/ Cl-EPDM/HA (3phr)	1.12	1.27	1.31	20.55	18.40	17.86	5.045	4.25	4.048
Cl-NBR/ Cl-EPDM/HA (5phr)	1.14	1.25	1.34	19. 98	17.63	15.17	4.854	4.039	3.211
Cl-NBR/ Cl-EPDM/HA (7phr)	1.19	1.32	1.39	13.47	11.45	12.84	2.851	2.115	2.462
Cl-NBR/ Cl-EPDM/HA (10 phr)	1.16	1.3	1.36	15.26	13.98	13.82	3.418	2.894	2.786
Cl-NBR/ Cl-EPDM/HA (15 phr)	1.13	1.28	1.36	16.72	15.84	15.01	3.886	3.472	3.143

8.2.9.4 Sorption mechanism

The mechanism of transport has been found out using the equation [358]

$$\mathrm{Log}\left(\frac{Q_t}{Q_\infty}\right) = \log k + n \log t \qquad \textbf{(Eq: 8.1)}$$

where Qt and Q∞ are as mentioned earlier. The value of constant 'k' cast light on to the structural characteristics of the matrix and its interaction with the solvent. The magnitude of constant 'n' describes the transport mode. For Fickian transport (n = 0.5), the rate of macromolecular chain relaxation is higher compared to the rate of diffusion of the penetrant whereas a slower chain relaxation than the penetrant diffusion rate suggest non-Fickian transport (n=1). If both the rubber chain relaxation process and rate of diffusion of penetrant are comparable, then the mode of transport is said to be anomalous ($0.5 < n < 1$). The values of 'n' and k are given in **table 8.6 (a)** and **8.6(b)**. The values of 'n' indicate that the mode of transport for the composites deviates from the regular Fickian trend and can be defined as anomalous. As the filler content increases, the matrix becomes more rigid due to the increased degree of reinforcement of the filler particles. Therefore, the rate of polymer chain relaxation become slow compared to the concurrent penetrant diffusion and the transport in filled system follow a relaxation-controlled diffusion process. As usual, the k values in the reinforced system are lower than the base blend due to

the reduced solvent-matrix interactions which can be attributed to better 'across phase' adhesion through the improved interface. Also, it is very obvious from the table that the blend composites shows less swelling in petroleum fuels than in aromatic solvents [359].

Table 8.6 (a) n and k values of values of Cl-NBR/Cl-EPDM/HA blend nanocomposites in aromatic solvents at room temperature

Samples	Benzene		Toluene		Xylene	
	n	k (min^{-1})	n	k (min^{-1})	n	k (min^{-1})
Cl-NBR/ Cl-EPDM (50/50)	0.68	0.19	0.76	0.18	0.76	0.15
Cl-NBR/ Cl-EPDM/HA (3phr)	0.74	0.17	0.78	0.16	0.77	0.12
Cl-NBR/ Cl-EPDM/HA (5phr)	0.78	0.16	0.79	0.14	0.78	0.11
Cl-NBR/ Cl-EPDM/HA (7phr)	0.80	0.12	0.82	0.11	0.83	0.08
Cl-NBR/ Cl-EPDM/HA (10 phr)	0.79	0.14	0.80	0.12	0.81	0.09
Cl-NBR/ Cl-EPDM/HA (15 phr)	0.78	0.15	0.79	0.13	0.81	0.09

Table 8.6 (b) n and k values of Cl-NBR/Cl-EPDM/HA blend nanocomposites in petroleum fuels at room temperature

Samples	Petrol		Kerosene		Diesel	
	n	k (min^{-1})	n	k (min^{-1})	n	k (min^{-1})
Cl-NBR/ Cl-EPDM (50/50)	0.32	0.34	0.41	0.29	0.45	0.27
Cl-NBR/ Cl-EPDM/HA (3phr)	0.34	0.33	0.45	0.28	0.46	0.24
Cl-NBR/ Cl-EPDM/HA (5phr)	0.36	0.32	0.46	0.26	0.48	0.23
Cl-NBR/ Cl-EPDM/HA (7phr)	0.4	0.28	0.49	0.21	0.51	0.19
Cl-NBR/ Cl-EPDM/HA (10 phr)	0.39	0.30	0.48	0.23	0.49	0.21
Cl-NBR/ Cl-EPDM/HA (15 phr)	0.37	0.30	0.47	0.24	0.49	0.22

8.3 Conclusions

In this study Cl-NBR/Cl-EPDM blend with different content of hydroxyapatite were prepared by a simple two roll mill mixing technique. The change in position of IR absorption peak of nanocomposite displays the better interaction of the hydroxyl groups on HA with the polar functional groups of Cl-NBR and Cl-EPDM. The XRD pattern showed that the blend composite attains an ordered arrangement pinpointing to the structural reorganization occurred in HA particles for the effective insertion in to the

polymer blend. The FESEM images revealed the polarity of blend matrix favors the uniform dispersion of nanoparticles inside the blend matrix. The higher glass transition temperature obtained for nanocomposites with increase in concentration of nanoparticles due to the confinement of elastomer chains. The TGA analysis disclosed the increase in the thermal degradation temperatures of the nanocomposites in addition to improved flame resistance due to better reinforcement of hydroxyapatite. The effect of fillers on the cure and mechanical properties of the blends have been investigated and found to be increased with increase in filler loading up to 7phr HA loading. AC conductivity, dielectric constant and dielectric loss of blend nanocomposites were higher than that of pure 50/50 blend. Cl-NBR/Cl-EPDM/7phr HA showed maximum electrical properties because tunneling mechanism is more dominant at 7phr loading of HA where optimum interfacial interactions between the nanoparticles and the polar segments of the matrix are achieved. Also, the HA filled samples have been found to show a reduced oil, fuel and solvent uptake compared to the bare matrix which can be explained by the increase in the rigidity of the polymer chains due to filler reinforcement and enhanced crosslink density of the matrix.

9.1 Conclusions

Synthetic rubber comes in nearly a dozen major types with potential benefits for various applications. Two common synthetic rubber compounds are known as EPDM and nitrile rubber. EPDM is a high-density, saturated, non-polar rubber and exhibits a number of useful properties, including heat stability, ageing resistance, and water resistance. On the other hand, NBR is a random copolymer of butadiene and acrylonitrile. It has high polarity, having polar C≡N groups, and is one of the most important industrial raw material. The biggest differences between these two rubber products lie in their resistance to petroleum-based fuel and lubrication products, and their resistance to weathering. As it is realized that synthesis of new elastomers are not always necessary for finding selected technological applications, three major strategies were used for tuning the physico-chemical properties of commercial diene rubbers. Thus there has been growing interest on producing new materials from existing ones via chemical modification, impregnation of fillers and blending. All have a positive impact on cost as well as a decreased impact on the environment.

The present work is an investigation of variation of different properties of chemically functionalized NBR and EPDM.

Nitrile rubber (NBR) based nanocomposite consists of different concentrations of HA nanoparticles were prepared and

characterized by FTIR, UV and X-ray diffraction studies. The FTIR spectra confirmed the interfacial interaction between NBR and the HA nanoparticles. The shift in the UV peak with broadness of composite indicates the formation of nanoparticles within the macromolecular chain of NBR. XRD pattern ascertained the ordered arrangement of nanoparticles with a decrease in the amorphous nature of parent polymer. Both the glass transition temperature and the thermal stability of the nanocomposites were higher than pure NBR and the glass transition temperature improved with the increase in concentration of nanoparticles in NBR composite indicate the strong interfacial adhesion between the polymer and nanoparticles. From DSC studies, thermodynamic parameters such as enthalpy and entropy change of the composites were also evaluated. AC conductivity of the nanocomposite was much greater than NBR and the magnitude of conductivity enhanced with the addition of nanoparticles. The observed enhancement in dielectric constant and dielectric loss tangent of composite with the increase in concentration of nanoparticle was attributed to the increase in number of interfacial interaction between the elastomer and the nanoparticles.

Hydroxyapatite nanoparticles filled EPDM rubber have been prepared and characterized. Nanocomposites of EPDM with HA nanoparticles were prepared by mechanical mixing in a two roll mill in presence of dicumyl peroxide (DCP) as crosslinking agent. The structural reorganization of nanocomposite was studied

by FTIR, UV-Visible spectroscopic techniques and XRD. Spectroscopic studies revealed that the incorporation of nanoparticles into the elastomer leads to an interfacial interaction between the nanoparticles and polymer. The XRD analysis ascertained the presence of HA nanoparticles in the EPDM chain. Optical and scanning electron microscopy was conducted to characterize the dispersion of nanoparticle inside the macromolecular chain of EPDM. The changes in thermal behaviour of EPDM rubber was characterized by TGA and DSC. The thermal stability and glass transition temperature of nanocomposites were increased with the increase in weight percentage of HA nanoparticles. The AC electrical conductivity and dielectric constant of nanocomposites were found to be increased with the increase in concentration of nanoparticles.

A systematic attempt has been done, through the present investigation, to develop and characterize chloro functionalized elastomers. Chlorinated acrylonitrile butadiene rubber (Cl-NBR) was prepared from NBR by the alkaline hydrolysis of chloroform, using phase-transfer catalysis. The formation of Cl-NBR was monitored by ^{1}H-NMR, UV-Vis, and Fourier transform infrared spectroscopic techniques. The percentage of chlorine attached to the rubber chain was estimated by Volhard method. The effect of polar groups on the structural and thermal properties of Cl-NBR was analyzed by scanning electron microscopy, X-ray diffraction analysis, differential scanning calorimetry and thermogravimetric

analysis studies. The flame retardant, oil resistance, cure behavior and mechanical properties of chlorinated elastomer were also analyzed. The proton NMR revealed the attachment of chlorine in the backbone of NBR with new chemical shift values. The C-Cl stretching of chlorinated NBR was confirmed from FTIR. The UV spectrum also supported the formation of chlorinated unit in the NBR chain through the shifts and broadening of absorption peaks. The X-ray diffraction analysis pattern indicated a decrease in the amorphous domain of NBR with an increase in the level of chemical modification. The increased glass transition temperature obtained from differential scanning calorimetry confirms the increased molecular rigidity of the chlorinated NBR and thermal transitions increased with increase in the level of chemical modification. The thermal stability of Cl-NBR decreased with an increase in chlorine content. The flame and oil resistance of Cl-NBR was greatly higher than pure NBR due to the increased polarity of modified rubber. The superior tensile strength of Cl-NBR (4 times higher than pure NBR) and higher oil resistance find applications in pump diaphragms, aircraft hoses, oil-lined tubing, and gaskets materials with the excellent flame resistant property. The transport characteristics of petroleum fuels and aromatic solvents through the membranes have been studied by a simple sorption gravimetric analysis in different temperature range. The diffusion results have been explained in terms of the size of liquid molecules and the diffusion mechanism was found to follow the anomalous trend. The activation energy for diffusion, sorption and

permeation process was evaluated. The solvent uptake tendency decreases up to sample containing 22% chlorine content and then increased. The change in transport properties can be correlated with the crosslink density calculated using Flory-Rehner theory. The oil resistance property of Cl-NBR was significantly higher than pure NBR. The electrical conductivity, dielectric properties of NBR was found to be increased with the increase in the chlorine content of NBR over the whole frequency range due to combined effect of increased hopping probability and crosslink density in the elastomer. The dielectric constant and loss tangent shows similar behavior to ac frequency and the increase of dielectric properties with the increase in chlorination is attributed to interfacial polarization and space charge distribution in the macromolecule as a result of the uniform arrangement of dipoles associated with the polar side groups. The higher AC conductivity and dielectric properties, solvent and oil resistance of Cl-NBR than that of NBR suggests that the chlorinated NBR can be used as multifunctional materials for flexible nano-electronic devices and high performance oil resistant applications.

Nanocomposite based on chlorinated acrylonitrile butadiene rubber loaded with different ratios of hydroxyapatite nanoparticles were prepared by using a simple and efficient mill mixing technique at room temperature to improve bulk properties. The inclusion of nano filler in the chlorinated elastomer matrix was investigated via spectral, morphological and thermal behaviour of

nanohybrid. The shift in characteristic FTIR and UV absorption frequencies of nanocomposites confirmed the presence of HA inserted between Cl-NBR chains. The XRD pattern investigated together with an examination of morphology by SEM showed better dispersion of HA with a decrease in amorphous nature of elastomer matrix. The addition of HA barely changes the glass transition temperature and decomposition behaviour as evidenced from DSC and TGA. Importantly, the processability and mechanical properties of nanocomposites are greatly reinforced by with varying concentration of HA filler due to the formation of polar networks in matrix which parallel their interactions. The present study well demonstrated the improved electrical properties, enhanced oil resistance in addition to fuel and solvent diffusion properties which can be due to the nanoscale effects and strong interactions between the Cl-NBR matrix and the nano HA interface. The magnitude of the increase in the physical, mechanical and diffusion properties reached the optimum level at 7 phr nanoceramic HA loading and above 7phr loading the particles became aggregated. Thus the newly fabricated Cl-NBR/ HA nano hybrid is very promising from the industrial viewpoint due to simplicity of the preparation technique of both matrix and filler, biodegradability and biocompatibility of ceramic filler and above all good cost/performance ratio. It is stressed that the Cl-NBR/ 7phr HA nano hybrid with superior strength may serve well in flexible nano-electronic devices, oil and solvent sealing products etc.

Halogenation of EPDM has been carried out by passing chlorine gas by a simple and inexpensive chemical method. Chlorinated EPDM was characterized by FTIR and UV spectroscopy, SEM, TGA, DSC and AC conductivity measurements. FTIR and UV spectra revealed the attachment of chlorine to double bond of EPDM. SEM images showed the coarsen morphology arising from polar nature of the resulting polymer. TGA and DSC analysis indicated that the chlorination on EPDM affected the basic decomposition pattern and glass transition temperature of synthesized polymer. Conductivity of halogenated polymer was significantly increased with increase in chlorine content and also with increase in frequency.

Nanocomposites composed of chlorinated ethylene propylene diene monomer rubber (Cl-EPDM) with various contents of hydroxyapatite nanoparticles (HA) were prepared in an open two-roll mixing mill. The effect of nanoparticle concentration on structural, morphological, thermal, and electrical properties were examined by different characterization technique such as FTIR, Uv-vis spectra, XRD, SEM, DSC, TGA and impedance analyzer. The shift in the IR and UV absorption frequencies of nanohybrid relative to that of chlorinated EPDM indicated the successful encapsulation of crystalline hydroxyapatite particles in the modified elastomer chain. The X-ray diffraction pattern of the fabricated composite revealed the more ordered arrangement of nanoparticles within the elastomer chains and the amorphous nature

of polymer decreases with raise in filler loading. The examination of nanocomposite morphology by SEM showed that the inorganic particles were well dispersed in the organic phases. TGA analysis showed the enhanced thermal stability of the composites with increase in the loading of nanoparticles. Shift in the glass transition temperature to a higher value in DSC thermograms of new hybrid indicated the increased orderness of the Cl-EPDM/HA nanocomposite. The significant increase in the interfacial interaction is evidenced by the values of maximum torque during the rheological studies. The tensile and tear properties of filled rubber increases with increase in concentration of HA, reached the maximum for Cl-EPDM/10phr HA nanocomposite and then decreased. Thus 10phr HA was observed as the optimum loading. The AC electrical conductivity was influenced significantly by the frequency of applied field and the concentration of nanofiller. Dielectric properties strongly distort at lower frequencies but became independent as frequency increased above 10^3 Hz. The marked increase in electrical and dielectric properties suggests that the Cl-EPDM/HA nanocomposite has potential application in the field of nanotechnology where flexibility is important criteria and in various electronic industries.

Cl-NBR and Cl-EPDM elastomers with different blend ratio were prepared, by simple two roll mill mixing technique using DCP as vulcanizing agent. The formation of blend samples were characterized by FTIR spectroscopy, XRD, SEM, TGA and DSC.

The effective miscibility of these blend components is revealed from FTIR spectrum which consist of characteristic IR absorption of both the components with a slight shift in frequency. The chlorine groups attached to each elastomer may itself act as compatibilising agent. The structural changes occurred in the fabricated samples can be clearly depicted from XRD and SEM images. The uniform mixing of both Cl-NBR and Cl-EPDM is higher in 50/50 blend ratio due to their optimum surface roughness and polarity. The TGA curves indicated the better thermal stability of blends than the homopolymers due to the effective interaction between blend components. The DSC analysis exhibit a single transition due to the "across-phase" interaction, indicative of the coupling reaction between the functional groups of the components. The AC conductivity and dielectric properties increased with increase in the mass percentage of Cl-NBR due to the intrinsic electric dipole polarization along with interface charge polarization. The optimum cure time of the blend increases with Cl-NBR due to fewer number of double bonds left after chlorination. The 50/50 blends showed better tensile and tear strength values because the effective interfacial interaction between the blend components is maximum at this ratio. The studies based on the sorption and transport properties of ASTM oils, petroleum fuels and aromatic solvents support the superior compatibility of Cl-NBR/Cl-EPDM blend.

Cl-NBR/Cl-EPDM blend composite with different loading of hydroxyapatite were prepared by a simple two roll mill mixing technique. The change in position of IR absorption peak of nanocomposite displays more homogeneous structure due to the better interaction of the hydroxyl groups on HA with the polar groups of base matrices. The XRD pattern and FESEM showed the uniform dispersion of nano particles inside the blend matrix so that the blend composite attains an ordered arrangement pinpointing to the structural reorganization occurred in HA particles for the effective insertion in to the macromolecular chains. The TGA analysis disclosed the increase in onset and completion of the thermal degradation temperatures of the nanocomposites in addition to improved flame resistance due to better reinforcement of hydroxyapatite. The glass transition temperature of the nanocomposites increases with increase in concentration of nanoparticles. The effect of fillers on the cure and mechanical properties of the blends have been investigated and found to be increased with increase in filler loading up to 7phr HA loading. AC conductivity, dielectric constant and dielectric loss of nanocomposites were higher than that of base matrix. Cl-NBR/Cl-EPDM/7phr HA showed maximum electrical properties because tunneling mechanism is more dominant at 7phr loading of HA where optimum interfacial interactions between the nanoparticles and the polar segments of the matrix are achieved. Also, the HA filled samples have been found to show a reduced oil, fuel and solvent uptake compared to the bare matrix and the

nanocomposites containing 7phr HA loading have achieved the maximum chemical resistance due to the uniform dispersion in the matrix with reduced domain size where the intermolecular interaction between filler and matrix chains has also reached the maximum value. The nanocomposites have been found to exhibit anomalous transport behaviour.

9.2 Future outlook

The scope for further studies on chemical functionalization, filler reinforcement and judicious blending of diene rubbers are of immense industrial importance. Some possible extensions include

- Biodegradability and biocompatibility studies of fabricated nanocomposites can be attempted
- Studies of HA incorporated composites have to be taken up for the application in dental composites, body implants and blood bags.
- The XPS studies has to be conducted to determine the elemental composition and electronic state of the elements that exist within the chemically modified elastomers
- Advanced studies like SAXS, XPS and solid state NMR can be utilized to elucidate the polymer/filler interaction
- Interface characterization has to be done by using highly sophisticated techniques like ellipsometry, small angle X-

ray scattering (SAXS) and small angle neutron scattering (SANS).

- The efficiency for the fabricated samples in membrane separation techniques can be explored
- Manufacture of oil seales, gaskets, fuel hoses, fire protective coatings can be attempted and tested.
- Electromagnetic shielding and microwave absorbing capabilities of developed samples can be studied.

1. P. Ghosh, Polymer Science and Technology: Plastics, Rubbers, Blends and Composites, (Third Ed.) 409, 2011.

2. P. K. Mallick, (1993). Fibre-reinforced composites-materials, manufacturing and design, 2nd edition, Marcel Dekker, New York.

3. S.A Ghany, M.H.A. Salam and G.M.Nasr, J. Appl. Polym. Sci. **77**, 1816 (2000).

4. M.T.Ramesan, Adv. Polym. Technol. **32**, 21362 (2013).

5. H.Bashir, A.Linares and J.L.Acosta, J. Polym. Sci:Part B:Polym. Phys. **39**, 1017 (2001).

6. M.T.Ramesan, Polym. Eng. Sci. **54**, 438 (2013).

7. S.Y. Lu and I. Hamerton, Prog. Polym. Sci. **27**, 1661 (2002).

8. D.J. Irvine, J.A. McCluskey and I.M. Robinson, Polym. Degrad. Stab. **67**, 383 (2000).

9. S.W.Park and R.A.Schapery, Int. J. Solids Structures **34**, 931 (1997).

10. D. Ponnamma and S. Thomas (eds.), Non-linear viscoelasticity of rubber composites and nanocomposites, Adv. Polym. Sci. **264** (2014).

11. A.N. Gent and L.Q. Zhang, Rubber Chem. Technol. **75**, 923 (2002).

12. P. B. Smith, A. J. Pasztor, M. L. McKelvy, D. M. Meunier, S. W. Froelicher and F. C.Y. Wang, Anal. Chem. **71**, 61 (1999).

13. A. Malas and C. K. Das, Compos. Part B Eng. **79**, 639 (2015).

14. G.B. Kauffman and R.B.Seymour, J. Chem. Educ. **67**, 422 (1990).

15. S. Thomas and H. J. Maria, Progress in Rubber Nanocomposites, Woodhead Publishing Series in Composites Science and Engineering **75**, 2016.

16. M. Morton, J. Macromol. Sci. A **15**, 1289 (1981).

17. K. Ahmed, J. Adv. Res. **6**, 811 (2015).

18. G.W. Coates,P. D. Hustad and S. Reinartz, Angew. Chem. Int. Ed. **41**, 2236 (2002).

19. N. M. Huntink, R. N. Datta, J.W.M. Noordermeer, Rubber Chem.Technol. **77**, 477 (2004).

20. S. Bhattacharjee, H. Bender and D. Padliya, Rubber Chem. Technol. **76**, 1057 (2003).

21. S. Chakraborty, S. Bandyopadhyay, R. Ameta, R. Mukhopadhyay and A.S. Deuri, Polym. Test. **26**, 38 (2007).

22. A.O. Patil and S.T. Coolbaugh, Rubber Chem. Technol. **78**, 516 (2005).

23. A.A. Shokri, G. Bakhshandeh and T.D. Farahani, Iranian Polym. J. **15**, 227 (2006).

24. K.C. Yong, P.J.S. Foot, H. Morgan, S. Cook and A.J. Tinker, Eur. Polym. J. **42**, 1716 (2006).

25. L. Ibarra and M. Alzorriz, J. Appl. Polym. Sci. **84**, 605 (2002).

26. A. Choudhury, A. K. Bhowmick and C. Ong, J. Appl. Polym. Sci. **116**, 1428 (2010).

27. L. S. Penn and H. Wang, Polym. Adv. Technol. **5**, 809 (1994).

28. A.Brydon and G.C. Cameron, Prog. Polym. Sci. **4**, 209, 1975.

29. J. W. Kang, US Pat., 3, 993, 885 (1976).

30. Y. Chamberlin, J. P. Pascoult, H. Razzowk and H. Cheradame, Makromol. Chem. Rapid Commun. **2**, 323 (1981).

31. H. Wang , L. Yang and G. L. Rempel, Polym. Rev. **53**, 192 (2013).

32. M.Sarkar, P. P. De and A. K. Bhowmick, J. Appl. Polym. Sci. **66**, 1151 (1997).

33. T. J. A. Graham, T. H. Poole, C. N. Reese and B.C.Goess, J. Org. Chem. **76**, 4132 (2011).

34. N. K. Singha, S. Bhattacharjee and S. Sivaram, Rubber Chem. Technol. **70**, 309 (1997).

35. D.N.Schulz, S.R. Turner and M.A.Golub, Rubber Chem. Technol. **55**, 809 (1982).

36. Y. Liu, H. Kim, Q. Pan and G. L. Rempel, Catal. Sci. Technol. **3**, 2689 (2013).

37. A.F.Halasa, J.M. Massie and R.J. Ceresa, Science and technology of rubber (Fourth Ed.) **497**, (2005).

38. R.T.Morrissey, Rubber Chem.Technol. 44, 1025 (1971).

39. C.O Weber, Chem. Ber. **33**, 779 (1900)

40. C.D Harries, Chem. Ber. **56**, 1048 (1923).

41. F.W. Hinrichsen, H. Quensell and Kindschen, Cheische Berichte **46**, 1283 (1913).

42. D.H.E. Tom, J.Appl.Polm.Sci **20**, 381 (1956).

43. R. Pummerer and P.A. Burkard, Chem. Ber. **55**, 3458 (1922).

44. C.Rouse, R.Pautrat, R.Cheriatat, F.Lederan, J.C. Danijard, R.Pautrat and R.Cheriatat, J.Appl.Polm.Sci. Part C **16**, 4687 (1969).

45. S. S. Sarkawi, A. K. C. Aziz, R. A. Rahim, R. A. Ghani and A. N. Kamaruddin, Polym. Polym. Compos. **24**, 775 (2016).

46. P. L. Teh, Z. A. M. Ishak, A. S. Hashim, J. Karger- Kocsis and U. S. Ishiaku, J. Appl. Polym. Sci. **94**, 2438 (2004).

47. X.H.Wang, H. X. Zhang, W.Jiang, Z.G.Wang, C.H Liu, H.J.Liang and B.Z. Jiang, Polymer **39**, 2697 (1998).

48. M.T.Ramesan and R. Alex, J. Appl. Polym. Sci. **68**, 153 (1998).

49. R.G. Bacon and E.H Farmer, Rubber Chem.Technol **12**, 200 (1939).

50. M.A Goulb, J.Appl.Polm.Sci. **25**, 373 (1957).

51. C. W. Bedford and H. A. Wilkinson, Syst. Surv. Rubber Chem. Chem. Cat. Co. New York (1923)

52. W. Arayapranee, P. Prasassarakich and G.L.Rampel, J. Appl. Polym. Sci. **89**, 63 (2003).

53. P.Prasassarakich, P.Sintoorahat and N.Wongwisetsirikul, J. Chem. Eng. **34**, 249 (2001).

54. B. George, S. N. Maiti, I.K. Varma, J. Elastom. Plast. **38**,319 (2006).

55. N. Subramaniam, M. J. Monteiro, J. R. Taylor, A. S.Gomes and R. G. Gilbert, Macromol. Symp. **152**, 43 (2000).

56. S. H. Botros and M. L. Tawfic, J. Elastom. Plast. **37**, 299 (2005).

57. N.Subramanian, R. Balic, J.R .Taylor, M.Griffiths, M.J.Monteim , R.G.Gilbert ,C.C. Ho, L. Abdullah and P.J.kioli, J.Nat. Rubb. Res., **12**,223 (1997).

58. S.H. Botros and M.L. Tawfic, Polym-Plast Technol. **44**, 209 (2005).

59. W. Work, K. Horie, M.Hess, R.Stepto, Pure Appl. Chem. **76**, 1985 (2004).

60. K.Müller, E. Bugnicourt, M. Latorre, M. Jorda, Y. E. Sanz, J. M. Lagaron, O.Miesbauer, A. Bianchin, S. Hankin, U. Bölz, G. Pérez, M. Jesdinszki, M. Lindner, Z. Scheuerer, S.Castelló and M. Schmid, Nanomaterials **7**,74 (2017).

61. A.Yasmin, J. J.Luo, J. L.Abot and I. M. Daniel, Compos. Sci. Technol. **66**, 2415 (2006).

62. A. Usuki, Y.Kojima, M. Kawasumi, A.Okada, Y.Fukushima, T.Kurauchi, and O.Kamigaito, J. Mater. Res. **8**, 1179 (1993).

63. S.Pavlidou and C.D.Papaspyrides, Prog. Polym. Sci. **33**, 1119 (2008).

64. J.J. Luo and I.M. Daniel, Compos. Sci. Technol. **63,** 1607 (2003).

65. R.Sengupta, S.Chakraborty, S.Bandyopadhyay, S.Dasgupta, R.Mukhopadhyay, K.Auddy and A.S.Deuri, Polym. Eng. Sci. **47**, 1956 (2007).

66. S. S. Ray and M. Bousima, Progr. Mater. Sci. **50**, 962 (2005).

67. S.Fu, X. Feng, B.Lauke and Y.Mai, Compos. B Eng. **39**, 933 (2008).

68. J. Jordan, K. I. Jacob, R. Tannenbaum, M.A.Sharaf and I. Jasiuk, Mater. Sci. Eng A **393**, 1 (2005).

69. T. Lan and T.J. Pinnavaia, Chem. Mater. **6**, 2216 (1994).

70. P.B. Messersmith and E.P. Giannelis, Chem. Mater. **7**, 1597 (1995).

71. A.K.Bhowmick, M. Bhattacharya, S.Mitra, K. Dinesh Kumar, P.K. Maji, A.Choudhury, J.J. George, G.C. Basak, Adv. Polym. Sci. **239**, 1 (2010).

72. W. Herrmann, C. Uhl, G. Heinrich and D. Jehnichen, Polym. Bull. **57**, 395 (2006).

73. Y.S.Lee, S.H. Park, J.C.Lee and K.Ha, J.Elastom.Plast. **48**, 659 (2015).

74. Z. Hana and A. Finab, Prog. Polym. Sci. **36**, 914 (2011).

75. P. Maa, N. A. Siddiqui, G. Marom and J. K. Kim, Compos. PART A Appl. S. **41**, 1345 (2010).

76. D. Yue, Y. Liu and Z. Shen, J. Mater. Sci. **41**, 2541 (2006).

77. M.A.L. Manchado, J. Biagiotti, L. Valentini and J.M. Kenny, J. Appl. Polym. Sci. **92**, 3394 (2004).

78. F. Gojny, M. Wichmann, U. Kopke, B. Fiedler and K. Schulte, Compos. Sci. Technol. **64**, 2363 (2004).

79. K.Rajkumar, N. Kumari, P.Ranjith, S.K.Chakraborty, P.Thavamani, P.Pazhanisamy and P.Jeyanthi, Int.J. Chem. Tech Res. **3**, 1343 (2011).

80. J. Yang, M. Tian, Q.X. Jia , J.H. Shi, L.Q. Zhang, S.H. Lim, Z.Z. Yu and Y.W. Mai, Acta Materialia **55**, 6372 (2007).

81. S.Yaragalla, C.S. Chandran, N. Kalarikkal, R.H.Y. Subban, C. H. Chan and S. Thomas, Polym. Eng. Sci. **55**, 2439 (2015).

82. Y. Zhan, M. Lavorgna, G. Buonocore and H. Xia, J. Mater. Chem. **22**, 10464 (2012).

83. Y. Kojima, K. Fukumori, A. Usuki, A. Okada and T. Kurauchi, J. Mater. Sci. Lett. **12**, 889 (1993).

84. C. M. Bhuvaneswari, S. D. Kakade, V. D. Deuskar, A. B. Dange and M. Gupta, Defence Sci. J. **58**, 94 (2008).

85. Y. Mohammadpour and A. A. Katbab, J. Appl. Polym. Sci. **106**, 4209 (2007).

86. J. Zhang, W. Zao, L. Wang, Y. Zhao and H. Bai, Polym. Compos. **35**, 1306 (2014).

87. S. Sadhu and A. K. Bhowmick, J. Polym. Sci. Part B: Polym. Phys. **42**, 1573 (2004).

88. S. Kango, S. Kalia, A. Celli, J. Njuguna, Y. Habibi and R. Kumar, Prog. Polym. Sci. **38**, 1232 (2013).

89. S.H. El-Sabbagh, M.E.Tawfik and F.M. Helaly, J. Appl. Polym. Sci. **109**, 2823 (2008).

90. S. Sahoo, M. Maiti, A. Ganguly, J.J. George and A.K. Bhowmick, J. Appl. Polym. Sci. **105**, 2407 (2007).

91. M. Kalaee, S. Akhlaghi, S. Mazinani, A. Sharif, Y. C. Jarestani and M. Mortezaei, J. Therm. Anal. Calorim. **110**, 1407 (2012).

92. G. Kofod, H. Stoyanov, M. Kollosche, S. Risse, H. Ragusch, D. Rychkov, M. Dansachmuller and D. N. McCarthy, 2010 10th *IEEE Int.* Conf. on Solid Dielectrics, 1 (2010).

93. G. Lin, M. Tian, Y. Lu, X. Zhang and L. Zhang, Polym. J. **38**, 498 (2006).

94. H.T. Ong, N.M. Julkapli, S.B.A. Hamid, O. Boondamnoen and M.F. Tai, J. Magn. Magn. Mater. **395**, 173 (2015).

95. V. C. Jasna, T. Anilkumar, G. Mathew and M. T. Ramesan, J. Mater. Sci. **53**, 9861 (2018).

96. M. T. Ramesan, A. Nihmath and J. Francis, AIP Conf. Proc. **1536**, 255 (2013).

97. L. M Walpita, W. M. Pleban and H. Eckhardt, U.S. Patent 5,962,122, Oct 5, 1999.

98. R. Popielarz, C. K. Chiang, R. Nozaki and J. O brzut, Macromolecules **34**, 5910 (2001).

99. M. A. Solomon, P. Kurian, P. A. Joy and M. R. Anantharaman, Int. J. Polym. Mater. PO. **53**, 565 (2004).

100. M. George, P. Kurian, M. R. Anantharaman, J. Appl. Polym. Sci. **119**, 3019 (2011).

101. J.Kruzelak, I. Hudec, R.Dosoudil and R. Sykrra, J. Elastomers Plast. **47**, 277 (2013).

102. M.H.Makled, T.Matsui, H.Tsuda, H.Mabuchi, M.K.El-Mansy and K. Morii, J.Mater. Process. Technol. **160**, 229 (2005).

103. L. Loganathan and S. Chandrasekar, J. Electr. Eng. Technol. **8**,345 (2013).

104. A. Patsidis and G.C.psarras, eXPRESS Polym. Lett. **2**, 718 (2008).

105. K.A. Gross and C.C. Berndt, J. Biomed. Mater. Res. **39**, 580 (1998).

106. A.A. White, S.M. Best and I.A. Kinloch, Int. J. Appl. Ceram. Technol. **4**, 1 (2007).

107. K. Balani, R. Anderson, T. Laha, M. Andara, J. Tercero, E. Crumpler and A. Agarwal, Biomater. **28**, 618 (2007).

108. P. Zhang, Z. Hong, T. Yu, X. Chen and X. Jing, Biomaterials **30**, 58 (2009).

109. Z. Hong, P. Zhang, C. He, X. Qiu, A. Liu , L. Chen, X. Chen and X. Jing, Biomaterials **26**, 6296 (2005).

110. M.C. Chang, C.C. Ko and W.H. Douglas, Biomaterials **24**, 2853 (2003).

111. Q. Hu, B. Li, M. Wang and J. Shen, Biomaterials **25**, 779 (2004).

112. J. Huang, L.D. Silvio, M. Wang, K.E. Tanner and W. Bonfield, J. Mater. Sci.: Mater. Med. **8**, 775 (1997).

113. K. Li and S. C. Tjong, J. Macromol. Sci. B **50**, 1325 (2011).

114. H. Nishikawa and K. Omamiuda, J. Mol. Catal. A: Chem. **179**, 193 (2002).

115. R.U. Mene, M.P. Mahabole, R.C. Aiyer and R.S. Khairnar, The Open Appl. Phy. J. **3**, 10 (2010).

116. H. Anmin, L. Ming, C. Chengkang, M. Dali, J. Mol. Catal. A: Chem. **267,** 79 (2007).

117. J.K. Battacharya, Polymer Blends and Alloys-An Overview, R.P. Singh, C.K. Das and S.K. Mustafi (Eds.), Asian Books Pvt. Ltd., New Delhi, (2002)

118. D.R. Paul and Newman, Polymer Blends, D.R. Paul and C.B. Bucknall, (Eds), John Wiley & Sons, New York, (2000)

119. C. Xu, Y. Wang and Y. Chen, Polym. Test. **33**, 179 (2014).

120. R. Manshaie, S.N. Khorasani, S.J. Veshare and M.R. Abadchi, Radiat. Phys. Chem. **80**, 100 (2011).

121. A.K. Maity and S.F. Xavier, Eur. Polym. J. **35**, 173 (1999).

122. S. George, K.T. Varughese and S. Thomas, Polymer **41**, 579 (2000).

123. Y.D. Lee and C. M. Chen, J. Appl. Polym. Sci. **33**, 1231 (1987).

124. U.Schulze, T. Fonagy, H. Kombar, G. Pompe, J. Pionteck and B. Ivan, Macromolecules **36**, 4719 (2003).

125. M .T. Ramesan and R. Alex, Polym. Int. **50**, 1298 (2001).

126. F. Ide and A. Hasegawa, Appl. Polym. Sci.**18**, 963 (1974).

127. B.G. Soares, M.S.M. Almeida and P. I. C. Guimarães, Eur. Polym. J. **40**, 2185 (2004).

128. S. Zhu and C.M. Chan, Polymer **39**, 7023 (1998)

129. S.H. Botros and M.L. Tawfic, J. Elastom. Plast. **38**, 349 (2006).

130. H. Ismail, Supri and A.M.M. Yusof, Polym. Test. **23**, 675 (2004).

131. D.K. Setua and Y.N. Gupta, Thermochim. Acta **462**, 32 (2007).

132. K. Jayanarayanan, S. Thomas and K. Joseph, J. Polym. Res. **18**, 1 (2011).

133. S. H. Botros and K. N. Abdel-Nour, Polym. Degrad. Stab. **62**, 497 (1998).

134. L.Wang, J.Hua and Z.Wang, Polym. Test. **76**,481 (2019).

135. A.K. Balan, S. M. Parambil, S. Vakyath, J. T. Velayudhan, S. Naduparambath and P. Etathil, J. Mater. Sci. **52**, 6712 (2017).

136. A. Das, K.W. Stöckelhuber and G.Heinrich, Macromol. Chem. Phys. **210**, 189 (2009).

137. S.Varghese, J.K. Kocsis and K.G.Gatos, Polymer **44**, 3977 (2003).

138. S.Varghese and J. K. Kocsis, Polymer **44**, 4921 (2003).

139. S. Varghese, K.G. Gatos, A.A. Apostolov and J.K. Kocsis, J. Appl. Polym. Sci. **92**, 543 (2004).

140. W.S. Chow, A.A. Bakar, Z.A.M. Ishak, J.K. Kocsis and U.S.Ishiaku, Eur. Polym. J. **41**, 687 (2005).

141. M. A. Z. Magda, Eur. Polym. J. **43,** 4415 (2007).

142. D.Voulgaris and D. Petridis, Polymer **43**, 2213 (2002).

143. M.Y. Gelfer, H.H. Song, L. Liu, B.S. Hsiao, B. Chu, M.Rafailovich, M. Si and V. Zaitsev, J. Polym. Sci. Part B Polym. Phys. **41**, 44 (2003).

144. M. Frounchi, S. Dadbin, Z. Salehpour and M.Noferesti, J. Membr. Sci. **282**, 142 (2006).

145. M. Mottaghi, S.N. Khorasani, M.N. Esfahany, A. Farzadfar, M.M. Talakesh, J. Elastom. Plast. 44, **443** (2012).

146. N. Mahmood, A.U. Khan, K. Stockelhuber, A. Das, D. Jehnichen and G. Heinrich, J. Appl. Polym. Sci. **131**, 40341 (2014).

147. S.T. Nair, P.P. Vijayan, P. Xavier, S. Bose, S.C. George and S. Thomas. Compos. Sci. Technol. **116**, 9 (2015).

148. R. Stephen, S. Varghese, K. Joseph, Z. Oommen and S. Thomas, J. Membr. Sci. **282**, 162 (2006).

149. T.E. Motaung, A.S. Luyt and S.Thomas, Polym. Compos. **32**, 1289 (2011).

150. M. A. M. Eid and D. E. El-Nashar, Polym. Plast. Technol. Eng. **45**, 675 (2006).

151. L.Mengjiao, Q.Zhang, C.Yin, L.Zhon and T.Xin, Polym. Compos. 34, 1809 (2013).

152. E. Abraham, P.A. Elbi, B. Deepa, L.A. J. Pothen and S.S. Narine, Polym. Degrad. Stab. **97**, 2378 (2012).

153. R.C.R. Nunes, M.M.L. Gonzalez and E.Riande, J. Polym. Sci. Polym. Phys. **43**, 2131 (2005).

154. R.C.R. Nunes and V.G. Costa, Eur. Polym. J. **30**, 1025 (1994).

155. M.A. Minnath, G. Unnikrishnan and E. Purushothaman, J. Membr. Sci. **379**, 361 (2011).

156. A. Bhattacharya, K.M. Ganguly, A. De and S. Sarkar, Mater. Res. Bull. **31**, 527 (1996).

157. R. Gangopadhyay and A. De, Eur. Polym. J. **35**, 1985 (1999).

158. B. Z. Tang, Y.Geng, J. W. Y. Lam, B. Li, X.Jing, X.Wang, F.Wang, A. B. Pakhomov and X. X. Zhang, Chem. Mater. **11**, 1581(1999).

159. M. S. Cho, H. J. Seo, J. D. Nam, H. R. Choi, J. C. Koo and Y. Lee, Smart Mater. Struct. **16**, S237 (2007).

160. Y. Wan, C. Xiong, J. Yu and D. Wen, Compos. Sci. Technol. **65**, 1769 (2005).

161. J.J.C. Busfield, A.G. Thomas and K.Yamaguchi. J. Polym. Sci. Part B: Polym. Phys. **43**, 1649 (2005).

162. I. Islam, S. Sultana, S. K. Ray, H. P. Nur, M. T. Hossain and W. M. Ajmotgir, J. Carbon Research **4**, 15 (2018).

163. R.M. Morsy, M.N. Ismaiel and A.A. Yehia, Int. J. Mater. Methods Technol **1**, 22 (2013).

164. A. M. Ghoneim and M. N. Ismail , Polym. Plast. Technol. Eng. **38**, 979 (1999).

165. K. Shin, S. Y. Yang, C. Yang, H. Jeon and C. E. Park, Org. Electron. **8**, 336 (2007).

166. A.Das, G.R. Kasaliwal, R. Jurk, R. Boldt, D.Fischer, K.W. Stöckelhuber and G.Heinrich Compos. Sci. Technol. **72**, 1961 (2012).

167. G. Kaur, R. Adhikari, P. Cass, M. Bown and P. Gunatillake, RSC Adv. **5**, 37553 (2015).

168. S. Praveen, P.K. Chattopadhyay, P. Albert, V.G. Dalvi, B.C.Chakraborty and S. Chattopadhyay, Compos. Part A **40**, 309 (2009).

169. K.C. Etika, L. Liu, L.A. Hess and J.C. Grunlan, Carbon **47**, 3128 (2009).

170. D. Feldman, J. Macromol. Sci. Part A **50**, 1241 (2013).

171. G. Unnikrishnan, S. Thomas and S. Varghese, Polymer **37**, 2687 (1996).

172. A.E. Mathai, R.P. Singh, and S. Thomas, Polym. Eng. Sci. **43**, 704 (2003).

173. M. E. Woods, J. A. Davidson, Rubber Chem. Technol. **49**,112 (1976).

174. M. G. Oliveira, B. G. Soares, C. M. F. Santos, M. F. Diniz and R. C. L. Dutra, Macromol. Rapid Commun. **20**, 526 (1999).

175. V. Jovanovic´, S. S.˘ija-Jovanovic´, J. Budinski-Simendic´, G. Markovic´ and M. M.Cincovic´ Composites: Part B **45**, 333 (2013).

176. V. C. Jasna, T. Anilkumar and M. T. Ramesan, J.Appl.Polym.Sci. **135**, 46518 (2018).

177. M.T. Ramesan, React. Funct. Polym. **59**,267 (2004).

178. M.T. Ramesan, J. Polym. Research **11**,333 (2004).

179. M.T. Ramesan, T.K.Manojkumar, R.Alex and B.Kuriakose, J. Mater Sci. **37**, 109 (2002).

180. Y.X. Pang and X.J. Bao, Eur. Ceram. Soc. **23**, 1697 (2003).

181. M. Makosza and M. Wawizyniewics, Tetrahedron *Lett.* **53**,4659 (1969).

182. G. C. Joshi, M. Pande, A. K. Mukhejee, K. K. Ganguli, P. K. Tiwari and S. *C.* Raman, Proc. Symp High Polym, Kanpur, India, 1972.

183. Annual Book of ASTM Standards, D3182-1989.

184. S. K. De and B. K. Dhindaw, J. Scanning Electron Micros. **3**,973 (1982).

185. M. Franson and N.A. Peppas, J. Appl. Polym. Sci. **28**, 1299 (1983)

186. A. Elwy, M.M. Badwy and G.M. Nasr, Polym. Degrad. Stab. **53**, 289 (1996)

187. K.P. Dasan, A.P. Haseena, G. Unnikrishnan, R. Alex and E. Purushothaman, Polym. Polym. Compos. **12**, 599 (2004)

188. C.K. Radhakrishnan, B. Ganesh, A. Sujith, G. Unnikrishnan and S. Thomas, Polym. Polym. Compos. **13**, 335 (2005)

189. S. Liang, L. Zhang and J. Xu, J. Membr. Sci. **19**, 287 (2007).

190. R. Rajendran, L.K. Shrestha, R.M. Kumar, R. Jayavel, J.P. Hill, K. Ariga, J. Inorg. Organomet. Polym. **25**, 267 (2015).

191. E. Bet-moushoul, Y. Mansourpanah, K. Farhadi, M. Tabatabaei, Chem. Eng. J. **283**, 29 (2016).

192. H.M. Shiri, A. Ehsani, Bull. Chem. Soc. Jpn. **89**, 1201 (2016).

193. V.K. Thakur, R.K. Gupta, Chem. Rev. **116**, 4260 (2016)

194. M.T. Ramesan, P. Jayakrishnan, J. Inorg. Organomet. Polym. **27**, 143 (2017).

195. R.P. Sing, A. Tiwari, C. Pandey, J. Inorg. Organomet. Polym. **21**, 788 (2011)

196. T. Yasin, S. Ahmed, F. Yoshii, K. Makuuchi, React. Funct. Polym. **57**, 113 (2003)

197. P. C. Thomas, S. P. Thomas, G. George, S. Thomas, J. Kuruvilla, J. Polym. Res. **18**, 2367 (2011).

198. P. Rybinski, G. Janowska, Thermochim. Acta. **549**, 6 (2012).

199. A. A. El-Wakil, Int. J. Polym. Sci. **2011**, 1 (2011).

200. P. Bhadane, M. Champagne, M. Huneault, F. Tofan and B. Favis, Polymer **47**, 2760 (2006).

201. F. Chen, Z.C. Wang and C.J. Lin, Mater. Lett. **57**, 858 (2002).

202. H. Tian, Z. Tang, X. Zhuang, X. Chen and X. Jing, Progr. Polym. Sci. **37**, 237 (2012).

203. C. Kealley, M. Elcombe, A.V. Riessen and B.B. Nissan, Physica B. **385–386**, 496 (2006).

204. J. Li, Y. Li, S. Ma, Y. Gao, Y. Zuo and J. Hu, J. Biomed. Mater. Res. A **95**, 973 (2010).

205. C.Z. Liao, K. Li, H.M. Wong, W.Y. Tong, K.W.K. Yeung and S.C. Tjong, Mater. Sci. Eng.C **33**, 1380 (2013).

206. E. Nejati, V. Firouzdor, M.B. Eslaminejad, F. Bagheri, Mater. Sci. Eng. C. **29**, 942 (2009)

207. M.N. Vîlsa, A. Meghea, M. Sonmez and M. Georgescu, University Politechnica of Bucharest Scientific Bulletin Series B **77**, 165 (2015).

208. P.M.S.L. Shanthi, R.V. Mangalaraja, A.P. Uthirakumar, S. Velmathi, T. Balasubramanian, M. Ashok, J. Colloid Interface Sci. **350**, 39 (2010)

209. M.S.M. Arsad, P.M. Lee and L.K. Hung, 2nd International Conference on Biotechnology and Food Science IPCBEE **7**, 184 (2011).

210. K. Suhailath and M.T. Ramesan, J. Therm. Anal. Calorim. **135**, 2159 (2018).

211. M.T. Ramesan, J. Appl. Polym. Sci. **131**, 3681 (2014)

212. P. Gill, T. T. Moghadam and B. Ranjbar, J. Biomol. Tech. **21**, 167 (2010).

213. M.T. Ramesan, J. Elast. Plast. **46**, 303 (2014).

214. P. Jayakrishnan, P.P. Pradyumnan and M.T. Ramesan, Chemist **89**, 27 (2016).

215. M.T. Ramesan, V.K. Athira, P. Jayakrishnan and C. Gopinathan, J.Appl. Polym. Sci. **133**, 5827 (2016)

216. M.T. Ramesan and K. Surya, J. Appl. Polym. Sci. **133**, 43496 (2016)

217. D. Yu, J. Wu, L. Zhou, D. Xie and S. Wu, Comp. Sci. Technol. **60**,499 (2000).

218. T. Anilkumar and M.T. Ramesan, AIP Conf. Proceed. **1620**, 28 (2014).

219. A. Qureshi, A. Mergen, M.S. Eroğlu, N.L. Singh and A. Gulluoglu, J. Macromol. Sci. **45**, 462 (2008).

220. Y. Chen, Y. Lin, Y. Luo and D. J. Liu, Poly. Adv. Technol. **27**, 830 (2016).

221. T. Witinuntakit, S. Kiatkamjornwong and S. Poompradub, Poly. Adv. Technol. **29**, 649 (2018).

222. K.I. Elizabeth, R. Alex, B. Kuriakose, S. Varghese and N.R. Peethambaran, J. Appl. Polym. Sci. **101**, 4401 (2006).

223. D. De, D. De and B. Adhikari, Poly. Adv. Technol. **15**, 708 (2004).

224. F. Cataldo, O .Ursini and G. Angelini, Polym. Degrad. Stab. **94**, 921 (2009).

225. V.C. Jasna and M.T. Ramesan, J. Inorg. Organomet. Polym. Mater. **27**, 968 (2017).

226. N. Lopattananon, D. Jitkalong and M.Seadan, J. Appl. Polym. Sci. **120**, 3242 (2011).

227. S. Radabutra, S. Thanawan and T. Amornsakchai, Eur. Polym. J. **45**, 2017 (2009).

228. T. Anilkumar, A. A. Naik and M. T. Ramesan, AIP Conf. Proc. **1849,** 020037 (2017).

229. M.T. Ramesan, Pet. Sci. Technol. **32**, 1775 (2014).

230. H. Yu, S.Li, J. Zhong and K. Xu, Thermochim. Acta. **410**, 119 (2004).

231. G. C. Joshi, N. Singh and L. M. Pande, Tetrahedron Lett. **15**, 1461 (1972).

232. T. M. Aminabhavi, S. B. Harogoppad, R. S. Khinnavar and R. H. Balundgi, J. Macromol. Sci. Part C **31**, 433 (1991).

233. U.K. Mandal, Polym. Int. **49**, 1653 (2000).

234. A. Nihmath and M.T. Ramesan, J. Inorg. Organomet. Polym. **27**, 481 (2017).

235. M. Subburaj, M.T. Ramesan and P.P. Pradyumnan, AIP Conf. Proc. **1620**, 541 (2014).

236. A. Pajak, P. Rybinski, G. Janowska and A.K. Jastrzabek, J. Therm. Anla. Calorim. **117**, 789 (2014).

237. M.T. Ramesan, Int. J. Polym. Mater. **60**, 1130 (2011).

238. M.T. Ramesan, M. Varghese, P. Jayakrishnan and P.Periyat, Adv. Polym. Technol. **37**, 137 (2018).

239. M.T. Ramesan, C. Jose, P. Jayakrishnan and T. Anilkumar, Polym. Compos. **39**, 38 (2018).

240. M. T. Ramesan and V. Santhi, J. Mater. Sci. Mater. Electron. **28**, 18804 (2017).

241. P. Jayakrishnan and M. T. Ramesan, Polym. Bull. **74**, 3179 (2017).

242. M. T. Ramesan, Polym. Compos. **35**, 1989 (2014).

243. A. Nihmath and M. T. Ramesan, Polym. Compos. **39**, 2093 (2018).

244. D.K. Setua, C. Soman, A.K. Bhowmick and G.N. Mathur, Polym. Eng. Sci. **42**, 10 (2002).

245. V. Tanrattanakul, B. Wattanathai, A. Tiangjunya and P. Muhamud, J. Appl. Polym. Sci. **90**, 261 (2003).

246. C. Sirisinha, P. Saeoui and J. Guaysomboon, Polymer **45**, 4909 (2004).

247. A. Mousa, U. S. Ishiaku and Z. A. Mohd Ishak, Polym. Bull. **53**, 203 (2005).

248. S. C. George and S. Thomas, Prog. Polym. Sci. **26**, 985 (2001).

249. P. V. Anil Kumar, K. T. Varughese and S. Thomas, Ind. Eng. Chem. Res. **51**, 6697 (2012).

250. I. C. Chukwujike, C. M. Ewulonu and M. Chukwu, Int. J. Multidiscip. Res. Dev., **2**, 154 (2015).

251. M. Balachandran and S. S. Bhagawan, J. Polym. Res. **19**, 9809 (2012).

252. A. E. Mathai and S. Thomas, J. Macromol. Sci. Part B Phys. **35**, 229 (1996).

253. H. J. Maria, N. Lyczko, A. Nzihou, C. Mathew, S. C. George, K. Joseph and S. Thomas, J. Mater. Sci., **48**, 5373 (2013).

254. N. Tabsan, S. Wirasate and K. Suchiva, Wear **269**, 394 (2010).

255. S. Chakraborty, R. Sengupta, S. Dasgupta,R. Mukhopadhyay, S. Bandyopadhyay, M. Joshi and S. C. Ameta, Polym. Eng. Sci. **49**, 1279 (2009).

256. S. Zhu, J. Guo and J. Zhang, J. Appl. Polym. Sci. **135**, 45936 (2018).

257. D. Grigorova, N Dishovsky and V.l. Iliev J. Univ. Chem. Technol. Metallurgy **42**, 355 (2007).

258. J. Kim, T. Oh and D. Lee, Polym. Int. **52**, 1058 (2003).

259. I . Armentano, M. Dottori, E. Fortunati, S.Mattioli and J.M.Kenny, Polym. Degrad. Stab. **95**, 2126 (2010)

260. Y. Zhang and J. Lu, J. Nanoparticle Res. **9**, 589 (2007).

261. Q.X. Dong, Q.J. Chen, W. Yang, Q. Chen, W. Yang, Y. Zheng, X. Liu, Y. Li and M. Yang, J. Appl. Polym. Sci. **109**, 659 (2008).

262. R. Bhowmik, K.S. Katti and D.R. Katti, Int. J. Nanotechnol. **6**, 511 (2009).

263. Y. Chen, T.H. Zhang, C.H. Gan and G. Yu, Carbon **45**, 998 (2007).

264. A. Dasari, Z. Z. Yu, Y. W. Mai and S. Liu, Nanotechnology **18**, (2007).

265. G. Bussu and A. Lazzeri, J. Mater. Sci. **41**, 6072 (2006).

266. D. Chayan and K. Bharat, Res. J. Recent Sci. **1**,357 (2011).

267. O.A. Al-Hartomy, A.A. Al-Ghamdi and F.R. Al-Solamy, Res. Rev. Polym. **3**, 93 (2012).

268. O.A. Al-Hartomy, F. Al-Salamy, A.A. Al-Ghamdi, M. A. Fatah, N. Dishovsky and F. El- Tantawy, J. Appl. Polym. Sci. **120**,3628 (2011).

269. K. Suhailath, M.T. Ramesan, B. Naufal, P. Periyat, V. C. Jasna and P.Jayakrishnan, Polym. Bull.**74**,671 (2017).

270. C.Sareena, M. Sreejith, M.T. Ramesan and E. Purushothaman, Polym .Bull. **72**,1683 (2015).

271. H.Ismail and S.Suzaimah, Polym. Test. **19**, 879 (2000).

272. C.Sareena, M.T. Ramesan and E. Purushothaman, Polym. Compos. **33**, 1678 (2012).

273. S. Padhi, P. G. R. Achary and N. C. Nayak, Bull. Mater. Sci. **38**, 925 (2015).

274. T. Johnson and S. Thomas, J. Polym. Sci. B Polym. Phys. **37**,415 (1999).

275. C.H.Obasi,U.M.Obidiegwu,N.G.Onyeagoro,O. I. Arukala m,C. G. Onuegbu N. F. Onuoha and M. C. Ewulonu, J. Polym. Environ. **25**, 544 (2017).

276. Y.D. Seo, H.S. Lee, S. Kim, and C. Song, Nucl. Eng. Technol., 43, 279 (2011).

277. M. Durandisha and A. Alipourb, Chin. J. Polym. Sci., 31, 660 (2013).

278. H. Zheng, Y. Zhang, Z. Peng, and Y. Zhang, Polym. Test. **23**, 217 (2004).

279. M.T.Ramesan, A.George, P. Jayakrishnan, G. Kalaprasad, J. Therm. Anal. Calorim. **126**, 511 (2016).

280. H.K. Tae, W.J. Lee, C.L. Dong, J.C. Hyoung, and M.S. John, Macromol. Rapid Commun. **23**, 191 (2002).

281. A. I. A.Kandil and M. S.Gaafar, J. Appl. Polym. Sci. **117**, 1502 (2010).

282. M.T.Ramesan, C.K.Premalatha and R.Alex, Plast. Rubber Comp. **30**, 355 (2001).

283. C.H.Lee and S.W.Kim, J. Appl. Polym. Sci. **78**, 2540 (2000).

284. M. Thakur, Macromolecules **21**, 661 (1988).

285. X. Yuan, B. Zhu, G. Tong, Y. Su, and Z. Zhu, Mater. Chem. B **1**, 6551 (2013).

286. Y. Han, X. Wang, and S. Li, J. Nanopart. Res. **11**, 1235 (2009).

287. M.T.Ramesan and D.S.Lee, Iranian Polym. J. **17**, 281 (2008).

288. M. T. Ramesan, Polym Comp. **33**, 2169 (2012).

289. S.S. Ray and M. Okamoto, Prog. Polym. Sci. **28**, 1539 (2003).

290. N. S. C. Mat, H. Ismail and N. Othman, Procedia Chemistry **19**, 394 (2016).

291. J. Prachayawarakorn, P. Sangnitidej and P. Boonpasith, Carbohydrate Polym. **81**, 425 (2010).

292. C. Sareena, M. T. Ramesan and E. Purushothaman, J. Appl. Polym. Sci. **125**, 2322 (2012).

293. M.T.Ramesan, Polym. Plast. Technol. Eng. **51**, 1223 (2012).

294. M.T.Ramesan and P.P.Pradyumnan, AIP Conf. Proc. **1391**, 658 (2011).

295. M.T. Ramesan, J. Appl. Polym. Sci. **128**, 1540 (2013).

296. Z.M. Elimat, A.M. Zihlif and G. Ragosta, J. Phys. D: Appl. Phys. **41**, 165408 (2008).

297. M.T. Ramesan, Int. J. Polym. Mater. Polym. Biomater. **62**, 277 (2013).

298. M.T. Ramesan, V.P.A. Raheem, P. Jayakrishnan, and P.P.Pradyumnan, AIP Conf. Proc., **1620**, 3 (2014).

299. R.C. Popielarz, K. Chiang, R. Nozaki, and J. Obrzutv, Macromolecules **34**, 5910 (2001).

300. P. Yu, H. He, C. Jiang, Y. Jia, D. Wang, X. Yao, D. Jia and Y. Luo, J. Appl. Polym. Sci. **133**, 42922 (2016).

301. R. Rajasekar, K. Pal, G. Heinrich, A. Das and C.K. Das, Mater. Des. **30**, 3839 (2009).

302. M. Tahir, K. W. St€ockelhuber, N. Mahmood, H. Komber and G. Heinrich, Macromol. Mater. Eng. **300**, 242 (2015).

303. B. G. Soares, M. Oliveira, D. Meireles, A. S. Sirqueira and R. S. Mauler, J. Appl. Polym. Sci. **110**, 3566 (2008).

304. C. W. Macosko, H. K. Jeon, T. R. Hoye, Prog. Polym. Sci. **30**, 939 (2005).

305. S. L. Abd-El-Messieh, D. E. El-Nashar and M. G. Khafagi, Polym. Plast. Technol. **43**, 135 (2004).

306. W. Arayapranee and G.L. Rempel, Int. J. Mater. Struct. Reliab. **5**, 1 (2007).

307. L. Wu, X. Luo and X. Wang, J. Appl. Polym. Sci. **102**, 5472 (2006)

308. M. Duin, Macromol. Symp. **233**, 11 (2006).

309. A.A. El-Gamal, H.M. Alsuhaiqi and H.H. Hassan, J. Macromol. Sci. **56**, 697 (2017).

310. K.N. Pandey, D.K. Setua and G.N. Mathur, Polym. Eng. Sci. **45**, 1265 (2005).

311. S.H Botros, A.F.Moustafa, J. Elast. Plast. **34**, 15 (2002).

312. M. G. Oliveira and B. G.Soares, J. Appl. Polym. Sci. **90**, 2408 (2003).

313. J. Lohmar, Kautsch. Gummi Kunst. **39**, 1065 (1986).

314. S. H. Botros and A. F. Moustafa, J. Appl. Polym. Sci. **89**, 3143 (2003).

315. J. Tyczkowski, I. Krawczyk, B. Woz´niak and J.M. Martin-Martinez, Eur. Polym. J. **45**, 1826 (2009).

316. A. Nihmath and M.T. Ramesan, Polym. Adv. Technol. **29**, 2165 (2018).

317. B. Yin, Y. Zhao, R. Yu, H. An and M. Yang, Polym. Eng. Sci. **47**,14 (2007).

318. M. Dionisio, L. Ricci, G. Pecchini, D. Masseroni, G. Ruggeri, L. Cristofolini, E. Rampazzo and E. Dalcanale, Macromolecules **47**, 632 (2014).

319. A. Sujith , G. Unnikrishnan and C.K. Radhakrishnan, J. Elast. Plast. **40**, 17 (2008).

320. M.T. Ramesan, G. Mathew, B. Kuriakose and R. Alex, Eur. Polym. J. **37**, 719 (2001).

321. M.T. Ramesan, R. Alex and N.V. Khanh, React. Funct. Polym. **62**, 41 (2005).

322. K. C. Manoj and G. Unnikrishnan, J. Appl. Polym. Sci. **105**, 908 (2007).

323. K. H. Rahiman, G. Unnikrishnan, A. Sujith and C.K. Radhakrishnan, Mater. Lett. **59**, 633 (2005).

324. K.P. Sau, T.K. Chaki and D.Khastgir, J. Mater. Sci. **32**, 5717 (1997).

325. S. George, K. T. Varughese and S. Thomas, J. Appl. Polym. Sci. **73**, 255 (1999).

326. A.L.G. Saad and S.El-Sabbagh, J. Appl. Polym. Sci. **79**, 60 (2001).

327. H. Ismail and H.M. Hairunezam, Eur. Polym. J. **37**, 39 (2001).

328. C. Kumnuantip and N Sombatsompop, Mater. Lett. **57**, 3167 (2003).

329. S. Mathai and S. Thomas, J. Macromol. Sci. Phys. B **35**, 229 (1996).

330. S.B. Harogoppad and T.M. Aminabhavi, J. Appl. Polym. Sci. **42**, 2329 (1991).

331. W.R. Brown, R.B. Jenkins and G.S Park, J. Appl. Polym. Sci. Polym. Symp. **41**, 45 (1973).

332. L.M. Lucht and N.A. Peppas, J. Appl. Polym. Sci. **33**, 1557 (1987)

333. M.T. Ramesan, Int. J. Plast. Technol. **19**, 368 (2015).

334. P.C. Vijayakumar, R. J. Kumar, A. Johns, N. Sathyan and J. Johns, Prog. Rubber Plast. Re. **31**, 55 (2015).

335. A. Sujith and G. Unnikrishnan, J. Mater. Sci. **40**, 4625 (2005).

336. T.M. Nair, M.G. Kumaran and G. Unnikrishnan, J. Appl. Polym. Sci. **93**, 2606 (2004).

337. V. Jovanovic´, J. Budinski-Simendic´, J. Milic´, A. Aroguz, I. Ristic´, S. Prendzˇov and L. Korugic-Karasz, Contemporary science of polymeric materials. ACS Symposium series,vol. **1061**, 167 (2011).

338. R.S. Rajeev and S.K. De, Rubber Chem. Technol. **75**, 475 (2002).

339. J. Fro¨hlich, W. Niedermeier and H.D. Luginsland, Compos. Part A Appl. Sci. Manuf. **36**, 449 (2005).

340. C. Shan, Z. Gu, L. Wang, P. Li, G. Song, Z. Gao and X. Yang, J. Appl. Polym. Sci. **119**, 1185 (2011).

341. D. E. El-nashar, E. Gomaa, and S. L. Abd-El-messieh, J. Polym. Sci. Part B: Polym. Phys. **47**, 1825 (2009).

342. S.A. AL-Gahtani, J. Amer. Sci. **7**, 804 (2011).

343. K.P. Sau, T.K. Chaki and D.Khastgir, J. Appl. Polym. Sci. **71**, 887 (1999).

344. V. Subramanian and S. Ganapathy, J. Appl. Polym. Sci. **70**, 985 (1998).

345. M. M. A. Zeid, Eur. Polym. J. **43**, 4415 (2007).

346. M. Tiwari, J. W. M. Noordermeer and W. K. Dierkes, Rubber chem. Technol. **81**, 276 (2008).

347. K. C. Manoj, P. Kumari and G. Unnikrishnan, J. Appl. Polym. Sci. **120**, 2654 (2011).

348. H. R. Le, S. Qu, R. E. Mackay and R. Rothwell, J. Adv. Ceram. **1**, 66 (2012).

349. M. Arroyo, M.A. Lo´pez-Manchado, J.L. Valentı´n and J. Carretero, Compos. Sci. Technol. **67**, 1330 (2007).

350. A.A. El-Gamal, H.M. Alsuhaiqi and H.H. Hassan, J. Macromol. Sci. B **56**,697 (2017).

351. S. Isaji, Y. Bin and M. Matsuo, Polymer **50**, 1046 (2009).

352. C. C. Ku and R. Liepins, Electrical Properties of Polymers, Chemical Properties; Hanser Publishers: Munich,1987

353. G. C. Psarras, Compos. Part A Appl. Sci. Manuf. **37**, 1545 (2006).

354. T. Sampreeth, M. A. Al-Maghrabi, B. K. Bahuleyan and M. T. Ramesan, J. Mater. Sci. **53**, 591 (2017).

355. H. Li, L. Wang, G. Song, Z. Gu, P. Li, C. Zhang and L. Gao, Iranian Polym. J. **19,** 39 2010.

356. F.W. Billmeyer, Jr., Text Book of Polymer Science, 2nd edition, John Wiley and Sons, (1971)

357. P.E. Cassidy, T.M. Aminabhavi and C.M. Thompson, Rubber Chem. Technol. **56**, 594 (1983).

358. D. Kim, J.M. Caruthers and N.A. Peppas, Macromolecules **26**, 1841 (1993).

359. S. J. Ahmad, H. Yudong and W. Li, Iranian Polym. J. **13**, 415 (2004).

Chapter 9
Conclusions and Future out look

Bibliography

List of publications

1. A. Nihmath and M. T. Ramesan, Synthesis, characterization, processability, mechanical properties, flame retardant, and oil resistance of chlorinated acrylonitrile butadiene rubber, Polym. Adv. Technol. **29**, 2165 (2018).

2. A. Nihmath and M. T. Ramesan, Preparation, Characterization, Thermal, and Electrical Properties of Chlorinated Ethylene Propylene Diene Monomer/Hydroxyapatite Nanocomposites, Polym. Compos. **39**,2093 (2018).

3. A. Nihmath and M. T. Ramesan, Fabrication, Characterization and Dielectric Studies of NBR/ Hydroxyapatite Nanocomposites, J. Inorg, Organomet. Polym. **27**, 481 (2017).

4. A. Nihmath and M. T. Ramesan, Effect of hydroxylapatite nanoparticles on structural and electrical properties of ethylene propylene diene monomer rubber, J. Chem. Pharm. Sci., special issue. **38** (2016).

5. A. Nihmath and M. T. Ramesan, Development, characterization and conductivity studies of chlorinated EPDM, AIP Conf. Proc. **1620**, 353 (2014).

6. M. T. Ramesan, A. Nihmath, and J. Francis, Preparation and characterization of zinc sulphide nanocomposites based on acrylonitrile butadiene rubber, AIP Conf. Proc. **1536**, 255 (2013).

7. A. Nihmath and M.T. Ramesan, Comparative Evaluation of Oil Resistance, Dielectric Properties, AC Conductivity and Transport Properties of Nitrile Rubber and Chlorinated Nitrile Rubber, Prog. Rub. Plast. Tech. DOI: 10.1177/1477760620 925490, 2020

8. A. Nihmath and M.T. Ramesan, Hydroxyapatite as Potential Nanofiller in Technologically Useful Chlorinated Acrylonitrile Butadiene Rubber, Polym. Test. 91, 106837 (2020).

9. A. Nihmath and M.T. Ramesan, Fabrication, Characterization, Dielectric Properties, Thermal Stability, Flame Retardancy and Transport Behavior of Chlorinated Nitrile Rubber/ Hydroxyapatite Nanocomposites, Polym. Bull., 2020**,** DOI: 10.1007/s00289-020-03469-w

10. A. Nihmath and M.T. Ramesan, Development of Novel Elastomeric Blends Derived from Chlorinated Nitrile Rubber and Chlorinated Ethylene Propylene Diene Rubber, Polym. Test. 89, 106728 (2020).

11. A. Nihmath and M.T. Ramesan, Development of Hydroxyapatite Nanoparticles Reinforced Chlorinated Acrylonitrile Butadiene Rubber / Chlorinated Ethylene Propylene Diene Monomer Rubber Blends, J. Appl. Polym. Sci., DOI: app.49912, 2020

12. A. Nihmath and M.T. Ramesan, Studies on the Role of Hydroxyapatite Nanoparticles in Imparting Unique Thermal, Dielectric, Flame Retardancy and Petroleum Fuel Resistance to Novel Chlorinated EPDM/ Chlorinated NBR Blend, Res. Chem.Intermed., DOI:10.1007/s11164-020-04239-z , 2020

Presentations

1. A. Nihmath and M. T. Ramesan, Development, characterization and conductivity studies of chlorinated EPDM, **Optics '14,** ***International Conference on Light,*** NIT Calicut, 19-21 March 2014.
2. A. Nihmath and M. T. Ramesan, Fabrication, Characterization And Dielectric Studies of Nbr/Hydroxyapatite Nanocomposite, **UGC Sponsered Graduate Seminar on** ADVANCES IN MATERIALS CHEMISTRY (AMC-2014), Department of Chemistry, University of Calicut on 5th December 2014.
3. A. Nihmath and M. T. Ramesan, Effect of hydroxylapatite nanoparticles on structural and electrical properties of ethylene propylene diene monomer rubber, **UGC Sponsered national seminar on** "Crystallography: Special Emphasis on Applications in Chemistry" N.S.S.College Manjeri on 6th and 7th January 2016.